The influence of surface functional groups of organic crystals on triboelectrification

by

James Robert Middleton

A thesis submitted in accordance with the requirements for the degree of Doctor of Philosophy in Chemical Engineering

The University of Leeds

School of Chemical and Process Engineering

September 2023

Intellectual Property and Publication Statement:

I confirm that the work submitted is my own, except where work which has formed part of jointly authored publications has been included. My contribution and the other authors to this work has been explicitly indicated below. I confirm that appropriate credit has been given within the thesis where reference has been made to the work of others.

Chapter 4 of the Thesis has been prepared as a paper and accepted into the American Chemical Society (ACS) journal Crystal Growth and Design. The other Authors are part of the supervisory team.

- J. R. Middleton, A. J. Scott, R. Storey, M. Marucci, and M. Ghadiri, "Prediction of the Effective Work Function of Aspirin and Paracetamol Crystals by Density Functional Theory – A First-Principles Study," Cryst. Growth Des., Jul. 2023, doi: 10.1021/acs.cgd.3c00218.

Acknowledgement

I would like to express my sincere gratitude to Professor Mojtaba Ghadiri and Dr Andrew Scott for their invaluable supervision and guidance throughout my PhD. I deeply appreciate their honesty, unwavering support, and the many hours they dedicated to providing feedback on my research.

I am also grateful to my fellow group members, Dr Wei Pin Goh and Saba Saifoori, for their friendship and camaraderie, which made my PhD far more enjoyable.

I extend my heartfelt thanks to my parents, Rob and Michelle Middleton, for their constant support and encouragement throughout this process.

Furthermore, I would like to acknowledge AstraZeneca for sponsoring this project.

Abstract

Triboelectric charging is a ubiquitous phenomenon with both historical significance in the discovery of electricity and contemporary importance in applications like particulate processing and small-scale power generation through ambient energy harvesting [1]. However, despite its long history, the fundamental mechanisms underlying triboelectric charging remain poorly understood. This complexity arises from the sensitivity of the phenomenon to a multitude of physical and environmental factors, making the interpretation of experimental results challenging [2]. Recent advances, particularly the development of triboelectric nanogenerators, have led to a growing consensus that the electron transfer mechanism dominates in triboelectric charging [3], although this perspective is not universally accepted among researchers [4]. First principles calculations have demonstrated their ability to probe the underlying mechanisms for charge transfer and this work has been applied to gain insight into various triboelectric charging phenomena observed in experiments [5]. This thesis employs Density Functional Theory (DFT) to gain insights into various aspects of triboelectric charging observed in experimental settings.

Firstly, the influence of surface properties, crystal facets, and the presence of surface contaminants on various electronic structure properties relevant to triboelectric charging is investigated. This analysis underscores the substantial impact that surface conditions can have on charge transfer phenomena. Secondly, the work function, a key parameter for modeling triboelectric charging, is predicted for different facets of pharmaceutical crystals using DFT. These calculations predict variations in work function, depending on the crystal facet and the presence of surface water. Finally, the charging characteristics of individual Active Pharmaceutical Ingredient (API) molecules are investigated through a theoretical "slab-molecule" approach. To elucidate the mechanisms of charge transfer, charge density difference, density of states and Hirschfeld charge analysis were employed.

This thesis aims to highlight, through the application of first principles calculations, the substantial influence that surface chemistry and contamination can exert on triboelectric charging. Additionally, it seeks to introduce innovative methods for gaining insights into the triboelectric charging properties of individual molecules.

This page is intentionally left blank.

Table of contents

List of Tables

List of Figures

List of Abbreviations

Abbreviation	Meaning
AFM	Atomic Force Microscopy
API	Active Pharmaceutical Ingredient
B3LYP	Becke, 3-parameter, Lee–Yang–Parr
BFDH	Bravais, Friedel Donnay and Harker
CA-PZ	Ceperley-Alder Perdew-Zunger
CPD	Contact Potential Difference
DC	Direct Current
DEM	Discrete Element Method
DFA	Density Functional Approximation
DFT	Density Functional Theory
DOS	Density of States
EFM	Electrostatic Force Microscopy
FF	Force Field
FFT	Fast Fourier Transform
GGA	Generalized Gradient Approximation
HF	Hartree-Fock
KPFM	Kelvin Probe Force Microscopy
KS	Kohn-Sham
LDA	Local Density Approximation
MD	Molecular Dynamics
MM	Molecular Mechanics
MP	Monkhorst-Pack
OEC	Overlapped Electron Cloud
OTFG	On The Fly Generated
PBE	Perdew-Burke-Ernzerhof
PDOS	Partial Density of States
PET	Polyethylene Terephthalate
PMMA	Polymethyl methacrylate
PTFE	Polytetrafluoroethylene
PVC	Polyvinyl Chloride
QM	Quantum Mechanics
SCAN	Strongly constrained and appropriately normed
SEM	Scanning Electron Microscope
TDOS	Total Density of States
TENG	Triboelectric nanogenerator
TS	Tkatchenko-Scheffler
UPS	Ultraviolet Photoemission spectroscopy
UV	Ultraviolet
XC	Exchange Correlation
XPS	X-ray Photoemission Spectroscopy

Chapter 1 – Introduction

Triboelectric charging, commonly referred to as contact electrification, is a widespread phenomenon in powder processing industries. It arises from the transfer of electrostatic charge when two surfaces slide, roll, or make direct contact, and most commonly arises from sliding or direct impact. In industrial powder processes, such as sieving, fluidising, conveying, pouring and grinding, triboelectric charging occurs frequently, leading to substantial electrostatic charge transfer [2,6]. Excessive charging can cause unwanted cohesion in powders, forming agglomerates [7]. It can also cause particle adhesion to vessel walls, also known as "sheeting" and can cause uneven inlet flow or blockages [8–12]. Excessive charging poses a notable risk of electrostatic discharges, carrying a significant threat of fire and explosions [13–15]. Conversely, triboelectric charging constitutes a key element in numerous valuable applications, including printing [16], powder separation [17], dry coating [18], gas cleaning [19], triboelectric nanogenerators [20] and preventing segregation in some mixtures [21]. However, despite being documented since antiquity [22], the underlying mechanisms of triboelectric charging remain poorly understood.

The concept of triboelectric charging has been known for thousands of years, the ancient Greeks for example observed that by rubbing a fur against amber it could attract small objects [22]. Despite this, there is still much that scientists do not fully understand about this phenomenon. Active debate continues over which mechanism dominates this process, electron transfer or ion transfer [1]. The magnitude and polarity of charging can vary significantly depending on numerous factors, mode of contact, i.e. friction, contact or separation [23], environmental conditions such as temperature [24], relative humidity [25] or external electric field [26], material properties such particle shape and size distribution [27,28] and surface roughness [29] all affect charge transfer. Charging propensity varies between different substances and these are typically ranked into a so-called triboelectric series, which is a list of materials arranged in order of their propensity to become electrically charged when they come into contact with another material [30]. Pharmaceuticals and excipients have significantly different charging behaviours in both polarity and magnitude [31]. Interestingly, particles in single component systems also experience charging when agitated [27,32], and it has been shown that contact between nominally identical materials with opposite surface curvature (concave vs convex) will consistently charge positively or negatively depending on curvature [33]. Also, ‘flexoelectricity’, arising from the coupling between polarisation and strain present in all insulators is shown to have a measurable effect on triboelectric charge transfer [34]. There is still significant disagreement among researchers on the underlying mechanisms of triboelectric charging. Three primary mechanisms are thought to govern the exchange of triboelectric charges during contact and separation processes: electron transfer, ion transfer and material transfer [1]. Electron transfer occurs when electrons are exchanged between two contacting surfaces, leading one material to gain electrons and acquire a negative charge, while the other material loses electrons, resulting in a positive charge. Ion transfer involves the migration of charged ions, either from the environment or ionisable surface groups, leading to a net charge difference after separation. Finally, material transfer refers to the microscale exchange of material between surfaces during contact which can potentially modify the charge distribution and influence the overall charging behaviour.

The charging of identical materials and the supposed prevalence of particle-particle contacts in powder flows [35] suggests that the cause of triboelectric charging in single component systems is most likely due to subtle structural differences between surfaces at contact points. The questions which naturally arise are whether the chemistry of the surfaces is anisotropic, does the uneven coating of surface water influence charge transfer or do the variations in surface electronic structure caused by temperature, mechanical stress or contamination play a role. Compelling evidence of the importance of water films in contact charging has been presented by Baytekin et al.[36], where they observed mosaics in surface potential were attributed to surface water. Additionally, Lee et al.[37] observed that the differences in surface hydrophobicity greatly increase the magnitude of transferred charges. There is a growing amount of research that suggests electron transfer is the dominant process in triboelectrification[3], but for adsorbed species on the surface, such as water, ion transfer cannot be ruled out. So further supporting evidence is needed by understanding the dynamics of charge transfer during contact.

Triboelectric charging has been a subject of extensive scientific research [1,2,25]. Generally, studying the behaviour of powder systems is complex as interparticle interactions are influenced by numerous physical and environmental factors, which in practice are difficult to "decouple" [38]. Additionally, electrostatic charging has been described as "unpredictable" [39], since triboelectric charging is impacted by both physical properties and environmental conditions. These factors make obtaining reliable experimental results challenging. Many published results are difficult to interpret and in some instances appear contradictory [1]. Modeling has shown great utility in studying triboelectric charging as computational methods offer precise control of the system in question and can reveal detailed underlying causes. Significant work has already been done on the macroscale modeling of triboelectrification in unit operations. A review of such techniques, applied to fluidised beds, is given by Fotovat et al. [40]. A detailed discussion of current modeling approaches is also given by Chowdhury et al. [41]. However, in both these publications the mechanisms for charging have not been addressed. *A priori* predictions could enable the triboelectric charging to be assessed more effectively [42].

Density Functional Theory (DFT) is a computational quantum mechanical modeling method that is widely used to study the electronic structure and properties of materials [43,44]. In recent years it has also been used to model triboelectric charging. Nikitina et al.[45] applied time-dependant DFT to produce *ab-initio* predicted triboelectric series. It has also been used to study how material deformation and mechanically induced-ionisation at a surface might impact charge transfer[46–48]. The work of Lin et al.[49] investigated how the presence of surface water can impact the electronic structure of a material, leading to a reversal in the polarity of transferred charges. Shen et al.[50] simulated charge transfer directly by calculating redistribution of atomic charges between contacting surfaces of quartz and sapphire. Furthermore, a significant amount of research is being devoted to the study of Tribo-Electric Nano-Generators (TENGs) [51,52] to optimise their design and predict their performance. This has contributed to an increase in the use of DFT to study triboelectrification [53–58].

This chapter contains a comprehensive literature review on the triboelectric charging phenomena. It begins with a historical overview, tracing the evolution of the field and highlighting significant contributions. The review explores the key electronic structure properties relevant to triboelectric charging, such as band theory and work function. This chapter provides an elucidation of the proposed mechanisms of triboelectric charging, encompassing electron transfer, ion transfer, and material transfer, supported by the most persuasive evidence available in the literature for each mechanism. Environmental and physical factors impacting charging behaviour, such as humidity, temperature, and surface roughness, are also discussed. Furthermore, the chapter reviews current experimental and computational methods, ranging from triboelectric nanogenerators to first principles quantum mechanical calculations, that aid in understanding charge transfer mechanisms.

1.1 – Historical overview

The study of triboelectrification is intrinsically connected to the exploration of electricity and magnetism throughout history. Ancient Greeks made the initial observations, noticing that rubbing animal furs on pieces of amber generated electrostatic discharges and enabled the manipulation of feathers. Although some debate remains over whether Aristotle or Thales of Miletus [22] was the first to document this phenomenon, the significance of their discovery is undisputed. The word "electricity" itself traces its origin back to the Greek word for amber, "ēlektron." [22]. Many of the early observations of behaviour of electricity and magnetism were carried out using what we know of today to be triboelectrically generated charges. In his seminal work “De Magnate” published in 1600 William Gilbert (1544 – 1603) recorded that amber became charged when rubbed with wool. He also identified many other substances in addition to amber that could be charged by rubbing, and termed these “electrics”. Those materials that he could not charge by rubbing “nonelectrics”. he likened the movement of charge from one material to another to that of a fluid [59].

In 1660, Otto von Guericke (1602 – 1686) created the earliest known electrostatic generator—a sulfur sphere revolving on a shaft. When electrified by a dry hand, the sphere attracted paper, feathers, and other light objects. Moreover, this apparatus generated small sparks and cracks during discharge which were attributed to electrostatic charging for the first time [60]. The electrostatic generator's design underwent improvement by Francis Hauksbee (1666 – 1713) [59] of the Royal Society, who demonstrated that a cylindrical tube of flint glass rubbed with silk was considerably more effective than dry hands on sulfur. Triboelectrically generated charges played a pivotal role in Steven Gray's (1666 – 1736) [59] discoveries of electrical conduction and insulation. Charles Francois de Cisternay du Fay (1690-1739) [59] became intrigued by electricity after learning about Gray's experiments, and he zealously attempted to electrify various natural objects through rubbing. It was during this endeavour that Du Fay first observed charge polarity, noting that glass rubbed with silk and amber rubbed with fur produced two kinds of electric charge, which he labelled as "vitreous" (positive) and "resinous" (negative) respectively [59]. John Carl Wilcke (1732-1796) recognized the possibility of categorizing materials according to their inclination to acquire positive or negative charges upon contact with other materials. This insight led him to develop the first triboelectric series, which organizes materials based on their polarity of charging [61]. During the 19th and 20th centuries, the triboelectric effect gained industrial relevance and found application in various techniques, such as electrostatic separation, electrophotographic printing, and the generation of exceptionally high voltages in the famous Van de Graaff generators. Despite its immense significance to the study of electricity, the mechanism of triboelectric charging remains inadequately understood, and uncontrolled charging has negatively affected powder processing industries since the industrial revolution.

A contemporary review of the field, presented in W.R. Harper's book "Contact and Frictional Electrification" [15] published in 1967, delves into the basic problem, theoretical aspects, and interpretation of experimental data, including a discussion of the quantum mechanical aspects of electron transfer. This work underscores ion transfer as a key mechanism. Subsequent highly cited review articles advocate for ion transfer [25] and electron transfer [3], respectively. Contemporary researchers continue to wrestle with identifying the dominant mechanism of triboelectric charging, facing the challenge that modest progress is often countered by experimental approaches encountering increasingly perplexing behaviours [1]. As a result, a consensus on the primary charging mechanism remains elusive, underscoring the complexity and intricacy of this phenomenon.

A pivotal advancement in the field of triboelectric charging emerged with the invention of the triboelectric nanogenerator by Zhong Lin Wang and co-workers [20], marking a significant breakthrough. This innovation opened up new possibilities for experimentation, enabling charging studies to be conducted at previously inaccessible temperatures and pressures [62]. Triboelectric nanogenerators (TENG) offer immense potential for microscale power generation, ranging from harvesting ambient mechanical energy to creating self-powered switches and devices. These developments have sparked a surge of research, utilizing first principles calculations [5] and atomic force microscopy (AFM) [63] to enhance the design and performance of triboelectric devices. This work has significantly advanced the understanding of the fundamental mechanisms of triboelectric charging. Ongoing efforts in this field has the potential not only to enhance the performance of TENGs but improve the modeling of triboelectric charging in applications such as powder processing, allowing for predictive modeling and charge mitigation techniques which would be of great interest to a range of industries. A comprehensive understanding of the triboelectric charging mechanism would offer substantial benefits to multiple sectors.

1.2 – The mechanisms of triboelectric charging

Fundamentally, charging arises from the transfer of elementary charge-carrying particles, such as protons or electrons. Different materials exhibit distinct charging propensities, leading to positive or negative charging, with varying affinities and magnitudes of charge build-up on their surfaces, allowing them to be ranked into various “triboelectric series” which will be discussed at length later on. Charging is highly sensitive to environmental factors contributing to the inconsistency and contradictions in published research [2,64,65]. The mechanisms underlying the movement of these charge carriers between surfaces, especially in insulating materials, remain unclear. In the early 90s Horn et al, [66] published a study where chemisorbed monolayers were used to study the adhesive and electrostatic forces between silica surfaces. In this paper he remarks that there are two ways to view electrostatic phenomena. From a physicist's standpoint, the concepts of electronic states and work functions are employed, which proves useful in describing electron transfer. On the other hand, a chemist's viewpoint favours the use of acid-base interactions, which proves useful in describing ion transfer. These mechanisms are undoubtedly the primary processes in triboelectric charging, however, it is also crucial not to overlook the significance of material transfer, as a secondary mechanism for charging when examining this phenomenon. This section will give a brief overview of each of the proposed mechanisms of triboelectric charging. A high quality and thorough overview of the theoretical framework of the tribocharging mechanisms is given by Harper [15], and also by Lowell and Rose-Innes [67].

1.2.1 – Charging by material transfer.

Material transfer, also known as mass transfer, describes the process of charged molecular fragments or macromolecules transferring between surfaces that causes triboelectrification. The triboelectric effect it thought to be closely related to the phenomenon of adhesion, when two materials undergo contact, they stick together due to intermolecular interactions such as ionic, van der Waals or hydrogen bonding. The precise nature of the intermolecular forces at interfaces are of significant interest to various fields and a covered extensively elsewhere [68]. Within the context for triboelectric charging, it is proposed that the mechanical and intermolecular forces at play at a contacting interface will result in a degree of bond cleavage at the interface. An extreme example of this process is the adhesion of polymer surfaces where cross-linking and entanglement of polymer chains at a given point of contact will induce bond cleavage producing charged radicals at the surface. This process is discussed at length in a review compiled by Raos and Zappone [69]. Disassociation of covalent bonds result in heterolysis or homolysis which forms a pair of either identical or cationic/anionic ions or cationic radicals respectively, which act as the prerequisite charge species required for charge transfer [4]. A striking example of this is the production of triboelectrically generated X-rays by the peeling of adhesive tape [70].

It is possible to define material transfer mechanisms as having two main components: charge transfer due to the cleavage of relatively large molecular fragments as discussed above, and the strain or triboelectrically induced formation of “mechano-ions”. Large molecular fragments are useful in explaining some unusual results that are observed during experiment. In the work of Baytekin et al. [36] where Kelvin Probe Force Microscopy (KPFM) measurements are used to highlight the mosaic of surface charge that develops on a surface after contact, it has been suggested by Williams [71] that these surface charge mosaics visually mirror the structural features of the transferred material. Nonetheless, it is important to acknowledge that an alternative interpretation of these results can be derived from an electron and ion transfer mechanism. Material transfer is sometimes used in publications to explain the reversal of charge during contact. Baytekin et al. [72] also studied the microscale material transfer between polymer beads and surfaces and found that over time, due to increased material transfer, it was possible for the polarity charge transfer to shift compared to the initial charge. Furthermore the magnitude of material transfer has also been addressed in the work of Pandey et al. [73] where polyvinyl chloride was contacted with hard and soft polydimethylsiloxane (PDMS) respectively, the general conclusion of this work being that a larger amount of material transfer corresponded with a larger amount of charge transfer. The work of Li et al. [74] also observed a correlation between and wear severity and triboelectrification in metal-metal contacts.

Mechano-ions are often invoked to explain the observed relationship between stress and strain gradients. There is a strong basis in literature that mechanical action on a surface can significantly impact the chemistry at surfaces. Evidenced by the reported phenomenon of triboluminescence [75] and tribo-excited chemical reactions on surfaces [76]. In the work of Piperno et al. [77] they used a modified Kelvin probe technique combined with X-ray photoemission spectroscopy (XPS) and contact angle measurements to show that rubbing produces free radicals at a surface. A phenomenon of particular interest is the impact of material strain on charging. In the work of Sow et al. [78] they observed that the magnitude and direction of charge transfer between contacting Polytetrafluoroethylene PTFE and latex rubber was proportional to the strain applied to the latex; it is argued that this is due to the strain induced ion/mechano-ions on the surface [79,80]. In more recent work published by Verners et al. [81] they investigated how surface roughness might impact the charge transfer between chemically identical polymers. Rough and smooth surfaces of polymers were prepared. Using faraday pail, profilometry and AFM experiments combined with finite element and molecular modelling approaches, it was found that the smoother surface always would charge negatively across all materials tested. The analysis indicated an inhomogeneous distribution of surface charge, influenced by surface geometry and driven by strain during contact and separation. The model predicted a distinct average charge sign resulting from bond breakages and charged material transfer-based CE reactions.

A significant fraction of published research investigating the material transfer mechanism deals with polymer contacts, be it polymer-polymer, metal-polymer etc. Polymeric materials are known for their high propensity for triboelectric charging [30], which can be attributed to their typically highly resistive properties. They are also ubiquitous in consumer and industrial problems and as a result the problems caused by their manufacture are well known. More recently they have emerged as a favoured material in tribo-electric generators due to their high triboelectric charging capacity and ready availability. As a result, a significant amount of research has emerged looking at how material transfer at the interface of polymeric materials might impact charge transfer. An extensive and recent review of engineering polymer materials for the design of more effective triboelectric nanogenerators which favours the material transfer mechanism is given by Šutka et al. [4].

In summary, it is highly probable that material transfer occurs to some degree during contact. Several studies have directly demonstrated microscale material transfer at interfaces [4]. Additionally, there is extensive evidence supporting the formation of mechano-ions and radicals at interfaces during contact. This is particularly valuable in explaining certain unusual charging behaviours, such as polarity reversal and the influence of strain gradients. Furthermore, there is a noticeable correlation between mechanical and wear properties and triboelectric charging. The material transfer mechanism undeniably plays a crucial role in polymer-surface contacts. However, its significance may vary when it comes to charging non-polymeric materials. In the subsequent sections, we explore the ion and electron transfer mechanisms, providing an alternative perspective.

1.2.2 – Charging by Ion transfer.

The ion transfer mechanism suggests that in any contact situation where triboelectrification occurs, a population of ions exists, constituting the primary charge carriers essential for this process. Upon contact, there is a redistribution of ions between the surfaces, leading to a charge separation upon separation. Unlike the material transfer mechanism, the ions in this context are not exclusively mechano-ions generated solely by mechanical impact. They encompass loosely bound surface ions as well as ions present in the surrounding environment. Ionic species required for charge transfer will always fall into two categories, surface or environmental [25]. The ion transfer mechanism is valuable for providing a convenient theoretical framework that elucidates triboelectric charging in electrically insulating materials, which has been extensively explored in the literature. A significant proponent of the ion transfer mechanism was W.R. Harper who authored the classic textbook on triboelectric charging "Contact and frictional electrification" [15] in which he states that the main charge carrier in triboelectrification is never electrons when the material is strictly an electrical insulator.

In 1953 Medley [82] published an article discussing the ion exchange process of common resins due to ionisable functional groups on their surface and ions from surface water due to humidity even on "dry surfaces". The key property of interest when interpreting triboelectric charging results is the materials Lewis acidity and basicity at a surface. Several studies have shown it is possible for ions to transfer across surfaces. In the work of Mizel et al. [83] they attempted to directly observe the ion transfer between a metal and a bromine salt doped insulating film using secondary-ion mass spectrometry. They were able to directly measure the transfer of bromine ions, significantly altering charging properties and in certain situations reverse the polarity of charge. Similarly, Law et al. [84] used a salt modified polymer surface to probe the charging properties of toner particles and polymer coated metal beads. They observed through XPS, secondary-ion mass spectrometry and Faraday cage experiments that the transfer of ions from the toner to metal coated polymer beads correlates with polarity and magnitude of charging. Using a different approach, Diaz [85], probed the charging behaviour of polymers/ionomers films and polymers/organic salts using a Kelvin probe reporting that films with mobile ions develop charge whereas films without mobile ions do not develop charge, and additionally proposed a model that relates charge to chemical structure of ions used to effect charge.

The transfer of ions between surfaces has been well addressed in literature. From a mechanistic standpoint what is the nature of the redistribution of ions at the surface during contact? The mechanisms of ion transfer at surfaces is covered at length in the review of McCarty and Whitesides [25]. Figure 1.1, shows a schematic representation of the mechanism of ion transfer during separation. The curves shown above the contacting surfaces show a complementary visualisation of the potential energy curves (which are described as being analogous to Lennard-Jones potential or Morse potential), and is intended to show the formation of a asymmetric double-well potential. At intermediate distance there is effectively a single well and the mobile ion can be found at any point within that well according to the Boltzmann distribution. At some distance the ion becomes trapped kinetically on one side of the well and the electrostatic energy (defined in the figure as ΔE) surpasses the thermal energy (kT) trapping the ion on the surface allowing for a separation of charge. A more though explanation of this process is described by McCarty and Whitesides [25].

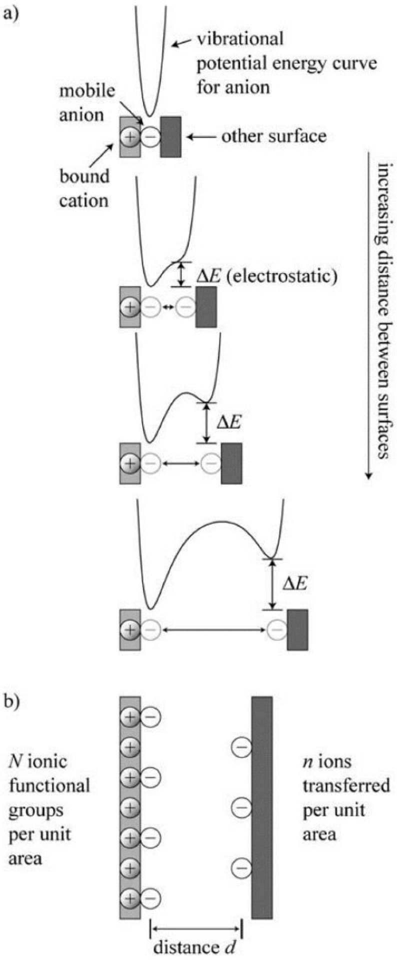

Figure 1.1 – *a) a schematic representation of the mechanism of ion transfer. b) An illustration of the charge transfer due to ions between surfaces (taken from reference [22]).*

In everyday manifestations of triboelectric charging, and in most practical applications the process will likely not be in high vacuum and a degree of contamination will be present on the surface typically in the form of surface water. The role of water in the triboelectrification is a topic of significant interest to researchers. It has been shown that in low humidity environments that the magnitude of charging is significantly reduced [86] and that high humidity environments increase the rate and magnitude of charging [87]. Water has also been observed to charge positively when contacted with any other material, putting it at the "top" of the triboelectric series [88]. A useful recent publication reported by Lee et al. [37] showed the use of acoustic levitation to repeatably contact a silanized glass sphere on to a similarly silanized glass plate and found that the largest degree of charge transfer occurs between dissimilar hydrophobic or hydrophilic pairs and is negligible or significantly reduced between similar hydrophobic/hydrophilic pairs, implying film transfer. Additionally the evaporation of water films have been observed to produce spontaneous charge mosaics on surfaces [89].

The ion transfer mechanism has significant merit in explaining experimentally observed correlations, particularly those pertaining to the Lewis acidity and basicity of surfaces. Moreover, it provides valuable insights into the substantial influence of water on the process. Most importantly, it offers an explanation for the charge transfer phenomena observed in insulating materials, which presents a conceptual challenge from the standpoint of electron transfer [15]. However, a critical limitation of this mechanism is its reliance on mobile ions at the surface to serve as the charged species. It has been observed that charging can persist in scenarios where no ionizable functional groups are present on the surface to provide these mobile ions [62]. Advocates of the ion transfer mechanism contend that, in such cases, the charged species are exclusively sourced from surface ions [25]. However, a significant drawback of the ion transfer hypothesis emerges when considering situations where water is absent. Triboelectric charging experiments conducted submerged in oil have demonstrated that contact electrification can occur independently of water, although water's presence does impact the magnitude of generated charges and the rate of charge decay [90]. Additionally, in Triboelectric Nanogenerator (TENG) experiments, it has been demonstrated that charging takes place even under conditions of elevated temperatures and in vacuum environments, involving materials that lack mobile ions. Under these circumstances, there are minimal ions available to act as charged species[1,62]. These findings provide a robust counter-perspective, suggesting that ion transfer may not be the exclusive mechanism governing charge transfer.

1.2.3 – Charging by electron transfer.

The final triboelectric charging mechanism to be discussed is the electron transfer mechanism which describes the process where materials exchange electrons at the point of contact. Following separation, electrons are either gained or lost by the respective materials, resulting in the retention of a residual charge. The specifics of this exchange process are significantly influenced by the electronic properties of a material, such as its work function. Conductive materials, characterized by their narrow band gap, exhibit electrons that are widely distributed throughout their bulk structure. Consequently, in metal-metal contacts, electrons can flow readily from one body to another. [67]. Harper [15], elaborates extensively on the theoretical foundation of electron transfer and concludes that it is likely the principal mechanism in conductive materials. However, he states that in case of insulating materials the charge species are always ions. Interestingly, many years later another popular and highly cited review article was published by Lowell and Rose-Innes [67] presents a contrasting perspective, suggesting that even insulating materials are capable of exchanging electrons. The electrical conductivity and insulating properties of a material significantly impact triboelectric charging. Triboelectric charge transfer can manifest in both conductive and insulating materials; however, it is of minor concern in conductive materials since any transferred charges swiftly disperse to earth [67]. Conversely, in insulating materials, triboelectrification poses a significant challenge because transferred charges tend to become localized at the point of contact. These trapped charges subsequently give rise to troublesome macroscopic effects, driven by electrostatic attraction and repulsion, along with the potential for electrostatic breakdown of the surrounding atmosphere, leading to the formation of sparks.

Materials can be categorized into three broad and overlapping classes: conductors, semiconductors, and insulators. Conductors permit charge carriers to move with little resistance through the material, exemplified by all metals, which possess a delocalized pool of electrons enabling bulk electron mobility and charge transfer. In contrast, insulators feature tightly bound electrons to atoms, with few mobile surface ions, resulting in restricted charge movement within both the bulk and on the surface. Semiconductors occupy an intermediate position, exhibiting properties that neither resemble excellent conductors nor excellent insulators but still charge significantly [91,92].

In insulators, charge mobility between the surface and the bulk is constrained, leading to its effective confinement at the point of contact. This scenario can result in a significant accumulation of charge on the surface, potentially surpassing the electric breakdown threshold of the surrounding air (or other gaseous medium), thus triggering electrostatic discharge [15]. The foundation of material conductivity finds its explanation through the principles of band structure theory. This theory elucidates the spectrum of attainable energy levels for electrons within a solid material. Valence electrons, the outermost electrons, primarily reside in the valence band. In conductive materials, these valence electrons can readily transition from the valence band to the 'conduction band,' where they gain the freedom to move unrestricted throughout the solid structure. The energy range between the valence and conduction bands is referred to as the 'band gap.' In materials with substantial band gaps, electrons find it challenging to access the conduction band and are largely confined to specific local regions, rendering the material insulating in nature [1]. Detailed descriptions of band structure theory are provided in literature [93]. These concepts are illustrated in Figure 1.2.

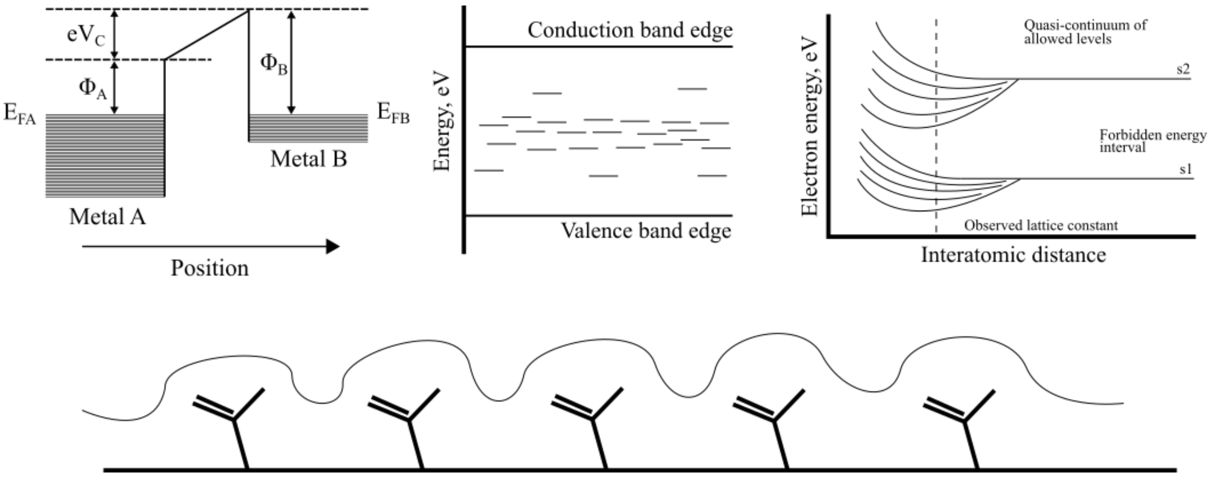

Figure 1.2 – *A schematic diagram of electron transfer between two metal surfaces where (Φ_A,Φ_B) is the work function of material A and B respectively. (V_A,V_B) is the contact potential and (E_{FA},E_{FB}) is the Fermi level of material A and B respectively. (V_C) is the contact potential difference and (e) is the elementary charge. Reproduced from reference [67]. Illustration of possible mid-gap states that form during contact of insulators, allowing conduction (top centre). Illustrations of the electron energy bands present in a material (top right), reproduced from reference [15]. Illustration of surface with protruding functional groups with an electron cloud extending out (bottom).*

Arguably the most important quantity that has been used to interpret the triboelectric charging is a materials work function. A good description of the theoretical concept of work function is provided by Lowell and Rose-Innes [67]. An electron's potential energy is directly related to its position within or outside a metal, stemming from electrostatic interactions with other charged particles, typically electrons or atomic nuclei. The theoretical zero potential point represents the energy of an electron positioned at an infinite distance from a surface. In the context of a positively charged metal, the material's work function (ϕ) is defined as the energy required to extract an electron from the solid and place it immediately outside the surface [94]. To move the electron from just outside the surface to an infinite distance, an additional amount of work is necessary, which is a product of the surface potential and the elementary charge, denoted as $V_s e$ [67]. The Fermi level denotes the energy difference between the highest and lowest occupied single-particle states in a quantum system at absolute zero temperature. The energy needed to relocate an electron from the Fermi level to an infinite distance is the electrochemical potential (ξ) and can be described by the equation $\xi = \phi + eV_s$. A conceptual illustration of this is given in Figure 1.3. Empirical evidence strongly suggests correlation between the work function (and Fermi level) and contact charging phenomena, not only in metal-metal contacts but also, to a certain extent, in metal-insulator contacts. [67].

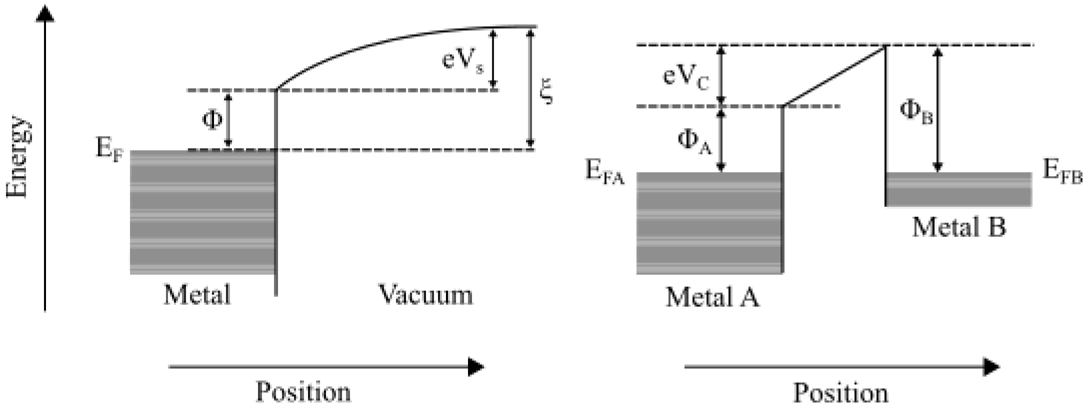

Figure 1.3 – *An illustration of the variation of the energy of an outside electron inside and outside a metal (left). Two metals in proximity exchange charge until their Fermi levels are coincident. The charge transferred is equal to* $(\phi_B - \phi_A)/e$*, the contact potential difference,* V_c *(right).* E_F *is the minimum energy of an electron added to the metal (reproduced from reference [67]).*

In the context of contact electrification in conductors, work function is widely used to model the charge transfer between metal surfaces. When two metals come into contact, electrons will naturally flow from the metal with a lower work function to the one with a higher work function, the amount transferred is proportional to the difference in work function [1,15,67]. The charge transfer mechanism, as described by electron transfer, operates as follows: consider two metal spheres with distinct work functions (ϕ_1) and (ϕ_2) respectively. Bring these spheres into contact and electrons will flow from one metal to another to establish the thermodynamic equilibrium [67]. The difference in surface potentials is called the contact potential difference (V_c) and is expressed as follows,

$$V_c = \frac{(\phi_1 - \phi_2)}{e_0}$$

Eq. 1.1 [67]

As the metals separate, the capacitance between them diminishes, leading to an increase in their surface potential difference. In response to this change, to uphold thermodynamic equilibrium, a portion of electrons may undergo tunnelling across the gap. Nonetheless, it is important to note that this tunnelling effect is constrained, typically ceasing after a very short distance (≈1 nm), with the resistance to further electron redistribution (R) increasing rapidly [67], as illustrated in Figure 1.4. Therefore, after separation there is expected to be a residual charge remaining on the spheres. An approximation of the charge remaining after separation (q) is given by Equation 4.6, where (C_0) is a constant and depends on the shape of the contacting bodies.

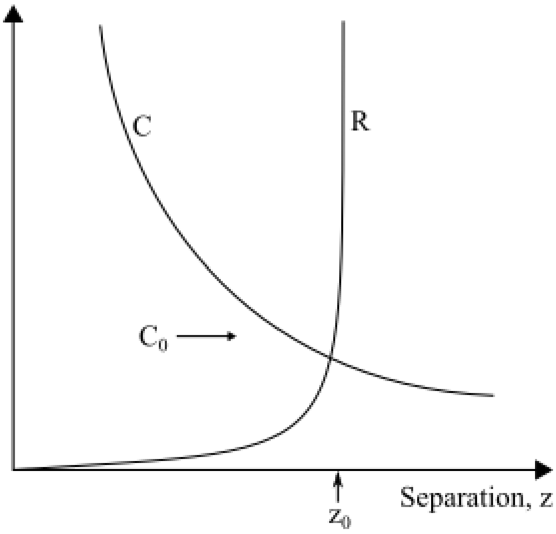

Figure 1.4 – *Schematic indication of the variation of capacitance (C) and resistance (R) between two metal surfaces, as a function of their separation (z)* [67].

$$q = C_0 V_c$$

Eq. 1.2 [67]

The model's performance in comparison to the experimental charge transfer when metals are brought into contact is illustrated in Figure 1.5.

Harper employs the work function model in an attempt to elucidate triboelectric charge phenomena. His work demonstrates a favourable correlation with experimental outcomes, as illustrated in Figure 1.5. Deviations from the theoretical model stem from the assumption of perfectly smooth spheres in the calculations, whereas practical spheres would exhibit varying degrees of roughness, including substantial protrusions exceeding the 1 nm limit of the tunnelling model [15,67]. Modeling the direction of charge in this way has been relatively successful in producing good correlations between work function, charge and material [67]. However this approach is imperfect as many metals will develop an insulating oxide layer with high surface resistivities altering the surface work function and interaction between the materials, meaning that the simple work function model can often give poor results [95]. A true understanding of metal charging requires a description of the process through these insulating layers.

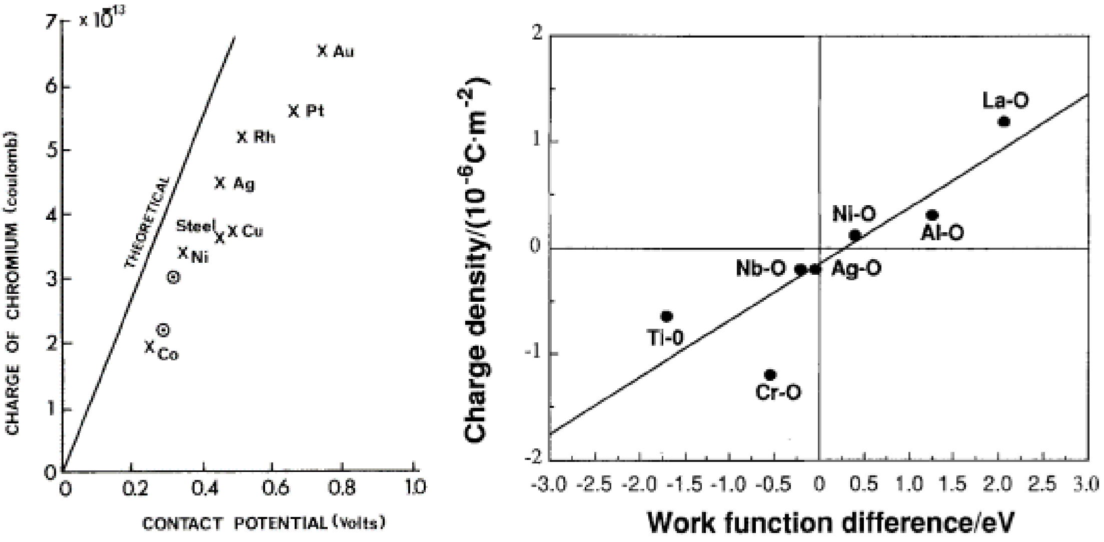

Figure 1.5 – *Charge on a Chromium sphere after contact with a sphere of another metal, plotted against the contact potential difference between the metal and Chromium. The "theoretical line" is based on the model defined in Equation 1.2* [67] *(Left). Charge densities of oxidised metal powders, calculated with particle surface area depending on the work function due to oxidation with gold as reference* [95] *(right).*

The concept of work function is firmly established for purely conducting materials, but it becomes less well-defined when applied to semiconductors and insulators. This challenge arises from the markedly distinct electronic structures of conductors and insulators. As mentioned earlier, conductive materials lack a band gap and possess a fully occupied conduction band, which results in a delocalized population of free electrons. In contrast, insulating materials exhibit a band gap with an unoccupied conduction band, meaning there are no 'free' electrons, and electron emission becomes localized and the concept of work function becomes less straightforward in such materials. [2,93]. Using work functions to model the triboelectric charging behaviour of insulating materials is challenging as experimentally measuring these work functions are, according to Gallo and Lama [96], “very difficult, time-consuming and inaccurate”. Despite these challenges, they underscore the critical importance of understanding work functions in the context of triboelectric charge transfer and emphasize its applicability to insulators. They define the work function of insulators as the minimum energy required to remove an electron from a fixed point charge. Additionally in this work Gallo and Lama [96] predict that small and large particles of the same material have different work functions, which is supported by recent experimental results [32]. By definition there is little to no electron mobility in insulating materials resulting in trapped charges on the surface, and more importantly this causes a significant build-up of charge on the surface during the experimental measurement of work function [97–99]. Early attempts to overcome this problem were made by Davies [100] who obtained the work function of a series of polymeric materials by contacting them with a metal with a known work function. The correlations observed in this work helped establish the concept of dielectric or “effective work function” [2]. Over time work function has remained a robust quantity of interest in the study of triboelectrification and is still used in recent works to interpret charging behaviour [101–103].

Obtaining reliable work function measurements, especially for materials used in the context of modeling triboelectric charging, can be challenging. Work function measurements are highly surface-sensitive. Even small surface impurities, contaminants, or changes in surface roughness can significantly affect the measured work function. Other factors affecting work function include: environmental factors such as humidity [104], temperature[105], and exposure to gases [106], or physical factors such as surface roughness

[107], curvature [108], particle size [109] or the materials response to stress or strain [102]. Interestingly it is also possible to view the correlation of Lewis acidity and basicity with triboelectric charging through the lens of the electron transfer mechanism. Two independent research groups correlated triboelectric charging with Lewis acidity and basicity, however in this work they interpret it using the electron transfer mechanism. In the work of Clint and Dusten [110] it is observed that there is a good relation between a between an “electron donor parameter” extracted from interfacial tension data and a material’s position on the triboelectric series, supporting an underlying electron transfer mechanisms. Furthermore, in the work of Veregin et al. [111] a theoretical framework in which the surface chemistry as determined by inverse gas chromatography can be related to the effective work function in provided. Both of these publications demonstrate the usefulness of work function, and by extension material electronic structure, to explain triboelectric charging results.

As a further complication, because of their negligible amount of charge carriers, insulators can undergo a process called polarisation. As the field passes through it interacts with the bulk of the insulator causing molecular dipoles to form which creates an opposing electric field. Any material that can be polarised is known as a dielectric. The degree to which a substance can be polarised is quantified by its dielectric constant (κ). This effect is commonly used in capacitors, as filling the space between the plates with a dielectric material increases the capacitance by a factor equal to the dielectric constant [112]. The dielectric properties of a material is known to be important to their triboelectric characteristics [113]. A high dielectric constant will weaken the electric field caused by contact or frictional charging, as the surface dipole will counteract the local surface charge. The relationship between the electric field (E) generated by a surface charge density (σ) is given by Harper (Eq 1.3) [15].

$$E = 2\pi\sigma\frac{2}{1+\kappa} \qquad \text{Eq. 1.3 }^{15}$$

If the field strength at the surface exceeds the electrostatic breakdown limit for the surrounding medium an electrostatic discharge can occur, causing sparking and presenting a significant explosion and fire hazard. This makes bulk materials’ dielectric properties significant when studying the charging of insulating materials. Polarisation has also been shown to enhance triboelectric charging in certain scenarios [114], highlighting it as a potential strategy to improve the design of triboelectric nanogenerators.

From the previous discussion it is shown that electron transfer can be used to successfully model the charge transfer behaviour in metal-metal contacts [15,67]. However, it has also been shown that the key quantity that is used to predict charge transfer, namely work function, is also sensitive to factors such as humidity and strain which, in some publications, are attributed to the ion [25] and material transfer [4] mechanisms respectively. With the recent increased interest in the design and development of TENG devices several compelling studies have been published showing strong evidence for electron transfer, even in insulating materials. In a recently published review article, electron transfer has been proposed as the dominant mechanism for triboelectric charging [3]. It has been established that water is not required for triboelectric charging to occur [90]. In the seminal work by Xu et al. [62], they investigate the contact electrification-effect at very high temperatures, using materials with no mobile ions at the surface. In this situation it can be assumed there are little to no mobile ions at the surface yet charge transfer still occurs. Additionally in the work of Wang et al. [115] their TENG device is shown to generate the largest amount of charge at very high vacuum. Strong evidence for the electron transfer mechanism is provided by the relationship between thermionic emission of electrons and charge transfer, and that charge evolution in both metal-insulator and insulator-insulator in TENG devices lines up well with a thermionic emission model [116,117]. Compelling evidence of these surface states is also given by Lin et al. [118] Ceramic films were coated with Polyvinyl chloride (PVC) and Polymethyl methacrylate (PMMA) polymers to study the effect of UV light on charge decay. Samples were triboelectrically charged using an AFM tip and the charge was measured using KPFM. It was found that the application of UV light accelerated the charge decay on the surface. Interestingly, this effect is dependent on the wavelength of light used with longer wavelengths producing little to no effect. This observation gives strong evidence that triboelectric charges occupy their own discrete energy levels on a surface, and can be liberated via photoexcitation [118]. This interaction between UV light and tribocharging has also been reported in earlier literature [119,120] and is strong evidence for the electron transfer mechanism.

The aspect of electron transfer that has always generated some controversy is the theoretical treatment of charge transfer in insulator-metal, insulator-semiconductor, and insulator-insulator contacts. As previously mentioned, insulators have a band gap which is too large for them to conduct electricity. However it is proposed that either defects on the surface or stained molecular bonds create surface states which act as intermediaries to bridge this large band gap [67]. In the work of Waitukaitis et al. [27] the impact of defect states on triboelectrification was investigated using thermoluminescence. While surface states were detected they reported that the magnitude of these charges on the surface were insufficient to produce the charges observed. However in other work, Xu et al. [33] the effect of surface curvature on the charge transfer between two plates of identical materials was looked at. It was found that the curvature of the plates produces a driving force for charge, repeatably charging either positively or negatively depending on convex or concave curvature. This is attributed to the formation of asymmetric surface states at a given contact.

Further support for electron transfer is given by a recent model proposed by Lin et al. [121] which describes electron transfer at an interface as a product of overlapping electron clouds. This is the overlapped electron-cloud model (OEC). It was found that contact electrification only occurred in the repulsive region not the attractive region. It was also found that thermal effects had no significant impact when the tip-sample difference was significantly large. The presence of an electric field was found to significantly impact charge transfer. The fact that contact electrification only occurs in the attractive region implies that electron transfer only occurs due to "electron cloud overlap". If a temperature difference is introduced the electron energy levels in the material will change, and therefore the electron transfer will change. In a strong enough electric field transfer was observed even in the attractive region [121].

The works of Cheng Xu [62,116] introduces a novel model for triboelectric charging, known as the "electron-cloud potential-well model". This model seeks to explain the phenomenon of triboelectric charge transfer across various materials, considering temperature effects. Before two materials make atomic-scale contact, their respective electron clouds remain separate, with no overlap. This corresponds to the attractive force region, as depicted in Figure 1.6. Within this region, electrons are tightly bound in specific orbitals by the potential well. As the two atoms, each from a different material, approach and contact each other, their electron clouds begin to overlap, forming either ionic or covalent bonds. If an external compression force is applied, the bonding lengths between the atoms are further reduced. In this scenario, the initial single potential wells transform into an asymmetric double-well potential, and the energy barrier between them decreases due to the increased overlap of electron clouds. This allows electrons to transfer from one atom to the other, resulting in contact electrification i.e. triboelectrification [3].

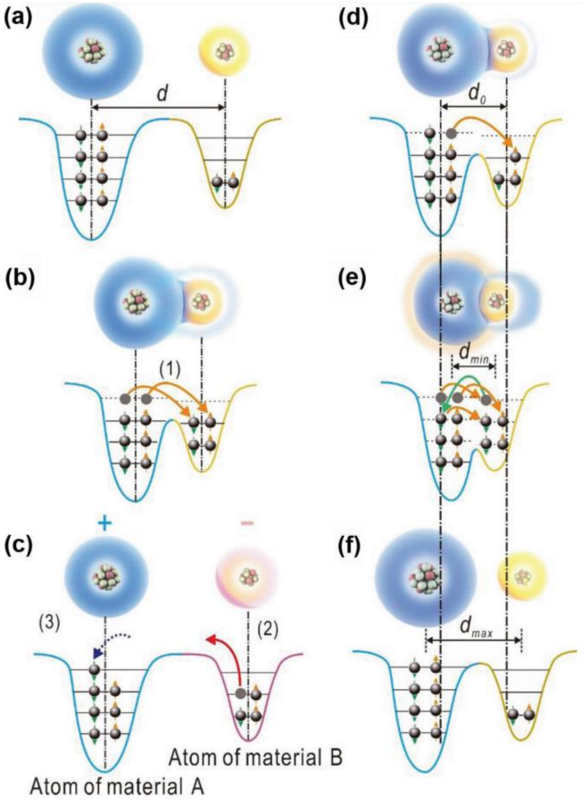

Figure 1.6 – *The General Electron-cloud-potential-well model for contact electrification. (a) prior to contact, (b) during contact, and (c) following contact for two atoms from dissimilar materials. The variable 'd' represents the distance between the electron clouds of the two atoms. (d)-(f) elucidate the same process however highlights impact of atomic thermal vibrations on charge transfer. (Adapted from reference [116]).*

The 'Electron-cloud-potential-well' model, also known as the interfacial potential barrier model, has undergone investigation by Ko et al. [5]. Their study employed a combination of experimental data and theoretical calculations to assess the validity of recent theoretical approaches, including the spatial charge redistribution model, the surface states model, the effective work function model, and the electron-cloud potential well model. This research culminated in the development of the 'Backflow-stuck charge model,', illustrated in Figure 1.7 which builds upon the concept that contacts generate a potential barrier drop at the interface. However, overcoming this barrier requires mechanical energy, and charges trapped within it, upon separation, lack the energy necessary for tunnelling back, resulting in the separation of charge.

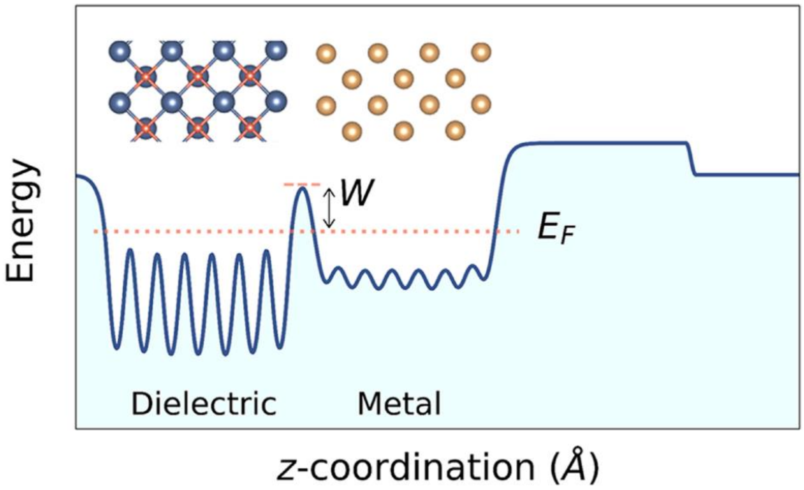

Figure 1.7 – *Schematic illustration of the previous interfacial potential barrier model of the Au-MgO interface distance, showing the average electrostatic potential along the z-axis. (Adapted from reference* [5] *)*

In summary, electron transfer stands as a fundamental mechanism in triboelectric charging, with applicability across various material types. The work function of a material emerges as a critical parameter in modeling triboelectric charge transfer, finding particular success in modeling charge transfer in metal-metal contacts. The challenge surrounding the application of work function to the modeling of charging in non-conductive materials revolves around the theoretical complexities of describing electron transfer in insulating materials and the experimental difficulties in obtaining accurate work function measurements for such materials. Nevertheless, it is feasible to view all environmental and physical factors affecting triboelectric charging through the prism of work function and electron transfer. For instance, this includes understanding the influence of surface contamination, humidity, and the dependency of work function on material stress and strain. Furthermore, numerous publications have reported scenarios where electron transfer is the primary mechanism for triboelectric charging. Examples include the relationship between thermionic emission and contact charging and the observation of charge transfer even at high temperatures and in vacuum conditions with materials lacking mobile ions. Recent theoretical advancements have also provided a framework through which the charging of insulating materials can be comprehended via the electron transfer mechanisms. In light of this, a compelling argument can be made regarding the paramount importance of electron transfer in the triboelectrification of various material types.

1.2.4 – The triboelectric series.

From the earliest days of triboelectrification research, it has been evident that the composition of the materials involved significantly influences the triboelectric charging mechanism. One of the earliest compilations of this phenomenon dates back to the 1700s, credited to John Carl Wilcke [61]. Since then, triboelectric series have become a fundamental aspect of this field. In contemporary research, Harper [15] has contributed significantly in his monograph titled 'Contact and Frictional Electrification,' where he delineates numerous series based on materials. The fundamental premise of a triboelectric series is that when a material is placed at the top of the series, it should charge either negatively or positively, depending on the series's orientation, in relation to all materials below it. Conversely, a material positioned further down the series would charge positively with all materials above it and negatively with all materials below it. Typically, researchers evaluate, and rank materials based on their capacity to donate or accept electrons through specific experimental techniques, thereby constructing a triboelectric series.

While many such series generally align, anomalies exist. For instance, non-polar materials like polyethylene and polytetrafluoroethylene consistently develop strong negative charges upon tribocharging, regardless of the material [121]. Due to the complex and poorly understood underlying mechanisms of triboelectrification, some series can be misleading, and inconsistencies exist in published works [122]. For example, in a recently published series, Zou et al. [30] introduced a novel method for quantifying charging propensity using liquid metal in a precisely controlled environment, claiming it as a new standard in the field (see Figure 1.8). This work contradicts several other published findings. It clearly indicates that substances like Nylon 6 and pig skin charge negatively. Yet, Kim et al. [123] reported that pig skin, Nylon 6, and most other organic lipid materials tend to charge positively. Additionally, it suggests that wood carries a measurable charge, while Özel et al. [124] argued that wood is largely 'immune' to tribocharging. Even identical materials can charge. A triboelectric series that ranks the charging properties of individual facets of common minerals in presented by Harper [15].

Interestingly, some triboelectric series deviate from the linear format, forming cyclical sequences of materials. Shaw and Jex [125] demonstrated that, when counted clockwise, the next material in such a series will charge positively relative to the first material. An example of an experimentally obtained cyclical series is presented in Figure 1.8. Several publications have reported these cyclic series[15,25,126,127], and it is suggested that their existence may be attributed to different charge media, charging modes, and electrification mechanisms. This phenomenon underscores the inherent complexity of triboelectric charging and the challenges in identifying the underlying mechanisms through these series.

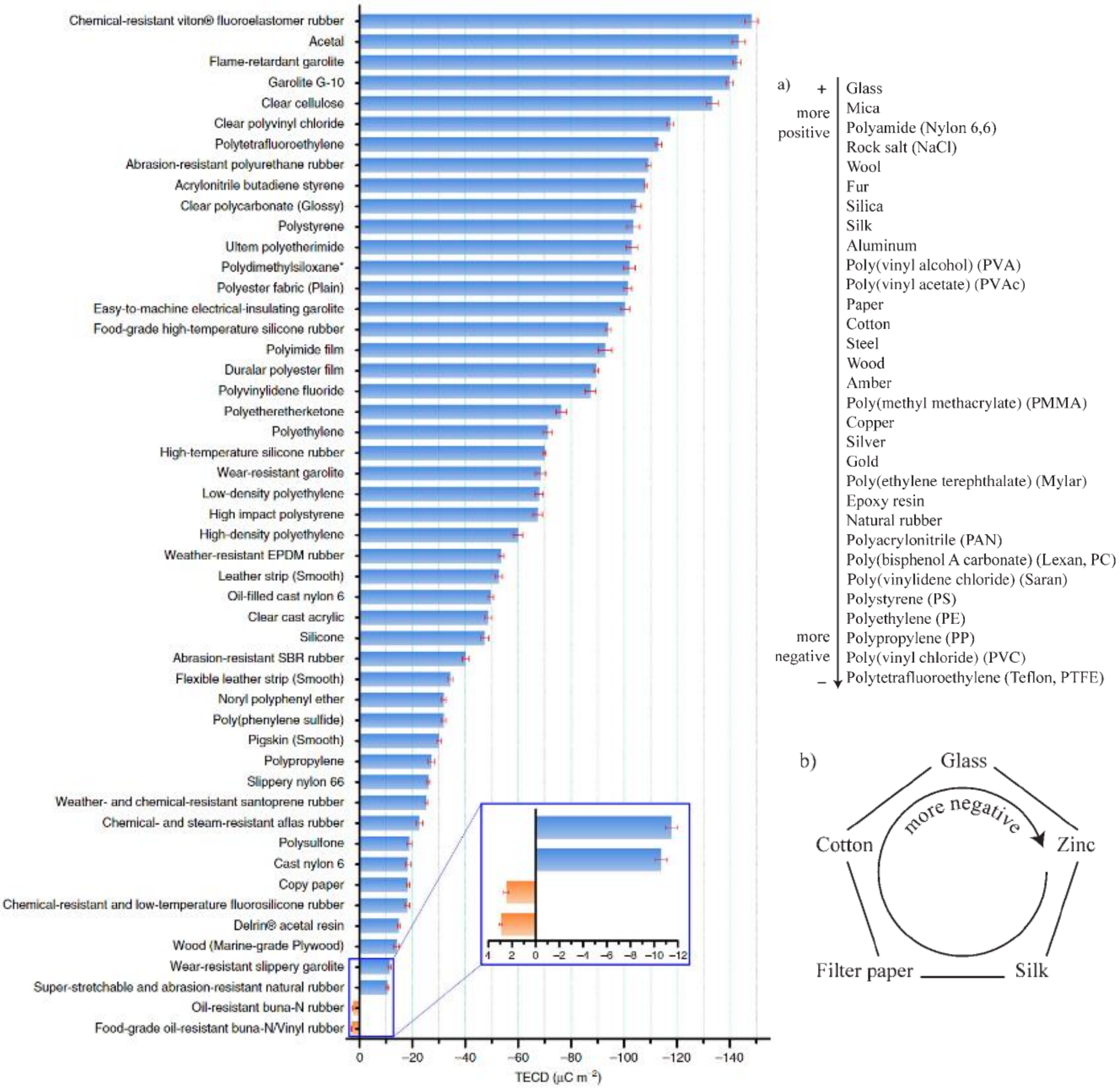

Figure 1.8 – *An example of a Triboelectric series presented by Zou el al.* [30]*. Obtained using a novel liquid-metal based method in a well-defined environment, which controls frictional effects and contact area. Hailed as the next "Textbook standard" for quantifying triboelectric charging (left). An example of a triboelectric series that combines several different series from literature* [25,122] *(top right). An example of a set of five materials which form a cyclic triboelectric series (bottom right)* [15,25].

Triboelectric series can exhibit dynamic characteristics, susceptible to alteration based on the system's conditions. In the research conducted by Liu et al. [128], a variety of elastomers were examined for their triboelectric properties under varying levels of strain and temperature. These conditions could induce shifts in the triboelectric series or even lead to a reversal in polarity, showing the importance of molecular spatial orientation to its electronic structure. The application of triboelectric series continues to evolve as researchers categorize the charging behaviours of increasingly exotic materials. Seol et al. [129] employed Kelvin probe microscopy to rank 2D layered materials for their suitability in triboelectric nanogenerators. In a highly innovative study by Yoo et al. [130], they compiled a liquid triboelectric series by submerging a PTFE sensing probe into various liquids and measuring the accumulated charge levels. This research highlights that common chemical groups tend to enhance the triboelectric effect in liquids.

In summary, triboelectric series play a valuable role in showing trends that contribute to a better understanding of triboelectric charging phenomena. However, due to the sensitivity of triboelectrification to environment and physical conditions, comparing series generated from different approaches and researchers may prove inconsistent and offer only limited insights.

1.3 – Material and Environmental factors that impact triboelectrification.

The impact of material and environmental conditions on triboelectrification are well known [2]. Several key variables have been identified as influential in triboelectrification, including surface conditions, particle size, processing parameters, and relative humidity [131]. More recently, emerging factors like light [132], external magnetic fields, and the evaporation of liquid films [133] have also demonstrated significant impacts on surface charges. Controlling all the factors that influence charging during experiments is an exceptionally challenging task, raising concerns about the reliability of conclusions drawn from comparing triboelectric series published by various researchers. While published works may differ on relatively minor details, such as the positioning of a material within the triboelectric series or its charging behaviour, it is evident that surface chemistry plays a substantial role in triboelectric charging, even in the presence of variations in experimental approaches [1]. Surface chemistry's significance is substantiated by numerous publications [37,113,134], although experimental results are frequently interpreted in accordance with the researcher's bias, whether leaning towards the ion [37] or electron [62] transfer mechanism. In this section, we will review various publications that explore the diverse environmental and physical factors influencing charging, aiming to illustrate the experimental challenges encountered by researchers.

1.3.1 – Surface chemistry

The charging of insulating materials is primarily regarded as a surface phenomenon because the prevailing models describing conductivity do not allow for the movement of charge from the surface to the bulk [15]. This suggests that proposed mechanisms involving electron transfer and ion adsorption are intricately linked to the interfacial physics and surface chemistry of the specific material in question. It is well-documented that when chemically distinct molecules come into contact and undergo rubbing, charge transfer occurs [15,67]. However it is also true that chemically identical materials can also experience triboelectrification. Particles, for instance, have been observed to charge based on their size [32]. Furthermore, experiments have indicated that particle-particle interactions might play a more substantial role in electrification than interactions between particles and surfaces [35].

Since insulating materials do not have free flowing delocalised electrons within their electronic bulk structure the transfer or charge carriers such as electrons or protons (ions) is limited to the surface of a material [15]. When studying the impact of surface properties on chargeability, it is important to keep the functional groups at the surface consistent, especially when dealing with powdered materials. This is commonly achieved through silanisation reactions or other surface modification techniques which are used to create a homogenous surface for testing [37,113,135]. In the research conducted by Byun et al. [113], KPFM experiments were conducted to investigate the charging behaviour of glass surfaces modified with various functional groups. Their findings underscored that the alteration of surface functional groups can have a significant impact on material chargeability, even when the monolayers are less than 1 nm thick. Surface condition also plays a significant role The application of dry powder coating has also been studied, in the work of Jallo and Dave [26], the nanocoating of micronized paracetamol has been shown to significantly influence charging behaviour.

In recent discussions regarding electron transfer mechanisms, various proposals have emerged to explain how electrons at the surface of insulating materials can transfer charge. However in the explanation of electron transfer given by Harper [15], the current models used to describe conductivity do not allow the movement of charge from the surface to the bulk. Hence, whether the mechanisms of charging involve ion transfer or electron transfer, they are intricately linked to the interfacial physics and surface chemistry of the specific material in question. Some publications focus on the transfer of ions between surfaces, suggesting the hydrophobicity is a key indicator [37,134]. Others focus more on the surface energy [136]. In some scenarios the ability to generate dipoles and their surface electronic states significantly impact charging [113]. In a recent paper by Mohanta et al. [137] the surfaces of coal and silica where functionalised, with the objective of modifying the work function of a material to alter its charging behaviour.

From the perspective of functional end-groups, isolating their impact on charging is difficult. A common method of achieving this is by silanisation glass beads or plates which applies a molecularly thin layer of functional end-groups to the surface [37,113,134,135]. However, there is a limitation studying triboelectricity in this way as it neglects how the supporting structure impacts the process. One of the main properties impacting surface charges is the dielectric constant of material which, to put it simply, treats the material in a region of charge as a local capacitor which stabilises the surface charge, preventing electrostatic discharge. An in depth description of this mechanism is given by Harper [15]. Materials with a large dielectric constant can stabilise large surface charges. In a regent paper by Burgo et al. [88] he places water at the top of the triboelectric serios as it leaves a positive charge on any material it is contacted with. This is attributed to water's extremely high dielectric constant. In some cases, the supporting structure can even supersede functional groups' impact on charging. When studying the triboelectric properties of organic lipids such as those found on tree leaves and animal skin Kim et al. [123] found that they all charged positively, even more than nylon 6. More interestingly he explored other synthetic lipids with different functional groups and found that functional group has little effect on the charging characteristics, which suggests that the supporting lipid structure was more important to the materials electron-donating ability.

It is well documented that the contact and rubbing of chemically distinct molecules causes charge transfer [15,67]. However, more perplexingly, chemically identical materials also undergo triboelectrification [33]. Particles have been shown to charge based on particle size [32]. Experiments have also been done which suggest that particle-particle interactions play a more significant role in electrification than the particle wall interactions [35].It is also argued that mechanical deformations act as a driving force for triboelectric charging [34,138,139]. This phenomenon is attributed to the generation of charged radicals in the form of mechano-ions resulting from stress and strain gradients, or to their influence on energy states, facilitating the transfer of charge. [33,34]. Additionally, in the event of deformation the lattice can become strained, resulting in an indentation or pull off at the surface On the atomistic level these strains manifest themselves in regions of high or low charge density as electrons are pushed together, which in turn can cause polarisation, causing a net charge to be generated on a surface [140], illustrated in Figure 1.9. This mechanism can contribute to understanding the perplexing effect of the tribocharging in identical materials [140], and the heterogeneous charging of insulators .

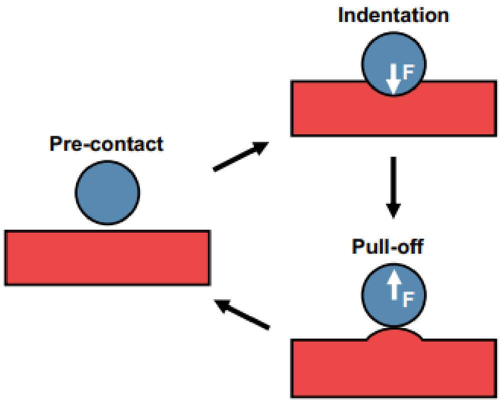

Figure 1.9 – *Schematic of asperity contact between a rigid sphere (blue) and an elastic body (red).During indentation and pull-off the elastic body will deform, developing a net strain gradient opposite to the direction of the applied force (reproduced from reference [34]).*

A recent review article by Kim et al. [141] focuses on the materials aspects of triboelectrification within the context of TENGs. In this work Kim describes the functional structure of a typical TENG device, it can be divided into four sections; the charge generation layer, the charge trapping layer, the charge collecting layer and the charge storage layer [141].

1.3.2 – Surfaces roughness

Surface roughness pertains to the nanoscale irregularities that may be present on a given surface, and the degree of roughness has long been associated with triboelectric charging. In the study conducted by Karner et al. [142], the impact of surface roughness on the charging behaviour of pharmaceutical materials relevant to dry powder formulations was investigated. Surface roughness was characterized using scanning electron microscopy (SEM). Rough powder exhibited higher charging, attributed to differences in contact mechanics. The relationship between roughness and charging is theoretically explained by Angus and Greber [143], who focused on the triboelectric charging of chemically identical materials. They reported that variations in local roughness result in differences in excited electron concentrations. These differences in electron concentrations are used to account for the formation of charging hotspots observed on a surface, akin to the surface mosaics documented in other studies [36,89].

Addressing the impact of surface roughness on contact electrification of surface water, Helseth [144] conducted experiments involving the measurement of the charge on a water droplet as it traversed a polymer surface. Interestingly, in contrast to some previous studies, it was discovered that water droplets picked up the largest tribo-charges from smooth surfaces. This observation was attributed to the reduced contact area for rough surfaces. Additionally, the capacitance of a surface plays a crucial role in the performance of Triboelectric Nanogenerator (TENG) devices. In the research conducted by Wen et al. [145], the role of surface roughness on capacitance, closely linked to the output of TENG devices, was thoroughly investigated. The study proposed a model that accounts for the impact of surface roughness on capacitance within TENG devices.

In the study conducted by Veners et al. [81], chemically identical polymer surfaces were meticulously prepared to investigate the impact of surface roughness. The findings revealed a noteworthy distinction: smooth surfaces exhibited a negative charge, whereas rough surfaces exhibited a positive charge. This difference was attributed to the easier bond-breaking process on rough surfaces. Similarly, in the research by Šutka et al. [146], focusing on polymer materials, it was observed that surface roughness could enhance the magnitude of charging. The most significant difference in charging magnitude was observed between surfaces with high and low roughness, attributed to the flexoelectric response. However, in a separate publication, Šutka et al. [147] also reported a notable shift in charging behaviour occurring at the glass transition of a polymer. This suggests that the impact of surface roughness may be somewhat "overrated" when compared to the influence of physical properties. The significance of the triboelectric charge mechanism in relation to surface roughness is that microscale asperities on the surface, resulting from roughness, create easily deformable regions. In addition, depending on the interpretation of the triboelectric charging mechanism, these regions can either provide mechano-ions or produce flexoelectric gradients required for charge transfer.

1.3.3 – Particle size

The triboelectric charging of identical materials has been observed in various natural and industrial contexts. In nature, this phenomenon is famously witnessed in the charging of volcanic ash plumes or the electrification of dust devils [148]. The occurrence of size-dependent charging poses particular challenges in the pharmaceutical industry, where blend heterogeneity can lead to significant regulatory issues [149]. In the study conducted by Sarkar et al. [150], changes in the properties of glass beads were investigated, revealing that tribocharging increased as particle size decreased. A similar effect was reported by Forward et al. [32], who studied the impact of bimodal particle size distributions on triboelectric charging. They used a novel particle fountain apparatus to isolate particle-particle interactions when agitating soda-lime glass. Various mass ratios of bimodal particle size distributions were tested, revealing that larger particles tended to acquire a more positive charge, while smaller particles tended to become more negatively charged. Similarly, Toth et al. [151] noted a size dependence in particle charging, where smaller particles tended to charge negatively and larger particles positively in low-humidity environments. However, it was reported that this dependence disappeared at higher humidities.

The dependence of particle size on triboelectric charging is interpreted in several ways. In a widely discussed topical review on the contact electrification of insulating materials, Lacks and Sankaran [152], likened this process to a probability game. They suggested that larger particles have a higher population of charge species trapped in different energy states, making identical material charging a consequence of the probability of impact. An alternative perspective posits that there is a curvature-induced change in the electronic structure, contributing to the asymmetry in charging [108,153]. The key takeaway is that surfaces do not necessarily have to consist of dissimilar materials to experience triboelectric charging.

1.3.4 – Humidity

Tribocharging is strongly influenced by the intrinsic properties of a material, however it is also very sensitive to the environmental conditions during charging. The notorious difficulty of obtaining repeatable results is often attributed to how difficult it is to keep conditions consistent across experiments [1]. Many publications record a reduction in charge intensity with humidity, some report a decrease followed by an increase [136], and others an initial increase followed by a decrease [86,132]. The presence of water undoubtably impacts contact electrification, however it remains difficult to quantify and precisely define its mechanisms in the general case [25].

The ion transfer mechanism is known to be one of the primary mechanisms in triboelectrification [15]. In the context of organic crystals, ionisable molecules are often found on functional end groups at the surface of the material. In the presence of environmental water, it is very common, if not ubiquitous, that a thin water film will form on the surface of the material. It is proposed that these films can become saturated with charged ions, and during contact form liquid bridges that allow for the moment of charge carriers between surfaces [25]. Alternatively, environmental water can react with co-called “mechano-radicals” caused by damage to surface creating mobile charge carriers [46].

In a published communication by Burgo et al. [88], water is said to exist near the top of the Triboelectric Series, as it charges positively when it comes into contact with any solid. This is rooted in its ability to donate either H^+or OH^- ions to other surfaces, charging them. Surface affinity for water molecule is therefore a governing factor in its chargeability [37,134,136]. In a paper by Biegaj et al. [134], glass beads were silanized to modify the surface functional end groups. It was found that the functionalised surface and the humidity significantly impacted charge transfer [134]. Following on from this, in an innovative study by Lee et al. [37], a single particle was suspended by acoustic levitation over a plate, and was then impacted onto the plate surface and the change in charge was characterised using an electric field passed through the particle. The particle and plate were made of boro-silicate glass and were subjected to different silanisation treatments to apply a hydrophobic and hydrophilic surface respectively. It was found that the largest charging effect was generated by contacting both hydrophobic and hydrophilic surfaces. This provides strong evidence that the charging seen in both insulating materials is due to the transfer of $\mathrm{H}^+$and OH^- ions.

It is also important to consider that adsorbed water at interfaces, can also significantly influence the electron transfer mechanism. In recent modeling work, first principles calculations have been used to study the charging behaviour of triboelectric nanogenerators, these studies highlight the importance of surface band structure when looking at charge transfer [53,54]. Earlier work by Zielinski et al [154]. showed experimentally that the presence of water on organic crystals alters its photoemission properties [154]. It has also be shown recently that there may be a mechanistic link between triboelectricity and photo emission [132]. From these studies it is implied that water could impact electron states at the interface. This relationship is explicitly studied from first principles by Fu et al [155], whereby he concludes that it is possible that electron states are impacted by the presence of water at the surface [155].

1.3.5 – Temperature

The influence of temperature on triboelectric charging has been well-documented by both Harper [15] and Lowell [67]. Previous research by Greason [24] emphasized the impact of temperature on metal spheres under varying environmental conditions, noting a reduction in the charge on the spheres with decreased temperature. Currently, a significant portion of research concerning the impact of temperature on triboelectric charging is conducted within the context of triboelectric nanogenerators. Lu et al.'s work [156] revealed a more complex temperature behaviour, as it observed a drop in charge transfer with increasing temperature. Lin et al. [157] conducted an in-depth study of the contact electrification mechanism for metal-insulator interactions. They reported that the temperature of a sample significantly affects both the magnitude and polarity of charging. Their findings align well with the thermionic emission model, with hotter materials becoming positively charged and colder materials becoming negatively charged.

In addition, Jantač et al. [8] examined the charging of polyethylene powder when in contact with an aluminium slide. They observed that polyethylene beads at higher temperatures reached a higher saturation charge compared to beads at lower temperatures. Similarly, Duesenberg et al. [158] reported a stronger charge at higher temperatures. The dependence of triboelectric charging on temperature can be interpreted in several ways. Regarding electron transfer, temperature might impact surface states, potentially making it easier for electrons to overcome a given energy barrier and return to the original material [5]. Tan et al. [159] provide a theoretical interpretation of how temperature affects triboelectric charging mechanisms in the context of the electron-cloud-potential well model. In terms of ion transfer, temperature could affect the formation and availability of ions at a surface [25]. Concerning material transfer, temperature might influence chain mobility at the surface of impacting polymers, thereby enhancing material nano-fracture at the surface [4].

1.3.6 – Light

In insulating materials triboelectric charges are restricted to their surface and there is a growing body of work which suggests that the electronic structure at the surface, the so-called "surface states" are responsible for the charge transfer with respect to electrons [54,113]. These surface states are sensitive to light as demonstrated experimentally by Zielinski et al [154]. Recently Lin et al. [118] attempted to apply first principles calculations and experiments to study the how light impacts triboelectric charging. He proposed that there is a threshold value for photo excitation which allows for charge to be transferred [118]. This interrelationship is further demonstrated in a recent paper by Liu et al. [132] concerning the development of photovoltaic methods for energy generation. Mechanical friction between a metal and semiconductor (analogous to silicon based solar cells) was found to significantly enhance the power output of the substrate when it was irradiated with laser light. This coupled tribo-photovoltaic method is able to generate significantly more electricity than standalone methods. While this effect has only been observed in metal-semiconductor junctions, excitation of surface electronic states and quantum tribo-tunnelling mechanisms has been shown to enhance charge transfer [132,160].

If the residual tribo-charges left on a surface are due to the electrons being trapped in these surface states, then it follows that triboelectric charges should interact strongly with light. Early work looking at how light interacts with surface charges was done by Yanagida et al [119], where charged pendant groups were characterised by photoemission. This work was built on by Hashimoto et al. [120] who observed a significant shift in the photoemission spectra of several contacting materials when charged. This phenomenon allows for a different interpretation of the relationship between charging and environmental humidity. Surface water has been shown to change the photoemission spectra in organic crystals [154] and humidity has been shown to significantly impact charging which is usually attributed to ions due to environmental water [25]. An alternative interpretation of this effect is that the presence of surface water effects the electronic structure of a material, creating surface states, which impacts contact electrification.

The relationship between light and charging has now been well established in literature and is being explored as a method to improve the performance of TENG devices and as a novel method to potentially simultaneously harvest ambient light and mechanical energy [132,160]. Interestingly UV light has been shown to both enhance [161,162] and reduce [118] surface charges. Working on the assumption that these electrons trapped in surface states are the primary charged species in contact electrification, can it be proven that it is possible to use UV-light to dissipate the trapped charges on pharmaceutically relevant powders? In this work we attempt to show that UV-light can be employed as a technique to mitigate charging in commercial powder processing.

1.3.6 – Other factors.

External electric fields are ubiquitous and will be present to some degree at anywhere on the Earth's surface. These fields are useful when performing electrostatic separations [17] or indirectly measuring charge using capacitance probes [135], however a recent study by Heinert et al. [133], suggests that external electric fields can significantly alter charging. They have found that the evaporation of methanol, ethanol and distilled water produced a strong charge on an insulated substrate when evaporated in an electric field, managing to artificially induce an electrostatic discharge. This effect was not observed in the absence of the field. The tests were repeated in several locations and found significant variance between locations, which is suspected to be due to differences in ambient electric field [133].

1.4 – Measurement techniques and the triboelectric series.

To quantify contact electrification several experimental techniques have been established. One of the most frequently used methods of characterising the charging of particulate materials directly is the Faraday pail/cup, where material is discharged into a conductive container, and the charge measured by an electrometer [131]. The assembly is placed inside another conductive container which is earthed. This approach is appropriate for measuring the bulk net charge on granular materials. Another popular technique is the Kelvin Probe Force Microscope (KPFM) [49,113,118,121,123,137,163,164], analogous to Atomic Force Microscopy (AFM). It uses a conductive probe tip with a known work function to measure the contact potential difference (CPD) between the surface and tip. This is more useful for investigating flat surfaces. Zou et al. [30] published a novel method of characterising charging tendency using liquid metal in contact with a material, touching with a consistent contact area, ostensibly giving the most accurate representation of a material's triboelectric properties. Since their development, Triboelectric Nanogenerators (TENG) have also become a popular technique used to study contact electrification [54,62,123,141,165,166]. This method allows for greater control of environmental conditions; however, this research area is focused on enhancing triboelectric power output rather than reducing it. Alternatively, the charge on particles can also be measured indirectly by observing the effect a charge particle has on an external electric field [37,135]. This method should be approached with caution as an external field has been shown to significantly impact charge transfer [121,133] .

1.4.1 – Faraday pail

The Faraday pail is a simple yet effective method for characterizing the net charge of a given powder. This design comprises an isolated cup grounded through an electrometer. When charged material is introduced into the pail, it induces a charge on the metal cup through electrostatic induction. This effect is then detected by the electrometer, enabling quantification of the charge on the material [2]. Murtomaa et al. [167] employed the Faraday pail to investigate the effects of different inhaler types, humidity, and the amorphicity of lactose on charging behaviour. One major advantage of the Faraday pail is its capability to measure the overall net charge of material mixtures. For example, in the study by Engers et al. [168], they comprehensively examined the behaviour of common pharmaceutical mixtures and identified correlations with humidity and dielectric properties. More recently, Zhang et al. [169] utilized a Faraday pail apparatus in combination with Kelvin Probe Force Microscopy (KPFM) to explore the impact of metal deposition on the charging behaviour of polymeric beads. This correlation between the charging behaviour of a material and its redox behaviour at the surface provides evidence for surface mosaic mechanisms. Ultimately, the Faraday pail is a robust method for determining the net charge of a distribution of particulate material. However, its primary limitation is that it can only measure the net charge of a dispersion and cannot provide information about potential charge distribution in terms of magnitude or polarity.

1.4.2 – Force microscopy approaches

Force microscopy techniques have become commonplace in the study of surface imaging, detection of surface charges and determination of the electronic structure of surfaces. One of the most fundamental of these techniques is Atomic Force Microscopy (AFM), which is widely used for mapping the topology of surfaces. AFM employs a small probe attached to a cantilever tip. When the tip is brought close to a surface, it experiences detectable forces due to their interactions. These signals are then translated into a high-resolution map of the surface. Kelvin Probe Force Microscopy (KPFM) is an analogous technique that utilizes a similar cantilever-probe setup, with the distinction that the probe tip is conductive. KPFM serves as a standard method for characterizing the surface potential and contact potential difference of materials. It achieves this by making contact with a material and applying a DC bias to the probe tip to compensate for electrostatic forces, thereby allowing the measurement of the Contact Potential Difference (CPD) of a material. An offshoot of KPFM is Electrostatic Force Microscopy (EFM), which directly images electrostatic forces without the use of a DC bias. For a comprehensive review of the KPFM technique, Melitz et al. [163] provide valuable insights, while a more comprehensive account of these methods can be found in the work of Sadewasser and Glatzel [170].

One of the pioneering precursors to modern-day Kelvin Probe Force Microscopy (KPFM) and Electrostatic Force Microscopy (EFM) was introduced by Nonnenmacher et al. [171]. This method was initially designed for characterizing material work function, absorption layers, oxide layers, and dopant concentration in semiconductors. Years later, Cunningham [172] expanded upon this work and applied it directly to the study of contact charging and triboelectrification. Cunningham's research delved into the investigation of point charges applied to conductive and insulating materials. Notably, this work was among the first to report that different polarity charges could be induced on different surfaces by altering the voltage bias of the contacting tip. An early example of using EFM to examine localized surface charges and electrostatic dissipation mechanisms was conducted by Morita and Sugawara [173]. Their work underscored the utility of EFM in exploring these fundamental processes at an "electron-by-electron and ion-by-ion basis," in future applications.

In the past 15 years, the utilization of KPFM/EFM techniques has witnessed significant advancements. A comprehensive article by Knorr and Vinzelberg [174] provides insights into the practical aspects of employing force microscopy techniques for measuring surface charges. In this article, they also introduce a combined AFM-KPFM method, where triboelectric surface charges are induced by agitating a surface using AFM and subsequently detected using KPFM. An exemplary demonstration of this process, involving charge "writing" by AFM and charge detection by KPFM, has been conducted by Palleau et al. [175]. Within the context of triboelectric charging, this approach has also found applications in the study of granular materials. Mirkowska et al. [63] employed this combined AFM/KPFM approach to investigate the charging properties of a large calcite crystal. Their research highlighted the influence of tapping versus rubbing and tip bias voltage on charging behaviour.

Some studies have looked into the influence of surface functional groups on triboelectrification. Byun et al. [113] utilized Kelvin Probe Force Microscopy (KPFM) to investigate the surface potential and contact potential difference of various glass SiO_2 surfaces that underwent chemical modifications to introduce different surface functional groups. This approach allowed them to isolate the contribution of individual surface groups. Similar research was conducted by Mohanta et al. [137] where they chemically modified the surfaces of coal and quartz to control their charging properties through the introduction of surface groups. They also employed KPFM to characterize the change in surface work function resulting from these surface modifications.

Yin et al. [164] conducted an extensive study on the charging mechanism of conductive and insulating fibres using Kelvin Probe Force Microscopy (KPFM), providing compelling evidence in favour of the ion transfer mechanism [164]. In their subsequent work, they further emphasized the inherent complexity of studying insulating polyester fibres using KPFM [176]. While this research primarily focuses on the investigation of insulating fibres, it addresses the primary limitations encountered when utilizing KPFM to study surface charges. Additionally, it presents a methodology for processing and interpreting results. By assuming that the surface can be approximated as a capacitor, the surface charge density can be estimated using a capacitor equation [173,174].

In other studies, Kelvin Probe Force Microscopy (KPFM) has served to complement Density Functional Theory calculations in exploring water-induced bipolar charging [49]. Furthermore, in an effort to quantify the charge tolerance of powder systems, Seidel et al. [177] employed a KPFM/EFM-based approach to investigate the relative permittivity of individual starch granules. This research revealed a correlation between relative humidity and the permittivity of the sample. In the work conducted by Gan et al. [97], KPFM was utilized to measure the work function of a pure insulating mineral, simulating the charging properties in non-earth environments.

In some of the most recent published works, Kelvin Probe Force Microscopy (KPFM) has been employed to probe the underlying mechanisms of charge transfer. For instance, Lin et al. [121], while investigating the so-called 'electron-cloud overlap model,' applied the KPFM technique to explore the distance at which charge transfer occurs between the tip and the sample. Their findings indicated that charge transfer occurred only when the tip was in the repulsive regime, thereby supporting Lin's hypothesis. In another recent study, Jin et al. [178] utilized KPFM as the primary experimental technique in the design of anti-static surfaces.

In conclusion, KPFM has become indispensable in the study of surface electronic states and charge transfer mechanisms. Notably, the combined AFM-KPFM approach demonstrated by Mirkowska et al. [63] proves to be highly suitable for investigating the charging properties of large pharmaceutical crystals.

1.4.3 – Photoemission.

Ultraviolet photoemission spectroscopy (UPS) provides valuable insights into the electron states near the Fermi level of a material, which are considered to be the primary electron states involved in triboelectric charging [120]. As previously mentioned, the electron transfer mechanism hinges on the movement of electrons between energy levels situated on, or just beneath, a material's surface. The presence of these transient surface states presents a compelling opportunity for experimentation, as theoretically, an electron excited by triboelectrification should manifest shifts in its photoemission spectra.

Pioneering work in this area was conducted by Zielinski et al. [154]. They examined the photoemission of adenine crystals in the presence of water using the Millikan-Pope-Arnold photoemission technique under pure nitrogen conditions. The findings revealed that crystals exposed to humid air displayed a shift in their photoemission spectra, with the presence of a water film lowering their ionization potential. Building upon this research, Yanagida et al. [119] employed photoemission techniques to directly characterize the electronic properties of various pendant group polymers. The results of this experiment were interpreted using the molecular-ion model proposed by Duke et al. [179]. It was discovered that there exists a correlation between the polymer's work function and the duration of material drying. Additionally, it was observed that the low-energy photoemission of polymers closely aligned with their work function energy, a phenomenon not observed in semiconductors. Evidently, the threshold energy aligns with a material's Fermi level, and the photoemission of polymers is closely linked to their charging tendencies [119].

More recently, the behavior of electrons at metal-polymer contacts was thoroughly investigated by Hashimoto [120]. In this study, polyethylene terephthalate (PET) films were brought into contact with aluminium, titanium, and copper oxide (CuO). After the charging process, their photoemission spectra were meticulously examined, with integration across this spectrum providing the density of states (DOS). The findings revealed that materials prone to strong charging, such as Al-PET, exhibited the most significant DOS shift, while CuO-PET displayed a smaller DOS shift and experienced the least amount of charging. Furthermore, a variety of functional groups were introduced to the polymer surface and subjected to testing. It was also observed that the addition of these functional groups induced noticeable shifts in the photoemission spectra of the functionalized polymers.

From this research, it becomes evident that photoemission is useful in probing the surface states of materials. In the context of triboelectrification, it sheds light on how surface electronic states are influenced by a material's chemical structure and the specific types of materials it comes into contact with. Moreover, it underscores the significant impact of water films on charging, which aligns with an electron transfer perspective on how humidity affects charge transfer [25].

1.4.4 – Triboelectric nano generators (TENG).

Triboelectric nanogenerators (TENGs) represent a ground-breaking development in the field of triboelectrification, as they utilize the triboelectric effect to generate practical electrical energy. These devices are characterized by a core design consisting of two thin insulating layers, typically made of polymeric materials, stacked on a metal substrate. When these insulating layers come into contact, they accumulate charges, which then flow into the underlying metal layer, creating a potential difference between the sheets and thereby generating electricity. The pioneering work in the field of TENG devices was conducted by Fan et al. [51], part of the research group led by Zhong Lin Wang [3], and introduced the concept of the "flexible triboelectric nanogenerator." Due to their simplicity and adaptability in design, these devices hold great promise for applications in ambient energy harvesting and powering microdevices. Given the increasing concern about climate change, the prospect of a new method for generating clean energy has generated significant excitement and has spurred extensive research efforts aimed at understanding TENG device performance and enhancing their design.

Triboelectric Nanogenerator (TENG) research has gained considerable attention and has been extensively reviewed [3,141,165]. TENG devices are incredibly versatile and find applications in four main categories. First, they serve as micro/nano energy sources, harvesting power from ambient energy sources like human motion [180] or machine vibrations [181]. This harvested energy powers various devices, including wearable self-chargers [180], self-powered watches [182], and medical equipment [183]. Second, TENGs play a pivotal role in self-powered sensors, responding to stimuli like touch [184], acoustics [185], or accelerations[186], making them valuable for passive chemical sensing [187]. Third, TENG technology enhances the power generation capabilities of established renewable energy sources such as wind [188] and wave energy [189], while also tapping into less common sources like rainfall [190]. Finally, TENGs are capable of producing exceptionally high voltages, making them suitable as portable and safe high-voltage power sources. These devices find applications in air purification within advanced face masks [191] and micro-plasma generation [192]. The versatility and potential of TENGs have led to a surge in research efforts, offering promising solutions for energy harvesting and a wide range of applications.

The vast array of potential applications for triboelectric charging has sparked substantial interest in the field, driving a surge of research into its fundamental mechanisms. This research has significantly advanced our understanding of the underlying processes governing triboelectric charging. The innovative aspect of TENG devices in the study of triboelectric charging lies in their capacity to facilitate highly controlled experiments. They offer the capability to systematically manipulate variables such as materials, temperature, environment, and contact pressure, making it straightforward to decouple these factors and analyse their individual influences on the overall triboelectric charging process.

A comprehensive exploration of the applications of TENG devices and their contributions to advancing the understanding of electron transfer mechanisms can be found in the work of Xu et al. [62]. Likewise, Šutka et al. [4] have provided an excellent and up-to-date review that delves into how TENG devices have enhanced our understanding of the material transfer mechanism.

1.5 – Computational methods simulations for Modeling Triboelectrification

Numerous methodologies have been devised to simulate the transfer of triboelectric charge and its impact on bulk powder systems [2]. The modeling of bulk powder behaviour typically entails the use of computational fluid dynamics (CFD) and discrete element method (DEM) simulations. However, these approaches have certain limitations in that they do not directly model charge transfer but instead rely on approximations derived from empirical data [38]. These meso-scale approaches have a limited capacity for studying the mechanisms of triboelectric charging since the governing mechanisms of triboelectric charging involve material, ion, and electron transfer, all of which operate at the molecular length scale. Therefore, a molecular modeling (MM) approach is essential to gain deeper insights into the mechanisms of triboelectric charging.

Molecular modeling is employed to investigate the fundamental nature of matter at the smallest length scales, representing materials as discrete particles such as molecules, atoms, and electrons. This approach has found applications in a wide array of systems, spanning from studies of chemical reactions and solid-state chemistry [1,193] to simulating the behaviours of planetary cores [194], and more recently, examining charge transfer phenomena from first principles [50]. In the early 2000s, many molecular modeling methods demanded significant computing power and yielded results of uncertain validity. However, the increased availability of computing resources and the maturation of these techniques have substantially enhanced the quality and accuracy of the outcomes generated [43,195].

This section offers an overview of the current molecular modeling practices and presents a review of recent publications that have applied molecular modeling techniques to investigate molecular crystals, surface processes, and charge transfer phenomena.

1.5.1 – Force field approaches

Despite significant strides in computing power, quantum mechanical calculations remain highly computationally demanding. In practice, quantum mechanical approaches are constrained to simulating systems containing approximately 1000 atoms [196,197]. This limitation imposes restrictions on the scale of systems that can be effectively simulated. To address this challenge, simplified 'force field' methods have been devised to alleviate the computational load of molecular modeling simulations. In this context, a force field encompasses the cumulative effects of all electrostatic and Van der Waals forces acting on a molecule or atom [197]. The use of force fields eliminates the need for frequent calculations of electronic states during simulations, substantially streamlining the complexity of the computations. Some force fields are in fact derived from first-principles calculations [198] However, this simplification comes at the cost of modeling chemical reactions or processes involving the formation or breaking of hydrogen bonds, effectively confining calculations to conformational searches [196].

Often, combined quantum mechanical and force field approaches are employed to reduce computational costs. In recent work by Zheng et al. [199], MD-generated interface morphologies were created using the GROMACS simulation package, followed by the use of high-precision DFT methods to study the quantum mechanical effects at the interface. Similarly, Fujita et al. [187] employed force field-based approaches to model atomistic structures, with subsequent use of DFT to analyse electronic behaviour at the interfaces [200]. It is evident that combining modeling approaches, such as applying the MM approach to optimize geometry followed by the required electronic structure calculations, can result in significant savings in computational resources.

1.5.2 – *Ab initio* modeling at surfaces

The first principles modeling of surfaces is of great importance to several fields. Surface interactions have a direct impact on the bulk properties of powder systems, affecting their processability [38]. Moreover, comprehending electronic properties such as photoexcitation is vital for the design of the next generation of photovoltaic materials [201], while studying surface states at interfaces is relevant to triboelectric energy devices [51]. From a modeling perspective, *ab initio* techniques offer a means to investigate these processes through first-principles calculations.

A growing body of modeling work suggests that *ab initio* methods can be effectively applied to study the underlying mechanisms of triboelectric charging from first principles. For instance, in a recent study by Le and Cheng [202], first-principles methods were employed to investigate how atmospheric water is adsorbed at electrochemical interfaces, revealing the presence of a permanent absorbed layer of water on pristine platinum surfaces. Some promising results have also been achieved in exploring the electronic properties of hybrid organic-inorganic interfaces. Schöttner et al. [192], for example, successfully modeled electron transfer at an organic/oxide interface using density functional theory (DFT) methods, demonstrating very good agreement with experimental observations [203]. Although these studies are in a different context, they highlight that quantum behavior at interfaces can be effectively studied and potentially applied to investigate the fundamental mechanisms of triboelectric charging.

In recent years, organic and inorganic semiconducting materials have become a focal point of intensive research. These materials find applications in various fields, including light-emitting diodes and photovoltaic cells, owing to their unique electronic structure and excitation properties [199–201,203,204]. Additionally, their complementary characteristics make them suitable for emerging technologies like thermoelectric materials [205] and spintronic devices [206]. Understanding their quantum behaviour at relevant interfaces is crucial for the rational design of these devices. While research into organic electronics may appear distant from the study of the triboelectric properties of pharmaceutical powders, they intersect at a crucial junction: understanding quantum interactions and charge transfer behavior at interfaces through first-principles calculations. A long-suspected link between photoemission, electron states, and charge transfer has been proposed. In an earlier study by Zielinski et al. [154], the presence of water on the surface of aniline microcrystals was found to alter the ionization energy at the surface [154]. A more recent experimental demonstration of this link can be found in a paper by Liu et al. [132], where the connection between electron excitation and triboelectric charge transfer is shown through a novel photo-tribo-co-harvesting technique. The study revealed that simultaneous triboelectric and photovoltaic energy co-harvesting significantly increased the power output of both phenomena, suggesting that incident light-induced excitations facilitate triboelectric charge transfer and vice versa [132].

The current first-principles approach to understanding charge transfer mechanisms at organic-organic and organic-inorganic interfaces involves the hybridization of electron states at the contacting interfaces. This hybridization occurs when the wave functions of the electrons overlap, effectively creating a new system at the interface. Furthermore, the number of free charge carriers also plays a crucial role in determining the charge transfer mechanism at the substrate. This can lead to either integer charge transfer, where a charge is localized on a molecule, or fractional charge transfer, where the charge is delocalized within the organic layer [201,204]. A comprehensive explanation of phenomena like hybridization can be found in existing literature [207]. Recent research papers demonstrate the capabilities of first-principles methods in modeling electronic structure properties of organic materials.

Through their research on the application of a monolayer on a zinc oxide substrate, Gruenewald et al. [204] experimentally demonstrated the formation of new electron states at the hybrid interfaces of contacting organic semiconducting materials. Additionally, they employed DFT methods to investigate dielectric properties, work function, and density of states, thereby analyzing the electronic properties of the system. These results provided strong evidence for charge transfer occurring due to the existence of hybrid interface states. In a recent study, Erker and Hofmann [201] utilized an advanced hybrid DFT approach to model the impact of surface doping on the band structure of a ZnO substrate. Their model successfully captured the phenomenon of "Band Bending" at the interface. Interestingly, they found that despite being a strong electron acceptor, the doped monolayer acquired a positive charge when absorbed onto the ZnO substrate, leading to a reduction in the surface work function. Their conclusion emphasized that the hybridization of electron states determines the charge transfer mechanism, with the number of free charge carriers playing a significant role in the amount of charge transferred [201].

Organic-organic interfaces are frequently encountered in the context of organic heterojunctions within cost-effective, large-area photovoltaic cells [199,200]. These studies are particularly intriguing because the electronic behavior at ordered organic heterojunctions bears modeling similarities to interactions at crystalline surfaces when two materials make contact. Fujita et al. [200] employed a combined approach involving force fields and DFT to investigate charge photogeneration at organic interfaces. Their research unveiled that interfacial morphology plays a crucial role in shaping interfacial charge transfer states, and the hybridization of excited states promotes long-range photoinduced charge transfer. Exploring further, Zheng et al. [199] delved into the influence of structural disorder and energy distribution on the electronic properties of organic surfaces using DFT methods. Their findings suggest a clear connection between the energy distribution of charge transfer states and the charge transport properties of the material. Furthermore, they established a correlation between surface functional groups and the charge transfer efficiency within organic solar cell systems.

1.5.3 – Density functional theory modeling of triboelectric charging

The computational methods used to theoretically model charge transfer have evolved significantly since researchers started applying these techniques in the mid-1970s. The first techniques to be used were the so-called molecular orbital methods which are semi-empirical methods that requires experimental input. These methods do not consider surface or interface structures however they are significantly less computationally expensive than semi-empirical methods. Two notable examples of applying this method to triboelectric charging are the work of Tanaka et al.[208] who used semi-empirical methods to correlated the energy of the frontier orbitals with contact potential difference. Similarly, Yanagida et al.[119] compared theoretically calculated HOMO and LUMO levels with the threshold of photoemission for several polymers, concluding that chemical structure influences the low energy states thought to be responsible for electron transfer in triboelectric charging.

Over time, researchers sought to transcend the limitations imposed by semi-empirical techniques i.e., the requirement of experimental inputs, and began using the more computationally expensive first-principles approaches such as the so called Hartree-Fock-Slater or Xα method which one of the first DFT-based schemes used to study systems with more than one atom [209]. In the work of Yoshida et al.[210] the Xα method is used to calculate more sophisticated electronics structure properties such as charge density difference and full density of states plots to investigate the impact and frictional charge characteristics of polymers. This approach was also used by Shirakawa et al.[211] who directly model the charge transfer between a metals and polymer surfaces, concluding that electron transfer is determined by the relationship between Fermi level of metals and the surface states and conduction band of PTFE.

Xα methods are considered as an important stepping-stone towards the development of modern DFT, which has now become the standard approach for materials modeling. From the year 2003 literature began to be published that used modern DFT-based approaches to calculate electronic structure within the context of charge transfer at interfaces. The theoretical framework of DFT will be discussed in detail in the next chapter. In some of the more recent papers the interface barrier is described as the direct characteristic parameter to determine the amount of charge transfer rather than effective work function[212],

Several published works have attempted to apply *ab initio* techniques directly to triboelectric charging. Earlier work by Yanagida et al. [119] performed modified neglect of diatomic orbital calculations to investigate the charge transfer in polymer metal-contacts, finding they correlate with experimental photoemission results. However this approach is criticised by Yoshida et al. [210] for restrictions in the type of material it is applicable to, and for requiring empirical input data. In polymeric materials the presence of dangling bonds are thought to contribute to charging, This phenomenon has been investigated using quantum calculations, using the DV-Xα Method, by Yoshida et al. [210] and then later by Shirakawa et al. [211]. More recently in a paper by Gil and Lacks [46], they describe a process where mechanical action creates “mechano-radicals” on the surface of polymetric materials, which react in the presence of water to form mobile charge carriers [46].

Simulations have also been used to complement experimental results, such as in the work by Mohanta et al. where DFT has been used to validate the change in work function of insulating materials during an investigation into the effect of the surface functionalisation of coal and quartz on its chargeability [137]. A recent study by Shen et al. [50], claims to be the first ever first-principles calculation of contact electrification, with validation, where the polarity of charging for a sapphire-quartz contact was predicted successfully using DFT. Arguing that charge redistributes due to the formation of new electron states at contact, during separation the electrons become trapped in these new states leaving residual charge, which is conceptually similar to the formation of new charge transfer state described by Gruenewald et al. [204] and Erker and Hofmann [17]. However, the study was limited in that arbitrary assumptions about the cut off point for electron backflow and the method failed to correctly predict the polarity in other systems [50].

Increasing prevalence of microelectronic devices has led to a new and innovated technology in Triboelectric Nanogenerators (TENG). It is hoped that these devices will eventually power the next generation of micro-electronics and self-powered switches [51]. However, the limited understanding of the underlying mechanisms of triboelectrification has made the conscious design of these devices difficult. As a result, several papers have been published attempting to simulate the charge transfer process with the objective of improving TENG performance [53,54]. In a study by Wu et al [53]. He presents evidence that the stress of mechanical contacts significantly impacts charge transfer, challenging the assumption that the work function is the main driving force of charge transfer. In a further study, Wu et al. [54] compared the contact charging of different functional groups, and has shown different functional group have different electron properties. In both these studies they state that control of the lowest unoccupied molecular orbital (LUMO) in the surface band structure is key to realising the design of TENGs [53,54].

In a very recent published work by Willatzen, et al. [213] he attempts to present a unified quantum mechanical model of contact electrification for fluids and solids, focusing on metal-metal, metal-insulator and insulator contacts. This work attempts to address two perplexing features of triboelectric charging, the contact charging of identical materials (size dependency) [214] and the occurrence of surface charge mosaics on contact [36]. In this 1-dimensional model Willatzen et al. [213] argues that the contact electrification of any system can be modelled by the selection of appropriate “hopping parameters”, dielectric constant and electron population on any site. This presentation of the approach neglects the band structure model, and ion transfer. However, it provides a basis for Volta-Helmholtz-Montgomery hypothesis (contact electrification due to quantum tunnelling and band structure) to be applied [213,215].

1.6 – Concluding remarks.

A comprehensive understanding of the mechanisms governing triboelectric charging has remained elusive, despite its significant contribution to the field of electricity. This complexity arises from the sensitivity of triboelectric charging to various environmental and physical factors. As highlighted in this chapter, researchers often propose multiple interpretations of experimental results, viewing them through the lenses of material, ion, or electron transfer, further complicating the issue. The advent of Triboelectric Nanogenerator (TENG) devices has paved the way for new avenues of experimentation, contributing to a growing consensus that electron transfer is the dominant mechanism underlying triboelectric charging [3], although some opposition still exists among researchers [4].

In recent years, Atomic Force Microscopy and Kelvin Probe Force Microscopy (AFM/KPFM) have emerged as powerful tools for investigating the triboelectric charging mechanism [216]. These techniques have provided experimental evidence supporting the "Electron-cloud-potential-well" model [121], which addresses the long-standing challenge of charge transfer in insulators. With the acceptance of the electron transfer mechanism, there has been a surge in research applying first principles modeling techniques to study triboelectric charging. These efforts contribute to realisation of the long-sought predictive model for charge transfer.

Computational modeling, particularly through first principles methods like Density Functional Theory (DFT), offers valuable insights into the underlying mechanisms of triboelectric charging. It provides precise control over system parameters, surpassing the limitations of experiments. This precision is crucial for enhancing our understanding of triboelectric charging, given its sensitivity to various factors. This work aims to explore fundamental aspects of triboelectric charging using first principles modeling. It delves into systems that are challenging to observe at the molecular level, shedding light on the roles of contamination, variations in surface work function, and the charging behaviour of individual molecules in triboelectric phenomena.

Chapter 2 – Density functional theory

Computational modeling has great utility; it can complement experimental work and enhance the understanding of the system being studied and predict the behaviour of systems without the need for expensive experiments. It can inspire new experiments with its results and can be used to model systems either too small or too extreme to be studied experimentally. Density functional theory has become the default approach for electronic structure calculations. It is often called a "first principles" or "*ab initio*" approach since theoretically it does not require any empirical input and is instead built on the fundamental quantum mechanical equations that describe the fundamental interactions in a material. There is tremendous scope for density functional theory calculations to improve the understanding of triboelectric charging as it allows the systems under study to be precisely defined removing uncertainties caused by environmental conditions or limitations in experimental approach. Furthermore, it can model length scales that are unreachable using currently available experimental techniques. This section will give a high-level overview of density functional theory and cover the key concepts of the approach.

2.1 – Quantum mechanical approaches

As mentioned previously, electron transfer is one of the primary proposed mechanisms for triboelectric charging. It would be impossible to model this process without considering the behaviour of individual electrons. First-principles (or *ab initio*) modeling at the atomic scale inevitably involves quantum mechanical (QM) calculations, which are categorised into either wavefunction-based or density-based methods, a description of these models is given by Brazdova et al [197] and Jensen [196]. The equations used to model quantum systems are notoriously complex, for example the Schrödinger equation can only be solved analytically for very simple systems; anything larger than a helium atom requires a numerical approximation [196]. A detailed account of the fundamental models, computational techniques as well as simulation methodologies are readily available in published literature [196,197].

Currently the two main established methods of numerical electronic structure calculations are Hartree-Fock (HF) and Density Functional Theory (DFT), both methods treat electrons as separate entities, unlike force field approaches (which are covered in the following section). A recent review into both these methods is given by Lehtola [217]. In the late 90s the application of electronic structure methods was limited, they required significant computational resource and produced results of questionable validity. However thanks to advances in computational power in the new millennium these methods have been more prominent and have emerged as one of the cornerstones of computational physics, chemistry and materials science [43,195,217].

DFT is now the workhorse of electronic structure calculations [43,197], however it can be unreliable when modeling transition metals, Van der Waals and dispersion interactions, and materials such as Mott insulators. DFT methods are remarkably good at calculating the band structures of materials, however struggle to accurately predict band gaps [197]. Another known limitation of DFT is the tendency of electrons to interact with themselves in calculations, the so-called many electrons self-interaction error (MSIE) which can lead to a tendency of charge "overdelocalisation" for common and semi local functionals, whereas limitations in HF methods can lead to overlocalisation of charge [218]. These limitations have led to the development of hybrid DFT functionals which use a Hartree-Fock-like exchange and generally perform better in terms of charge transfer, which have been used to study charge transfer behaviour in organic semiconductors [201].

2.2 – The Schrödinger Equation

The basis of first principles calculations is the Schrödinger equation which is very often simply expressed as,

$$H\psi = E\psi \qquad \text{Eq. 2.1 } [219]$$

which describes the general form of time independent, nonrelativistic equation, where E is defined as the ground state energy of a system, H is the Hamiltonian operator and ψ is a set of eigenstates of the Hamiltonian. The definition of the Hamiltonian depends on the system being studied, for simple systems such as a single particle in a 1-dimensional box, the Hamiltonian is simple and the Schrödinger equation can be solved exactly. For more complex systems where multiple electrons are interacting with multiple nuclei the Schrödinger equation is described as,

$$\left[\underbrace{\frac{\hbar^2}{2m}\sum_{i=1}^{N}\nabla_i^2}_{\text{Kinetic energy of each electron}} + \underbrace{\sum_{i=1}^{N}V(r_i)}_{\text{Interaction energy between the electron and nuclei}} + \underbrace{\sum_{i=1}^{N}\sum_{j<1}U(r_i, r_j)}_{\text{Interaction energy between the electron and other electrons}}\right]\psi = E\psi$$

Eq. 2.2 [219]

Which relates the kinetic energy of each electron, the interaction energy between the electron and nuclei and the interaction energy between the electron and other electrons in an N electron system to the electronic wave function ψ and the ground state energy of the system E. The results from this equation can theoretically be extrapolated to predict all material properties such as material electronic structure, reaction pathways, Young's moduli and even reproduce experimental spectra obtained from techniques such as Raman Spectroscopy or Magnetic Resonance Imaging.

Solving the Schrodinger equation can be viewed as one of the fundamental problems of quantum mechanics. Given unlimited computer time, wave-function based approaches can converge towards to the exact solution to the Schrodinger equation, however these methods will typically be prohibitively expensive for most practical calculations. This computational difficulty arises from the that fact that each wave function of a system is influenced by every other wave function in the system, a so-called "many-body problem", in this scenario the full wave function solution to the Schrödinger equation would be a function of 3N coordinates. It is also useful to note that the quantity of electrons in a given region of space, the electron density $n(r)$, can be written in terms of the individual electron work functions,

$$\rho(r) = 2\sum_{i}|\psi_i(r)|^2$$

Eq. 2.3 [220]

Electron density is a function of only 3 coordinates, compared to a full electron wavefunction which is a function of 3N coordinates, and still contains a great deal of information about the system in question. This property of the wavefunction and its relation to electron density is the foundational of DFT.

2.3 – The Kohn-Sham equation

DFT offers an alternative view of quantum mechanics, which forgoes the use of wavefunctions for electronic charge density, which is intended to make these calculations practically feasible. The basis of DFT are the theorems of Hohenberg and-Kohn which are as follows.

Hohenberg-Kohn 1st theorem - the ground state energy from the Schrödinger equation is a unique *functional* of the electron density.

A functional is similar to a mathematical function where it takes the value of a variable (or variables) and produces a single number. A functional is similar, however it takes a function and defines a single number from that function, i.e., a function of a function. So, in the context of DFT the ground state energy, E , is a functional of the electron density, $\rho(\boldsymbol{r})$, which is a function of position, r, fully expressed as $E[\rho(\boldsymbol{r})]$ hence the name density fucntional theory. This theorem states that there exists a one-to-one mapping between the ground state electron density and the ground state wavefunction.

Hohenberg-Kohn 2nd theorem - the electron density that minimises the energy of the overall functional is the true electron density corresponding to the full solution of the Schrödinger equation.

In other words, if the true functional form were known then electron density could be varied until the energy of the system was minimised i.e. it reaches its ground state, which is stated to be the same and the ground state for the full wavefunction. However, some properties, such as electron kinetic energy cannot be calculated from the electron density therefore it is converted back into a wave function with a caveat. DFT converts a many-body Schrodinger equation for N electrons, which is effectively impossible to solve for larger systems, into fictitious single particle orbitals i.e. each electron is effectively its own single body wave function. Therefore, is modelled as N 3-dimentional equations each with one quasi-particle:

$$\left\{-\frac{\hbar^2}{2m}\nabla^2 + V[\rho(r)] + V_H[\rho(r)] + V_{XC}[\rho(r)]\right\}\psi_b = \varepsilon_b\psi_b(r)$$

Eq. 2.4 [219]

This is known as the Kohn-Sham equation, forming the foundation of Density Functional Theory (DFT). It represents a considerable simplification compared to Equation 2.2, primarily because the summation terms are absent. This simplicity arises from the nature of the solutions to the Kohn-Sham equations, which are single-electron wavefunctions characterized by only three spatial variables. The equation comprises a kinetic energy term ($(-\hbar^2/2m)$), the wave function of the electronic state (ψ_b), the Kohn-Sham eigenvalue (ε_b), and three potential terms (V, V_H,V_{XC}), all of which are density functionals. These potentials describe various aspects of electron behaviour. (V) describes the interaction between and electron and the collection of atomic nuclei. (V_H) represents the Hartree potential, as defined in Equation 2.5. It describes the Coulombic interaction between the electron under consideration in the Kohn-Sham equations and the total electron density arising from all electrons within the system. However, it is important to note that this term introduces the well-known self-interaction error in density functional theory. In simple terms, it quantifies the interaction between an electron and the average electron density, which includes the electron itself, leading to a non-physical self-interaction.

$$V_H(r) = e^2\int\frac{\rho(r')}{|r \quad r'|}d^3r'$$

Eq 2.5 [219]

This problem is corrected in the final term (V_{XC}) which is the exchange and correlation functional, this is a key parameter in DFT calculations and will be discussed in more detail in the following section. (V_H) is defined by Equation 2.6 and is described as a "functional derivative" of the exchange correlation energy.

$$V_{XC}(r) = \frac{\delta E_{XC}(r)}{\delta\rho(r)}$$

Eq 2.6 [219]

The solution to this is an iterative process requiring an initial guess. To solve the Kohn-Sham equation the Hartree potential must be known and by extension also the electron density. To obtain this requires the single electron rave functions to be defined which requires a solution to the Kohn-Sham equations and so on. The solution procedure is as follows:

1. *Make and initial guess of the electron density* $\rho(r)$.
2. *Solve the KS equations using the initial guess to approximate the single-particle wave functions.*
3. *Use the electron density outputted and feed it back into the KS equations.*
4. *Repeat step 3 until the electron density converges and the input and output electron density match.*

This is a simplified description of the calculation procedure, a more in-depth explanation is provided by Payne et al. [220]. The specific convergence criteria for these calculations and instructions on how to update or establish an appropriate initial guess for the electron density have not been elaborated here but can be found elsewhere [221]. This procedure, which is repeated until the input and output densities are consistent, is known as self-consistency.

2.4 – Charge Sloshing and Density mixing schemes:

As described by Brázdová and Bowler [197], the process of finding a charge density that is self-consistent can be extremely difficult. Simply taking the output charge density from one step as the input density could easily prove problematic and produce instability in the calculation. To remedy this an approach known and density mixing is employed where the output charge density from one step is mixed with the input charge density from that step and used as the input for the next step, which can speed up convergence but also lead to instabilities.

A major source of this instability is known as "charge sloshing" which can make self-consistency and convergence in larger systems challenging. This effect is characterised by a significant shift of charge from one point in the cell to another point between the input and the output. This can lead to an oscillation of charge back and forth between iterations, hindering convergence. This effect is particularly acute for metal surfaces where charges can "slosh" to and from the surface with essentially no cost in energy [222]. Selecting an appropriate mixing procedure enhances the electronic convergence and also avoids charge sloshing. Examples of two common mixing schemes are presented by Broyden [223] and Pulay [224].

2.5 – The exchange-correlation functional

The exchange-correlation (XC) functional stands out as arguably the most crucial parameter in a Density Functional Theory (DFT) calculation. All other terms, apart from (V_{XC}), represent the 'known' components, describing kinetic energy and potential energies arising from interactions within the system. The exchange-correlation functional encompasses all quantum mechanical effects that are not explicitly considered in the known terms. In this context, the “exchange energy” embodies the Pauli exclusion principle's impact, stating that no two electrons can share the same quantum numbers within a system. This means that electrons must have asymmetric wave functions if they occupy the same orbital. On the other hand, “correlation” accounts for the Coulombic interactions among electrons, including their natural tendency to avoid each other. In more precise terms, as defined by Payne et al. [220], it is “The difference between the many-body energy of an electronic system and the energy of a system calculated using the Hartree-Fock approximation”.

Sholl and Steckel [219] state that, according to the Hohenberg-Kohn theorem, the existence of the true form of the exchange-correlation functional, which would perfectly describe all the physical effects currently unaccounted for in the 'known' terms, is guaranteed. However, this true form is unknown. Developing accurate exchange-correlation functionals remains an active field of research, with numerous options presently available. The choice of exchange-correlation functional can significantly impact the accuracy of DFT calculations. Researchers often select the functional that best suits the system they are studying based on its known strengths, limitations and computational costs. Descriptions of the most commonly encountered functionals are presented below.

2.5.1 – Local density approximation (LDA)

The earliest and most simple and computationally inexpensive functional is the local density approximation functional, commonly abbreviated to LDA. Uniquely this is the one functional that can be derived exactly by treating the system in question as a uniform electron gas (jellium) i.e. $\rho(r)$ is constant and the exchange correlation is defined in Equation 2.7.

$$V_{XC}(r) = V_{XC}^{electron-gas}[\rho(r)] \qquad \text{Eq 2.7}^{219}$$

LDA is useful due to its simplicity and is computationally inexpensive compared to other functionals however, it is of course a non-physical description of a system. Despite this, LDA performs very well when compared with more sophisticated exchange correlation functionals such as generalised gradient approximation [225]. This makes LDA ideally studied for initial calculations where accuracy can be sacrificed in exchange for speed and computational resource.

2.5.2 – Generalised gradient approximation (GGA)

The Generalized Gradient Approximation (GGA) is a highly popular functional frequently employed in DFT calculations. Among these GGAs, the Perdew-Burke-Ernzerhof approach (GGA-PBE) [226] is notably the most extensively utilized. The fundamental concept behind GGA-PBE is its consideration of electron density gradients, which offers a more realistic representation compared to modeling the system as a homogeneous electron gas, as defined in Equation 2.8.

$$V_{XC}^{GGA}(r) = V_{XC}[\rho(r), \nabla\rho(r)] \qquad \text{Eq 2.8}^{219}$$

The $\nabla\rho(r)$ term in GGA functionals accounts for the spatial variation in electron density, providing a more accurate description of the electronic structure compared to the local density approximation (LDA). GGA functionals represent a significant advancement in density functional calculations, especially for materials with slowly varying electron densities. However, it is important to note that GGA calculations are computationally more expensive than those using LDA, and in certain scenarios they may not significantly outperform LDA in terms of accuracy [227].

2.5.3 - Jacob’s ladder, Hybrid functionals and post – DFT methods

DFT is the standard approach for first principles materials modeling, and as such, a significant amount of work is devoted to its improvement. As previously mentioned, the exact exchange-correlation functional is still unknown. The list of available functionals is extensive, with LDA and GGA functionals falling into the more general category of density functional approximations (DFA). DFA encompasses the full range of exchange-correlation functionals developed to enhance the performance of DFT. The analogy of Jacob’s ladder, as presented in Figure 2.1, is often used to describe the improvement of XC functionals beyond the original LDA functional.

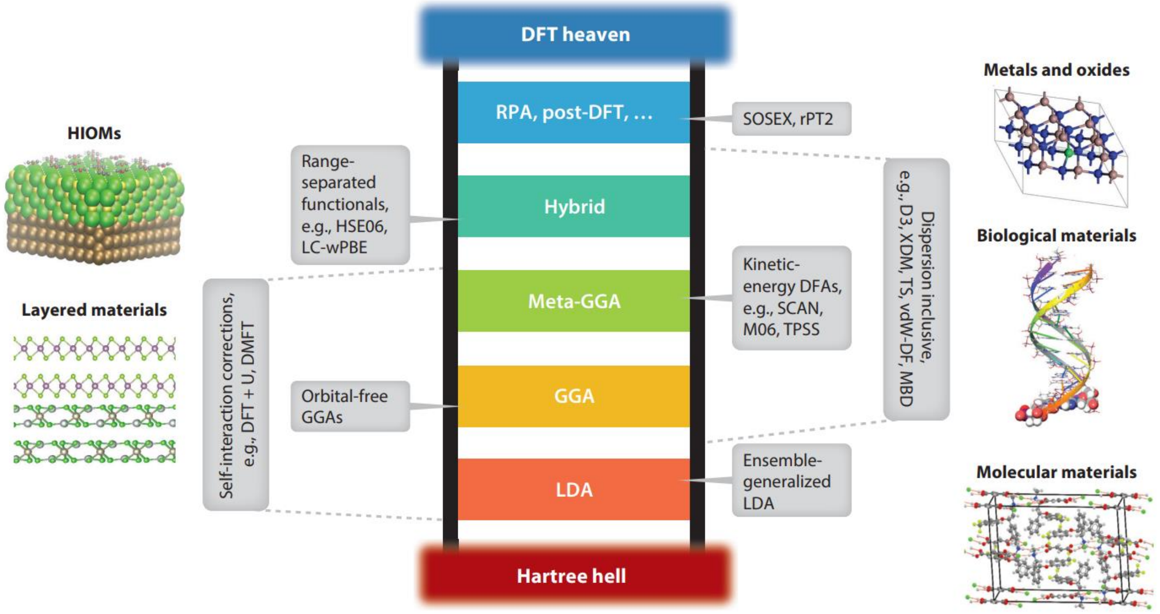

Figure 2.1 – *The Jacob’s ladder analogy illustrating the improving approximations of DFT methods (adapted from reference* [43]*)*

Beyond GGA, there are the meta-GGA functionals, such as the SCAN functional [228], which employ a more sophisticated treatment of the electron density. On the next rung of the ladder, there is the hybrid functional class, which combines so-called "exact exchange" (a mathematically rigorous but computationally expensive way of determining exchange energy) with a GGA exchange functional. These functionals address issues like self-interaction and band structure calculations but come at a significantly increased computational cost. A commonly used hybrid functional is B3LYP [229]. A high level overview of common density functionals is given by Sholl and Steckel [219]. Additionally, an excellent review article on the progress made in the development of DFT functionals and advances in DFT more generally has been provided by Maurer et al. [43].

To conclude, there is a significant choice available in regard to the available functionals for DFT calculations, which are categorized into the Jacob's ladder analogy. However, functionals that offer better approximations usually come with a significantly increased computational burden, and in some cases, they do not appreciably increase accuracy. The selection of an appropriate functional should be balanced between the required accuracy and computational cost.

2.6 – Bloch's Theorem, Plane waves, K-points and basis sets

DFT is a computationally expensive approach to model material properties. Even in modest settings with simple exchange-correlation (XC) functionals, simulations involving hundreds of atoms can become computationally expensive, and those involving thousands, such as those seen in force field approaches, become unfeasible. This challenge is overcome by taking advantage of the periodicity of extended systems e.g., crystals. A common concept in materials science is that of the unit cell, which is an arrangement of a relatively small number of atoms that can be said to repeat infinitely in each direction. DFT calculates the electronic structure of this unit cell, or a small infinitely repeating "slab" of a surface, to dramatically reduce the computational resources required, making them feasible to calculate. An important concept in DFT, and in material science more generally, is that of Bloch's theorem which states that in a periodic solid each electronic wave function can be written as the product of a cell periodic part and a wavelike part [220]. Bloch's theorem in terms of solutions to the Schrodinger equation are presented in equation 2.9.

$$\phi_k(r) = \exp(ik \cdot r)u_k(r) \qquad \text{Eq 2.9}^{219}$$

Where r represents the vector in real space and k represents the vector in reciprocal space. Reciprocal space, a central concept in DFT is covered in more detail by Sholl and Steckel [219], a large real space system has a small representation in reciprocal space. Likewise a small real space system has a large representation in reciprocal space, the primitive cell in reciprocal space is often called the Brillouin zone. This concept is important for practical DFT calculations as it introduces the key settings when performing a calculation, k-point sampling and plane wave basis sets. Functions of the form $\exp(ik \cdot r)$ are defined as planewaves so calculations involving them are referred to as plane-wave calculations [219,220] and u_k represent the periodicity of the wavefunction. The translation of this into a practical solution is somewhat in depth and will not be covered. However the basis set effectively corresponds to an expansion set of this equation, the so called "kinetic energy cutoff" corresponds to a truncation of this set to only include solutions with a kinetic energy below a given value [219]. This parameter will always be reported in any publication using DFT. The other key quantity that will always be reported in a publication using DFT is the k-point sampling which represents the number of points used in calculation in the Brillouin zone. An important and counterintuitive feature of k-point sampling is that larger unit cells required fewer k-points as and are inversely proportional to the real space dimensions of the cell. From Bloch's theorem wave functions are treated as periodic, in larger systems additional k-points are not required as the whole periodicity of the wavefunction has been captured [219].

2.7 – Pseudopotentials

The peudopotential approximation is a commonly employed technique in DFT calculations to further reduce computational costs. In the context of Bloch's theorem description of electronic wave functions, these functions can be expanded into a discrete basis set of potentially infinite plane waves. This set is truncated by setting a kinetic energy cut-off mentioned above however the number of plane waves required can be further reduced by applying "Pseudopotentials" to represent the core electrons of atoms in the system. A very large number of plane waves are required to model the tightly bound core electrons of a system, furthermore in practical situations the valence electrons that govern bonding and chemical reactions are of much greater importance than the core electrons [220]. Pseudopotentials reduced the computational burden by replacing the electron density of a chosen set of core electrons with the density of a "frozen core," which serves as a representative of the true ion core [219]. According to Sholl and Steckel [219] one of the most widely used methods of defining these are the so-called ultrasoft pseudopotential based on the work of Vanderbilt [230] which substantially reduces the required kinetic energy cut-off and, consequently, the computational resources needed for a calculation.

2.8 – Long range dispersion interactions:

Classical physics fails to explain the attraction that is present between two non-polar molecules, evidenced by the tendency of all gasses to condense at some temperature. The origin of this interaction is attributed to the high frequency oscillations of electrons around a nucleus creating momentary polarity changes. Attractive orientations are said to have a higher probability than repulsive ones which, on average, leads to an average attractive force. These are the so called London or "dispersion" forces, and are discussed in more detail elsewhere [68]. A known shortcoming of DFT is the difficulty it has in correctly modelling these long-range dispersion forces. The development of functionals that can correctly capture dispersion forces is an active area of research [43].

An excellent perspective on the treatment of van der Waal dispersion forces is given by Klimeš and Michaelides [231]. In this work they comment on the inability of "standard" XC functionals to describe the long-range electron dispersion forces, give examples of some poorly performing systems, and give a good overview of the most commonly encountered dispersion correction schemes. As described by Klimeš and Michaelides [231], many dispersion correction attempt to solve the dispersion forces problem by adding an additional energy term the DFT equation,

$$E_{tot} = E_{DFT} + E_{disp} \qquad \text{Eq 2.11}$$

Where E_{DFT} is the uncorrected energy of the system obtained by DFT and E_{disp} is the dispersion correction energy. The simplest description the of the dispersion correction energy is given below, where C_6^{AB} is the dispersion correction coefficient, based on the elemental pairs (A and B) and r_{AB}^6 is the distance between particles.

$$E_{disp} = -\sum_{A,B} C_6^{AB}/r_{AB}^6 \qquad \text{Eq 2.12}$$

These so called "DFT-D" methods are simple and have a low computational requirement and are therefore widely used. However, there are many issues with this approach. Firstly, that the function C_6/r^6 exhibits divergent behaviour at small r. To solve this typically a damping function is applied, for example,

$$E_{disp} = -\sum_{A,B} f(r_{AB}, A, B)\, C_6^{AB}/r_{AB}^6 \qquad \text{Eq 2.10}$$

Where the value of $f(r_{AB}, A, B)$ will vary between one and zero depending on depending on the interatomic distance r. An example of such a damping function is provided by Grimme[232,233]. Often it is unclear how the dispersion correction coefficient C_6 should be obtained. In rudimentary dispersion correction schemes, as exemplified by Grimme[232,233], predefined input parameters, usually derived from experimental data, are employed. Alternatively, more intricate schemes exist, generating these coefficients *a priori* [234].

Generally, maintaining coefficients that remain constant throughout calculations is undesirable, as they overlook potential influences arising from the chemical state of the atom or the surrounding environment. Tkatchenko and Scheffler [235] propose a "parameter-free" approach in their Tkatchenko-Scheffler (TS) dispersion correction, aiming to address this issue and move towards a genuinely first-principles dispersion correction. Another noteworthy scheme is the many-body dispersion (MBD) method. Unlike prior methods employing atom-pairwise additive correction for the C_6term, these approaches disregard many-body effects [236], known to exert a substantial impact on real systems [237]. The MBD method, introduced by Tkatchenko et al. [238], represents a dispersion correction scheme designed to account for interactions involving multiple bodies.

The previously discussed dispersion corrections primarily belong to the category of posteriori methods, referring to approaches that apply dispersion corrections atop existing functionals. Alternatively, there are approaches that directly integrate dispersion forces into energy functionals, eliminating the need for separate dispersion correction schemes. However, these methods demand significantly more computational resources compared to posteriori methods. Klimeš [231] and Maurer [43] describe these methods in greater detail.

2.9 – Atomic charge schemes & Hirshfeld Charges:

Atomic charge schemes are methods designed to accurately represent the partial charges of atoms within a system, exemplified by the partial positive and negative charges observed around hydrogen and oxygen atoms in a water molecule. The atomic charge, or charge distribution, significantly influences the electronic and chemical properties of a system and is considered a fundamental property [239]. These schemes are commonly applied to model properties related to chemical reactivity, such as electrophilicity, nucleophilicity [240], and charge transfer[241] , contributing to a better understanding of diverse systems like corrosion inhibition [242], catalysis [239], and triboelectric charging [50,243,244]. There are currently many charge analysis methods available, a summary of the commonly encountered schemes is given below.

One of the earliest atomic charge density schemes is by Mulliken [245], which pre-dates the publication of the foundational equations of DFT the Kohn-Sham equations. Mulliken's approach quantifies the so-called *overlap populations* derived from the linear combination of atomic orbitals, predicting bonding and anti-bonding while assigning values to their strengths. Additionally gross charges i.e. partial charges can be detrained using this approach. A criticism of this approach is that is it highly dependent on basis set. However is recognized for its straightforwardness and simplicity, making it a prevalent choice for charge analysis in catalysis[246] and corrosion inhibition [242].

The later work of Hirshfeld [247] offers an alternative approach. It estimates the partial charge of an atom by comparing the calculated molecular charge density with the free-atom density at the corresponding distances from the nuclei. The free-atom density is taken as the spherically averaged ground state density of a free atom. The difference, defined as the deformation density, is multiplied by a sharing function based on the relative proportion of an atom in the free atom density which gives a Hirshfeld charge. Hirshfeld charges are widely used, demonstrating strong correlations when exploring reactivity-related properties [240].

Bader charge analysis [248] is based on a so called "Atoms in molecules" approach, where any given atom will have a region of charge density surrounding it. Assuming, as Bader does, that the charge density maximum is at the centre of a molecule it then follows that there will be a charge density minimum between the two atoms. The position of this minimum in a surface creates a so called zero flux surface it is used to divide atoms. The volume within this surface, the Bader volume, is then used to calculate the Bader charges using the total charge density partitioned within the volume. Notably, similar to charge partition schemes proposed by Mulliken and Hirshfeld, Bader's scheme is widely used despite its age. Interestingly, Bader charge analysis finds significant application in literature dedicated to the investigation of triboelectric charging using DFT [244,249,250].

While various atomic charge density schemes exist, Mulliken, Bader, and Hirshfeld analyses are prevalent in literature, especially in density functional theory studies of triboelectric charging [50,243,244]. Ongoing developments, including Charge Model 5 (CM5) [251] and Density Derived Electrostatic and Chemical Approach (DDEC6) [252], emphasize the continually evolving nature of this field. However, with numerous studies comparing these schemes [239,253–255] there is no consensus on the superior atomic charging scheme. Despite available comparisons in literature, no single scheme universally outperforms the others. The interpretation of charges should be approached cautiously, considering the limitations of each method. The work of Wang et al. [239] suggests that newer atomic charge schemes often yield comparable results to traditional ones, underscoring the importance of method selection aligned with specific research objectives.

2.10 – Molecular mechanics

Molecular mechanics serves as a comprehensive umbrella term, encompassing diverse modeling approaches that, at a minimum, treat atoms as discrete elements. Perhaps the most straightforward approximation of a molecule's structure involves conceptualizing atoms as individual balls interconnected by springs. According to Hinchliffe [256], this analogy can be traced back to the work of D. H. Andrews [257] in the 1930s, and was known by at least two names, the Westheimer method and the force-field method. The term molecular mechanics was coined in the 1970s to describe the application of classical mechanics to the determination of molecular structures [256].

The objective of molecular mechanics is to capture all of the forces of a given molecule and translate that into meaningful data about the possible structure, potential energy profile and, when approached correctly, chemical properties of a system. Assuming a system of balls attached with strings, where each ball can be a different chemical element, the main quantities parameters of this system that must be captured are the mechanical terms i.e. bond stretching, bond bending and any torsions in the system. Any van der Waal and electrostatic interactions. Crucially, practical considerations acknowledge that a molecule is rarely fully isolated; it interacts with surrounding molecules. Therefore, additional Cross and non-bonded terms due to other molecule in the system must be considered. A detailed and comprehensive overview the equations that govern molecular mechanics calculations is given by Cramer [258].

In order for a molecular mechanics simulation to give meaningful information the most energetically favourable configuration of the atoms in the system must be found. Figure 2.2 presents the well-known Lennard-Johns potential which to this day remains a good approximation of the van der Waal (non-bonded) interactions which are individually weak but collectively important in all materials [197]. An analogous version of this curve also describes the potential of a bond length. The key features of this curve are, as the distance to the molecule increase, the potential tends towards zero. The region of exponential increase in potential as the molecule is approached illustrates the repulsive force between molecules. As the molecule is approached, there is a clear potential well and the minima of this well corresponds to the energetically favourable position of the molecule, which in this case applies to a two-atom system. In practical simulations in 3D and with N atoms, this is done through the application of a potential energy surface where the positions of the atoms are varied until a minimum is found. An important caveat is that even if a local minimum is found it is difficult to prove that it is the true global minimum. A typical safeguard against this is to use many different starting points to see if they all converge to the same value [256,258].

It is important to emphasize that molecular mechanics calculations inherently neglect temperature effects. At the atomistic length scale, temperature corresponds the vibrational movement (the kinetic energy) of molecules. This is typically simulated by obtaining an energy minimised structure calculation then adding momentum (or kinetic energy) to the molecules until the system attains the desired temperature according to the Boltzmann distribution. This computational approach is now categorized as a molecular dynamics (MD) simulation. One way of thinking about energy minimization is as an MD simulation at absolute zero temperature where the lack of momentum (or kinetic energy) results is the molecule getting trapped in the closest energy well. Therefore, reaching an energy minimum with a molecular mechanics calculation corresponds to a systems temperature of 0 K [196,256].

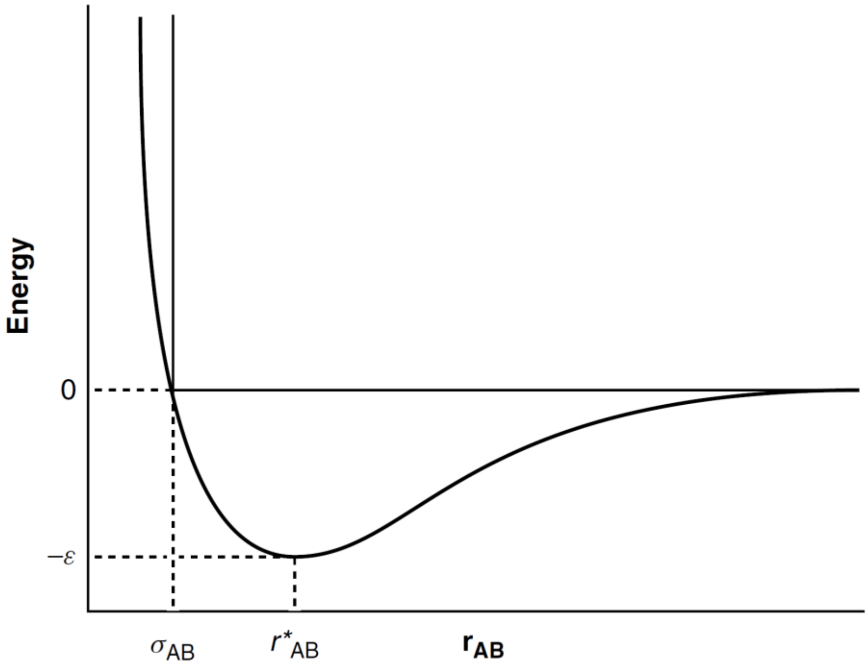

Figure 2.2 – *Illustration of Lennard–Jones potential (curve) and non-attractive hard-sphere potential (straight lines). (ε) specifies the Lennard–Jones potential well depth. (σ) is the point where the attractive and repulsive forces exactly balance and (r^*) is the bond length minimum. (Figure taken from Cramer [258]).*

Molecular mechanics simulations fall broadly into two categories. *Ab initio* molecular mechanics simulations the forces between molecules are calculated from a first-principles approach, such as DFT. However, as mentioned, first-principles calculations are computationally expensive, and in many cases unnecessary for conformational searches. The other category is the force-field based approaches where the interatomic and intermolecular forces are approximated into a so-called force-field, which offers a significant saving in terms of computational time however these methods are unsuitable for calculating the electron structure properties available to DFT [197]. Force-fields approximate the forces acting on atoms by parameterizing the interactions among atoms and fitting the parameters either to experimental data or theoretical data from quantum mechanical simulations. Some notable examples of force fields are DREIDING [259], Universal [260], CVFF [261], PCFF [262], COMPASS [263], COMPASSII [264] and COMPASSIII [265]. Forcefields require significantly less computational resource and simulation time since these methods to not explicitly model electrons and have been shown in some works to preform just as well if not better than DFT based approaches [266].

2.11 – Density functional theory and molecular mechanics codes

Both Density Functional Theory (DFT) and Molecular Mechanics (MM) have reached advanced stages of development, resulting in a wealth of available codes that empower scientists to conduct electronic structure and classical mechanics calculations efficiently, without the need for difficult computer programming. This section contains a brief outline on how molecular modeling calculations are performed. The initial step in atomistic scale simulations involves precise structure definition. The system can be isolated (e.g. a molecule) or periodic in all three dimensions (a crystal with or without defects), or pseudo two dimensional (a surface). Internal coordinates, representing atom positions must be defined. Additionally any molecular symmetry should be defined and exploited to minimize computational costs [197].

Boundary conditions play a crucial role in simulations. In an isolated system, a single molecule is modeled in a vacuum. An extended system is represented by a series of infinitely repeating periodic cells. Isolated boundary conditions dictate that the electrostatic potential reaches zero at a specific distance. Periodic boundary conditions involve copies of the simulation cell being made in each direction. This approach can be visualized as creating a condition were exiting the simulation cell on one side brings you back in through the opposite side. Once the system is defined and encoded in a format interpretable by the chosen code, subsequent calculations can be executed [197]. A more extensive explanation of the practical aspects of atomistic computer simulations is given by Brázdová and Bowler [197].

MM force-field-based approaches are preferable. Notable MM codes, such as AMBER [267], CHARMM [268], GROMACS [269], LAMMPS [270], NAMD [271], OpenMM [272], and FORCITE from Materials Studio. While their implementations undoubtedly differ, these codes universally operate on classical mechanics principles. They leverage force fields to investigate the behaviour of substantial molecular structures, spanning proteins, nucleic acids, biomolecules, and applications in material science. FORCITE [273], a proprietary tool within the Materials Studio suite, offers a simplified workflow by integrating structure building and simulation within a single program. It is the exclusive molecular mechanics tool employed in this work. Relative to DFT geometry optimisation calculations using FORCITE offers an immense time saving [266]. Furthermore, it grants access to high-quality force fields, notably the Materials Studio Compass including COMPASSII [264], which has demonstrated superior performance compared to DFT in specific cases [266]. As a proprietary program accessible solely through Materials Studio, precise details regarding its implementation are not publicly available. However, details on its capabilities are available from the online datasheet [273]. The FORCITE package integrated into the Materials Studio 2023 was used in this work.

Likewise, a multitude of Density Functional Theory (DFT) codes is available, with notable examples such as VASP [274], Quantum ESPRESSO [275], Wien2K [276], and CASTEP [277]. These can differ considerably terms of their implementation. However, a recent comprehensive review by Lejaeghere et al. [278], comparing 40 DFT methods, underscores that the shift from small, personalized codes to more widely adopted general-purpose packages has compelled developers achieve the utmost consistency and reproducibility, resulting in great agreement between results obtained using different codes.

The package that is the focus of this for work is CASTEP which is a fully featured first principles code with numerous capabilities such as total energy, electronic structure, Geometry optimisation, Molecular dynamics, Transition states, Phonons, Electric field response, including having access to the newly developed exchange and correlation functionals. It is also well suited to modelling extended systems, i.e. periodic bulk unit cells for crystals, or surfaces. While available in a stand-alone version, it is also available within the Materials studio suite, which also possesses a graphic interface which can be easily used to generate structure files and input files for the novice user, including running calculations on smaller systems. A more detailed description of CASTEP is given by Clark et al. [277]. The CASTEP version 20.11 was used in this work.

Chapter 3 – First principles calculations on the electronic structure of common surfaces and the role of different surface contaminants.

3.1 – Motivation and overview

Triboelectric charging is a common industrial nuisance, posing safety hazards due to electrostatic discharge and issues during powder processing such as particle aggregation, inconsistent powder flow and problems in formulation and packaging[2]. More recently triboelectric nanogenerators (TENGs) have emerged as a promising and sustainable technology for generating electricity[51]. These innovative devices have the potential to harvest ambient mechanical energy from various sources, such as wind, water flow, or human movement, offering a new and environmentally friendly approach to clean energy production[279].

The study of triboelectric charging has been a topic of interest for scientists and researchers for many years and is the focus of many highly cited review articles[1,2,25]. While significant progress has been made, the complexity of triboelectric charging continues to provide new challenges and opportunities for further research. The triboelectric charging process involves intricate interactions between materials at the atomic and molecular levels, making it a challenging phenomenon to fully comprehend. Triboelectric charging exhibits some perplexing features and phenomena that continue to intrigue researchers such as the charging of identical materials[32], the role of surface curvature in charge transfer[153,280], and the triboelectrically induced X-ray generation[281].

There is a growing body of work that supports the electron transfer mechanism as the dominant mechanism in triboelectric charging[3], this is highly dependent on the electronic structure of a system during contact. Work function of materials has successfully explained the observed charging behaviour in many material pairs and has proven to be an essential parameter in modeling triboelectrification[282]. In recent studies, researchers have developed more sophisticated models for understanding the triboelectric charging phenomenon based on the electronic structure of materials. Such as the 'electron-cloud potential well'[62] and the 'backflow-stuck charge'[5] models which delve into more fundamental features of material electronic structure.

Triboelectric charging is very sensitive to environmental and material conditions which makes it very difficult to form robust conclusions and consistent results across publications[1]. Computational techniques have shown great utility in modeling triboelectric charging [54,57,244,283]. Advances in high-performance computing and computational methods have expanded the scope and applicability of *ab initio* calculations, enabling researchers to gain valuable insights into the behaviour of precisely defined systems, that are not feasible to study directly in experiments. The ability to accurately model triboelectric charging would be very beneficial for preventing unwanted charging in particulate processing and transport and in improving the design and performance of triboelectric nanogenerators.

Humidity, contact force and temperature are all known to impact triboelectric charging [1]. Interestingly, in the realm of semiconductor, photovoltaic and piezoelectric research, work function is known to vary significantly with these environmental conditions. Currently there is a great scope for using *ab initio* calculations to improve our understanding of how environmental conditions might impact triboelectric charging by examining how these factors might impact underlying electronic structure of materials.

In this work the work function of several high index facets of common metal surfaces are calculated using Density Functional Theory. The role of surface contamination is then explored by looking at the role that surface contamination has on the surface work function of these materials. Further analysis of the charge transfer mechanism is done by examining the charge transfer using electrostatic potential, Hirschfeld charges, density of states and charge density difference between the contamination and substrate.

3.2 – Theoretical approach

This work leverages a combined first-principles DFT and force-field based molecular mechanics approach to model several selected surfaces. A molecular-mechanics based approach was used to optimise the surface of the material tested, including optimising contaminant molecules on to the surface being modelled. For DFT calculations CASTEP [284], the plane wave, pseudopotential modeling code was used throughout. For MM calculations the Materials Studio Forcite tool is used with the COMPASSIII force field [265] throughout. The initial part of this work focuses on the viability of the combined DFT-MM approach, which involves comparing the results of geometry optimisation calculations obtained using two different exchange correlation functionals, the Local density Approximation (LDA) (CA-PZ) and the general gradient approximation (GGA) of Perdew-Burke-Ernzerhof (PBE) [226] and the COMPASSIII [265] force field. For the DFT geometry optimisation calculations several different k-point and settings were used which are listed in Table 3.1. with a kinetic energy cut-off of 560eV and a Monkhorst-pack grid of 15x15x15 for bulk calculations.

Table 3.1 – *Kinetic energy cut-off and k-point sampling settings used for geometry optimisations of metal unit cells used in sensitivity analysis.*

System	Kinetic energy cut-off (eV)	k-points
Al	210	6x6x6
Ag	570	6x6x6
Au	360	6x6x6
Cu	450	8x8x8
Pt	360	6x6x6
Si	210	6x6x6

A sensitivity analysis was carried out on the bulk unit cells, comparing simulation results with key input settings such as the FFT grid, k-point sampling, and kinetic energy cut-off. Additionally, a further sensitivity analysis is conducted on the surface, examining the system's energy and work function in response to variations in slab and vacuum thickness, as well as the influence of surface relaxation on the work function. Subsequently, a brief explanation is provided regarding how the work function is calculated using DFT, along with theoretical details concerning Hirshfeld charge analysis and charge density difference calculations.

3.2.1 – Comparison of Molecular Mechanics and DFT Structural optimisation approaches

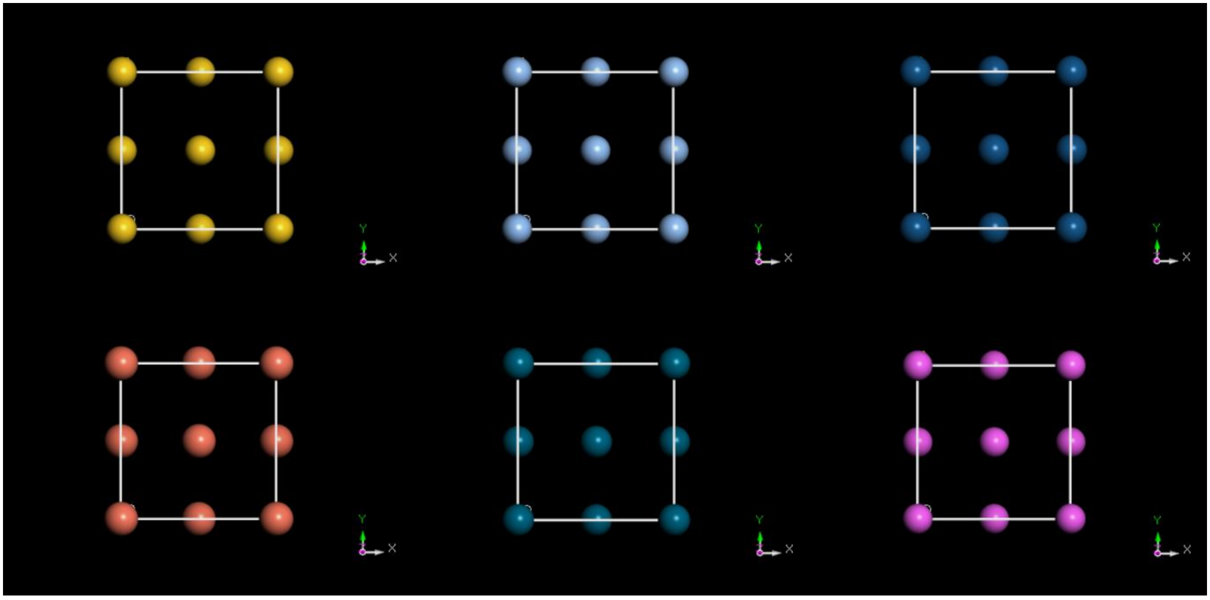

Figure 3.1 – *Unit cells of simple metals used in bulk optimisation calculations. Viewed through Materials Studio visualiser. Gold (top left), Silver (Top centre), Platinum (top right), Copper (bottom left), Palladium (bottom centre), Aluminium (bottom right). Structures obtained from Materials Studio.*

The following calculations covers the sensitivity analysis carried out to ensure appropriate settings were used in this work. The simulation boxes shown in figure 3.1 are the simple metals chosen for the bulk optimisation study, Ag, Au, Al, Cu, Pt and Pd. Each unit cell has a face-centred-cubic crystal system with an Fm-3m space group. All Bulk systems were obtained through the structure database within Materials Studio. The purpose of this work is to determine the optimal approach for calculating these structures based on their lattice parameters and calculation time. In total three calculations are performed on each system. A forcefield based geometry optimisation using the Material Studio molecular mechanics tool Forcite with the COMPASSIII [265] force field at 0 K with assigned charges using the Ewald Summation Method and atom based van der Waals interactions. Convergence tolerances for this optimization are 5.0×10^{-6} kcal/mol for change in energy, 1.0×10^{-2} kcal/mol/Å for force, 5.0×10^{-4} Å for displacement and a stress tolerance of 2.0×10^{-2} GPa. Then two DFT calculations using the LDA (CA-PZ) and GGA-PBE functionals respectively. OTFG ultrasoft pseudopotentials with Koelling-Harmon relativistic treatment is used throughout. For these functionals DFT calculations of this type run in trivial computational time, so the remaining settings are significantly over-converged. A full cell optimisation is done with a custom Monkhorst-Pack Grid of 15x15x15 in line with recommendations from Al-Mahayni et al. [285] with 120 irreducible k-points and with a kinetic energy cut-off of 560eV. Sensitivity analysis in regard to these settings is carried out later. Convergence tolerances for these DFT geometry optimizations include 5.0×10^{-6} eV for change in energy, 1.0×10^{-2} eV/Å for force, 5.0×10^{-4} Å for displacement and a stress tolerance of 2.0×10^{-2} GPa. For the electronic minimisation, a tolerance of 5.0×10^{-7} eV was selected for the total energy per atom. The initial structures used in these calculations are imported from the Materials Studio database and are assumed to be representative of experimentally obtained unit cells. Geometry optimisation calculations are then performed on the structures using these different approaches and then the change in lattice parameters is compared against the unoptimized imported structures from the Material Studio database to determine the accuracy of each method. Calculations are performed through the Materials Studio Suite Interface.

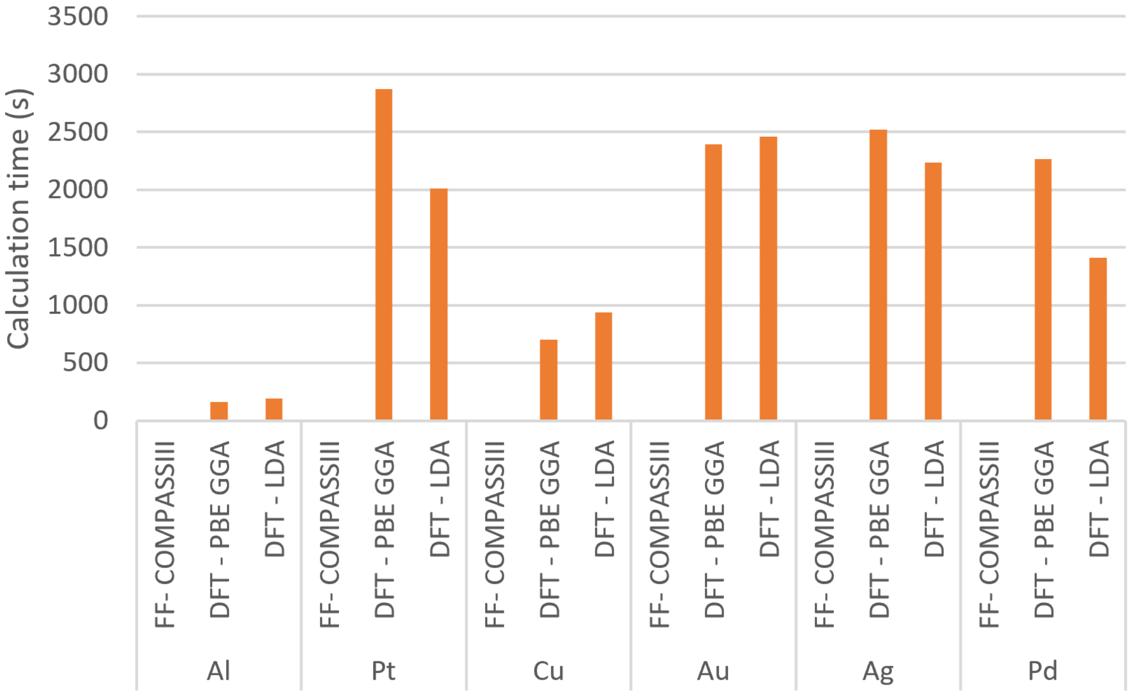

Figure 3.2 – *Calculation time of each simulation vs material and Forcefield (FF) and Density functional theory (DFT) geometry optimisation technique.*

From Figure 3.2 It is clear that DFT calculations take orders of magnitude longer than COMPASSIII with simulation run times consistently under a second. Figure 3.3 shows the percentage change in lattice parameters compared to the initial structure due to geometry optimisation. COMPASSIII generally performs better than DFT calculation, with the exception of GGA-PBE on Aluminium. This justifies the use of COMPASSIII for all geometry optimisations in this work. Raw data for this work is available in the Appendix. COMPASSIII demonstrates strong performance in geometry optimization calculations, leading to a notable reduction in computational time. However, to determine crucial quantities relevant to the investigation of triboelectric charging, such as work function, electrostatic potential, and charge density, additional electronic structure calculations employing DFT are necessary. Therefore a hybrid approach is adopted for this work to reduce computational resource requirement, similar to other works [54,199], where geometry optimisations are performed using molecular mechanics and electronic structure calculations are performed by DFT.

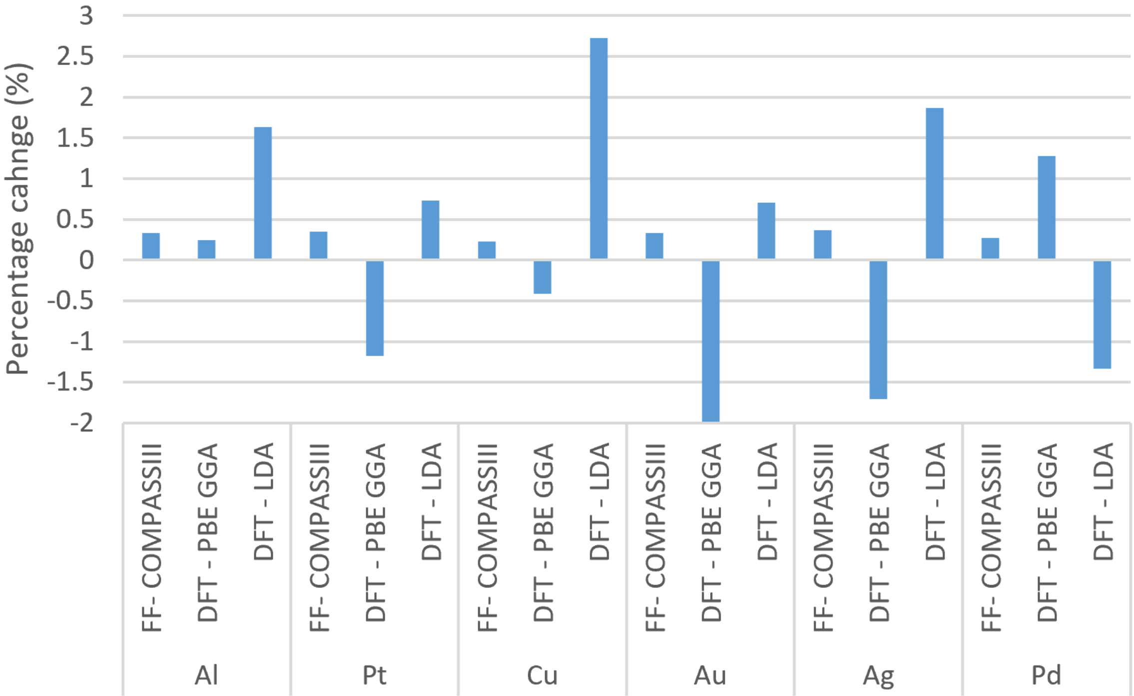

Figure 3.3 –*Percentage change in lattice parameters for each material and geometry optimisation technique compared to unoptimized bulk unit cells.*

To ensure the reliability and accuracy of numerical simulations in the context of density functional theory (DFT), convergence tests are conducted , as recommended by Brazdova and Bowler [197], which address key simulation parameters necessary in achieving meaningful results. First and foremost, the convergence of basis sets is assessed, ensuring that all pertinent properties exhibit convergence with respect to the chosen basis sets, and that the selected basis set is suitable for the employed pseudopotential. Next, k-point sampling convergence is scrutinized, ensuring that the number of k-points in each direction scales inversely with the simulation cell parameters and that total energy differences are convergent based on the selected k-point sampling. Lastly, the convergence of properties with respect to the reciprocal space grids in Fast Fourier Transform (FFT) calculations is examined. Detailed descriptions of these parameters and their significance can be found in Chapter 2 of the referenced material. Further information and recommended tests can also be explored in relevant literature sources[196,286].

For all electronic structure calculations in this work the Plane-Wave basis set is used with on the fly generated (OTFG) Ultrasoft Pseudopotentials. Ultrasoft pseudopotentials allow calculations to be performed with lower energy cut-offs [230,287,288]. Using this basis set the convergence of total energy with kinetic energy cut-off is tested.

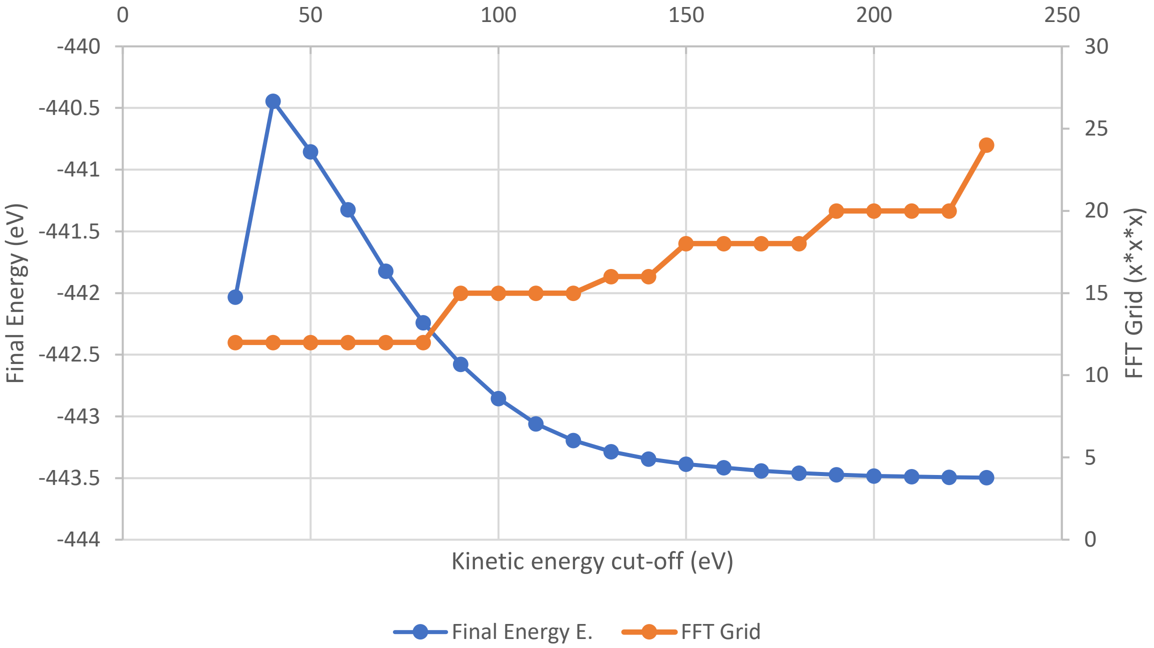

Figure 3.4 – *Graph showing the Total calculated energy of the system vs the kinetic energy cut off for a unit cell of bulk Al (Blue). The density of the FFT grid at each cut-off is also shown (Orange). Calculated using CASTEP simulation package.*

Each simulation uses a 15X15x15 Monkhorst-Pack grid with 120 irreducible k-points and a 12x12x12 FTT Grid. Figure 3.4 shows the expected trend of the total energy converging to a value with increasing kinetic energy cut-off. The density of the FFT grid is at each selected cut-off is also shown. From this it is recommended that all electronic structure calculations are performed at a kinetic energy cut-off

>230 eV. The Monkhorst-Pack grid is an unbiased method that defines the number the k-point sampling k-points in the Brillouin zone in reciprocal space required for calculations. Figure 3.5 shows total energy convergence with the Monkhorst-pack grid. The figure shows that the calculation has converged at a grid density of 10x10x10. The total energy of each calculation converged within a tolerance of 7x10^{-7} eV per atom.

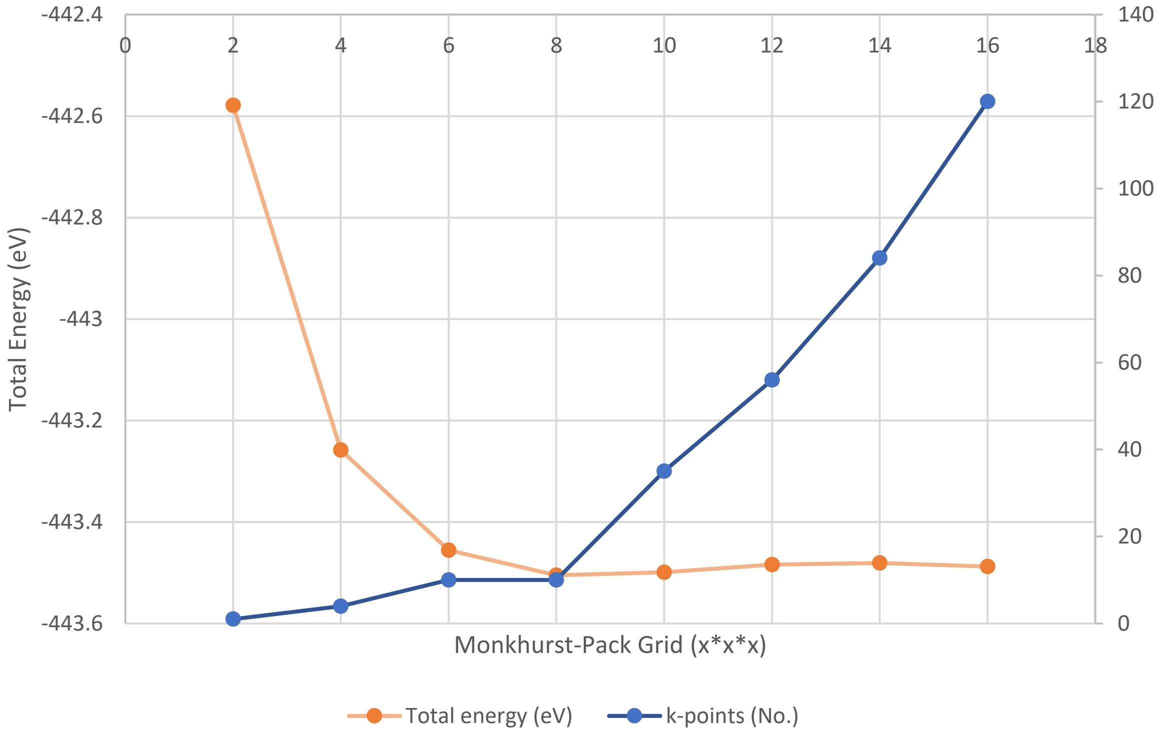

Figure 3.5 – *Graph showing the convergence of total energy with Monkhorst-Pack Grid Density. The number of irreducible k-points at each grid density is also shown. Calculated using the CASTEP simulation code.*

3.2.2 – Vacuum and slab thickness model and Surface Geometry optimisation

Triboelectric charging of insulating materials is a surface phenomenon, there is effectively no charge migration between the surface and the bulk [15]. Therefore, requires a model surface for calculations. To create an ideal model surface, a computational approach involves generating a slice of material that periodically extents infinitely in two dimensions but is finite along the surface's normal direction. Practically this is achieved by using periodic boundary conditions in three dimensions The atomic structure fills a designated section or "slab" within the supercell along the x and y directions, while vacant space or a vacuum region is positioned both above and below the slab. A periodic unit cell of this vacuum-slab model is illustrated in Figure 3.6.

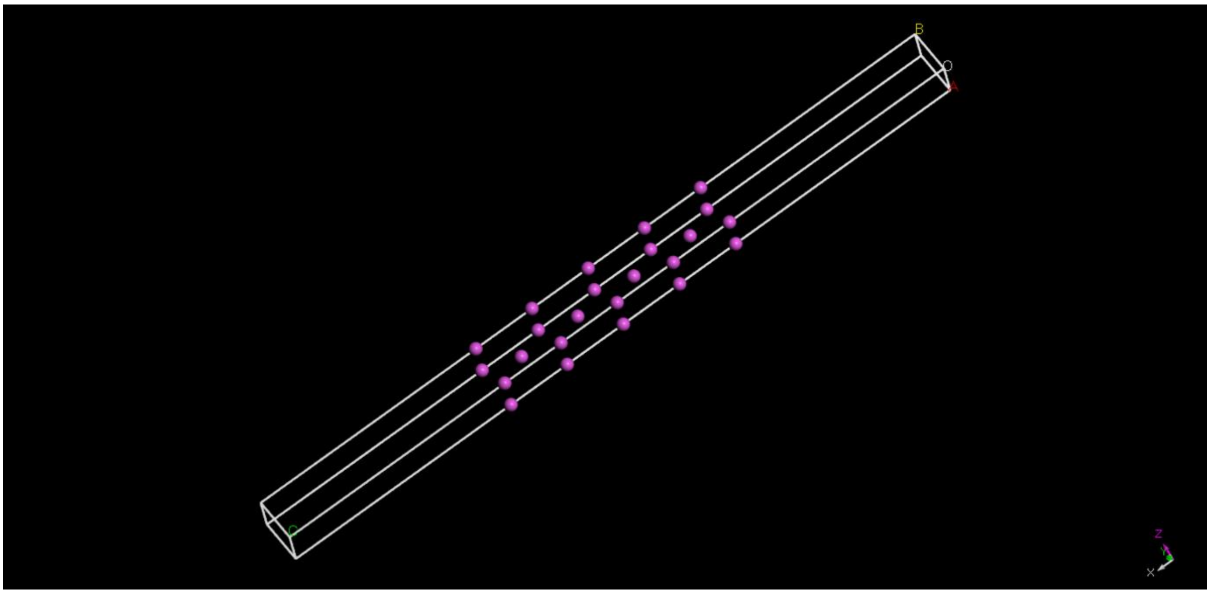

Figure 3.6 – *A periodic simulation box showing a nine-layer thick aluminium (100) surface. Visualised using the Materials Studio Visualiser Interface.*

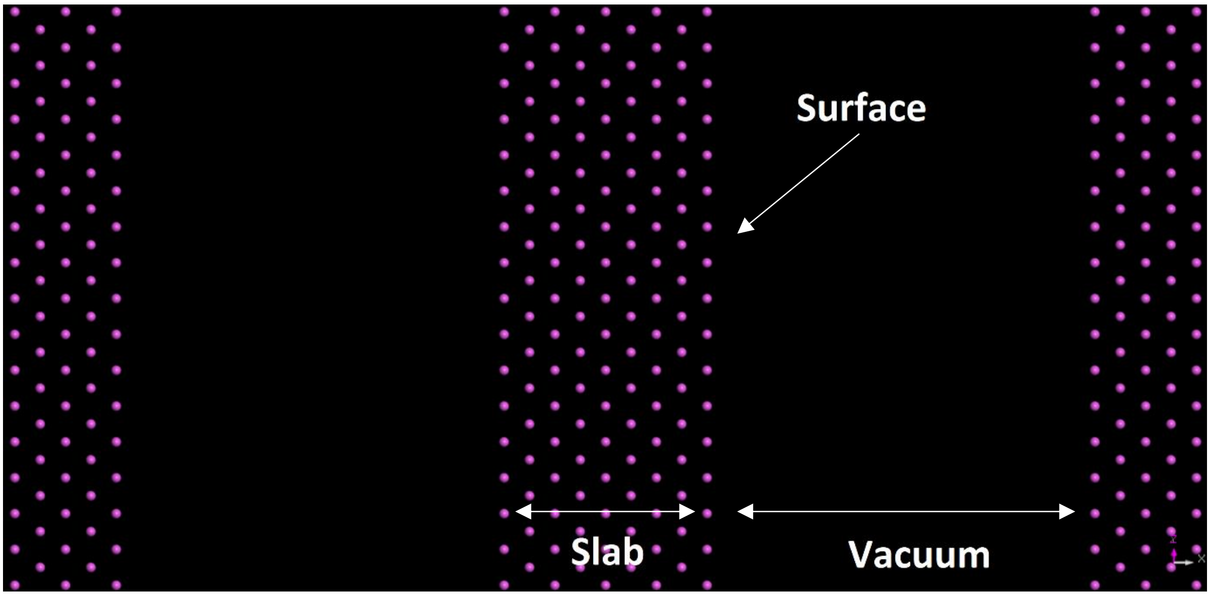

Figure 3.7 – *Schematic of the vacuum-slab approach showing periodically repeating layers of and Aluminium (100) surface sandwiched between periodically repeating layers of vacuum.*

Figure 3.7 demonstrates an expanded view of the unit cell, indicating directions parallel and normal to the surface. It is of utmost importance to ensure an adequate thickness of the vacuum region to allow the electron density between the two slabs to approach zero, as no interaction should occur between periodic slabs. The vacuum-slab approach is the established technique for modeling surfaces with DFT. Further details about this modeling are available elsewhere[219].

3.2.4 – Work function calculation

In this calculation of work function is based on Equation 3.1, which takes it as a relationship between the vacuum energy and the fermi level of a system. Vacuum energy (E_{vac}), as described by Kahn [289], is the energy of an electron positioned "a few nanometres" away from the surface with zero kinetic energy with respect to the surface. How the vacuum energy is derived from a slab-vacuum surface is illustrated in Figure 3.8. This value is subtly different to the energy of a theoretical electron removed to an infinite distance from the surface, which is not experimentally accessible [290]. This energy difference is due to the contributions from the surface dipoles or extra charge possibly present on the surface. The Fermi level, also called the chemical potential, (E_F) is defined as the topmost filled orbital at 0K [291].

$$WF = E_{vac} - E_F \qquad \text{Eq. 3.1 [289]}$$

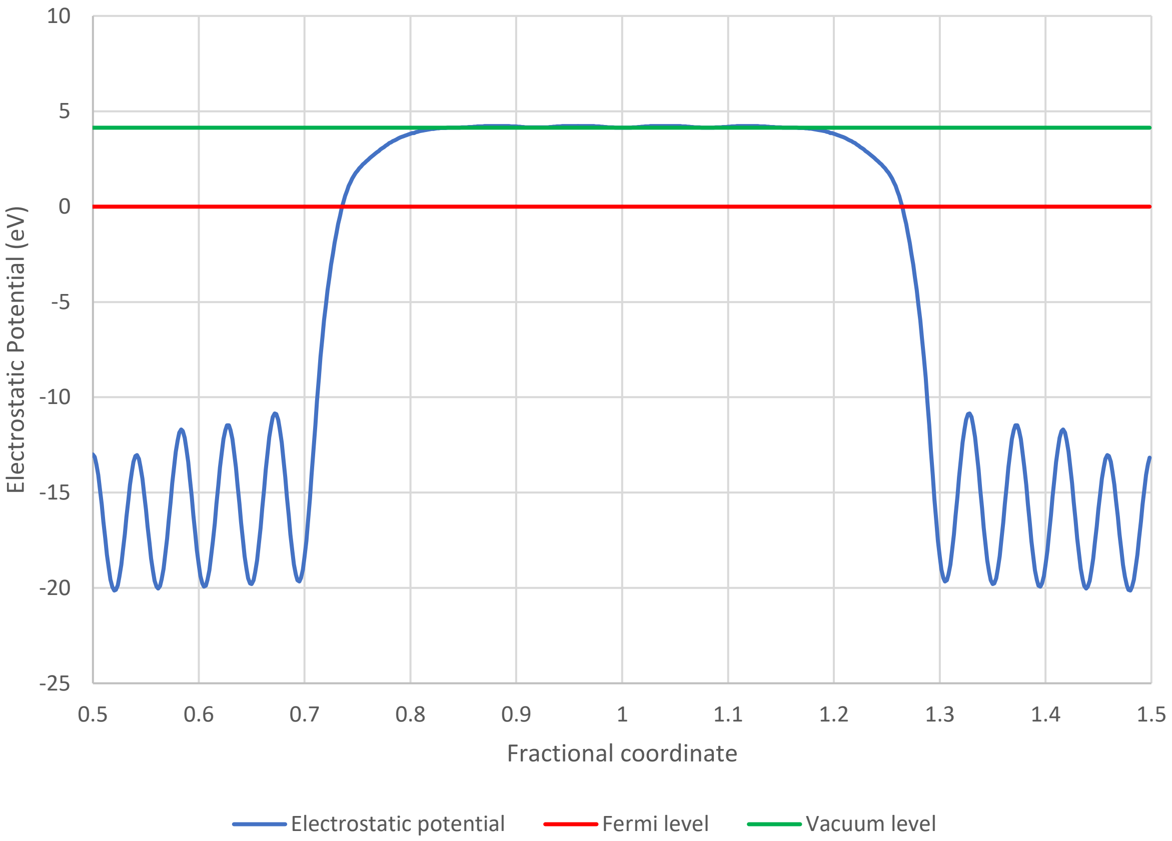

Figure 3.8 – *Calculated planar averaged electrostatic potential normal to a clean aluminium (100) surface with calculated fermi energy and a vacuum level shown.*

3.2.3 – Vacuum and Slab Thickness

Like kinetic energy cut-off and k-point density, it is imperative to demonstrate convergence with respect to slab thickness, vacuum thickness, and surface relaxation. To initiate this process, the surface is derived from a bulk unit cell. It is important to note that molecules on the surface may have different conformations compared to those in the bulk due to altered surface coordination, particularly within the top few layers. Surfaces reconstructions are significant and observed in literature [292], therefore it is important to ensure discontinuities at a surface are properly accounted for. This phenomenon is referred to as surface relaxation, necessitating a subsequent geometry optimization step to properly prepare these surfaces for further calculations. Sufficient vacuum must be provided to ensure that there are no interactions between but also the slab must be of sufficient thickness to simulate the bulk. In this study the quantity of interest is the work functions so the converge of work function and the total energy of the system with vacuum thickness.

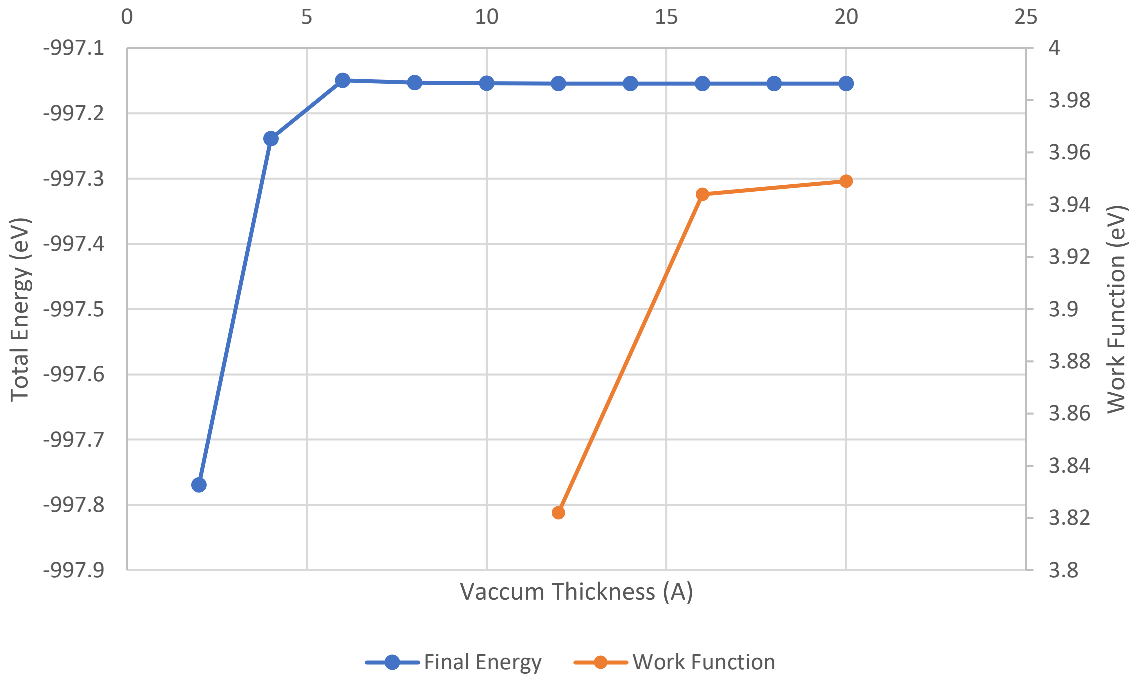

Figure 3.9 – *Graph showing the total convergence of total energy and work function with vacuum slab thickness for a 9-layer thick 111-Aluminium surface. Calculated using the CASTEP code with GGA-PBE functional, ultrasoft pseudopotentials with a 300eV kinetic energy cut-off.*

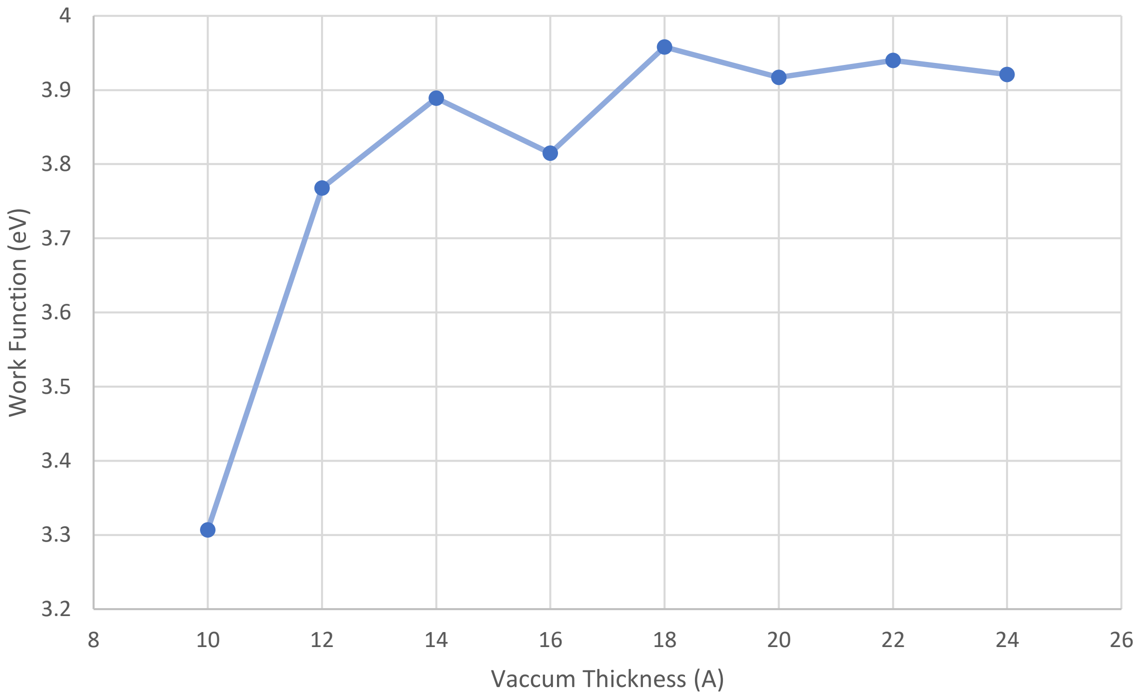

Figure 3.10 – *Graph showing the expanded total convergence of work function with vacuum slab thickness for a 9-layer thick 111-Aluminium surface. Calculated using the CASTEP code with GGA-PBE functional, ultrasoft pseudopotentials with a 300eV kinetic energy cut-off.*

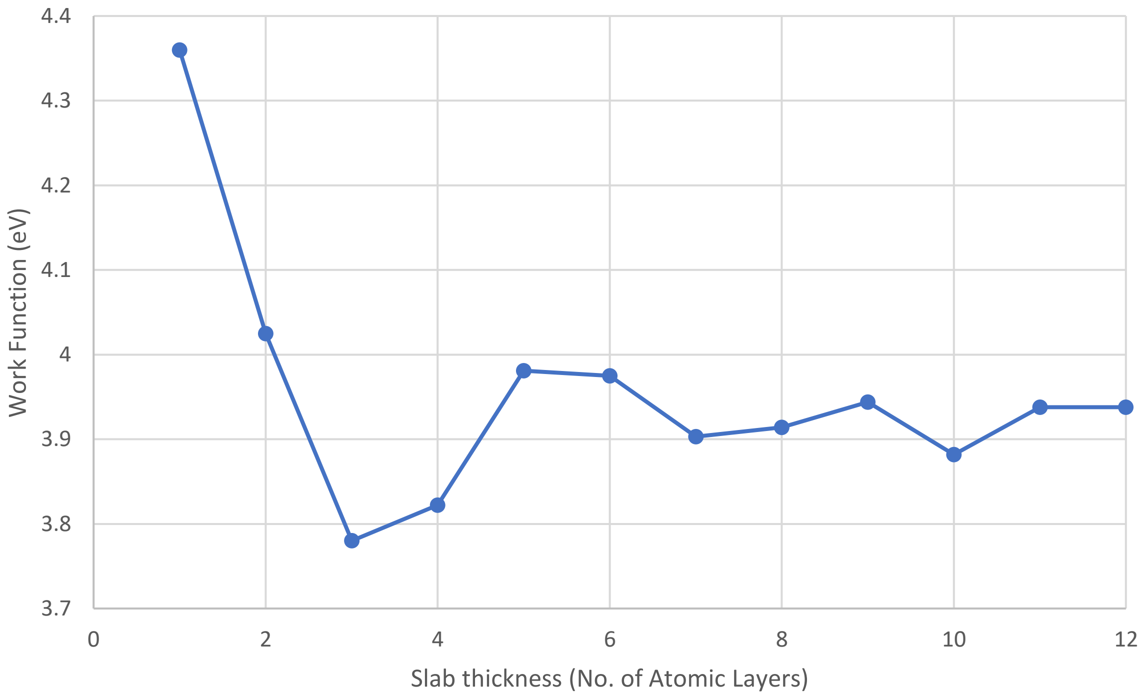

Figure 3.11 – *Graph of work function vs slab thickness of a (111) Al surface. Calculated using CASTEP with a constant vacuum slab thickness of 20A. PBE-GGA functional with Ultrasoft Pseudopotentials with a 210eV kinetic energy cut-off.*

It becomes evident from Figure 3.9 and 3.10 that the total energy of a vacuum-slab system achieves convergence at around 6 Å Angstroms, and the calculated work function stabilizes at approximately 20 Å. Therefore, any subsequent calculations should incorporate a vacuum thickness of at least 20 Angstroms for accurate results. Regarding the slab thickness, as depicted in Figure 3.11, the system demonstrates decent convergence beyond 8 layers of slab atoms, with the final calculated WF values being within 1x10^{-3} eV. Further calculations were carried out to investigate the effect of constraining surface atoms on the surface work function. In a geometry optimization calculation, "constrained" surface atoms have their coordinates fixed, while "unconstrained" atoms are free to adjust their positions until they reach their energetically favourable configuration. Typically, a system undergoing surface geometry optimization resembles the one shown in Figure 3.12, with surface atoms allowed to move and a core of constrained atoms at the centre representing the bulk material. The convergence of work function concerning the number of relaxed surface layers is also illustrated in Figure 3.13.

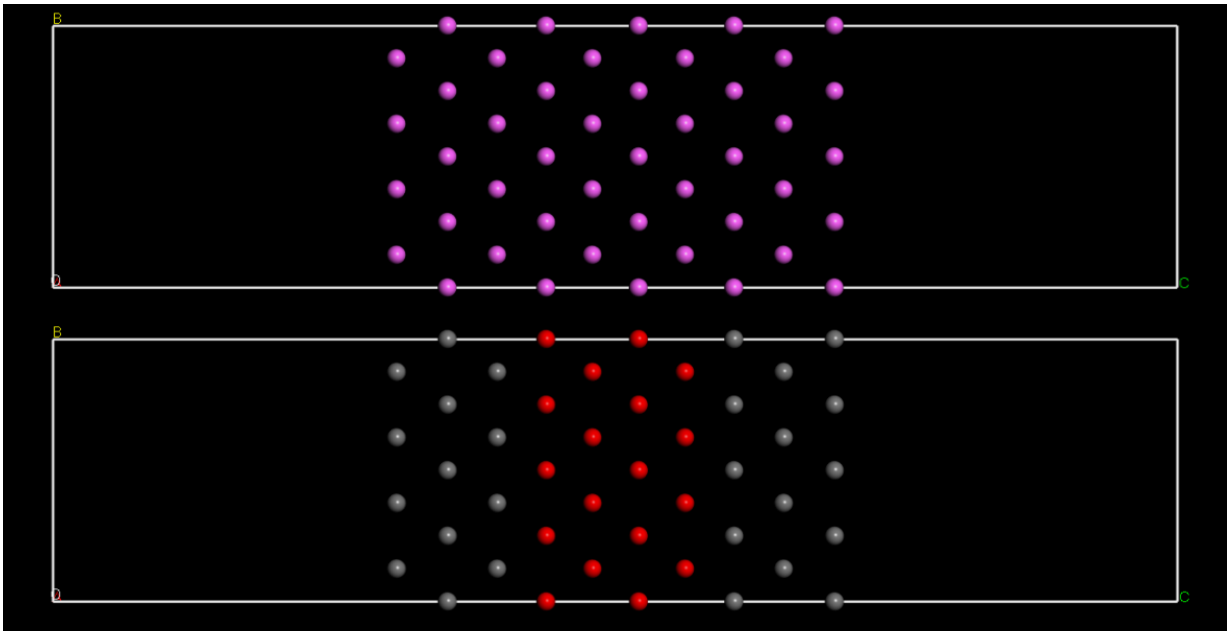

Figure 3.12 – *Supercell of Aluminium (111) surface showing constrained bulk atoms (red) and unconstrained surface atoms (Gray). In this system 3 surface layers are unconstrained.*

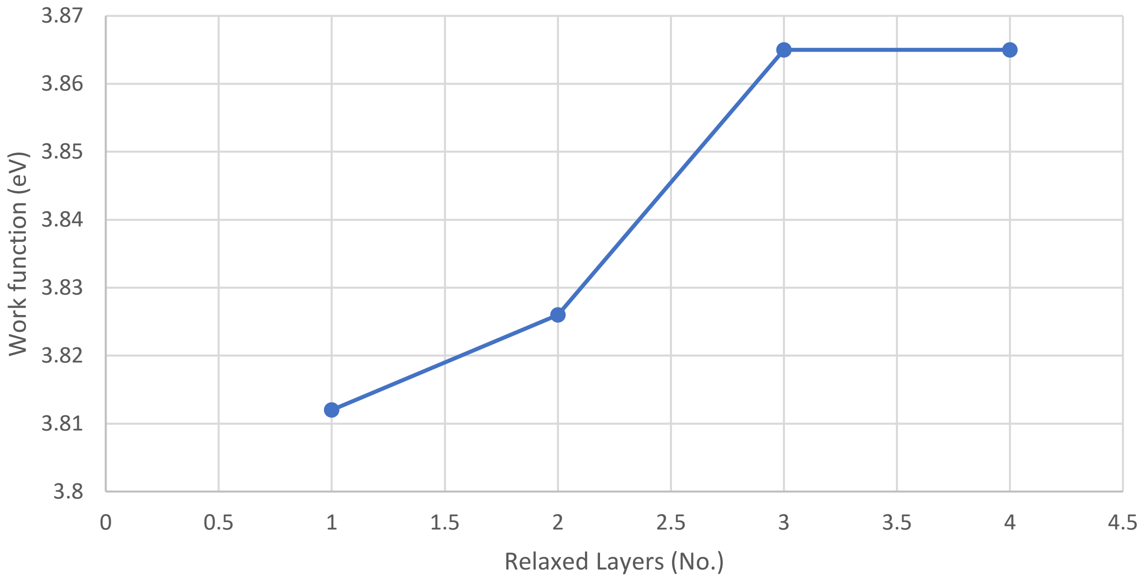

Figure 3.13 – *Calculated work function vs number of constrained surface layers of 9-layer 111 Al surface after CASTEP geometry optimisation. PBE-GGA functional with Ultrasoft Pseudopotentials with a 210eV kinetic energy cut-off and a k-point sampling of 10x10x1.*

3.2.4 – Effect of water molecules on metal surfaces

The influence of water on triboelectrification is well-established, and has historically been attributed to the ion transfer mechanism [25]. Work function, as mentioned earlier, plays a key role in modeling charge transfer. Interestingly, the effect of contamination on work function is a common subject of study in fields such as semiconductor and photovoltaic research. Fortunately the behaviour of water has been studied extensively using first principles calculations, a recent review on the topic has be published by Groß and Sakong [293]. However, the shift in work function resulting from contamination is rarely addressed. This research aims to investigate how common environmental contaminants might impact the electronic structure of metals and speculate on their effects on triboelectric charging. The initial testing focused on examining the role of surface water on the work function of several noble metals. Examples of the unit cells used in an initial test are shown in Figure 3.14. Unconstrained water molecules are placed on the material slab with 3 layers of unconstrained surface molecules and 3 constrained core atoms to simulate the bulk. They are then subjected to a geometry optimisation calculation. K-point sampling of 10x10x1 and a kinetic energy cut-off of 630eV is used throughout.

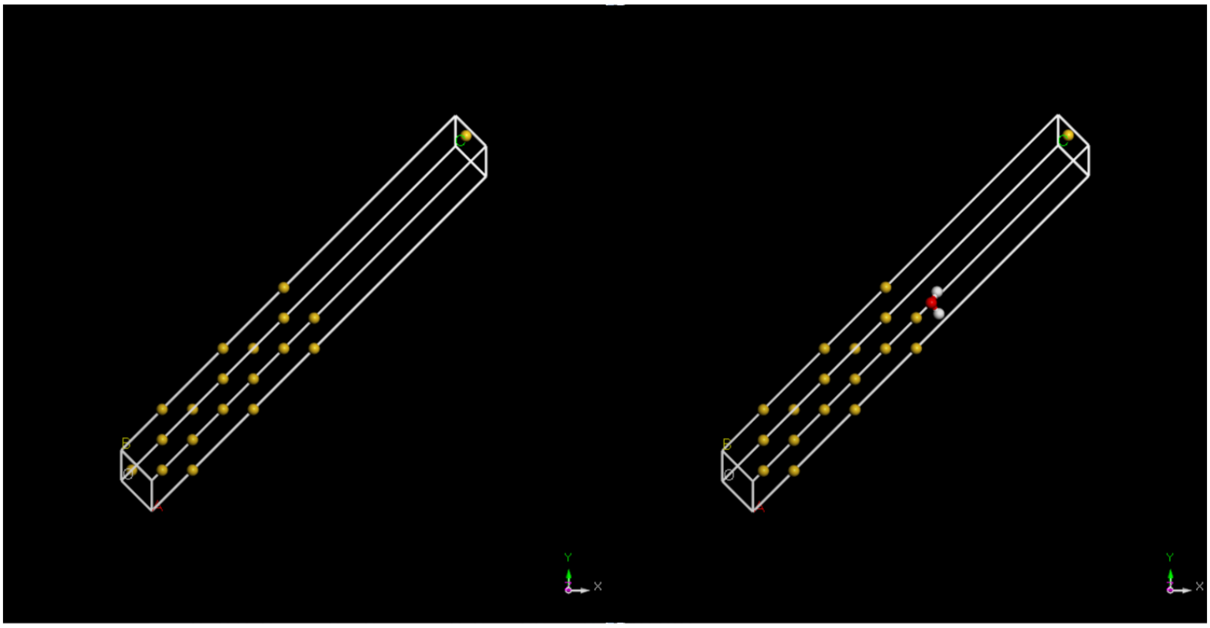

Figure 3.14 – *Visualisation of vacuum slab system of 111 Gold surface using Materials Studio Visualiser. Clean surface (left). Surface with a monolayer of absorbed water, geometry optimised using COMPASSIII (right).*

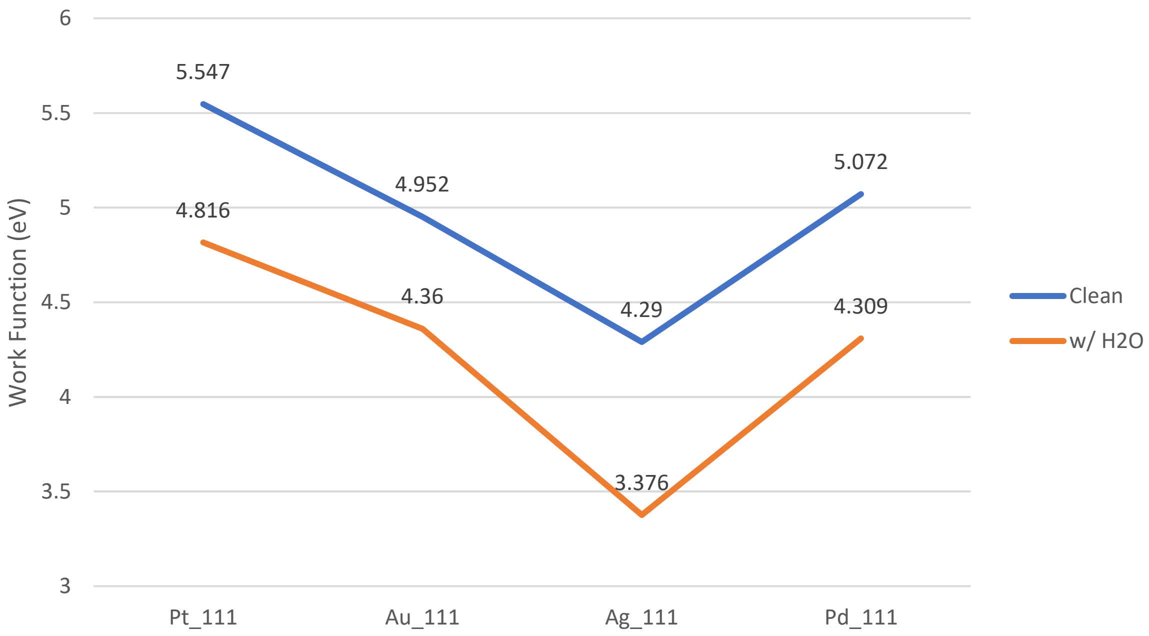

Figure 3.15 – *Graph showing the calculated work function drop by adding a water monolayer to a 111 Noble metal surface. Geometry optimised using Forcite simulation package with COMPASSIII forcefield (FF). DFT single point energy calculations were done using CASTEP (GGA-PBE) with ultrasoft pseudopotentials.*

In the initial tests, a substantial drop in work function, exceeding 0.6 eV, was observed on each metal surface when a water molecule was introduced to the surface. In this scenario, the periodic system had a large aspect ratio, and it's highly likely that water molecules interacted with the surface. To further investigate the effects of multiple water molecules on the surface, a larger supercell of aluminium was created, as shown in Figure 3.15. Several water molecules were placed on the surface to assess their impact on the surface work function.

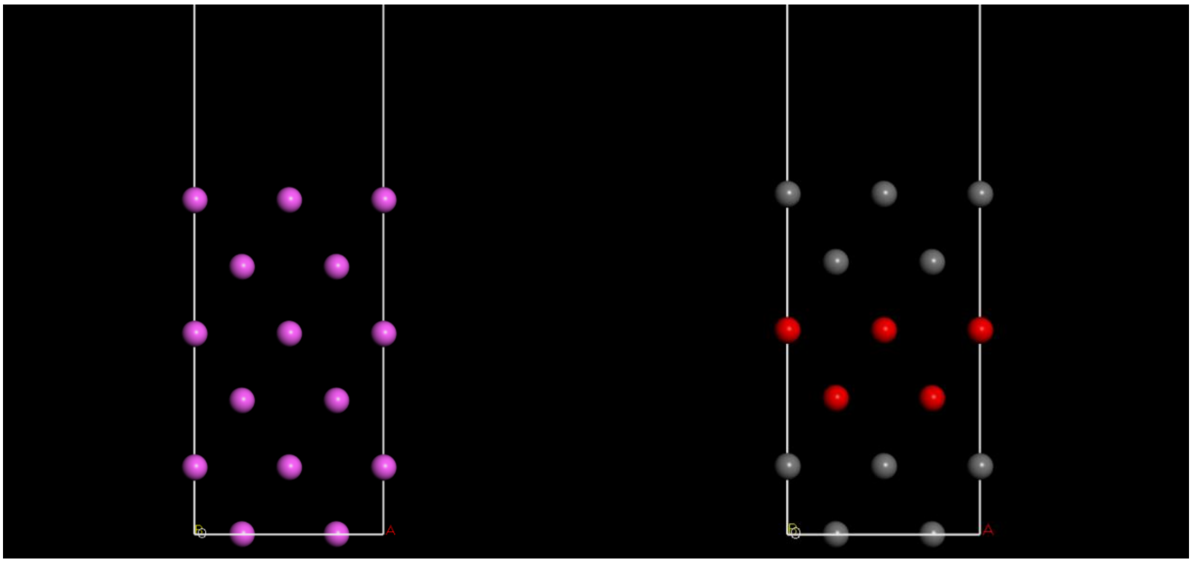

Figure 3.16 – *Vacuum-slab of a 6-layer (001) Aluminium surface (left). The core "bulk" layers have their positions constrained, highlighted in red, the remaining surface layers are highlighted in Gray and their positions are unconstrained (right).*

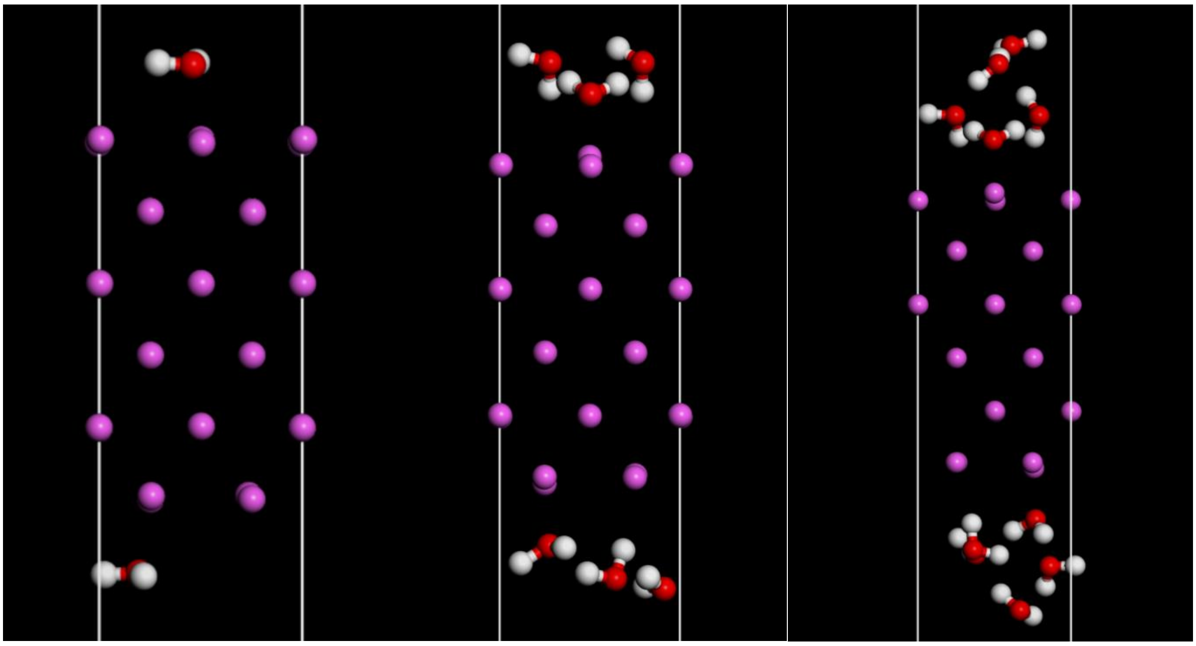

Figure 3.17 – *Visualisation of several optimised structures used in calculations. 1-H_2O (Left). 3-H_2O (Centre). 5-H_2O (Right).*

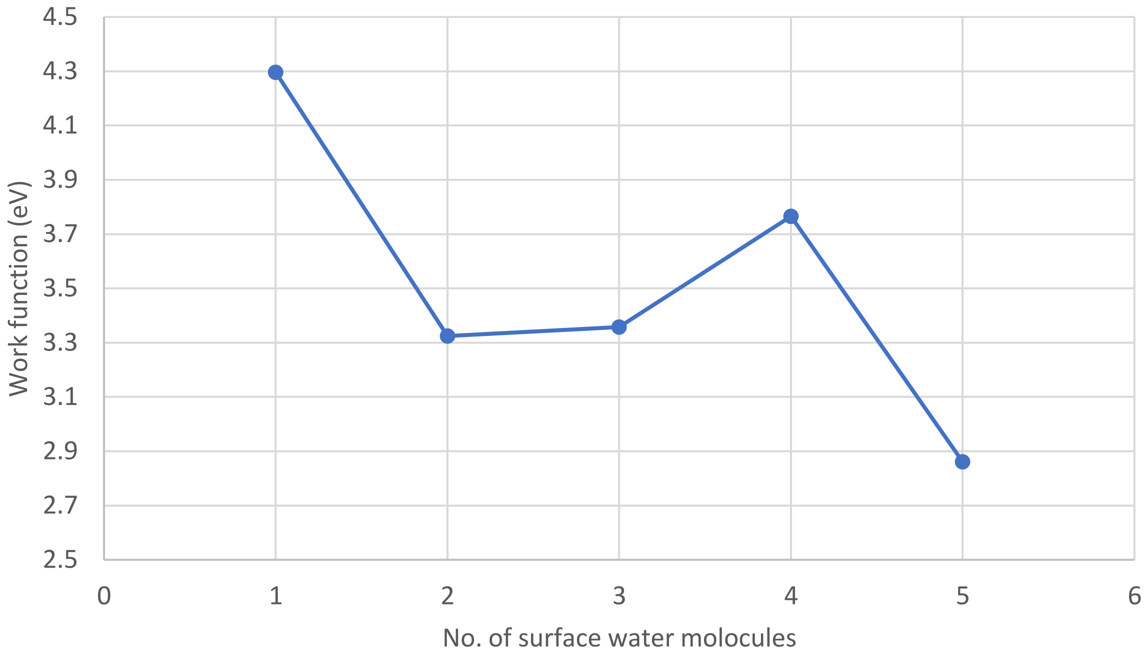

Figure 3.18 – *The dependence of calculated surface work function on the number of optimised molecules on the surface.*

The initial tests clearly indicate that the presence of multiple water molecules has a substantial impact on the calculated work functions of materials. However, it is important to note that these tests have limitations, as they do not account for factors such as temperature and the specific arrangement of water molecules at the surface. Nevertheless, these initial findings underscore the potential for networks of water molecules at the surface to exert a significant influence on the calculation results.

To conclude, comparing different geometry optimisation techniques shows that DFT simulations are significantly more expensive computationally, and do not offer significant improvement of FF based approaches. It is therefore valid for initial optimisations do be done using COMPASSIII force field combined with a single point energy DFT calculation to reduce the required computational time. In terms of grid density, the total energy of a system is shown to converge at a Monkhorst-Pack grid of 10x10x10. For the vacuum slab model, the system is shown to converge in terms of total energy and work function at a vacuum thickness of >20Å. The convergence of work function with slab thickness is less clear, however is taken at a minimum of 9 layers. In regard to, surface relaxation, there should be at least 3 layers of relaxed unconstrained surface molecules for work function to converge.

3.2.5 – Calculation details for contaminated and clean surfaces

The primary objective of this study is to leverage DFT calculations to gain deeper insights into how surface contamination could potentially affect the phenomenon of triboelectric charging. Work function, a key parameter, is frequently associated with charging data. Similarly, the influence of adsorbate molecules on the electronic structure and work function of a surface has been extensively explored in various fields. However, the application of DFT to systematically investigate the impact of contamination on charge transfer mechanisms remains a relatively unexplored area of research.

Humidity and atmospheric conditions impact triboelectric charging [1]. In parallel fields of research, work function has been found to be influenced by the level of environmental contamination [294]. This study seeks to explore the impact of potential contaminants on the surfaces of metals, each with distinct work functions, in order to shed light on their potential effects on the triboelectric charging mechanism. Specifically, common atmospheric contaminants, including water, carbon dioxide, and nitrogen dioxide, have been selected for investigation, given their prevalence in the environment. Modeling the impact of contamination from particulate matter resulting from fossil fuel combustion poses a more intricate challenge. These particulates are too large to be simulated as a whole, so the molecules of butane, cyclo-hexane, and benzene have been optimized to represent their effects on respective surfaces. As triboelectric charging has been observed to correlate with work function, three different metals with varying work functions have been chosen to explore potential variations in surface interactions between the metal and the adsorbed molecules. The systems prepared for this study are visually represented in Figure 3.18. Each system consists of a 9-atomic layer thick slab of a (111) surface of aluminium, gold, or platinum. Geometry optimisation calculations are calculated by Materials Studio Forcite with the COMPASSIII force field. The contaminant molecules are left unconstrained and additionally 3 surface layers of the surface are also unconstrained with the 3 layers at the centre of the slab, constrained to simulate bulk. DFT energy calculation are done using CASTEP with a k-point sampling of 2x2x1 and a 600eV energy cut-off used throughout.

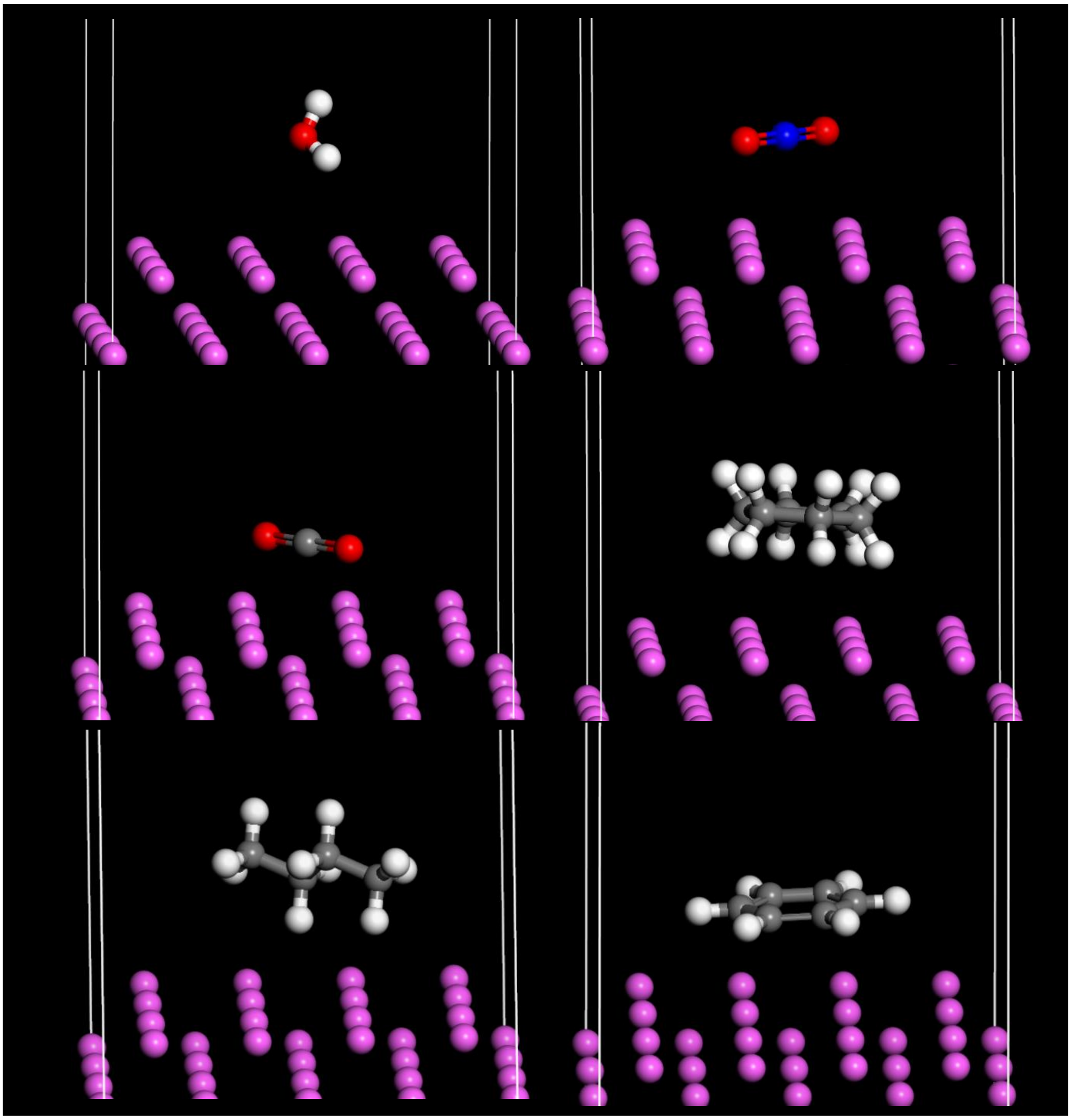

Figure 3.19 – *Unit cells prepared to simulate various environmental contaminants such as water (top left), nitrogen dioxide (top right), carbon dioxide (middle left), cyclo-hexane (middle right), butane (bottom left) and benzene (bottom right).*

In order to accommodate the larger surface molecules, larger supercells of the surfaces were prepared. This approach was employed to prevent of any undesired interactions between the periodic cells. The cross-sectional dimensions of these supercells were set to 11.10 Å for Aluminium, 11.64 Å for Gold, and 11.13 Å for Platinum.

3.2.5 – Hirshfeld charge analysis

Hirshfeld charges, as defined by Hirshfeld [247], are an approach designed to succinctly summarize the charge redistribution of a specific atom within a molecule. This is achieved by quantifying the change in atomic electron density through a comparison between the calculated electron density of an atom within a molecule and the electron density of an isolated atom in its free state. These charges provide valuable insights into how electron density is distributed among atoms within a molecule, aiding in the understanding of chemical bonding and reactivity. Hirshfeld charge analysis has also been applied in numerous studies to model triboelectric charging [155,243,295–297].

3.2.6 – Charge density difference analysis

Charge density difference calculations are routinely performed in triboelectric charging studies to quantitatively assess charge transfer and redistribution across surfaces[49,54,298]. An illustration of the planar-averaged charge density difference of NO_2 on Al(100) is provided in Figure 3.20, obtained using Equation 3.1. ρ is defined as the electron density.

$$\Delta\rho = \rho_{surf-mol} - \rho_{surf} - \rho_{mol} \qquad \text{Eq. 3.1}$$

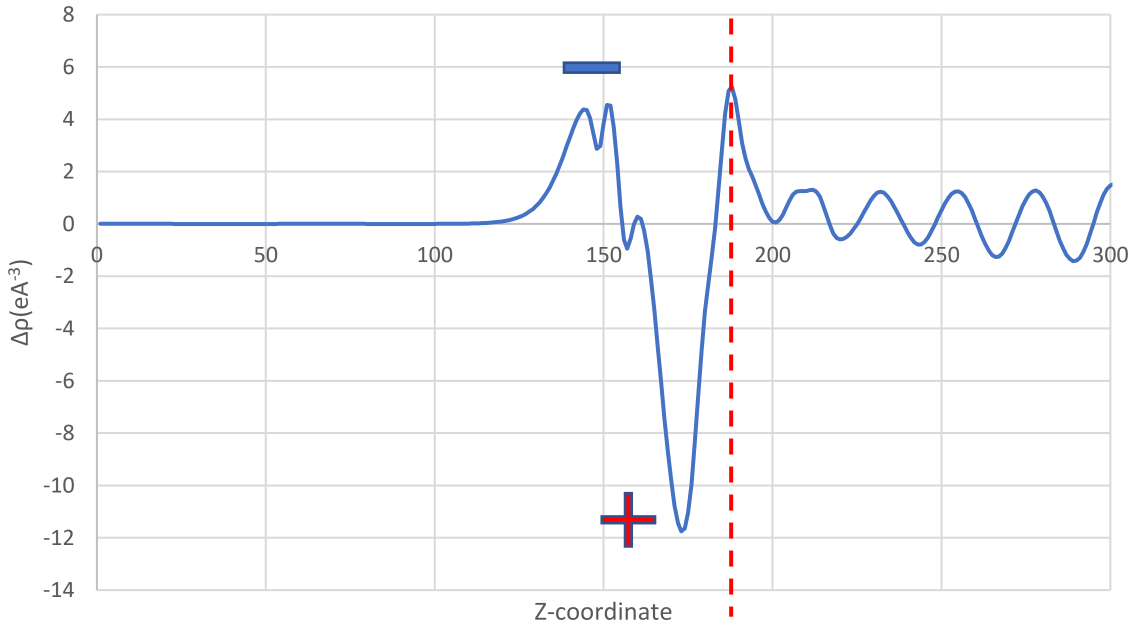

Figure 3.20 – *Calculated charge density difference between nitrogen dioxide molecule and an aluminium (100) surface. Dashed red line indicates position of interfacial aluminium atom. Regions of expected positive (+) and negative (-) charging labelled.*

3.4 – Results and discussion

The work functions of common metals have undergone extensive study, using both theoretical and experimental approaches. A comprehensive database comprising reported work function values for various elemental materials, collected from numerous publications, has been compiled by Kawano [299]. This publication highlights the significant variation in reported work functions across all the materials considered. The initial calculations involve the determination of work functions for several surfaces that have been commonly examined in experimental literature. These calculated values are subsequently compared with the data obtained from Kawano's work [299]. Following this, the impact of different contaminants on the (100) surfaces of aluminium (Al), gold (Au), and platinum (Pt) is thoroughly investigated.

3.4.1 – The work function of the high index surfaces of elemental materials

The initial simulations focused on theoretically studying the different work functions of a range of elemental materials and any differences that might occur due to difference between the facets of that surface. It is observable from Figure 3.21 and Table 3.2 that work function is sensitive to both material and facet. Platinum surface are observed to have the highest work function with aluminium having the lowest of the surface tested. Interestingly there does not seem to be a consistent trend between the Miller indices of the facets e.g. the calculated work function of the facets of aluminium are ordered (111)<(110)<(100) however the facets of silver, copper, gold and platinum are ordered (110)<(100)<(111). Similar orderings are reported elsewhere [300].

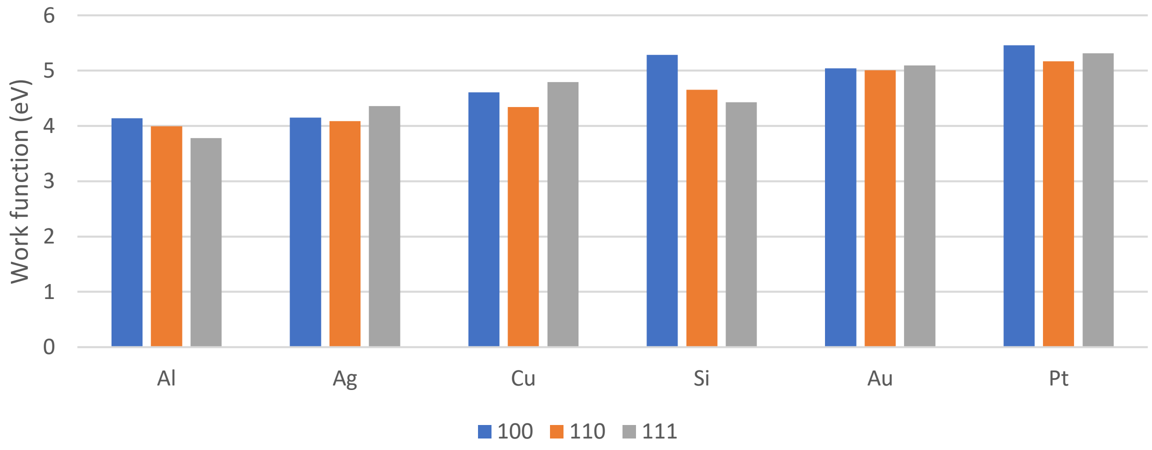

Figure 3.21 – *Calculated work function of the high index surfaces of several elemental metals and pure silicon.*

Table 3.2 – *The "recommended" work function values reported by Kawano* [299] *compared to the calculated work function values from this study.*

	Experimental [299]			Calculated		
	100	110	111	100	110	111
Al	4.28	4.05	4.24	4.14	3.99	3.78
Ag	4.46	4.28	4.64	4.15	4.09	4.36
Au	5.39	5.33	5.46	5.04	5.01	5.10
Cu	4.58	4.43	4.95	4.61	4.34	4.79
Pt	5.74	5.54	5.80	5.46	5.17	5.31
Si	4.82	4.44	4.86	5.29	4.65	4.43

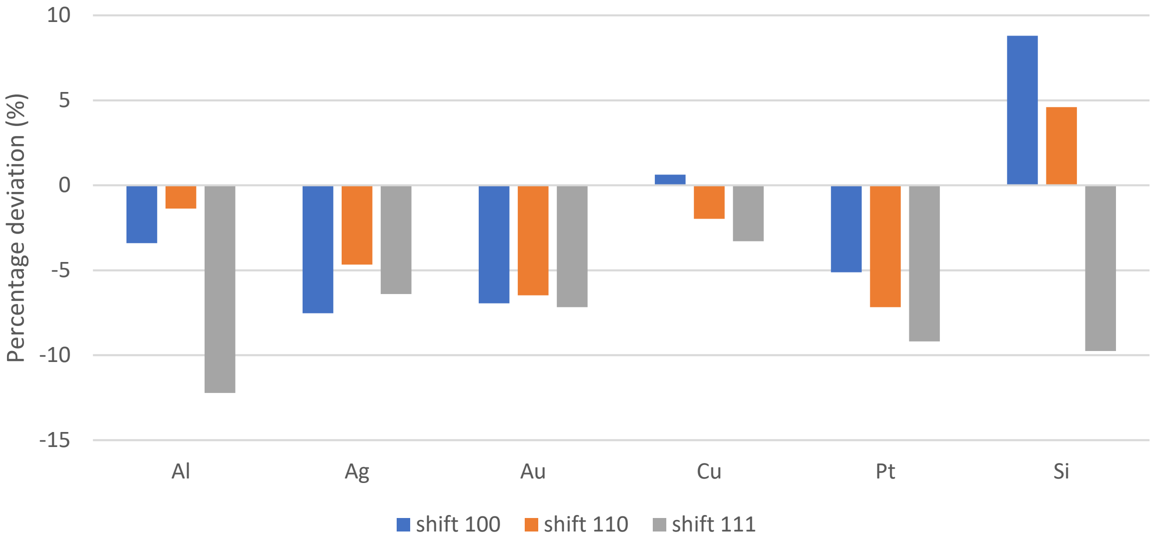

Figure 3.22 – *Discrepancy in work function between values calculate in this study compared to work functions recommended by Kawano* [299].

The calculated work functions show varying degrees of deviation from the "recommended" work functions reported by Kawano [299], which recommends work function values based on a database of theoretical calculations and a range of different experimentally obtained values from a range of techniques. Nevertheless, upon closer examination of this database, it becomes evident that a wide range of work function values obtained from theoretical calculations align with those reported in this study. Lin et al. [98] have discussed the accuracy of work functions calculated using Density Functional Theory (DFT). It is noted that Generalized Gradient Approximation (GGA) functionals, which are commonly employed in DFT calculations, are known to underpredict work functions compared to experimental values; however, they typically agree within a range of 0.2-0.3 eV in most cases, consistent with the results presented in this research. Furthermore, it is important to acknowledge that there are inherent limitations to experimental accuracy when making direct comparisons with theoretical values.

3.4.3 – The role of contamination on work function and surface electronic structure

The impact of water on the work function of common metals is a well-documented phenomenon. Notably, the influence of water on the copper (110) surface has been rigorously examined. Bange et al. [301] conducted a comprehensive study, providing intricate insights into how water exposure affects the work function (WF) of copper. Their findings revealed a notable decrease in the work function in the presence of water. Furthermore, Musumeci and Pollack [302] experimentally observed a reduction in the work function of metals such as platinum, gold, and copper, with the magnitude of these changes falling within ranges similar to those illustrated in Figure 3.17. Additionally, other research has demonstrated that the presence of water can induce bipolar charging during triboelectrification processes [49]. In this work, DFT calculations have revealed that the presence of various surface molecules simulating contaminants can significantly impact the calculated work function of the surface.

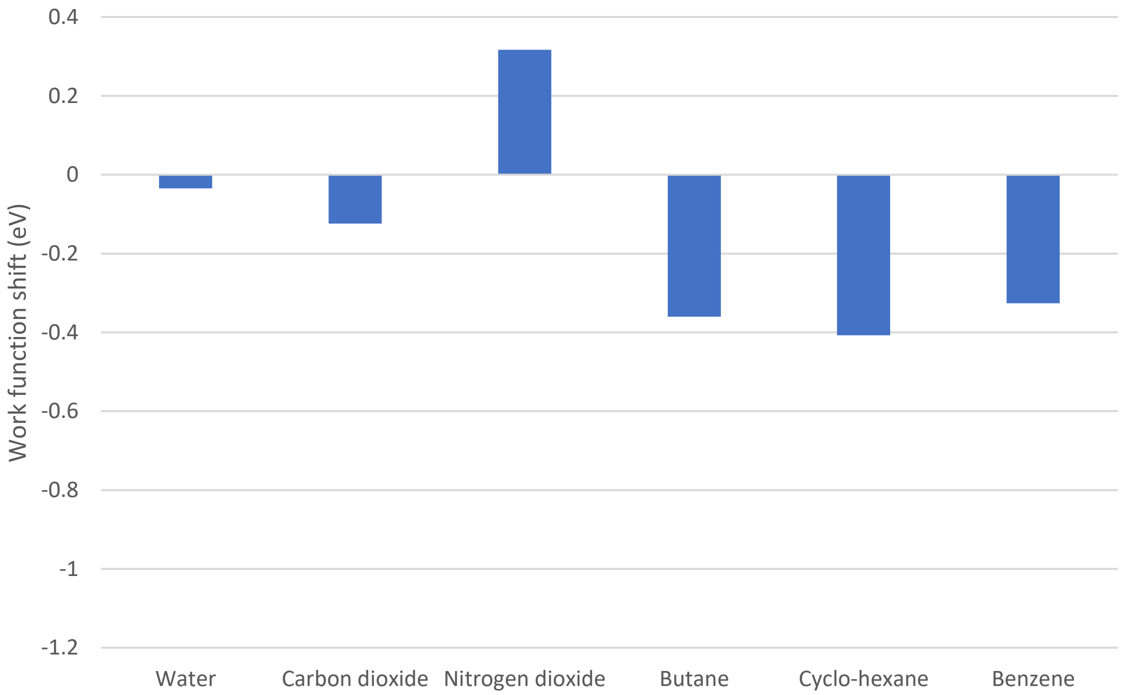

Figure 3.23 – *The calculated work function shift due to the presence of a contaminant molecule on a aluminium (100) surface.*

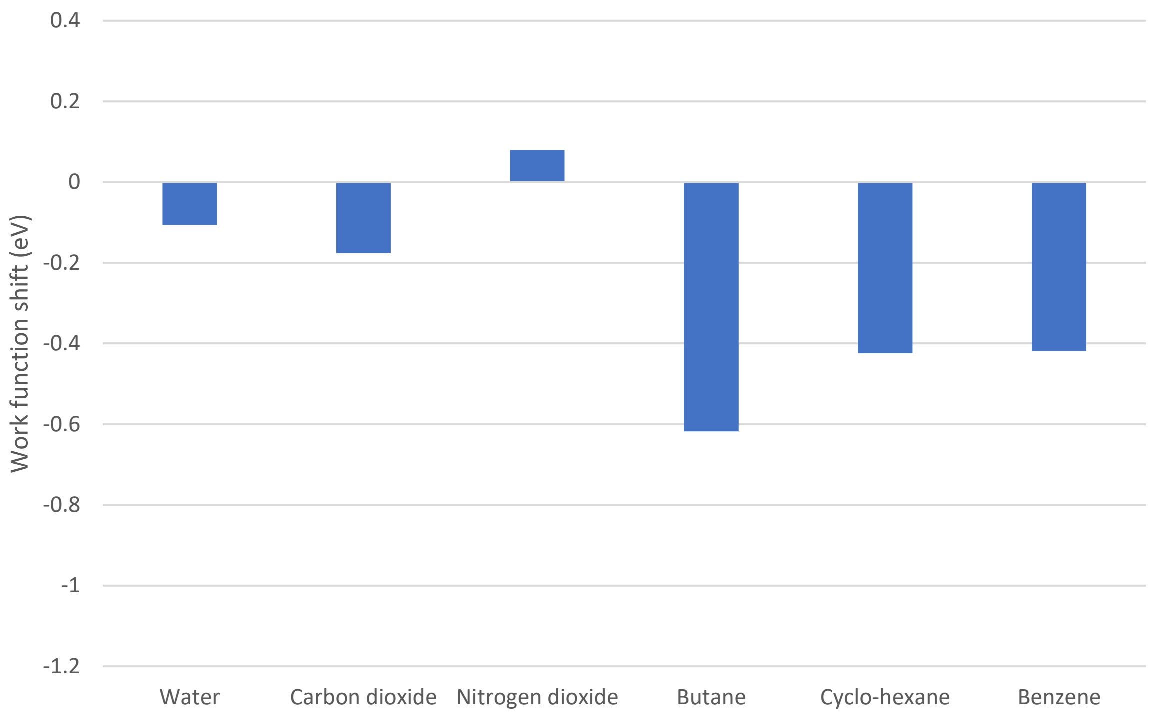

Figure 3.24 – *The calculated work function shift due to the presence of a contaminant molecule on a gold (100) surface.*

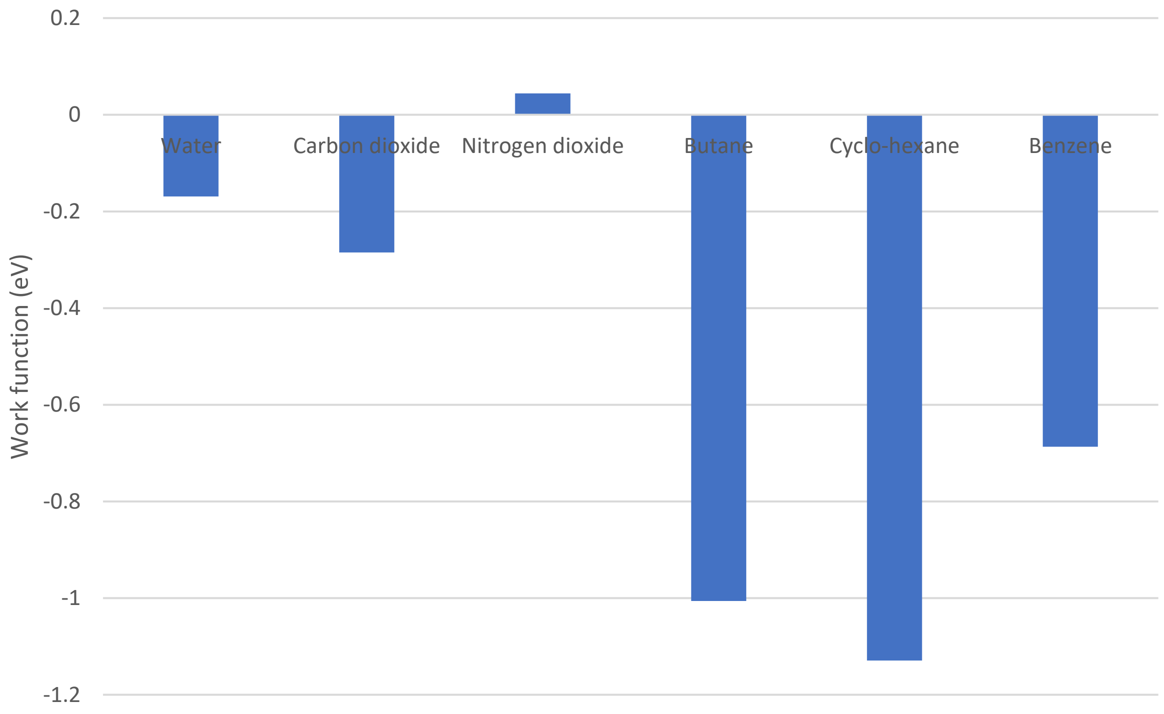

Figure 3.25 – *The calculated work function shift due to the presence of a contaminant molecule on a platinum (100) surface.*

Figures 3.23, 3.24, and 3.25 illustrate the observed work function shifts resulting from various contaminant molecules on the surfaces of aluminium, gold, and platinum, respectively. Firstly, it was consistently observed that water caused a decrease in work function on every surface tested, in line with expectations. However, the decrease in work function was notably less pronounced compared to the initial test cases (Figure 3.18). This can be attributed to the larger unit cell employed to prevent interactions between adsorbate molecules across periodic boundaries. Similarly, carbon dioxide induced a decrease in work function on every material tested. Notably, nitrogen dioxide led to an increase in work function on every surface tested, with this effect being more pronounced on the aluminium surface. In contrast, hydrocarbon contaminants generally resulted in a significant drop in surface work function.

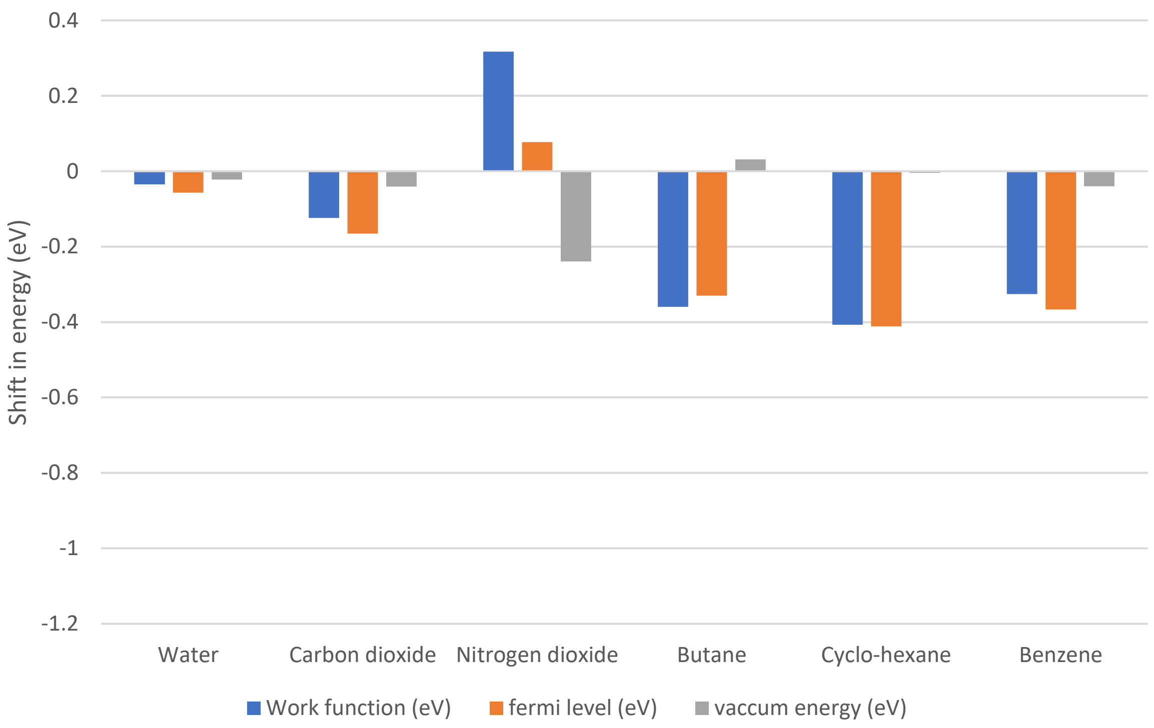

Figure 3.26 – *Shift in work function, fermi level and vacuum energy due to presence of surface contamination molecule on an aluminium (100) surface.*

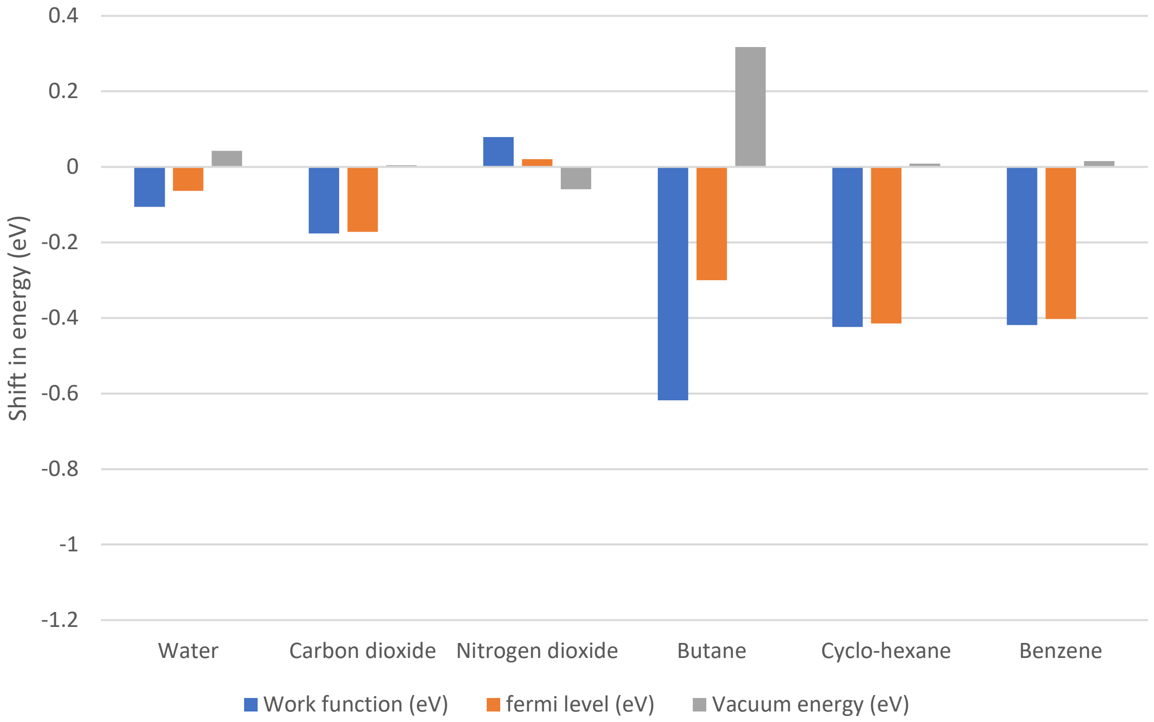

Figure 3.27 – *Shift in work function, fermi level and vacuum energy due to presence of surface contamination molecule on a gold (100) surface.*

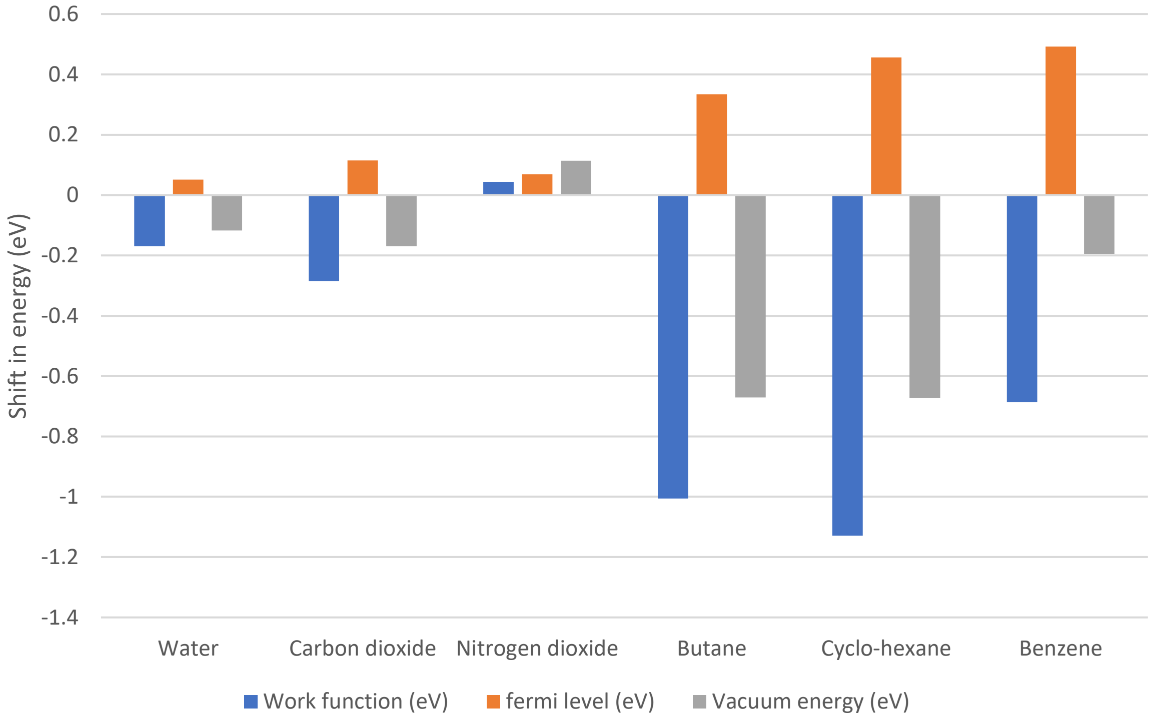

Figure 3.28 – *Shift in work function, fermi level and vacuum energy due to presence of surface contamination molecule on a platinum (100) surface.*

The work function is the difference between the vacuum energy and the Fermi level of the system. Figures 3.26, 3.27 and 3.28 show the calculated works functions alongside the contributions from the fermi energy and the vacuum energy of the surface. Breaking down the contributions in this way presents a more complex picture of the interactions occurring at the surface. In other publications an increase of the Fermi level indicates is taken to indicate an enlarged barrier for electrons [244].

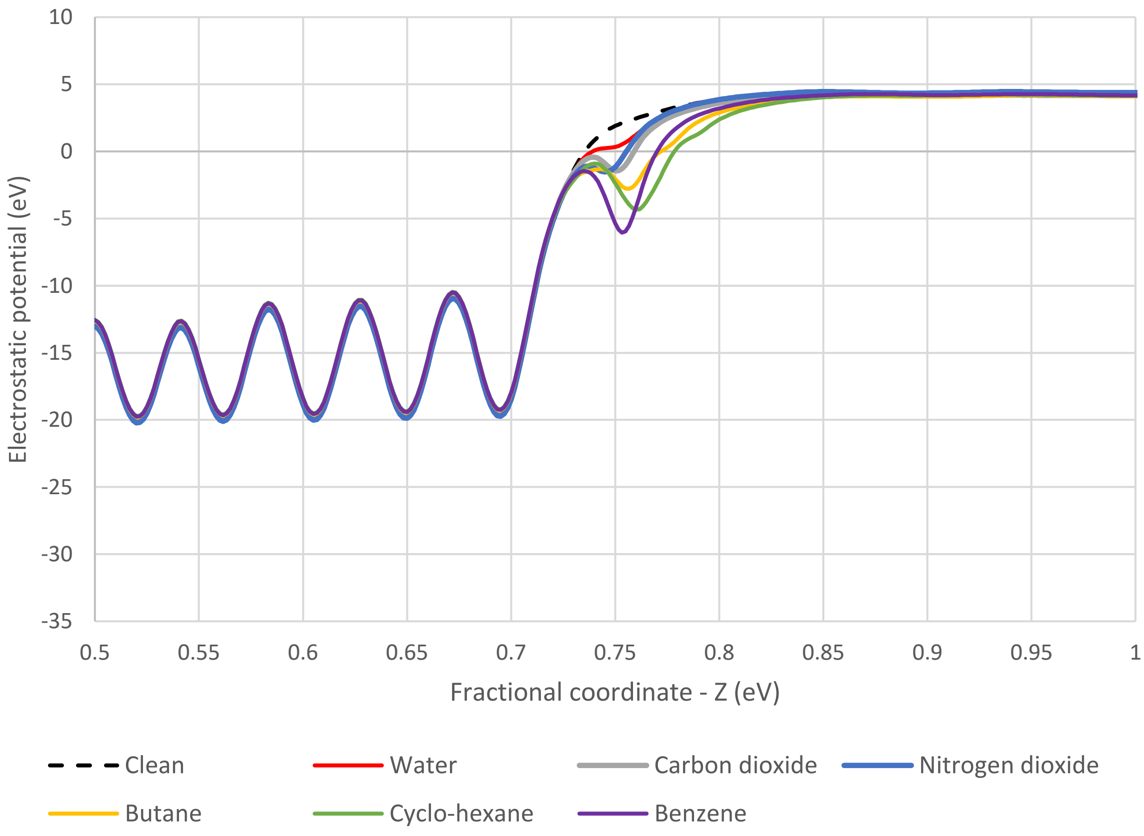

Figure 3.29 – *Shift in surface electrostatic potential due to contaminant molecule on aluminium (100) surface.*

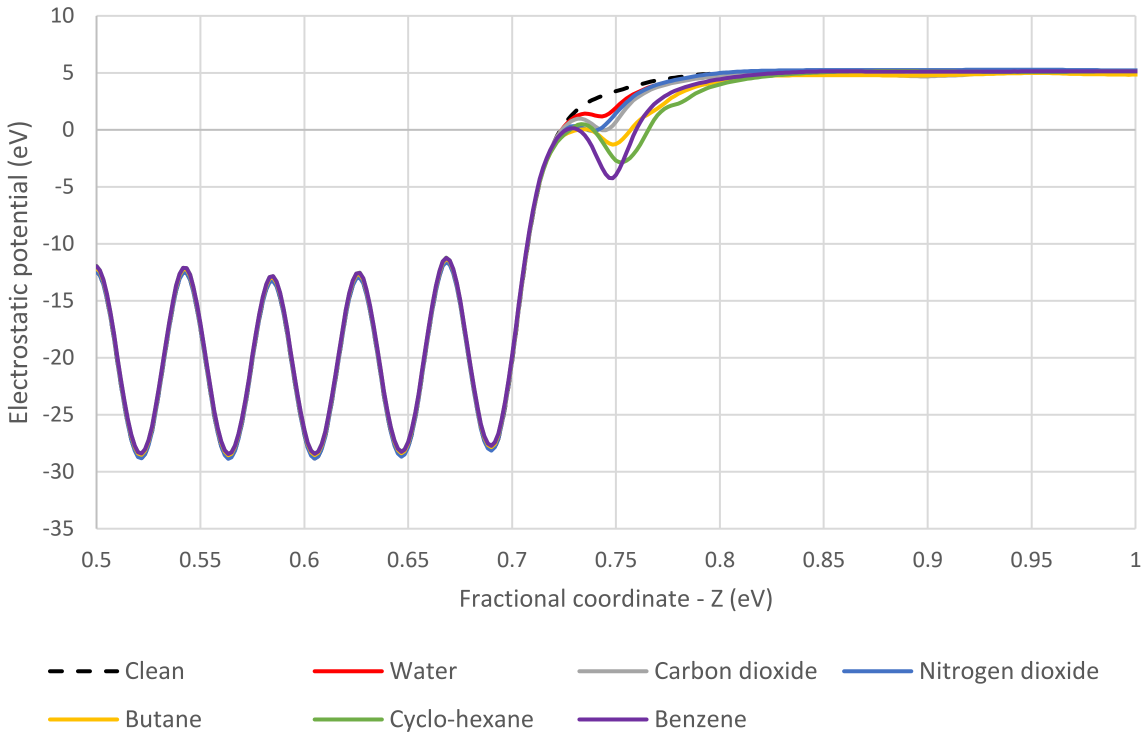

Figure 3.30 – *Shift in surface electrostatic potential due to contaminant molecule on gold (100) surface.*

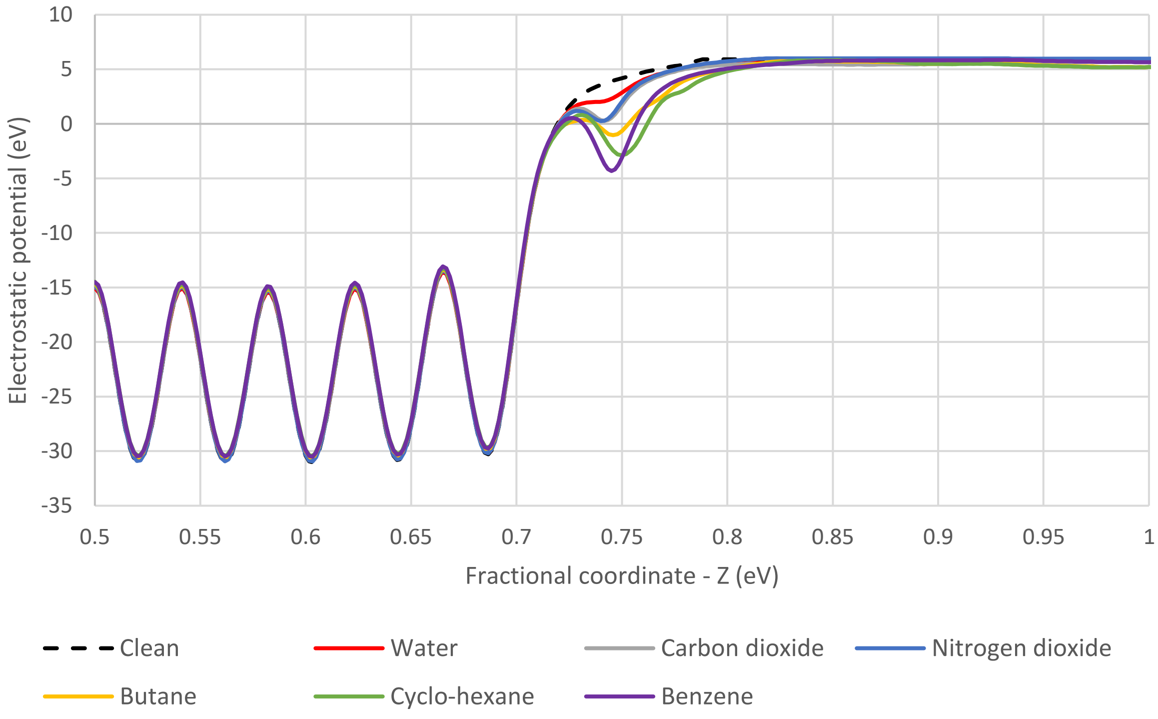

Figure 3.31 – *Shift in surface electrostatic potential due to contaminant molecule on platinum (100) surface.*

Electrostatic potential represents the potential energy of an electron at any point in space, several publications use the calculated electrostatic potential of a system to gain insight into the triboelectric charging mechanism[5,303]. Figures 3.29, 3.30 and 3.31 show the impact of the contaminant molecule on the surfaces of aluminium, gold, and platinum respectively. The fractional coordinate 0.5 represents the centre of the slab and the fractional coordinate represents midpoint of the vacuum region. As expected, a wavelike electrostatic potential is observable in the bulk of the material and this is attributable to the electrostatic potential of individual atoms. The bulk electrostatic potentials of gold and platinum are significantly more negative than that of aluminium and this is attributable to the higher number of filled orbitals in both these materials. When studying electrostatic potential curves there are three main quantities of interest: the vacuum energy which is required to calculate work function, the electrostatic potential offset between two materials and the interfacial energy barrier.

In Shen et al.'s work [155], the electrostatic potential was used in an unsuccessful attempt to predict the direction of charge transfer by modeling the electrostatic potential offset, which is the difference between the macroscopically averaged electrostatic potentials of two surfaces. A similar concept was applied by Jia et al. [303], but in this case, it was used to assess the stability of charges on a material. In the studies conducted by Ko et al. [5] and Gao et al. [212], an increase in electrostatic potential energy above the Fermi level (shown as 0 electrostatic potential in Figures 3.29, 3.30, and 3.31) at the interface between two materials indicates the barrier to charge transfer, as illustrated in Figure 1.7. In this work, only a small interface barrier is observed on surfaces with a hydrocarbon contamination layer, suggesting that a minimal amount of energy is required for electrons to move between surfaces. There is a negligible barrier on surfaces with carbon dioxide and nitrogen dioxide, signifying that no additional energy is needed to transfer electrons to those surfaces.

A slight slope of increasing electrostatic potential is observable at the surface of each material towards the vacuum. This trend appears to be most pronounced for aluminium and is also clearly observable in Figure 3.8. These slopes are indicative of dipole moments forming due to surface contamination [304].

The figures also show a clear influence of the contaminant materials at the surface on the electrostatic potential at the surface, perhaps the most useful comparison is made between the molecules of water, carbon dioxide and nitrogen dioxide. CO_2 and NO_2 display similar electrostatic potential profiles due to their similar composition. The larger hydrocarbon molecules induce the largest electrostatic potential at the surface, with benzene producing the largest peak. This is likely explained by the planar structure of benzene.

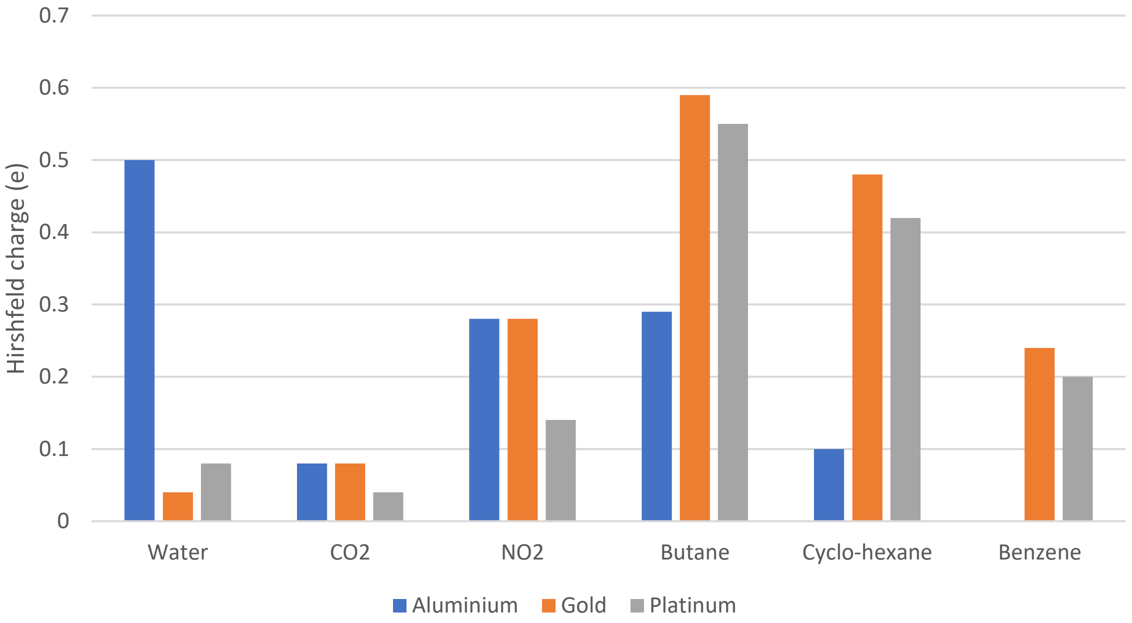

Figure 3.32 – *Change in the calculated sum of the Hirshfeld charges of isolated contaminant molecule versus molecule on the surface.*

Hirshfeld charge analysis has been done on each of the contaminant molecules placed on the surface. Comparing the difference in the calculated Hirschfeld charges between an isolated molecule. Calculations show that the calculated net Hirschfeld charges of the molecule always increase. Water is shown to gain a significant amount of Hirshfeld charge when compared water on a gold or platinum surface. Carbon dioxide and nitrogen dioxide exhibit very similar charging profiles, with the largest net charges being obtained when contacted with a gold or aluminium surface. However, nitrogen dioxide is observed have a significantly larger magnitude of net Hirshfeld charge increase. The hydrocarbon molecules tested they are also observed to share a similar Hirshfeld charge redistribution profile with gold followed by platinum gaining the most significant amount of charge and aluminium gaining significantly less. Benzene offers an interesting case as when in contact with an aluminium surface there is next to no Hirshfeld charge redistribution to the molecule.

Figures 3.33, 3.34, and 3.35 show the redistribution of charge density at the surface due to the presence of a contaminant molecule. For the aluminium surface a restructuring of charge was observed across the surface however overall, there was a charge depletion from the molecule to the surface. For the aluminium surface, the largest charge redistribution is observed at the surface with nitrogen dioxide contaminant. This aligns well with the observation from Figure 2.6 which shows a large shift in the vacuum energy indicating a polarisation at the surface leading to a significantly increased work function. For the hydrocarbon molecules there is a noticeable enrichment of charge on the substrate molecules and for butane and cyclo-hexane there is an observable overall depletion of charge the molecules however there is a move complex restructuring occurring at the surface of benzene. The charge density difference calculations are relatively large compared to those observed from at the aluminium interface. This is like due to the significantly higher number of electrons in these systems. For the gold and platinum surface, in all cases studied there seems to be a significant redistribution charge occurring at the surface molecules indicating regions of positive charge. Unfortunately, due to this significant restructure the more subtle details of the charge distribution occurring outside the surface and within the bulk are being downed out. However, this profile is consistent across all surfaces studied. Of the platinum and gold interfaces the magnitude of the charge density shift also seems to correlate with module used. The hydrocarbons at the surface have a noticeable increase magnitude of redistribution.

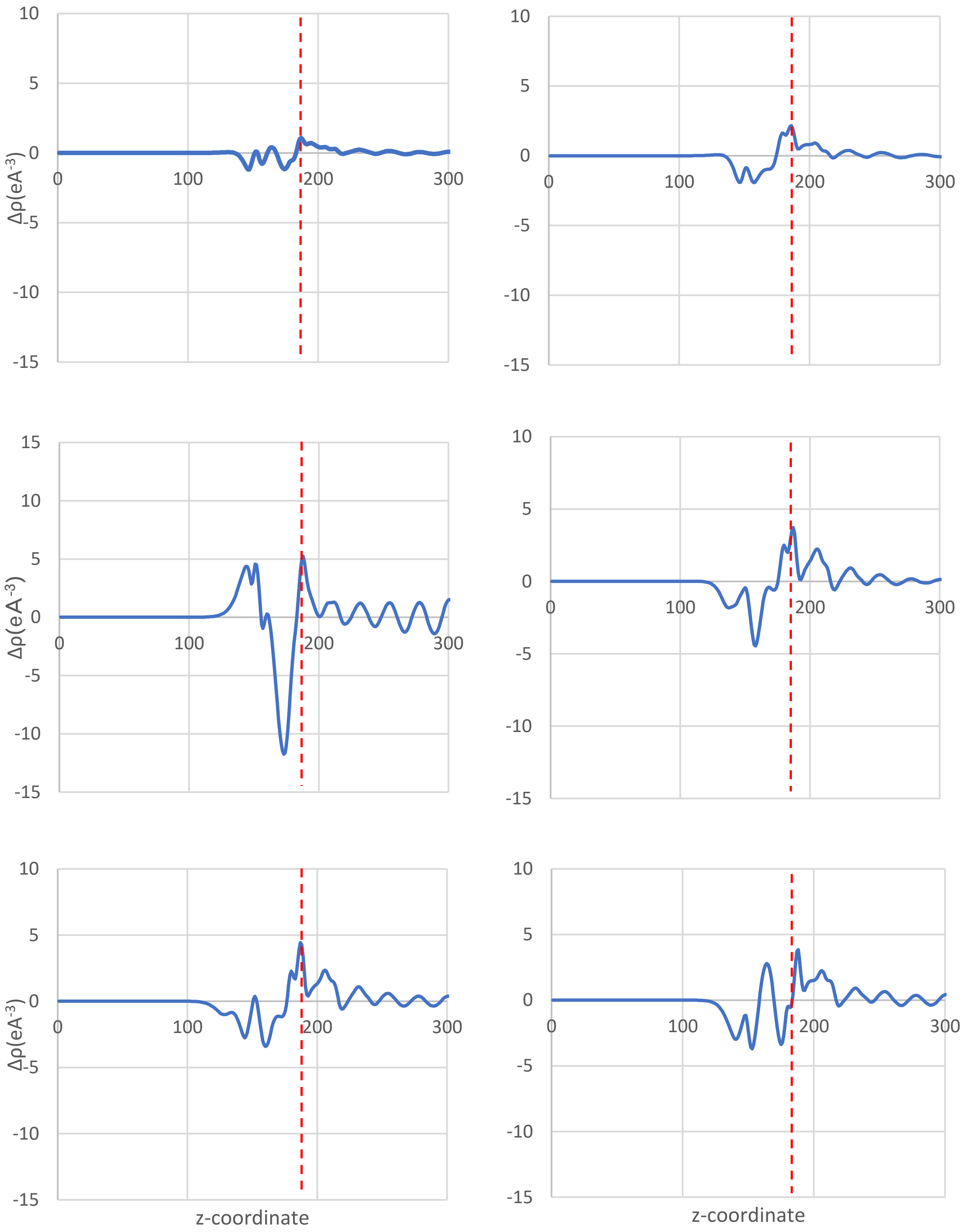

Figure 3.33 – *Charge density difference plot of several contaminants on aluminium (100) surface. Dashed red line highlights the position of the surface aluminium atom. water (top left), carbon dioxide (top Right), nitrogen dioxide (middle left), butane (middle right), cyclo-hexane (bottom left), benzene (bottom right).*

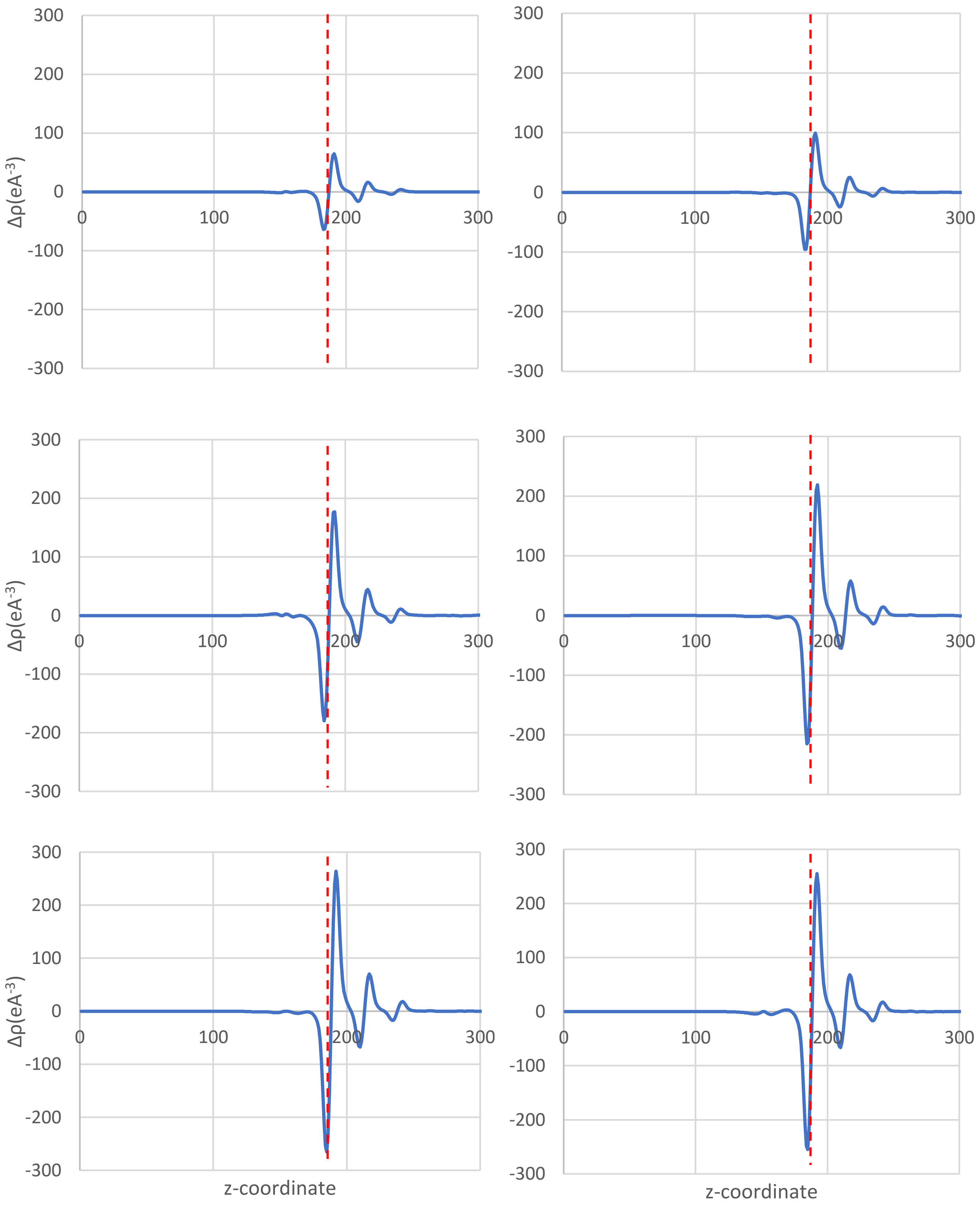

Figure 3.34 – *Charge density difference plot of several contaminants on gold (100) surface. Dashed red line highlights the position of the surface gold atom. water (top left), carbon dioxide (top Right), nitrogen dioxide (middle left), butane (middle right), cyclo-hexane (bottom left), benzene (bottom right).*

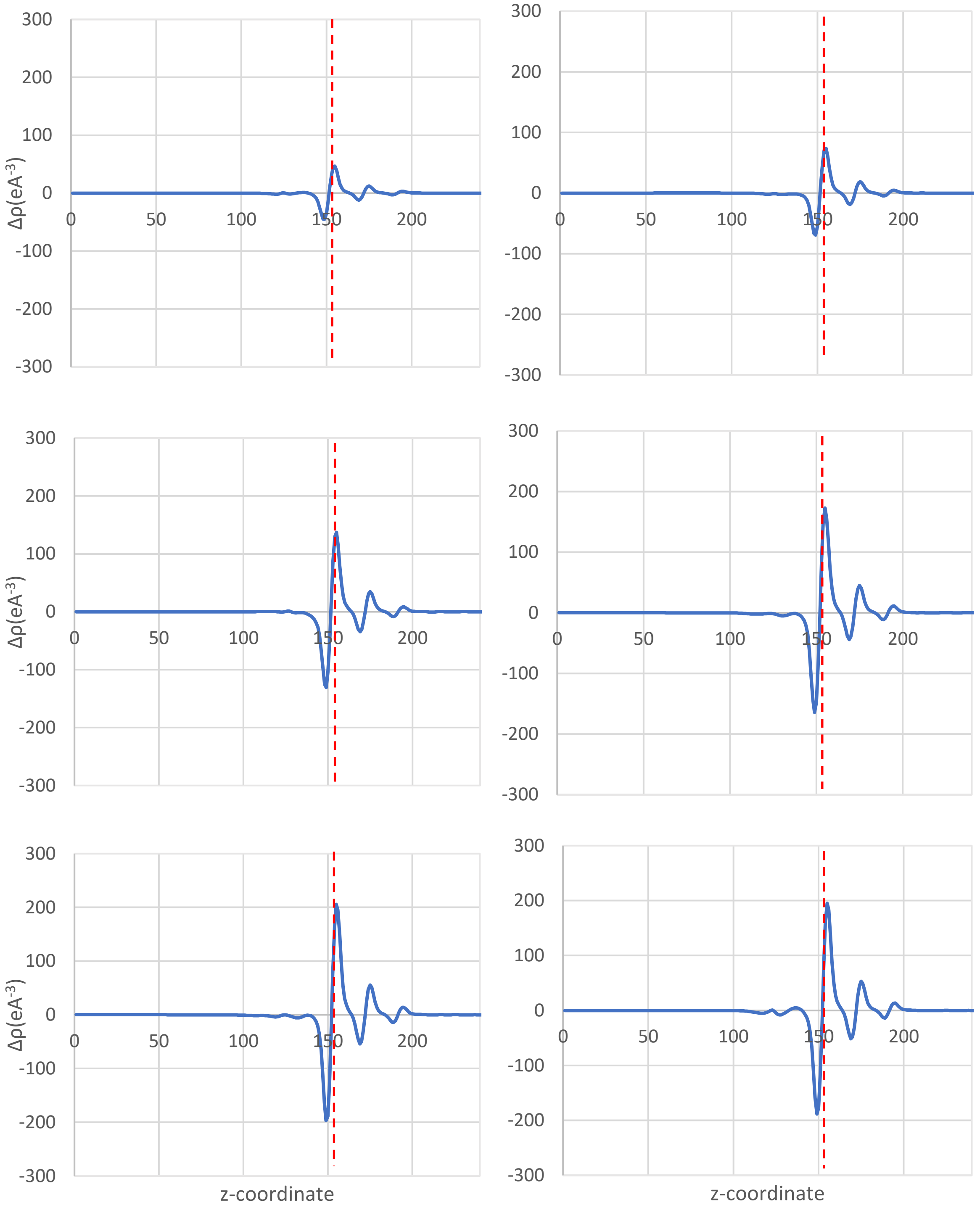

Figure 3.35 – *Charge density difference plot of several contaminants on platinum (100) surface. Dashed red line highlights the position of the surface platinum atom. water (top left), carbon dioxide (top Right), nitrogen dioxide (middle left), butane (middle right), cyclo-hexane (bottom left), benzene (bottom right).*

3.5 – Summary

DFT calculations have been employed to determine the work functions of high-index surfaces for several common metals and pure silicon. These calculations have revealed substantial differences in work functions among different materials and even among facets of the same material. These findings are in line with expectations and align with previously reported work functions from experimental and theoretical sources available in the literature [299].

Three metal surfaces were chosen based on their varying work functions, and the influence of various contaminant molecules was examined. These contaminants were selected to simulate atmospheric, or hydrocarbon pollutants commonly encountered in the environment. The study revealed that the work function shift induced by each type of contaminant was consistent across the tested surfaces. For instance, water consistently led to a decrease in work function, while nitrogen dioxide caused an increase. Notably, hydrocarbon contamination resulted in a significant reduction in work function, a finding supported by previous experimental literature [294].

The introduction of contaminant molecules to the surface demonstrated that environmental contaminants have the potential to significantly impact both the Fermi level, indicating electron transfer and its effect on electronic states, and the vacuum energy, indicating a shift in electrostatic forces at the surface, possibly due to polarization. Hirshfeld charge analysis showed, at least from a theoretical perspective, that it is possible to measure net charge redistributions from a surface to a contaminant molecule. Additionally, the choice of substrate plays a significant role in the amount of charge redistributed, as indicated by the charge density difference plots. Both the contaminant molecule and the choice of metal substrate significantly influenced the charge density distributions at the surface. In preliminary investigations, the influence of several water molecules on the surface was examined, revealing a notable decrease in work function as the number of water molecules on the surface increased. These findings closely align with experimental values reported in the literature [302]. Future research should aim to delve deeper into the study of water films, particularly by investigating the impact of more realistic, disordered networks of water molecules at the surface.

This theoretical work would be greatly assisted by experimental work obtaining quantitative measures of charging of difference surfaces at different facets. From a modeling point of view this work could be further improved by modeling surfaces with total surface coverage to better understand the subtle when modeling the effects of single molecules vs thin films.

Chapter 4 – Prediction of the effective work function of aspirin and paracetamol crystals by Density Functional Theory – A first principles study

4.1 – Motivation and overview

In the preceding chapter changes in the work function and electronic structure due to surface contamination was investigated using DFT calculations, it becomes evident that shifts in material work function are likely to occur not only due to its inherent chemistry or atomic arrangement at the surface but also due to the interactions with environmental molecules adhering to surface, resulting from factors such as atmospheric gases, humidity, or contamination from pollutants. While first principles calculations have been used extensively to investigate this phenomenon beyond the topic of triboelectrification, especially in fields like photovoltaics and semiconductors, there remains a lack of research utilizing these methods to understand and predict the charging behaviour of pharmaceutical materials.

Triboelectrification is a significant problem within the pharmaceutical industry. Given that a substantial portion of drug and excipient substances are managed in powder form, they become susceptible to triboelectric charging and undesired charging can be highly disruptive to pharmaceutical processes. Just as observed in other procedures involving powdered materials, there is a propensity for these substances to adhere to vessel walls and pipelines, leading to product loss and increased downtime for cleaning. More specifically to pharmaceuticals, the agglomeration induced by triboelectric charging holds the capacity to jeopardize the uniformity of blends. which can result in the non-compliance of a material batch with regulatory standards. Moreover, the ramifications of triboelectrification extend to drug delivery methods. This is notably critical in the context of aerosolized medications like inhalers, where the behaviour of micronized drug particles is significantly affected. Gaining deeper insights into the triboelectric charging of pharmaceutical powders holds significant value for the industry. Such insights empower pharmaceutical companies to refine their processes and design their active pharmaceutical ingredients (APIs) in ways that mitigate these detrimental effects.

Modeling charge transfer in materials has historically relied heavily on the material work function, a key parameter. However, this method is notably less accessible when it comes to insulating materials compared to metals. Established techniques like photoemission spectroscopy and Kelvin probe force microscopy are effective for assessing the work function of metallic and semiconducting materials[99,163]. However, their utility diminishes when attempting to characterize the work function of insulating materials[305,306]. The intrinsic high resistivity of these materials leads to charge accumulation and low electron mobility at the surface, presenting challenges in achieving accurate measurements.

Consequently, investigations into the experimental or theoretical determination of the work function for pharmaceutical materials, primarily comprising insulating molecular crystals, are rare. In recent times, Density Functional Theory (DFT) has garnered significant attention as a tool for investigating the impact of crystal orientation[300,307], surface chemistry[308], deformation[47], and surface water[57] on the work function. Recent progress has been made through the use of Density Functional Theory (DFT) to explore the influence of crystal orientation, surface chemistry, deformation, and surface water on the work function. DFT has great utility in predicting the work function of conducting and semiconducting materials from first principles, and its and has also been successfully applied to the electronic structure calculations of insulating crystals[309]. This methodological framework forms a robust foundation for calculating the 'effective' work function of pharmaceutical materials, showing promise for future research.

Electronic structure calculations, such as those done by DFT, offer a potential way to understand and predict charging in pharmaceutical materials. There is limited research on applying DFT to study the triboelectric charging of pharmaceutical materials in literature. However, one notable exception is the work done by Brunsteiner et al.[310]. In this study the charging behaviour of several pharmaceutical materials was predicted from first principles using DFT by comparing the calculated work function, ionisation potential and the highest occupied molecular orbitals (HOMO) to experimentally obtained charging data.

In this work, DFT is used to predict the effective WF of several crystal facets of paracetamol and aspirin and explore the effect of adsorbed water molecules. Electronic structure calculations are performed using the CASTEP Density Functional Theory package[277], to determine the electrostatic potential and effective WF and how these quantities change in the presence of water.

4.2 – Theoretical Approach

Electronic structure calculations are performed to determine the electrostatic potential and WF within the framework of periodic Density Functional Theory (DFT). The Generalised Gradient Approximation (GGA) Perdew-Burke-Ernzerhof (PBE) exchange-correlation functional is used[226]. On-the-Fly Generated (OTFG) ultrasoft pseudopotentials are used in all cases. Dispersion forces are expected in this system, so the Tkatchenko-Scheffler (TS) dispersion correction is applied to account for van der Waals interactions and hydrogen bonding[235]. The kinetic energy cut-off for the plane wave basis is set at 630 eV, to ensure the system is well converged. The crystal structures of aspirin and paracetamol are obtained from the Cambridge Structural Database as a starting point for calculations (Figure 4.1) [311]. A geometry optimisation calculation is then performed on these structures to minimise the total energy of the system with respect to atomic positions. The structures are optimised using the limited memory Broyden–Fletcher–Goldfarb–Shanno (LBFGS) method [312]. Convergence tolerances for the geometry optimizations were 5.0×10^{-6} eV for change in energy, 1.0×10^{-2} eV/Å for force, 5.0×10^{-4} Å for displacement and a stress tolerance of 2.0×10^{-2} GPa. For the electronic minimisation, a tolerance of 5.0×10^{-7} eV was selected for the total energy per atom. These convergence criteria are used throughout. For geometry optimisation calculations of the bulk unit cell a Monkhorst-Pack grid of (2x4x2) and (2x3x4) is used for k-point sampling for aspirin and paracetamol, respectively.

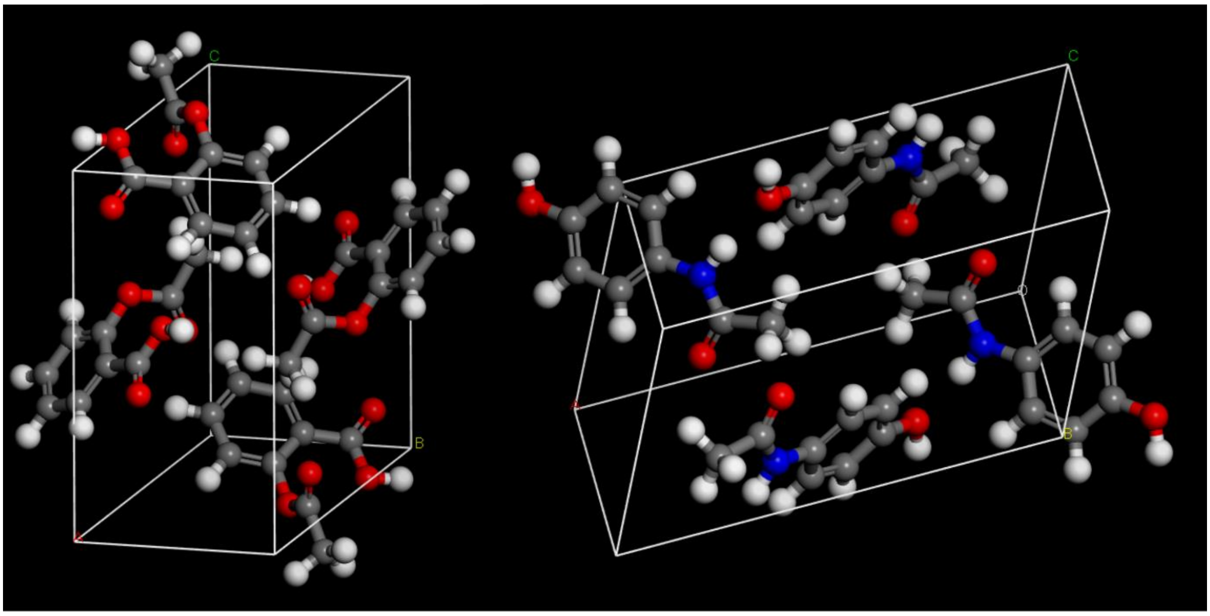

Figure 4.1 – *Bulk unit cells of aspirin (ACSALA01) (left) and paracetamol (HXACAN01) (right). Crystallographic Information Files downloaded from the Cambridge Crystallographic Data Centre website* [311].

The shape of these crystals is predicted by using the Bravais, Friedel Donnay and Harker (BFDH) model. This is a geometrical approach that relates external shape to inter-plane distance, but does not take into account atom type, bonding or partial charges which all impact crystal growth[313]. However, this technique has been applied successfully to study the facets of crystalline materials[314–316] and has also been previously paired with DFT calculations to study surface electronic structure in other studies[317]. CCDC Mercury software is used to generate the BFDH morphologies of aspirin and paracetamol shown in Figure 4.2. Four surfaces are selected from each morphology which are considered to represent the primary facets of the crystal and are listed in Table 4.1.

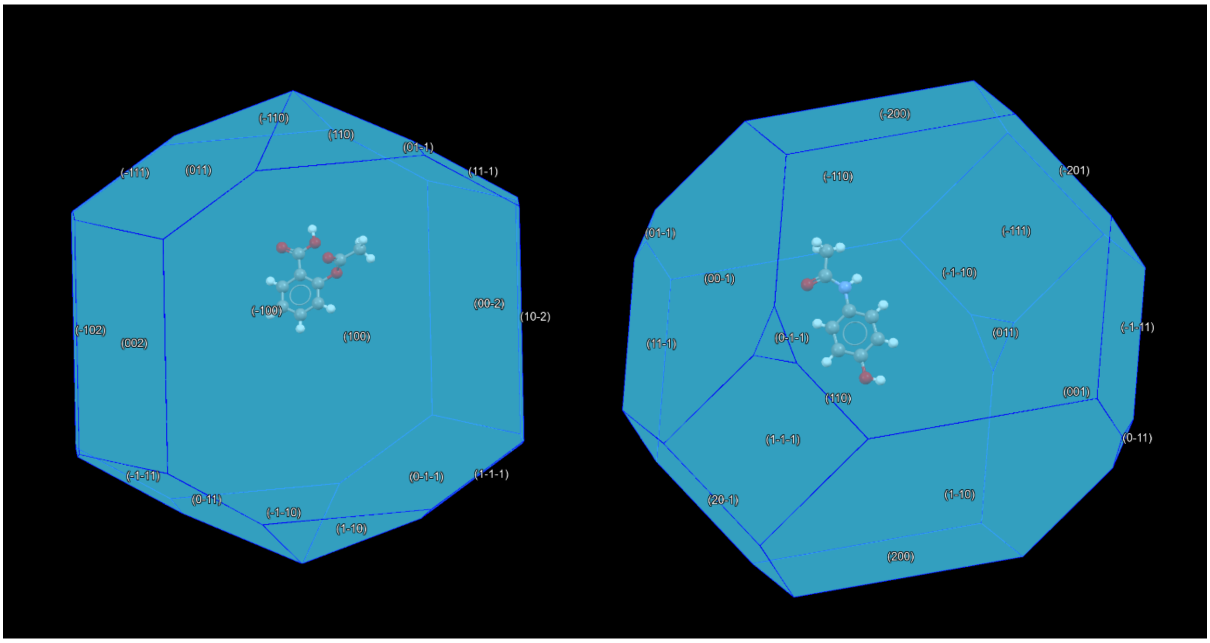

Figure 4.2 – *Crystal morphologies of aspirin (left) and paracetamol (right) generated using the BFDH facility in CCDC Mercury.*

Surfaces are constructed from these optimised structures using the Materials Studio – Materials Visualiser. Supercells are constructed consisting of a thin slab of material separated from its periodic images by a layer of vacuum (Figure 4.3). To ensure that the top and bottom surfaces of the slab are identical, a slab thickness of *N* unit cells equivalent length are always used. A vacuum gap of 30 Å is used to prevent interaction between periodic slabs so that the vacuum energy can be accurately determined. DFT calculations require that the number of k-points in each direction are inversely proportional to the simulation cell parameters [197]. The Monkhorst pack grid used for each surface is given in Table 4.1.

Table 4.1 – *The selected surfaces of aspirin and paracetamol with their associated Monkhorst-Pack grid.*

Material	Surface	Monkhorst-Pack grid (a x b x c)
Aspirin	(002)	2 x 4 x 1
Aspirin	(011)	2 x 2 x 1
Aspirin	(110)	2 x 2 x 1
Aspirin	(100)	2 x 4 x 1
Paracetamol	(200)	3 x 4 x 1
Paracetamol	(011)	2 x 3 x 1
Paracetamol	(110)	2 x 2 x 1
Paracetamol	(001)	4 x 2 x 1

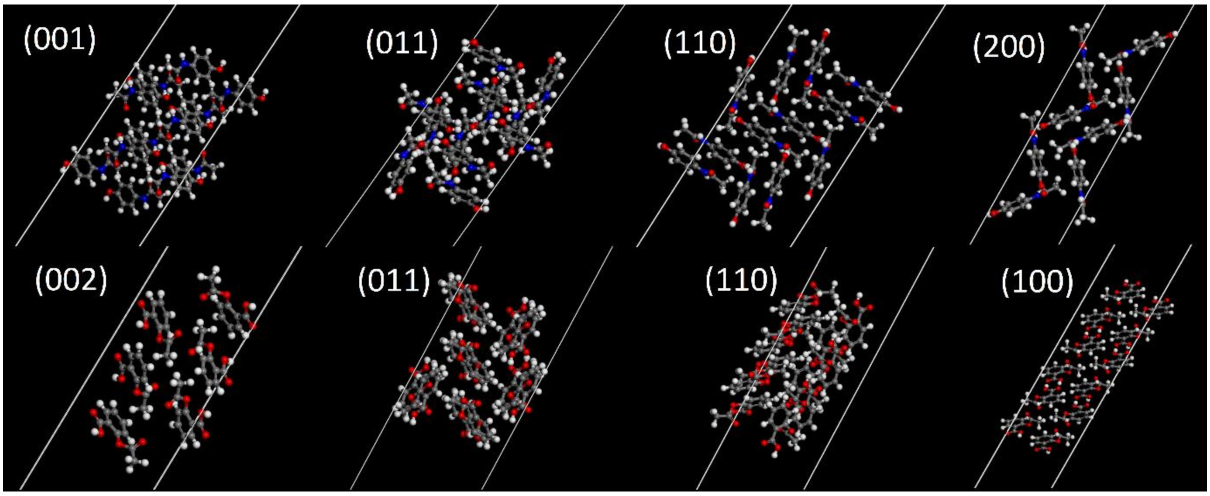

Figure 4.3 – *Labelled periodic cells of paracetamol (top) and aspirin (bottom) used in calculations. Visualised using the Materials Studio – Materials Visualiser.*

The work function (WF) is calculated using the equation,

$$WF = E_{vac} - E_F \qquad \text{Eq. 3.1}$$

where (E_{vac}) is the vacuum energy, defined as the electrostatic potential in the vacuum gap when it reaches an asymptotic value. The Fermi energy (E_F), the highest energy electron of the system at 0 K, is calculated at half of the energy gap [318]. This is shown in Figure 4.4. A convergence study was carried out testing the dependence of calculated effective WF on the kinetic energy cut-off, slab thickness and layers of constrained molecules at the surface. These tests were performed on an aspirin (100) surface (Figure 4.5) and additional slab-thickness calculations were performed on an aspirin (011) surface for comparison (Figure 4.6). Testing the dependence of cut-off energy on effective WF, single point energy calculations were performed on the aspirin (100) surface at values ranging from 25-800 eV using a 3N unit cell thickness slab. It was found that calculated WF values had converged well by 300 eV. The impact of the number of constrained surface layers was also tested and found to be negligible to the predicted effective WF.

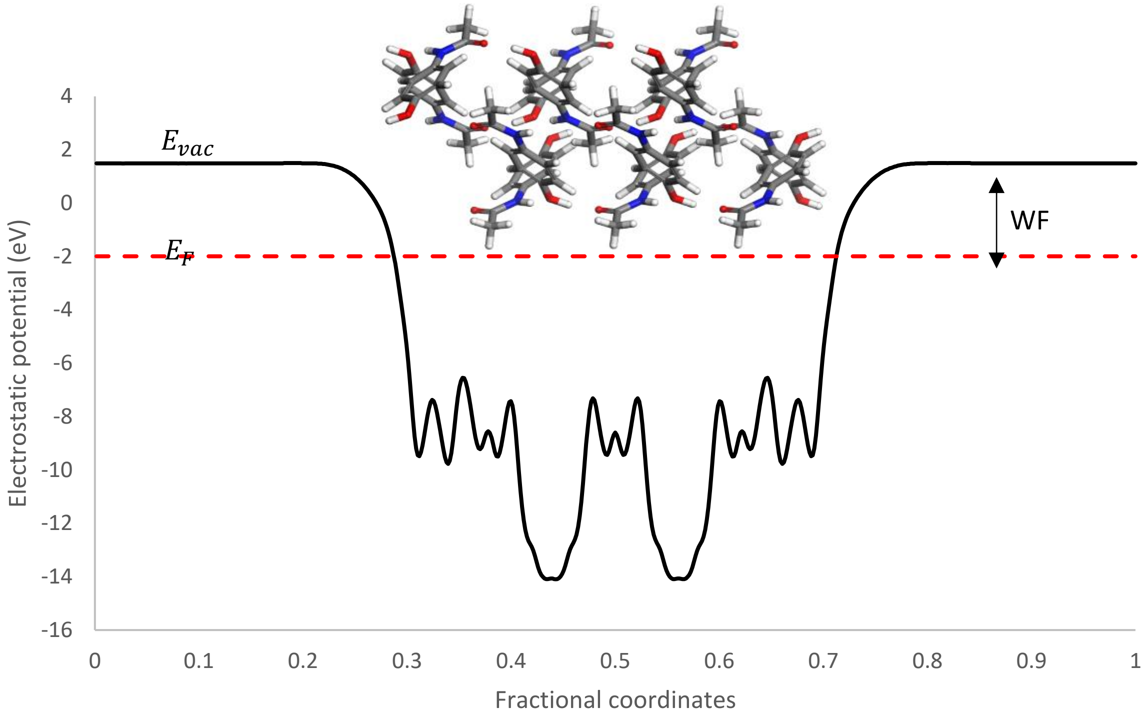

Figure 4.4 – *Electrostatic potential of a (001) paracetamol slab. Slab thickness = 23 Å. Vacuum thickness = 30 Å . Fermi energy of the system (E_F), the vacuum energy (E_{vac}) and the effective WF are labelled in the graph.*

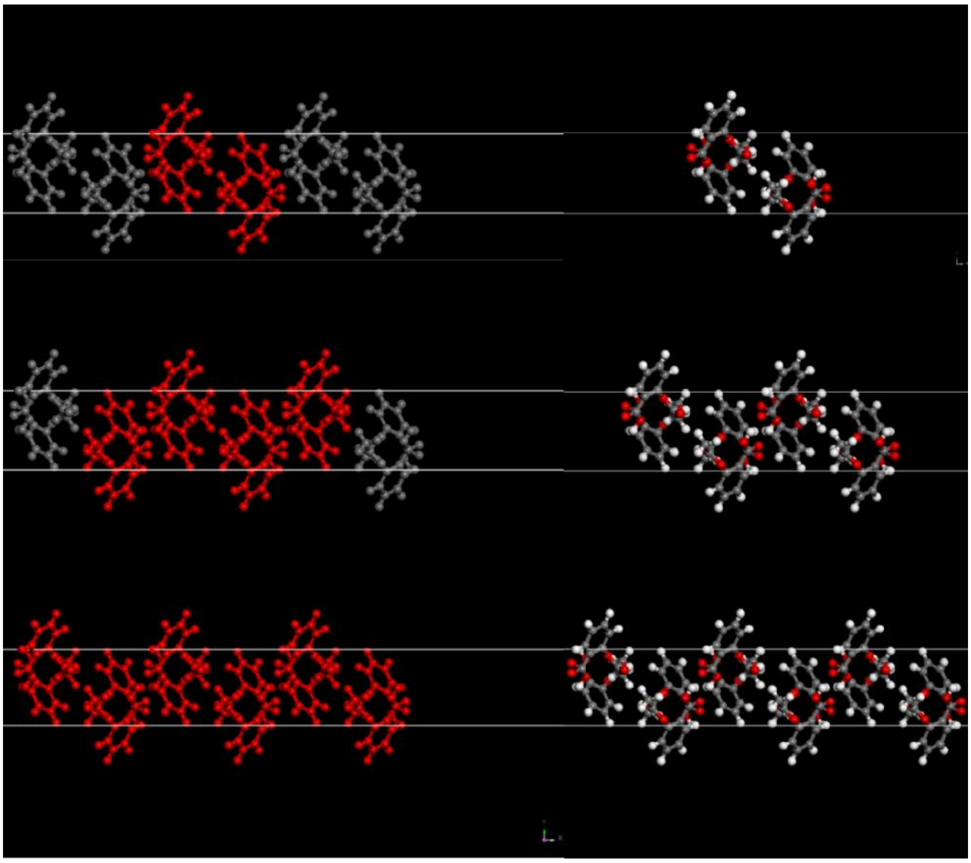

Figure 4.5 – *Illustration of different levels of constraint and slab thickness to an aspirin 100 surface. Fully constrained (bottom left), 1 layer unconstrained (middle left), 2 layers unconstrained (top left). 1 unit cell thickness (right top), 2 unit cell thickness (right middle), 3 unit cell thickness (right bottom).*

Changes in effective WF due to the number of unconstrained surface layers were found to be negligible. However, one layer of surface molecules was left unconstrained for each surface tested to accommodate structural changes due to the presence of surface water. Figure 4.6 shows the variation of calculated effective WF with slab thickness, in terms of length and N unit cell thickness, for both surfaces tested. The relatively large unit cells associated with aspirin and paracetamol show that a thin slab of one unit cell equivalent length has largely converged. However, a slab thickness equivalent to three unit cells was used for all materials to ensure good electrostatic potential calculations within the bulk and to provide surface layers for structural relaxation in the presence of water.

The surfaces of pharmaceutical molecules are complex and will typically consist of several different elements, chemical bonds and interacting molecules. This creates many local minima, where a water molecule might settle in a geometry optimisation calculation. Furthermore, the work of Li et al.[319] highlights the profound impact that adsorption location can have on the electronic structure of a surface within the context of triboelectric charging. Thus, the role of the aforementioned adsorption location should be considered when optimising a surface. Due to this, the impact of surface water was also investigated by placing a single molecule of water on each selected surface. A coarse grid search and DFT geometry optimisation of the water molecule was performed on each surface to find the lowest energy configuration. The effective WF was then calculated for this structure. The grid search was done using the FORCITE molecular mechanics module of Materials Studio 2021. The Universal force field [260] was selected to model interactions, due to its ready availability and also proven performance in calculating adsorption energies, being in good agreement with experimental results in other studies [320].

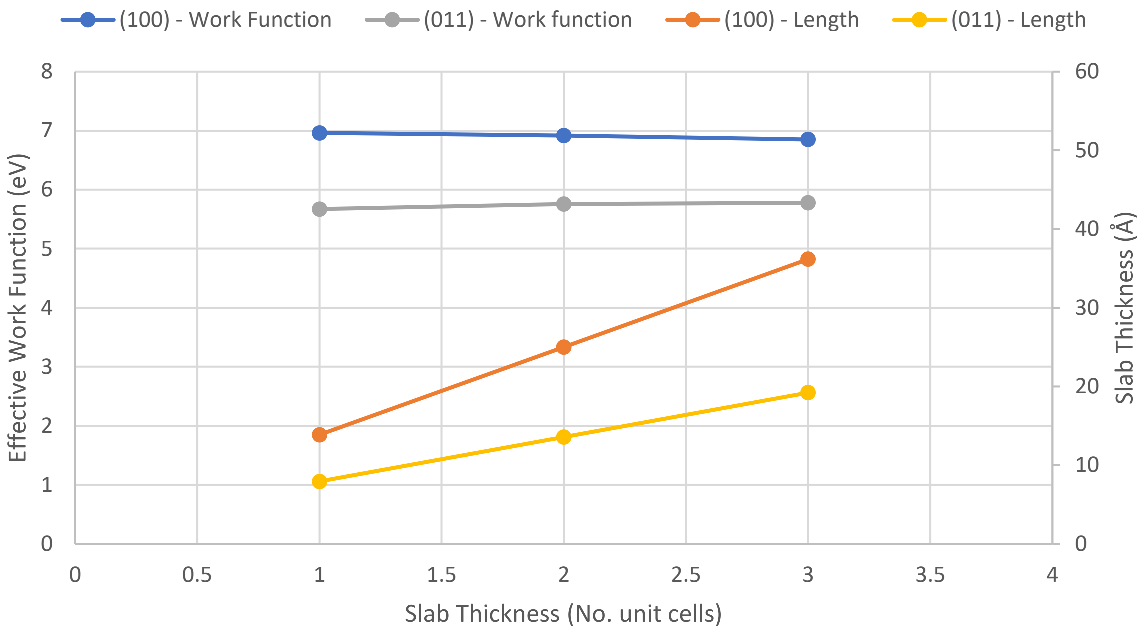

Figure 4.6 – *Effect of Slab thickness in terms of equivalent unit cell distances on slab length perpendicular to the surface on calculated effective WF.*

4.3 – Results and Discussion

The results of the calculated effective WF of several aspirin and paracetamol surfaces with and without the presence of water are summarised in Table 4.2. They change significantly depending on both the material and surface tested, as also shown graphically in Figure 4.7. The highest effective WF observed is associated with aspirin (100) at 6.9 eV and the lowest being paracetamol (001) at 3.5 eV. The range of values observed is itself interesting. A comprehensive review of experimentally-determined WF for a wide range of elemental materials has been compiled by Kawano [299]. The majority of the WF published in this work are within the range or 2-6 eV. The effective WF calculated here are in a similar range. Pharmaceutical materials are primarily composed of carbon, hydrogen oxygen and nitrogen. However, these calculations show that despite similarities in elemental composition, the differences in the calculated effective WF can be significant. This observation shows the importance of atomic structure, bonding and surface termination. From Table 4.2, comparing the surfaces of the same material, the effective WF of both systems varies by up to 1.4 eV and 1.3 eV for aspirin and paracetamol, respectively.

Table 4.2 – *Calculated effective WF of selected surfaces of aspirin and paracetamol. Clean and in the presence of a single water molecule. The change in effective WF due to water (ΔWF) is also shown.*

System	Surface	Effective work function (eV)		ΔWF (eV)
		Clean	H_2O	
Aspirin	002	5.5	5.7	0.2
Aspirin	011	5.9	6.3	0.4
Aspirin	110	6.4	6.2	-0.2
Aspirin	100	6.9	7.0	0.1
Paracetamol	200	4.8	4.9	0.1
Paracetamol	011	4.5	4.3	-0.2
Paracetamol	110	4.6	4.7	0.1
Paracetamol	001	3.5	3.9	0.4

Other works comparing the WFs shift due to different surface functionalities are within this range [308,321]. There is a noticeable distribution of the effective WF between facets. This result is in line with expectations, as anisotropic WFs have been observed in many crystals [299,309,322]. Even metal surfaces, whose surface terminations are extremely similar, have experimentally-verified variations in their WF due to differences in the atomic packing at the surface, which is comparatively minor compared to the differences in surface termination expected for pharmaceutical materials[323]. It is therefore not surprising that the systems tested in this work also show this effect. Additionally, the effective WF of aspirin is consistently higher than that of paracetamol for all surfaces. The extent of charge transfer between two materials is dependent on the difference in their WF, and a material with a lower WF is expected to transfer electrons to materials with higher WF, resulting in a negative charge for the latter [67]. The WF of stainless steel is reported as 4.3 eV [324], and is indicated in Figure 4.7, which is consistent with the negative polarity and stronger charging propensity of aspirin as compared with paracetamol. The trend is also in line with the experimental work by Šupuk et al. [31], who tested the charging propensity of a large number of pharmaceutical powders against stainless steel, and found that both aspirin and paracetamol charged negatively against stainless steel, with aspirin charging more strongly. Other calculated effective WF values for pharmaceutically relevant materials are reported in literature, however this surface anisotropy is typically neglected [310,325,326].

The effect of adsorbed water on the calculated effective WF of each surface was also investigated. The impact of surface chemistry and surface contamination on effective WF are of great interest in other fields [327,328]. Humidity is known to significantly affect the charging process [25]. Atomistic studies on surface water in the context of triboelectric charging will typically use either a film-based[57,155] or molecule-based[319,329] based approach. A film-based approach models multiple layers on the surface, which is arguably more analogous to a real surface; however, it adds significant complexity to the calculation. Molecule-based approaches are less computationally intensive and allow for more detailed study of the different co-ordinations of water at the surface. In this work, water was simulated on each surface by optimising a single water molecule on to the surface, similarly to Li[319]. It was found that in the presence of water an effective WF shift in all surfaces was produced (Figure 4.9). Interestingly, the magnitude of this effective WF shift was found to change depending on which surface the water molecule was placed. The effective WF was found to increase in the presence of water for six out of eight surfaces analysed, indicating that more energy is required to remove electrons from such surfaces, so a surface with adsorbed water is more likely to get charged negatively. However, for aspirin (110) and paracetamol (011) the effective WF was found to decrease, therefore making it easier for electrons to be removed from the surface. The effective WF shift due to humidity is significant, relevant to the charging of similar materials, which has also been reported in the literature[32]. This shows that, theoretically, there is an apparent driving force for charge transfer between water-adsorbed and dry surfaces, even for idealised surfaces. This result is also reported by Mukherjee et al. [325] who calculated a similar decrease in effective WF due to surface water on multi-crystalline cellulose. The role of surface coverage was also examined by calculating the fractional coverage of a water on the surface (Figure 4.8) and comparing it to the magnitude of the WF shift (Figure 4.9) to determine if it is correlated with the amount of water per unit area. No significant correlation was observed between surface water coverage and effective WF shift.

Figure 4.9 shows an increase and decrease in effective WF depending on the coordination of water molecules on the specific facet is very interesting. In the work by Anagaw et al.[308] their theoretical calculations suggest that a shift in effective WF is strongly correlated with the surface dipole due to surface modification. In this work a highly polar molecule, water, is added to the surface. The observation that the effective WF can both increase and decrease in the presence of water shows that the bonding location of the water molecule on the surface is an important consideration. The unit cell parameters used to calculate surface coverages are given in Table 4.3.

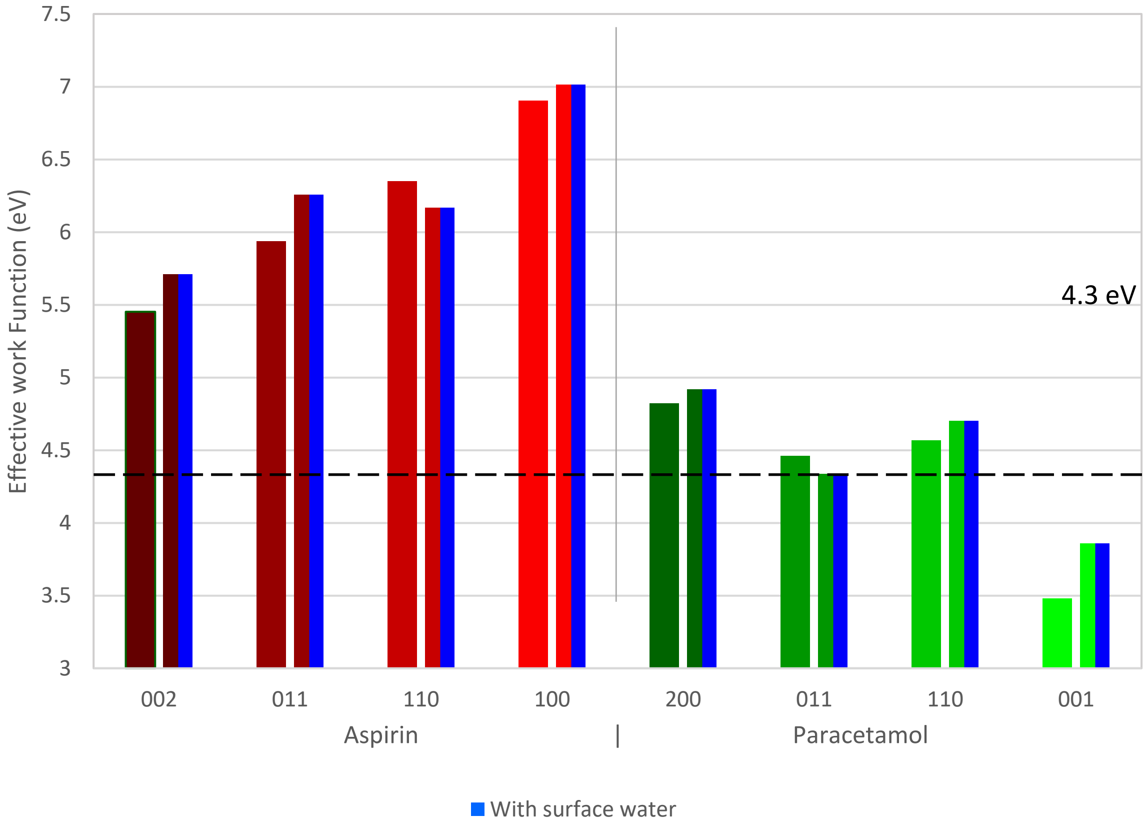

Figure 4.7 – *Calculated effective WF of selected surfaces of aspirin (002, 011, 110, 100) and paracetamol (200, 011, 110, 001) and showing the effective WF difference between facets and effective WF shift induced by the fractional coverage of water onto the surface. The dashed line represents the effective WF of stainless steel as reported by Wilson*[324] *and its difference with various facets represents the propensity for charge transfer.*

Table 4.3 – *Cross sectional dimensions of each-unit cell axis normal to the surface (a and b) and their intersecting angle (γ), with calculated values of area of exposed surface and the fractional coverage of water, respectively. Diameter of water is taken as 2.8 Å based on the work of D'Arrigo*[330]*. Illustration of periodic unit cell presented alongside.*

System	Surface	a (Å)	b (Å)	γ (°)	Exposed surface (Å^2)	Fractional Coverage
Aspirin	002	11.24	6.51	90.00	73.23	0.08
Aspirin	011	11.25	13.10	83.55	146.39	0.04
Aspirin	110	11.37	13.00	96.43	146.78	0.04
Aspirin	100	6.51	11.37	90.00	73.99	0.08
Paracetamol	001	12.68	9.04	90.00	114.66	0.05
Paracetamol	011	12.68	11.43	75.73	140.55	0.04
Paracetamol	110	7.00	14.84	82.66	103.02	0.06
Paracetamol	200	9.04	7.00	90.00	63.28	0.10

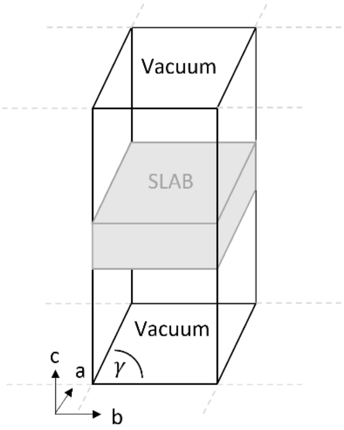

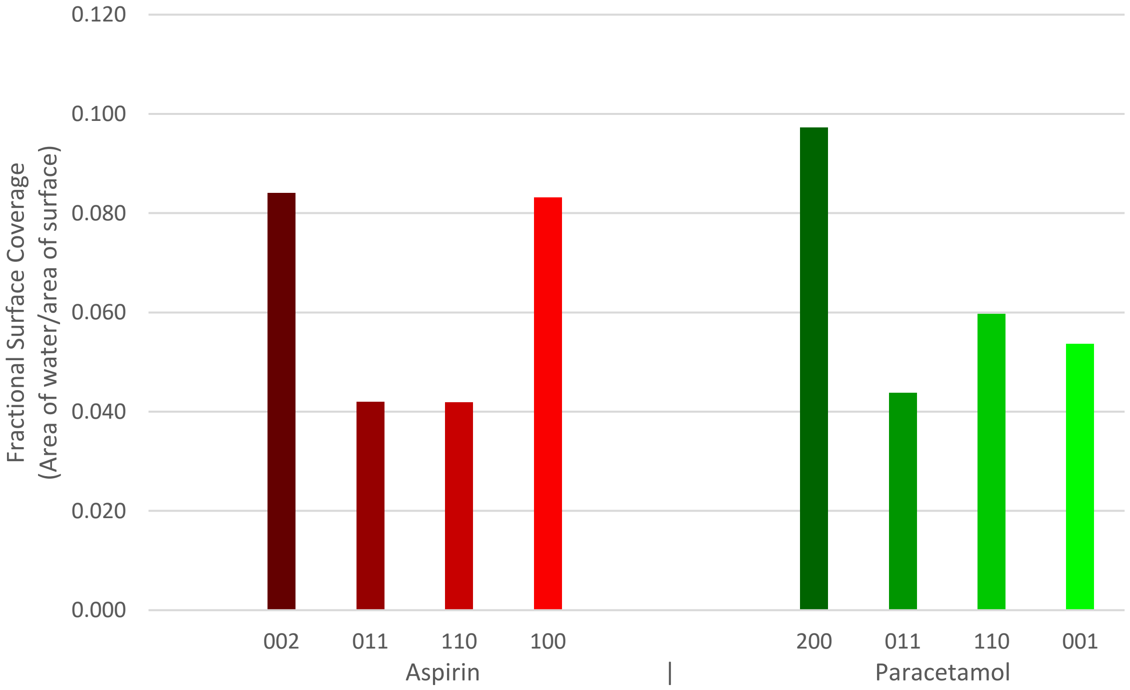

Figure 4.8 - *Surface coverage of water for each system, taken as the fractional coverage. The coverage area is based on the circular area of a water molecule with a diameter of 2.8 Å.*

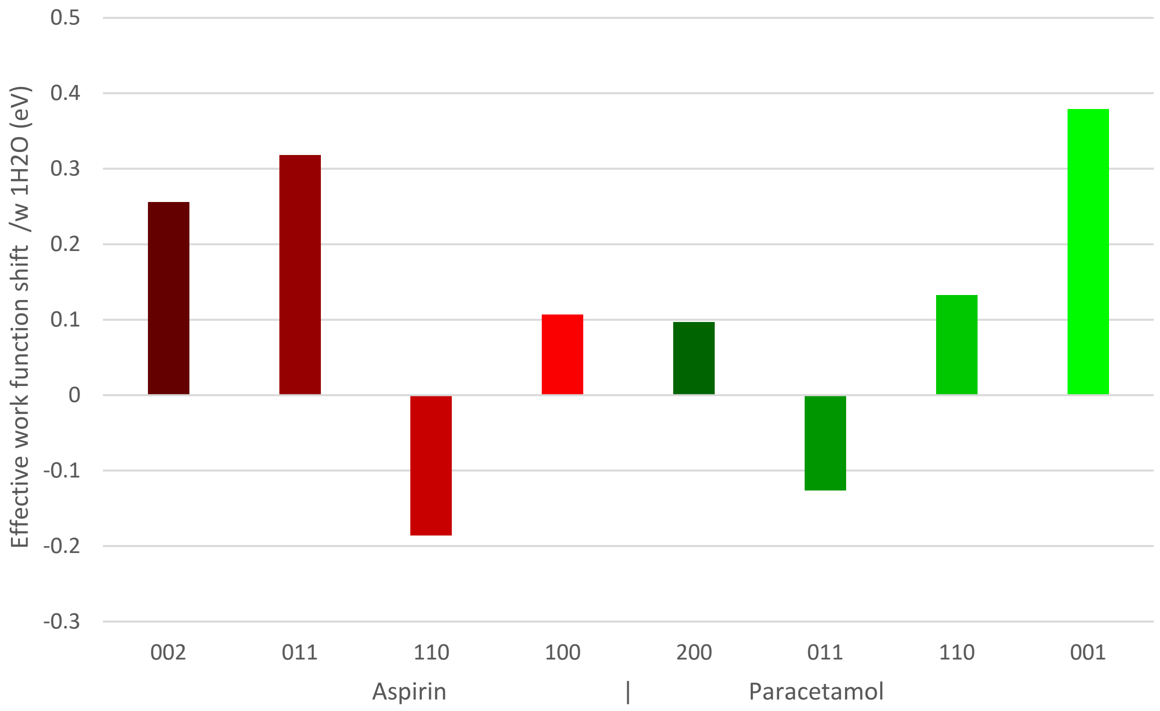

Figure 4.9 – *Effective work function shifts due to the presence of water on the surfaces of selected facet of aspirin (002, 011, 110, 100) and paracetamol (200, 011, 110, 001)*

The surface termination of paracetamol and aspirin is shown in Figures 4.10 and 4.11 respectively, with their calculated effective WF values shown. They reveal the different orientations of molecules at the facet and the population of functional groups exposed at the terminating layer. On visual inspection of the aspirin surface there are several electron withdrawing carboxyl groups, placed prominently at the interface. For comparison, Heng et al.[331] observed that a higher degree of hydrophobicity was observed on the (100) compared with (011), which is attributed to more prominent carboxyl groups. This is consistent with the surfaces used in this work. Conversely, for paracetamol surfaces there is a greater population of electron donating hydroxyl groups at the surface and electron withdrawing amide groups are less prominent. In other work Heng et al.[332] has confirmed the surface anisotropy of paracetamol using X-ray photoelectron spectroscopy, where (001) surfaces were found to have the highest proportion of polar hydroxyl groups which is also consistent with our model.

Anagaw et al.[308] studied the impact of adsorbed organic molecules on semiconductor surfaces, and reported a WF shift due to the electron donating/withdrawing properties of several organic functional groups and the dipole formation at the surface. Therefore, it is possible to hypothesise, in the context of the surfaces of pharmaceutical crystals, that facets with relatively high populations of electron withdrawing groups should be expected to have high WF, whereas facets with high populations of electron donating groups have lower WF.

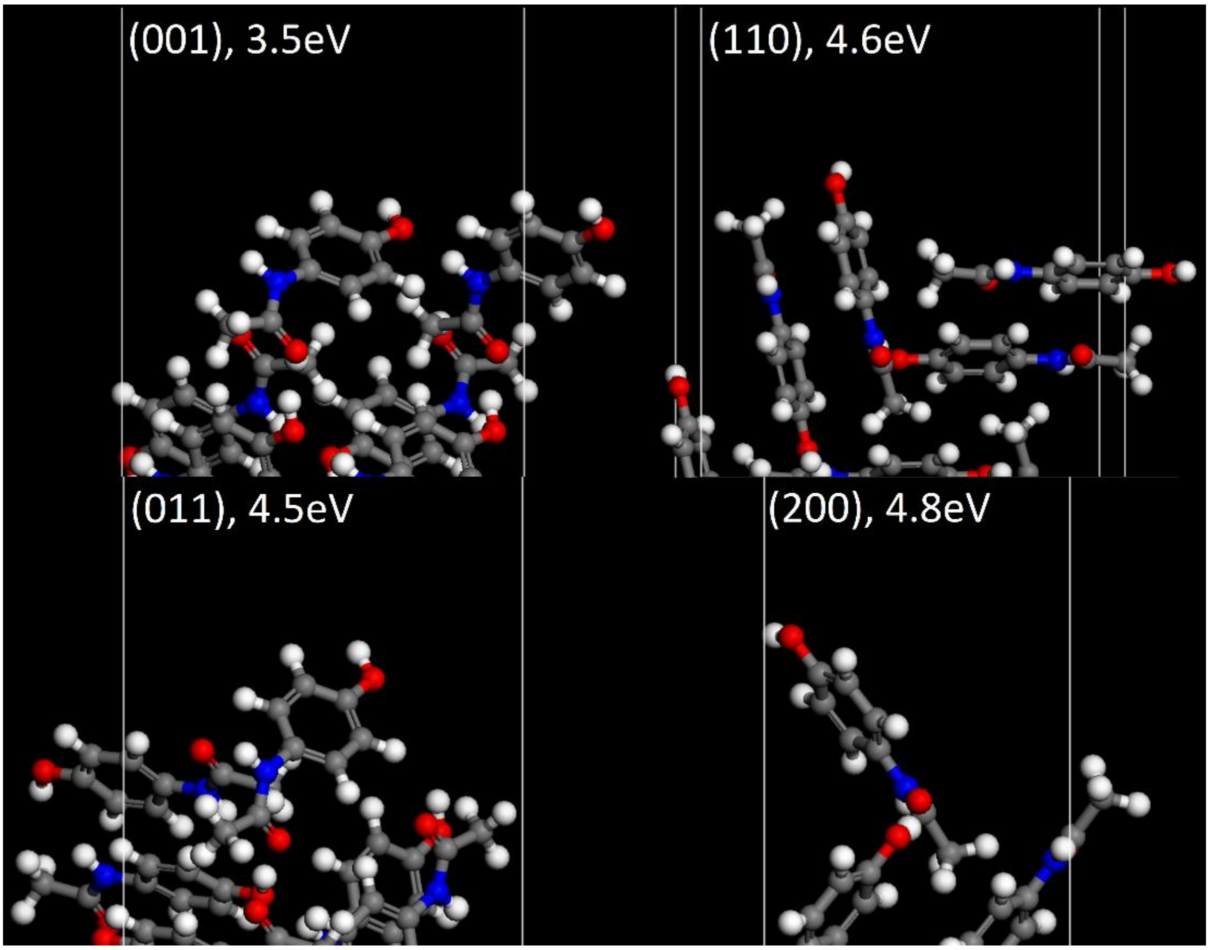

Figure 4.10 – *The termination of each paracetamol surface simulated. Calculated effective WF shown above.*

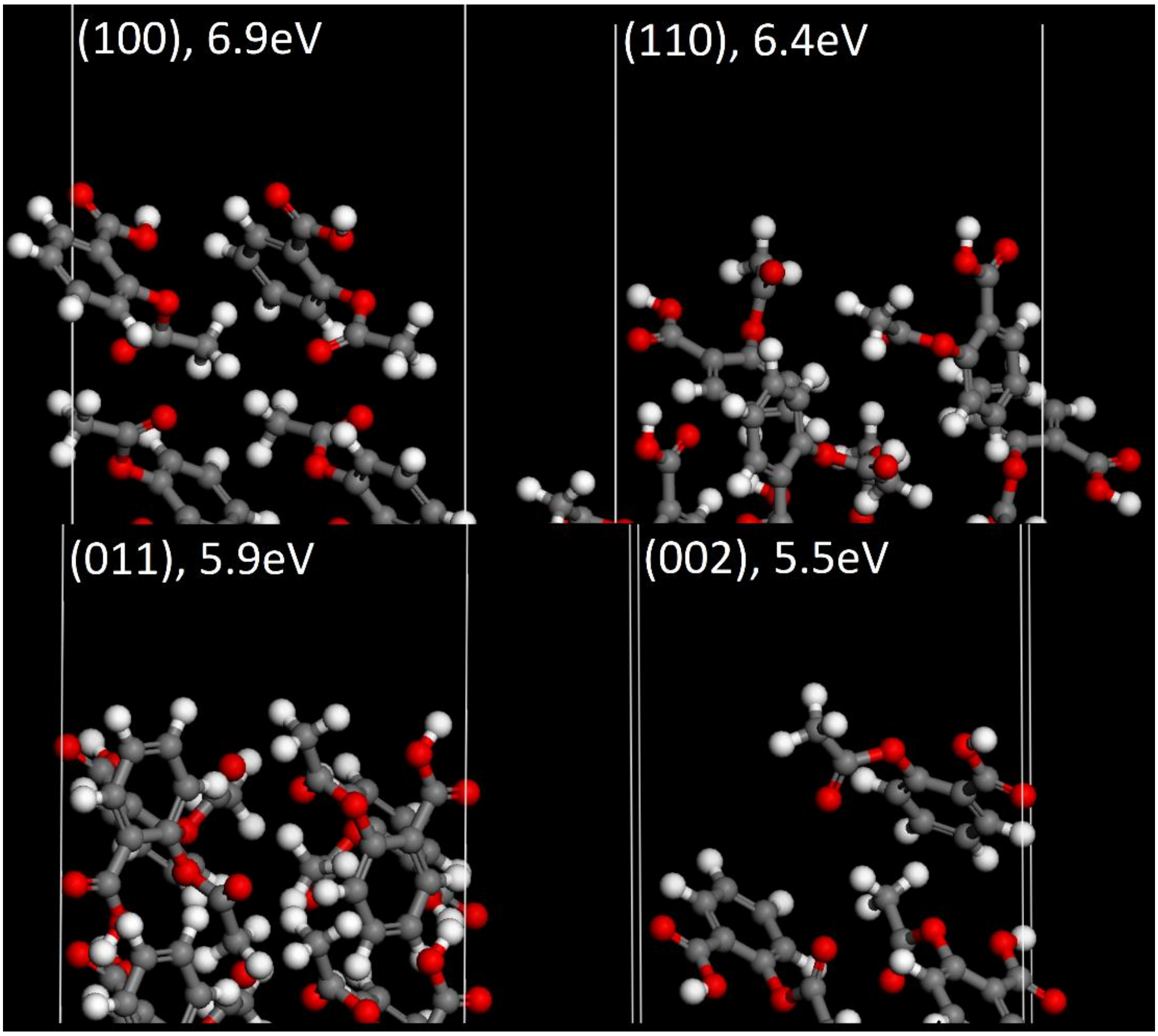

Figure 4.11 – *The termination of each aspirin surface simulated. Calculated effective WF shown above.*

Figure 4.12 shows the electrostatic potential of the aspirin (002) slab, highlighting a shift in potential caused by the addition of water molecules to the surface. The graph is superimposed onto an image of aspirin (002) as a visual aid to show the position of molecular water relative to the slab with the water molecules labelled A and B. As previously mentioned, a coarse grid search was performed to determine the most energetically favourable position of the water molecules on each surface. During this search, it was observed that the positions of the water molecules would always converge towards two well defined locations, depending on the initial search position of the water. Position A is more energetically favourable and taken as the global minimum for this surface, and B is taken as a local minimum. Due to this, aspirin (002) is selected to investigate the impact of multiple water molecules adsorbed onto the surface at different locations.

Comparing the clean surface, shown in black, to the surfaces with adsorbed water, shown in blue and red in Figure 4.12, shows the addition of water molecules causes a perturbation in the electrostatic potential towards the surface. The perturbation caused by molecule A is consistent between simulations. Black arrows emphasize the electrostatic potential attributed to the water molecules, illustrating the formation of a potential well that signifies a region of heightened stability. The potential energy then quickly returns to typical bulk behaviour towards the centre of the slab (fractional coordinate = 0.5), and is unaffected by the surface water, showing the electrostatic potential of the bulk is not influenced by surface water. Since WF is effectively a measure of binding energy of electrons on a surface, the electrons of a material with a higher WF take more energy to remove. For aspirin (002) the addition of several water molecules appears to make this surface more energetically favourable for it to accept electrons.

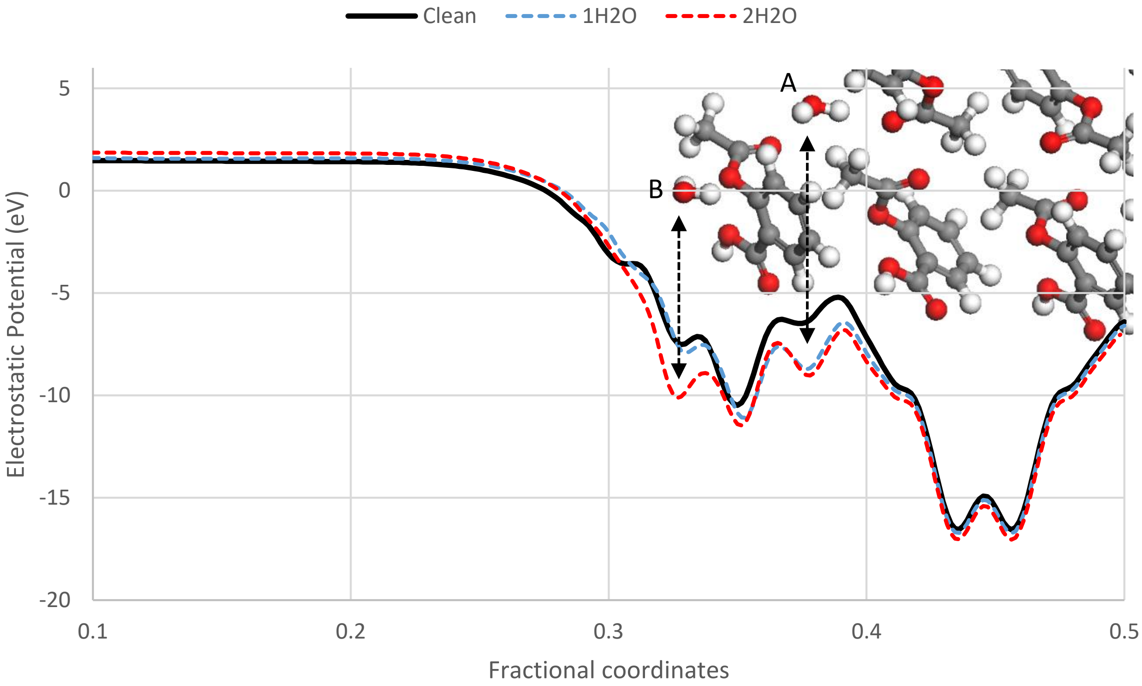

Figure 4.12 – *Comparison of the calculated electrostatic potential of aspirin (002) surfaces used to derive the effective WF with and without water molecules. Clean surface (black); single H_2O molecule adsorbed on surface of the unit cell, labelled A (blue); two H_2O molecules adsorbed on surface of the unit cell, labelled A and B (red).*

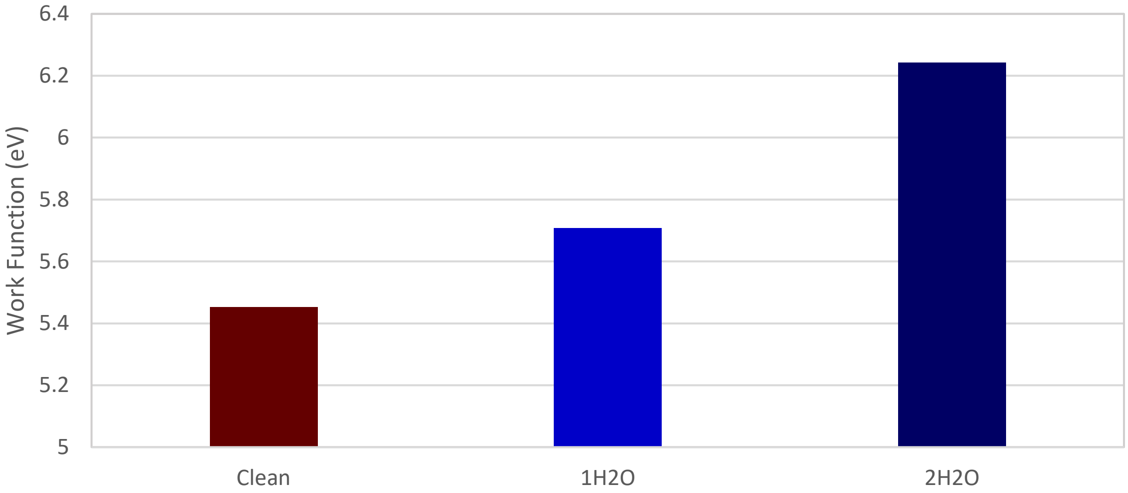

Figure 4.13 – *The calculated change in effective WF caused by the addition of water molecules to an aspirin (002) surface.*

Our results show that the calculated, effective WF of pharmaceutical materials vary significantly depending on surface and material tested. Similar to other works[244,308,327,328], the molecular termination and level of contamination at the surface can be expected to cause a shift in the surface WF. The significance of this relates firstly to the predication of charging in pharmaceutical materials, since reliable experimental measurement of these materials can prove difficult to obtain. The work shown here provides a basis on which an understanding of charge transfer between different pharmaceutical crystals can be built. Secondly, it provides insight into the poorly understood phenomenon of the triboelectrification of chemically identical materials[333]. Based on this work and the papers previously discussed[244,299,309], it is very unlikely that the surface effective WF profile of any particulate solid is homogenous, implying that triboelectric charge transfer can readily occur for the same material. This has implications for transport and fluidisation of homogeneous particulates. These subtle differences in the effective WF and surface electronic structure caused by surface orientation and contamination could provide the driving force for charge transfer in these systems. Finally, the calculated impact of water offers an alternative to the popular belief that the correlation between humidity and triboelectric charging is due to environmental water providing ions for charge transfer. The shift in effective WF caused by adsorbed surface water could itself be facilitating the electron transfer mechanism without necessarily involving ions for the charge transfer.

4.4 – Summary

The results of this study provide insights into the triboelectric behaviour of aspirin and paracetamol crystals by calculating the effective work function of various crystal facets. Significant variations in the effective WF are observed among the facets. Material composition also influences the WF shift. The presence of water molecules on the surface is found to have a noticeable impact, causing changes in the effective WF. This variation may be attributed to the influence of water on the molecular dipole and/or electrostatic potential of the interface, underscoring the importance of atomic coordination and bonding at the surface. Moreover, the calculated effective WF is found to depend on the number of water molecules present, expressed as fractional coverage, highlighting the significance of surface saturation.

This study emphasizes that a substantial distribution of effective WF can be expected in pharmaceutical systems due to surface termination, chemical composition, or surface condition. The findings have implications for understanding charging phenomena in single-component systems and the role of humidity in the charging of pharmaceutical materials. Further research is needed to establish connections between these calculated values and experimental measurements. Currently, there is limited research on facet-specific charging of organic crystals, and expanding the investigations in this area would greatly enhance our understanding of the underlying mechanisms.

Chapter 5 – Characterising the contribution of individual functional groups using the slab-molecule approach – A first principles study.

5.1 – Motivation and overview

In the rapidly evolving landscape of drug discovery and development, digital drug design has emerged as a transformative approach, leveraging the power of computational methods and advanced modeling techniques to revolutionize the way we search for new pharmaceutical agents. While digital drug design and computational methods have made significant strides in various aspects of drug discovery and development, predicting a drug's tendency to become triboelectrically charged during transport remains a challenging task.

Modeling triboelectric charging using first-principles calculations is an active area of research, with the majority of recent publications focused on improving the design and performance of triboelectric nanogenerators. However, the accurate *ab initio* prediction of triboelectric charging could offer several significant benefits to the pharmaceutical industry. In the realm of drug development, precise predictions of triboelectric charging tendencies could lead to improved drug formulation and stability, enabling the a priori identification of potential issues caused by agglomeration, adhesion, or electrostatic discharges during transport and processing[42].

The impact of surface functional group on triboelectric charging tendency is well known in various fields. By considering the impact of functional groups on triboelectric charging tendencies, drug designers can make informed choices about the composition and structure of drug molecules. Careful selection and placement of functional groups might help minimize undesirable triboelectric charging effects while maintaining drug efficacy. This is especially relevant for aerosolised drug particles where triboelectric charging can significantly impact pulmonary drug delivery.

Currently little research is available on the DFT prediction of the triboelectric charging tendency of pharmaceutically relevant materials, fortunately DFT is used extensively to model, predict, and gain mechanistic insight into the triboelectric charging mechanism in other fields, providing a strong methodological basis for this work.

Ab-initio calculations can be used to calculate the electronic structure of individual molecules and even analyse the electronic properties of individual functional groups within those molecules. This enables researchers to gain valuable insights into the behaviour of small systems that may not be feasible to study directly in experiments. In the context of organic electronic devices Li et al.[334] investigated how polymer surface treatments impact surface electronic structure by putting a single monomer on a NiO surface. This work inspired the work of Wu et al.[54] who used this same 'slab-monomer' approach to assess the properties of different polymers for their use in triboelectric nanogenerators. More recently Nan et al.[244] used DFT to study the charge transfer of several polymers between an idealised water layer to comprehensively study the contact electrification mechanism at water polymer interfaces.

In this work the charging tendency of several functional groups attached to common pharmaceutical materials is studied by density functional theory calculations. Using a 'slab-monomer' approach analogous to other publications molecules of aspirin, ibuprofen, mannitol and paracetamol are each placed on two layer atomic layers of several metals that have a range of work functions respectively. Looking at charge transfer of each functional group under a variety of conditions using Hirshfeld charge analysis, plotting the charge density difference between the surface and the API molecule, location of frontier orbitals (HOMO and LUMO) and observing the shift in density of states. The objective of this work is to provide insight on how the functional groups exposed at the facets of pharmaceutical crystals might influence triboelectric charging.

5.2 – Theoretical approach

This work aims to investigate the relative charging properties of the individual functional groups of common pharmaceutical molecules using a "slab-monomer" approach. The molecule of interest is placed on a slab of material. A molecular mechanics geometry optimisation calculation is performed using Materials Studio Forcite tool with the COMPASSIII [265] forcefield and is followed a single point energy DFT calculations if necessary to determine electronic structure quantities. This approach has been used in the work of Wu et al.[54] and Nan et al.[244] to study triboelectric charging. This approach is most often seen in the study of corrosion inhibition which is very commonly done using DFT[335]. An example of a simulation box used in calculation is showing in Figure 5.1. In this work a combined MM and DFT approach was used. Geometry optimisations MM calculations were performed by the Materials Studio molecular mechanics tool Forcite tool using the COMPASSIII force field[265]. Using the SMART optimisation algorithm. Convergence tolerances for this optimization include 2.0×10^{-5} kcal/mol for change in energy, 1.0×10^{-3} kcal/mol/Å for force, 5.0×10^{-4} Å for displacement and a stress tolerance of 2.0×10^{-2} GPa. An Ewald summation of electrostatic terms was used and an atom-based summation method for van der Waals interactions.

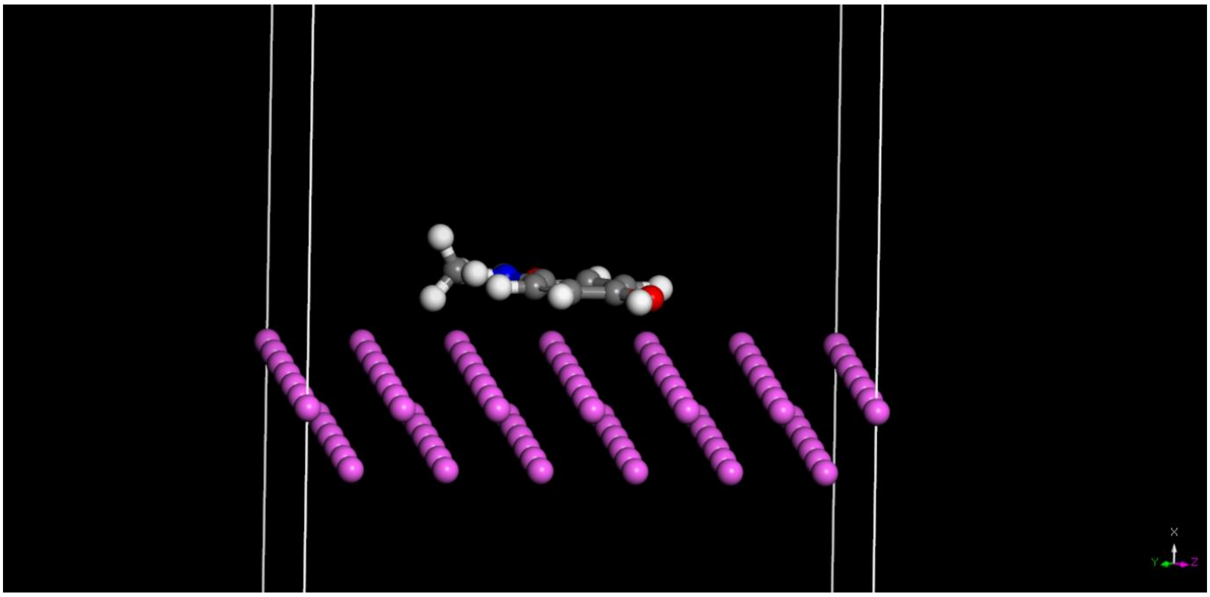

Figure 5.1 – *A periodic vacuum-slab unit cell containing a two atomic layer thickness (100) aluminium surface.*

The CASTEP simulation code was used for electronic structure calculations, using the GGA-PBE exchange correlation fucntional, which is consistent with other studies [54,244]. For the electronic minimisation, a tolerance of 5.0x10^{-7} eV was selected for the total energy per atom. Hirshfeld charge analysis is used to quantify the charge transfer between atoms and different surfaces and charge density difference calculations are also done to investigate the regions of the molecule which exchange charge density with the surface. In the work of Wu et al.[54] a molecule is place on a metal slab several atoms thick, however in the work of Nan et al.[244] molecules are put on only a single layer of ordered water. The convergence of Hirshfeld charges is with layer thickness is presented in Figure 5.2.

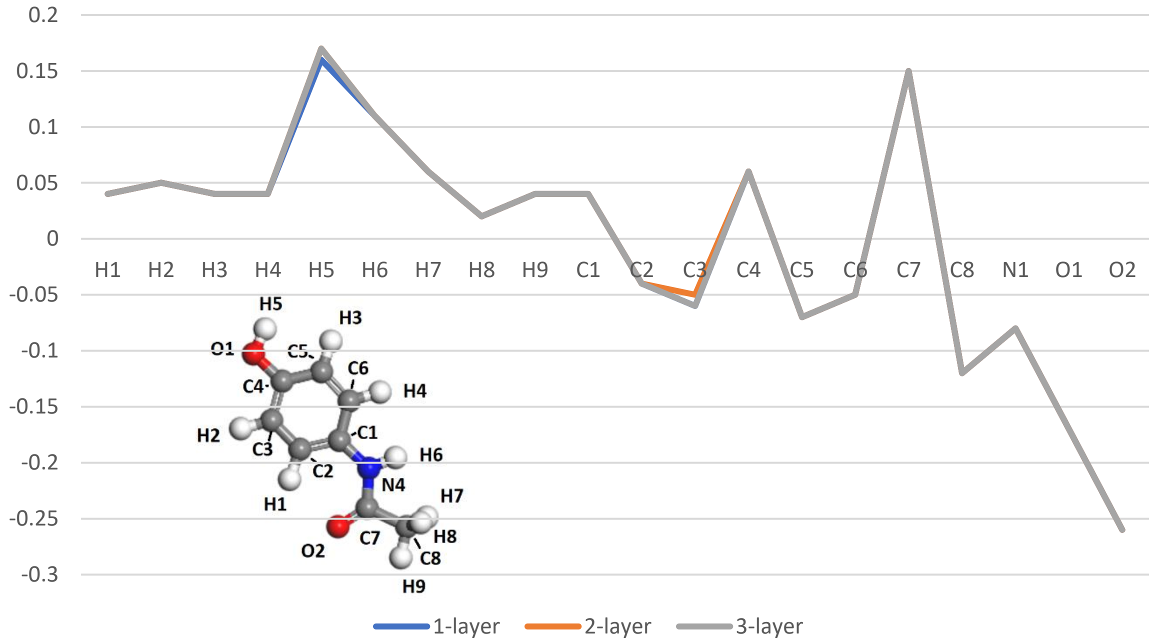

Figure 5.2 – *Convergence of Hirshfeld charge distribution with number of atomic layers. Calculated using a 600eV kinetic energy cut-off and a 2x2x1 Monkhorst-Pack.*

From this a slab thickness of two atomic layers was deemed to be sufficiently converged for these calculations, therefore a slab thickness of two was always used throughout this work. Density of states calculations were also performed to investigate the conductivity and frontier orbitals of the systems studies. DOS calculations usually require more precise energy cut-off and k-point sampling. A sensitivity analysis on an example paracetamol on aluminium (100) surface showing the dependence of energy cut-off and k-point sampling is shown in Figures 5.3 and 5.4 respectively.

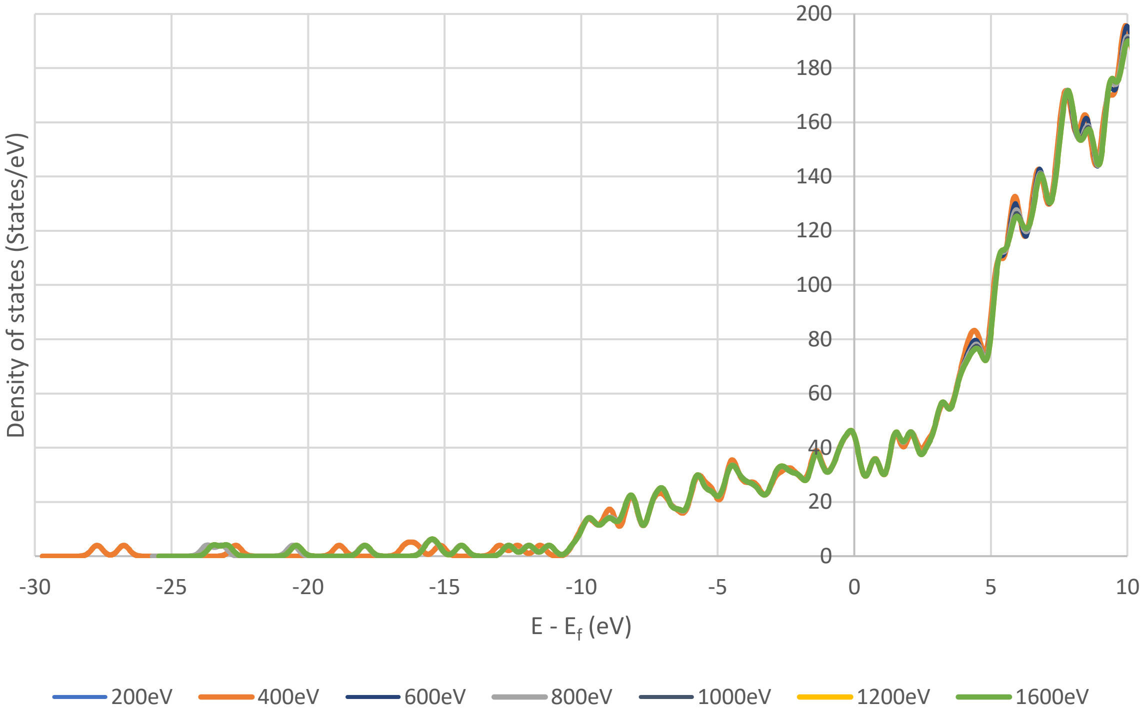

Figure 5.3 – *Density of states convergence with e-cutoff of a paracetamol on an aluminium (100) surface. Each test case was simulated with a 2x2x1 Monkhorst-Pack grid.* E_f *= fermi level.*

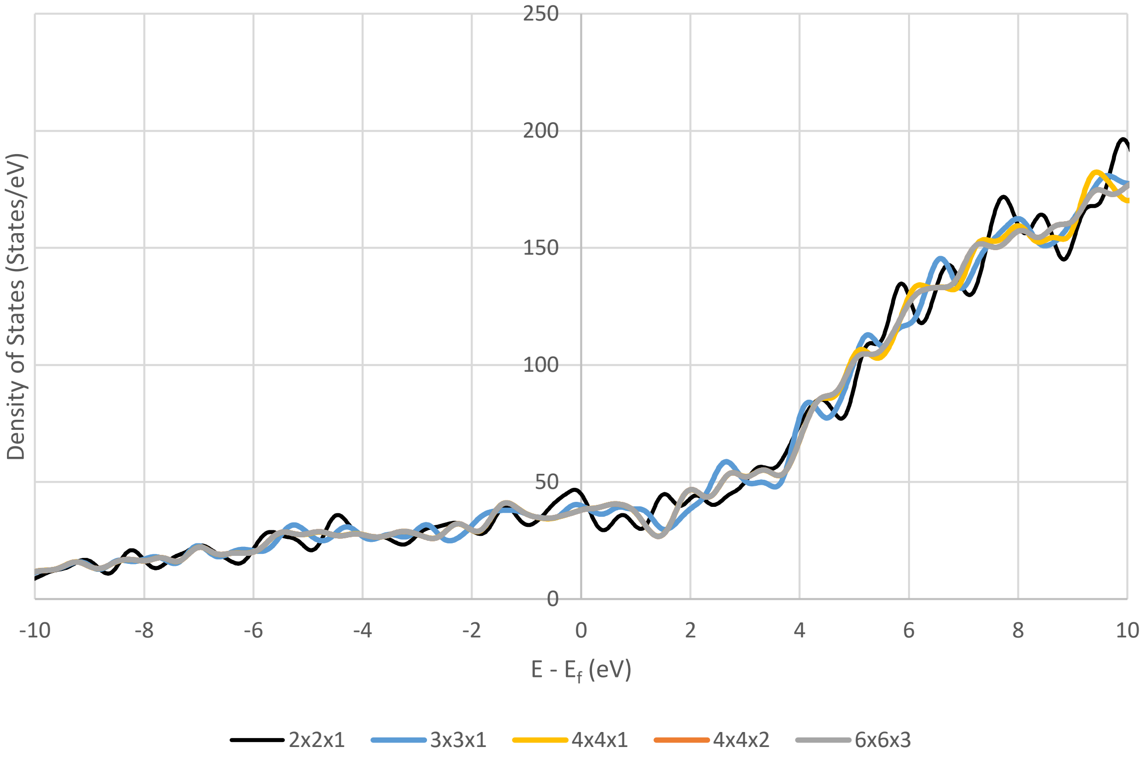

Figure 5.4 – *Density of states convergence with Monkhorst-Pack k-point sampling. Each test case was simulated using a kinetic energy cut-off of 150eV.* E_f *= fermi level.*

The states of primary interest for modeling triboelectric charging are the frontier orbitals, i.e. the states in closest proximity to the Fermi level (the HOMO and LUMO). Fortunately Figure 5.3 shows good convergence of the DOS near the Fermi level even at relatively low energy cut-off, however lower energy states show good convergence at a kinetic cut-off of above 400eV. The impact of Monkhorst-Pack sampling shows that decent convergence of the DOS near the Fermi level occurs after a k-point grid of 4x4x1. Based on these test cases higher a kinetic energy cut-off of was chosen at 600eV to ensure high quality results was used throughout this work. For Hirshfeld charge analysis and charge density difference calculations a cut-off of Monkhorst-Pack k-point sampling of 2x2x1 is used, for DOS a sampling of 4x4x1 is used. During geometry optimisation relaxation of the surface is not considered and all atoms are fully constrained, surface molecules are allowed to fully relax. The charge density difference induced by the molecules placed on the slab is given calculated by,

$$\Delta\rho = \rho_{surf-mol} - \rho_{surf} - \rho_{mol} \qquad \text{Eq. 3.1}$$

Where charge density of the surface (ρ_{surf}) and molecule (ρ_{mol}) are subtracted from the charge density of the combined surface and molecule ($\rho_{surf-mol}$), which allows for visualisation of areas of electron depletion and electron enrichment due to contact. Hirshfeld charge analysis [247] is performed to quantify the transferred surface charge density,

$$\sigma_{H,trasnfered} = \sigma_{H,mol} - \sigma_{H,surf-mol} \qquad \text{Eq. 5.2}$$

Where ($\sigma_{H,mol}$) is defined as the Hirshfeld charges present on an isolated molecule and ($\sigma_{H,surf-mol}$) the charges on a molecule placed on a surface. Obtaining these quantities requires three separate calculations on an isolated surface, isolated molecule and combined surface and molecule. An example of the systems used for paracetamol on a 100 aluminium surface shown in Figure 5.5. The following results contain the DFT predicted location of the frontier orbitals on isolated molecules. The contact-induced shift in electron charge density between the surface and molecule. Hirshfeld charge analysis and density of states are used to elucidate the charge transfer mechanism of common pharmaceutical materials.

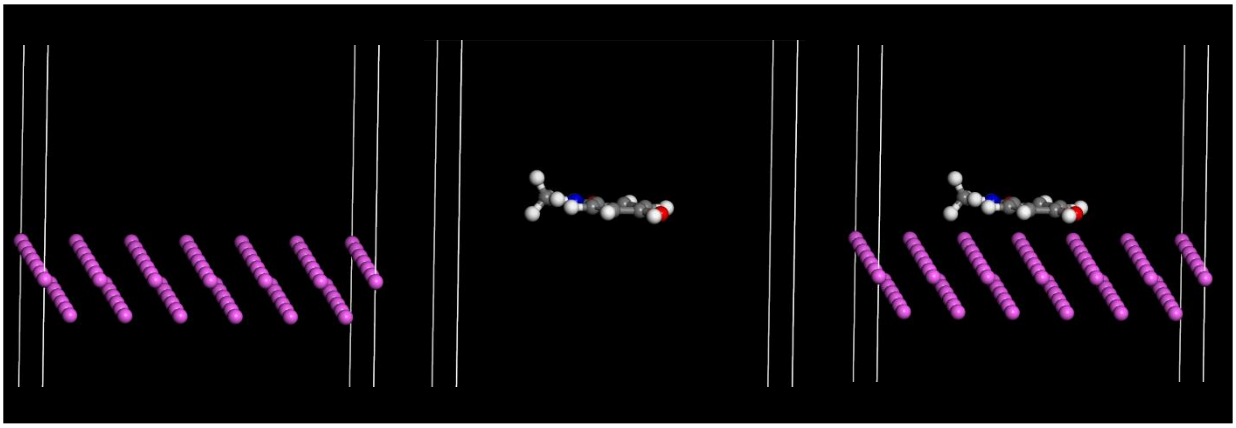

Figure 5.5 – *Visualisation of the unit cell used to calculate a isolated surface (left), isolated molecule (centre) and combined surface and molecule (right)*

5.3 – Results and discussion

In order to effectively probe the charging behaviour of these molecules initial calculations were done to look at the electronic structure of common pharmaceutical materials in isolation. The frontier orbitals of the system are reported to be of crucial importance to charge transfer [53,319,336]. These orbitals contain electrons or relatively low energy and therefore, in a low energy process like triboelectric charging these electrons are the ones that are most likely to move between molecules. The predicted locations of the HOMO and LUMO of the molecule of all API molecules tested are displayed in Figure 5.6 and some clear trends are observable. HOMOs are typically focused on oxygen molecules implying they readily donate electrons. For aspirin and paracetamol HOMOs tend to distribute around the oxygen molecules and the LUMOs appear to distribute around the arene rings. In line with expectations for Ibuprofen and mannitol HOMO distribution does favour the oxygen orbitals however there appears to be a distribution and overlapping of orbitals on the arene ring. On mannitol the LUMO seem to focus on the functional groups with the HOMOs favouring the oxygens and the LUMOs appearing to distribute to the hydrogen atoms.

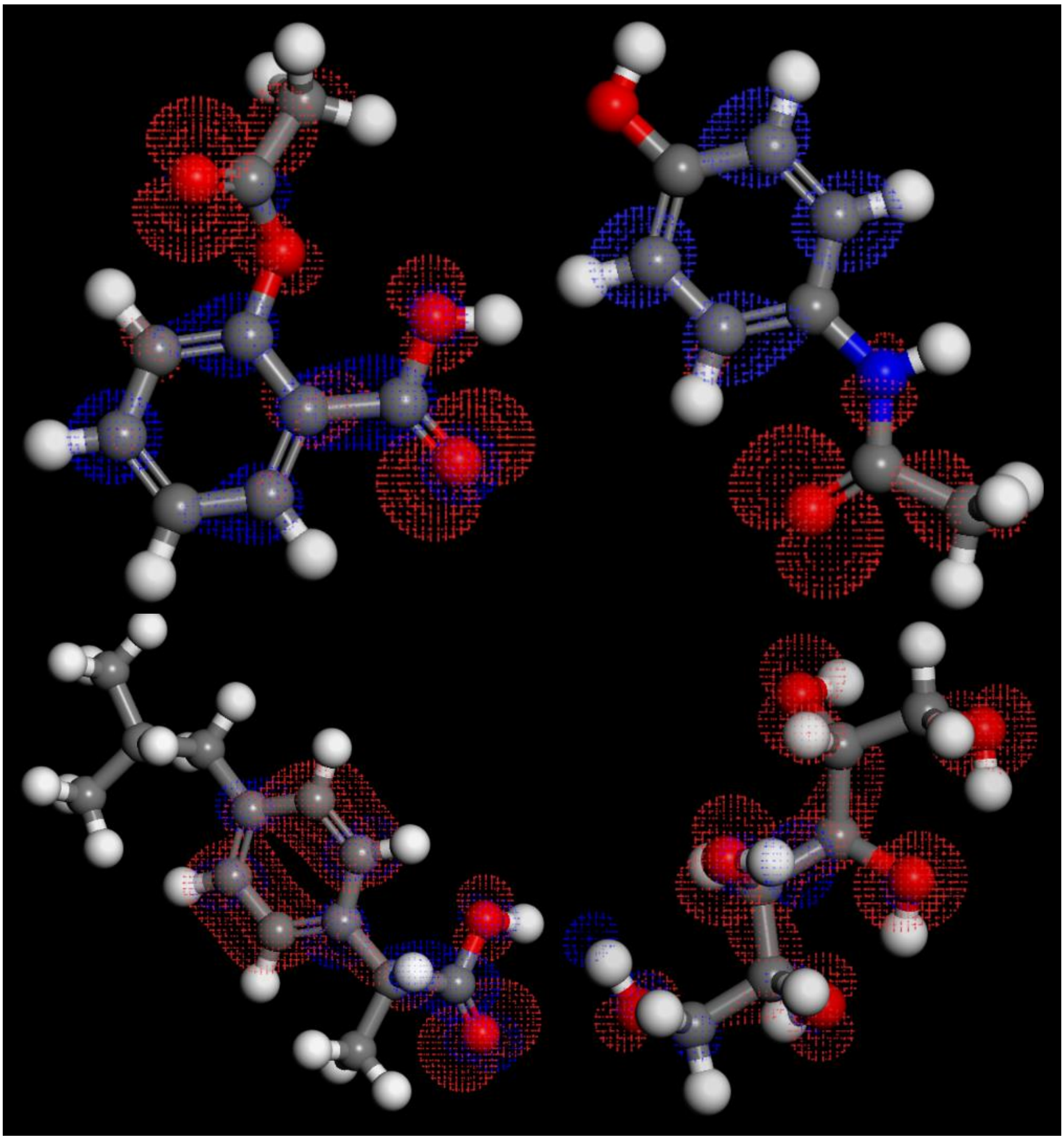

Figure 5.6 – *The calculated frontier orbitals of isolated aspirin, paracetamol, ibuprofen and mannitol. Highest occupied molecular orbital (HOMO) highlighted in red. Lowest unoccupied molecular orbital (LUMO) highlighted in blue.*

In the work of Wu et al. [54] the slab-molecule approach is leveraged to probe the triboelectric charging characteristics of individual molecules. The molecules of aspirin, paracetamol, ibuprofen and aspirin are tested against the surface of aluminium, gold and platinum. The charge density difference iso-surfaces are presented in Figures 5.7 to 5.10.

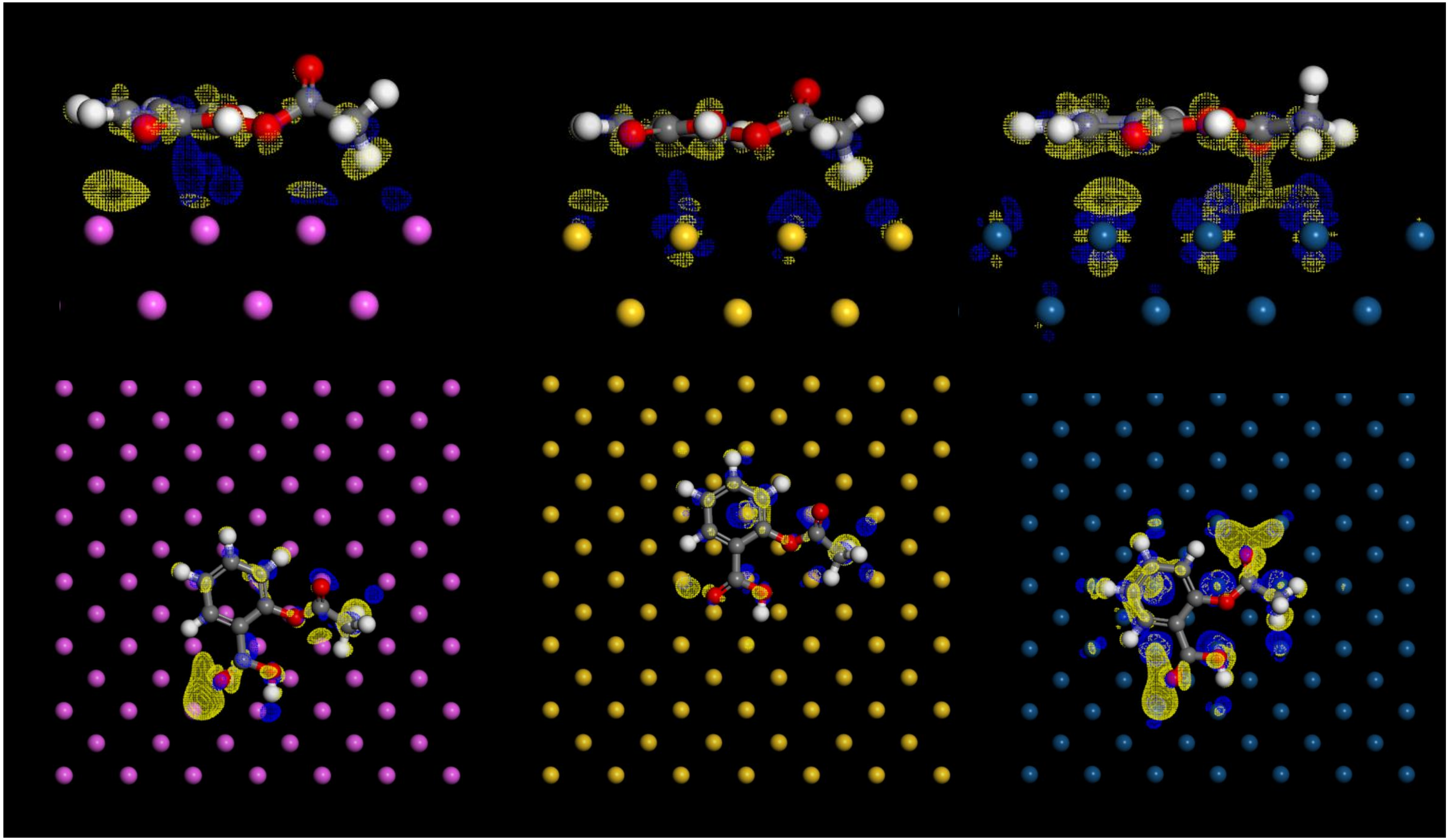

Figure 5.7 – *Comparison of the charge density difference at the aspirin-metal interface. Yellow iso-surfaces indicate areas of electron depletion and blue areas indicate areas of electron enrichment. Iso-surfaces set at a value of 0.008 electrons Å^{-3}. Surface colour indicates aluminium (Pink), gold (gold), platinum (blue) respectively.*

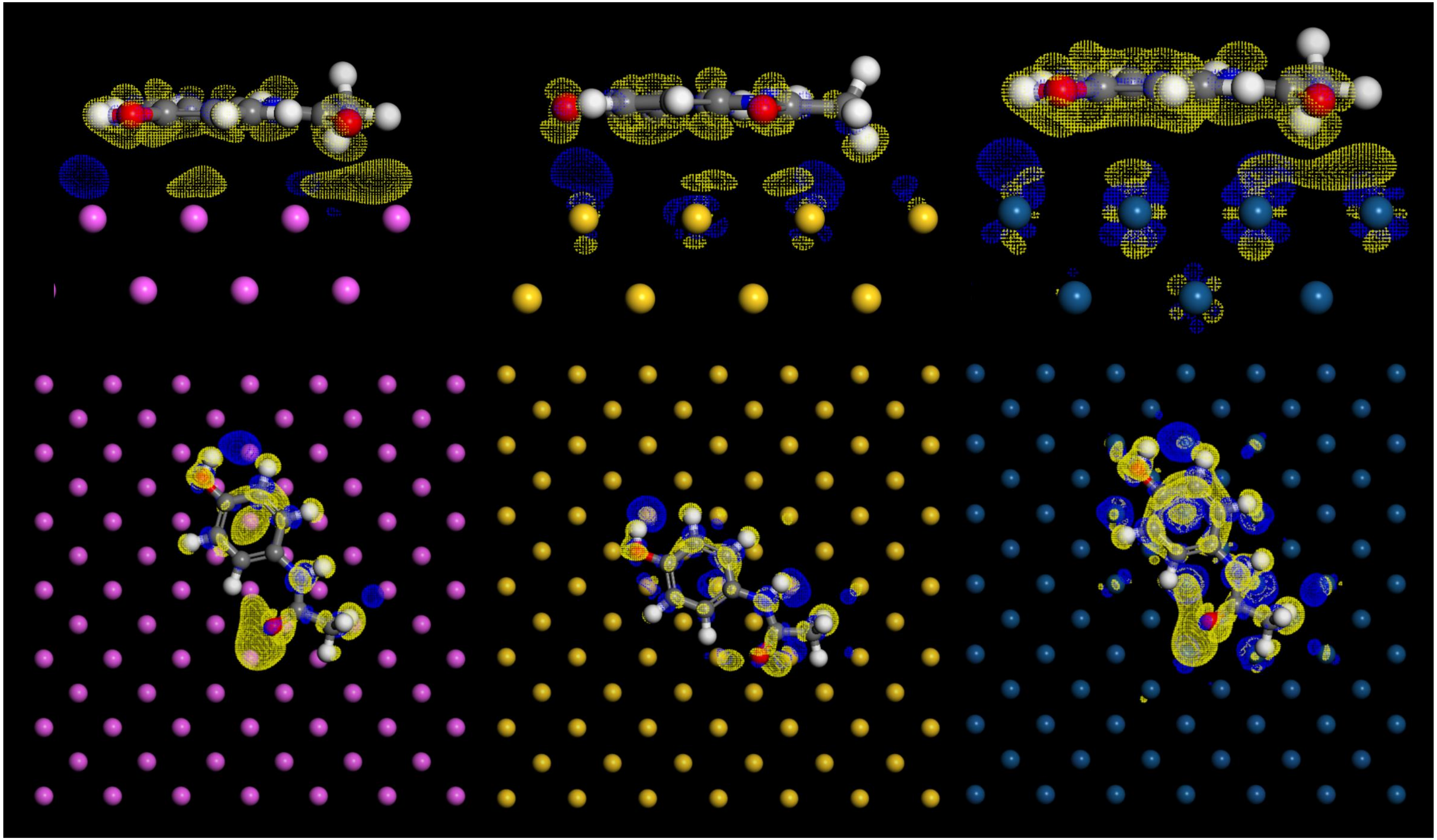

Figure 5.8 – *Comparison of the charge density difference at the paracetamol-metal interface. Yellow iso-surfaces indicate areas of electron depletion and blue areas indicate areas of electron enrichment. Iso-surfaces set at a value of 0.008 electrons* Å^{-3}. *Surface colour indicates aluminium (Pink), gold (gold), platinum (blue) respectively.*

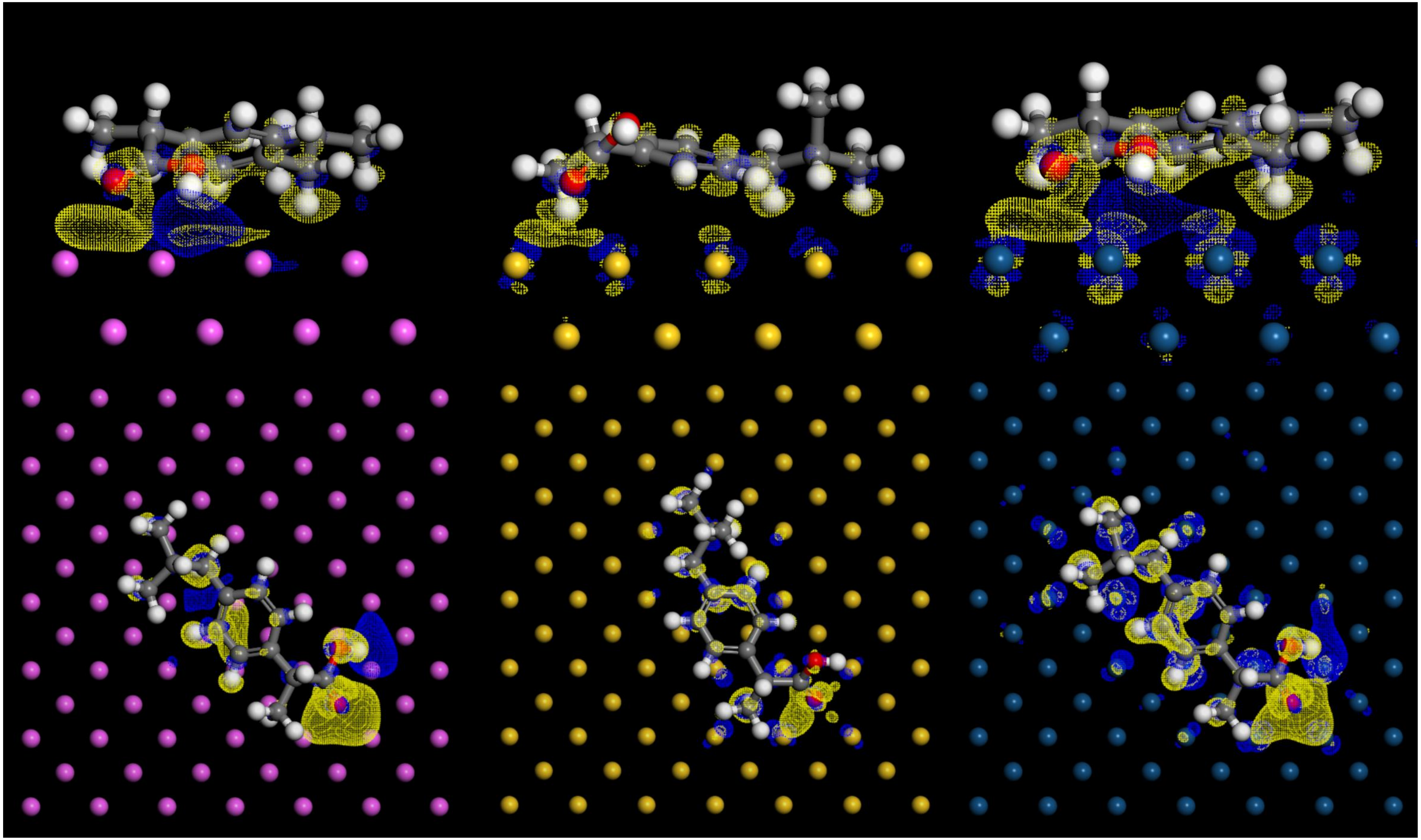

Figure 5.9 – *Comparison of the charge density difference at the paracetamol-metal interface. Yellow iso-surfaces indicate areas of electron depletion and blue areas indicate areas of electron enrichment. Iso-surfaces set at a value of 0.008 electrons Å^{-3}. Surface colour indicates aluminium (Pink), gold (gold), platinum (blue) respectively.*

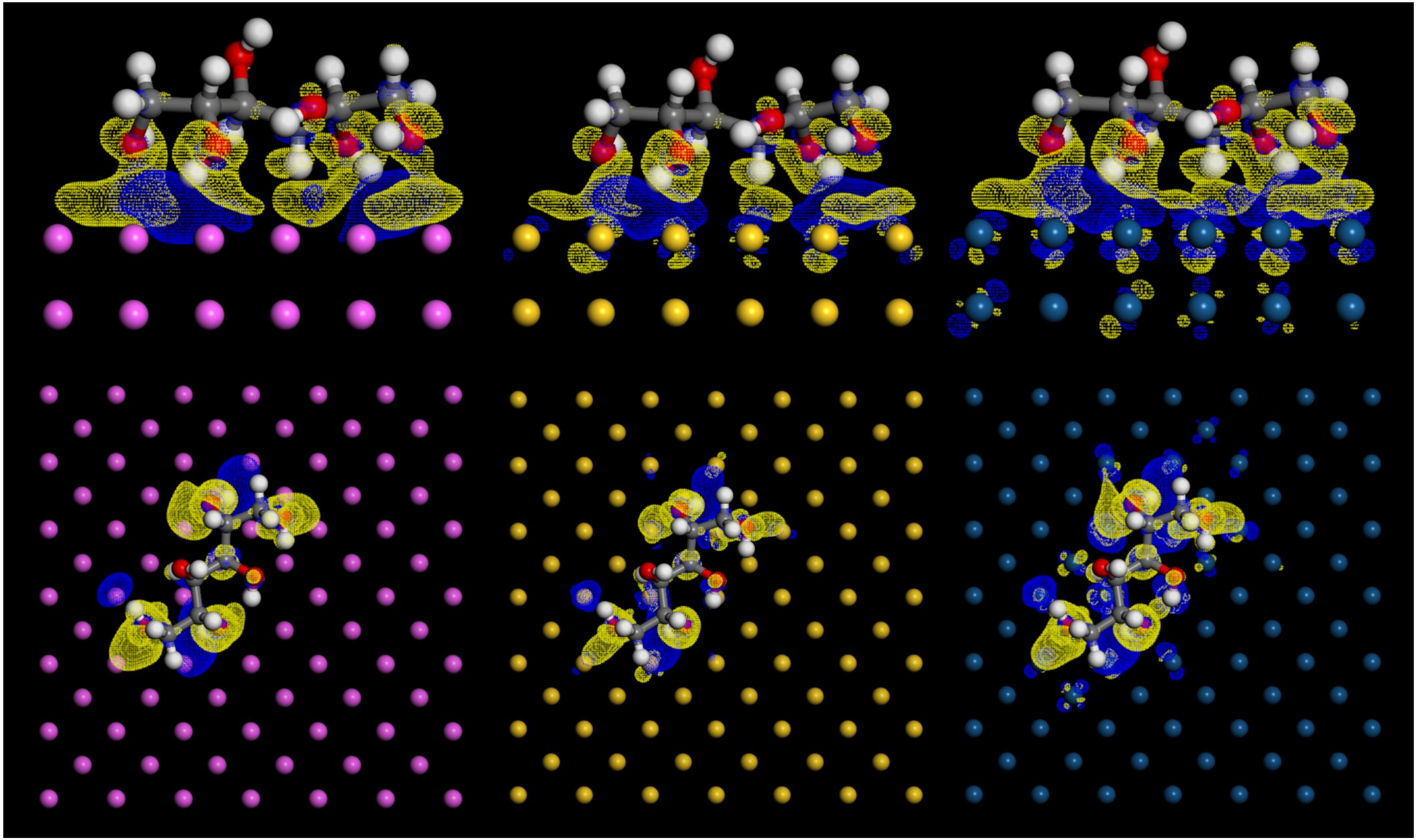

Figure 5.10 – *Comparison of the charge density difference at the paracetamol-metal interface. Yellow iso-surfaces indicate areas of electron depletion and blue areas indicate areas of electron enrichment. Iso-surfaces set at a value of 0.008 electrons Å*$^{-3}$*. Surface colour indicates aluminium (Pink), gold (gold), platinum (blue) respectively.*

Charge density difference plots are commonly used in the literature when applying DFT to study triboelectric charging [54,297,337]. Typically, they are employed to examine the redistribution of charges in molecules that are chemically bonded to a surface. In triboelectric charge transfer studies, these plots are utilized to highlight charge transfer occurring between surfaces. Across all materials studied, noticeable regions of electron depletion are observed around the carbonyl groups. However, there does not appear to be a clear correlation between the size of these depletion/enrichment regions and the charge transfer predicted by the Hirshfeld charge analysis. Notably, in the case of aspirin on platinum, the molecule is optimized with the carbonyl group much closer to the surface, resulting in a large region of electron depletion at the surface. This suggests a more complex scenario where multiple regions within single molecules may be involved in charge transfer.

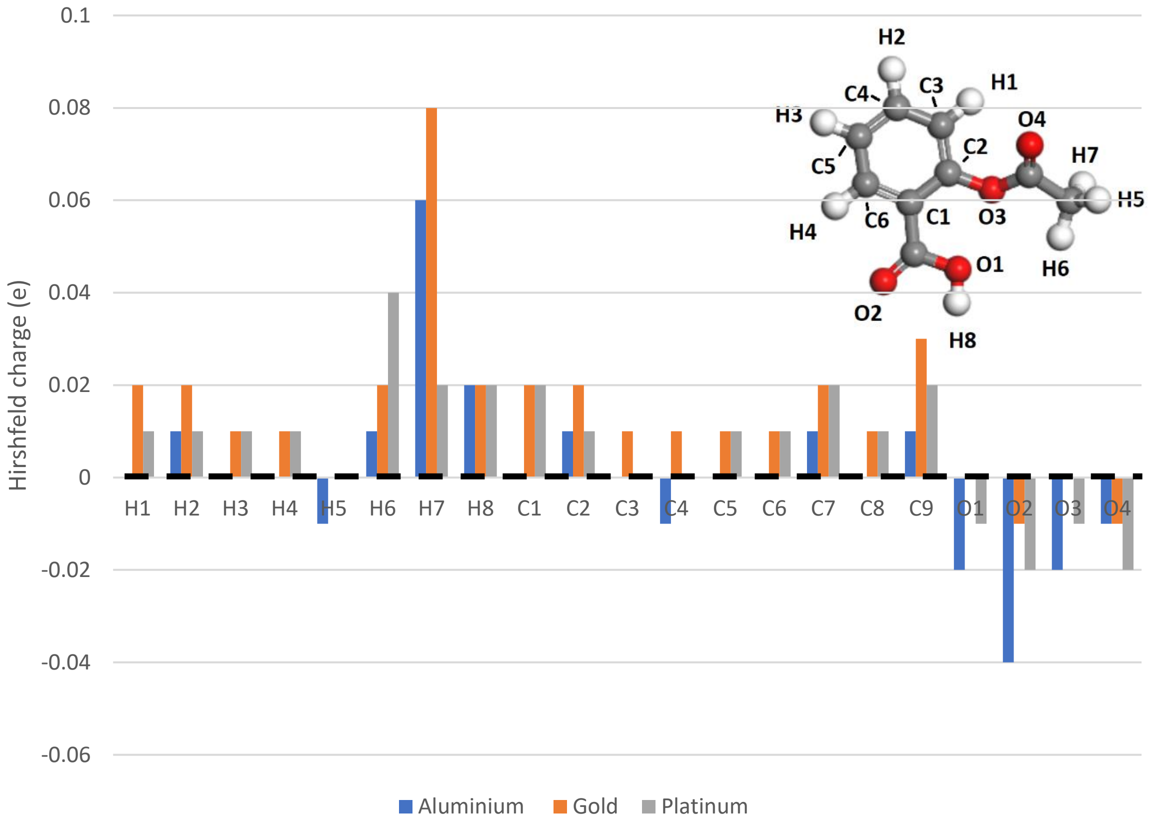

Figure 5.11 – *Hirshfeld charge difference of aspirin molecule on a Al, Au and Pt surface compared relative to the Hirshfeld charges on an isolated aspirin molecule.*

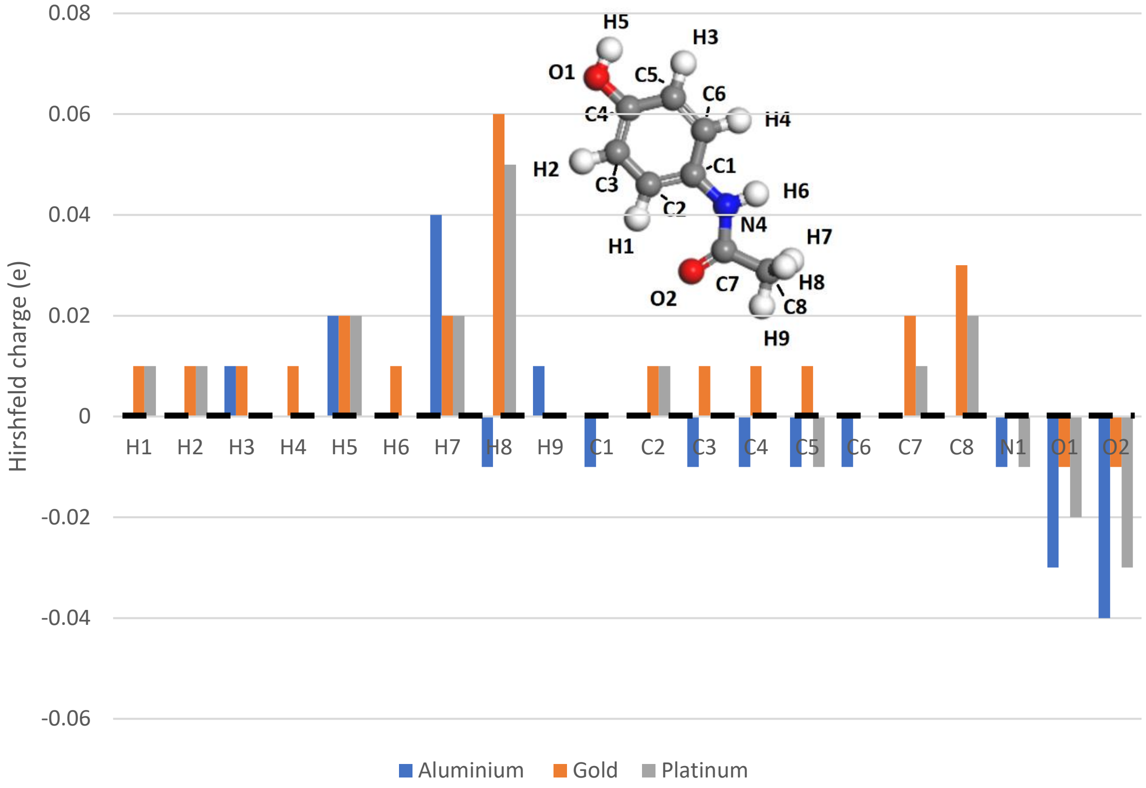

Figure 5.12 – *Hirshfeld charge difference of paracetamol molecule on a Al, Au and Pt surface compared relative to the Hirshfeld charges on an isolated paracetamol molecule.*

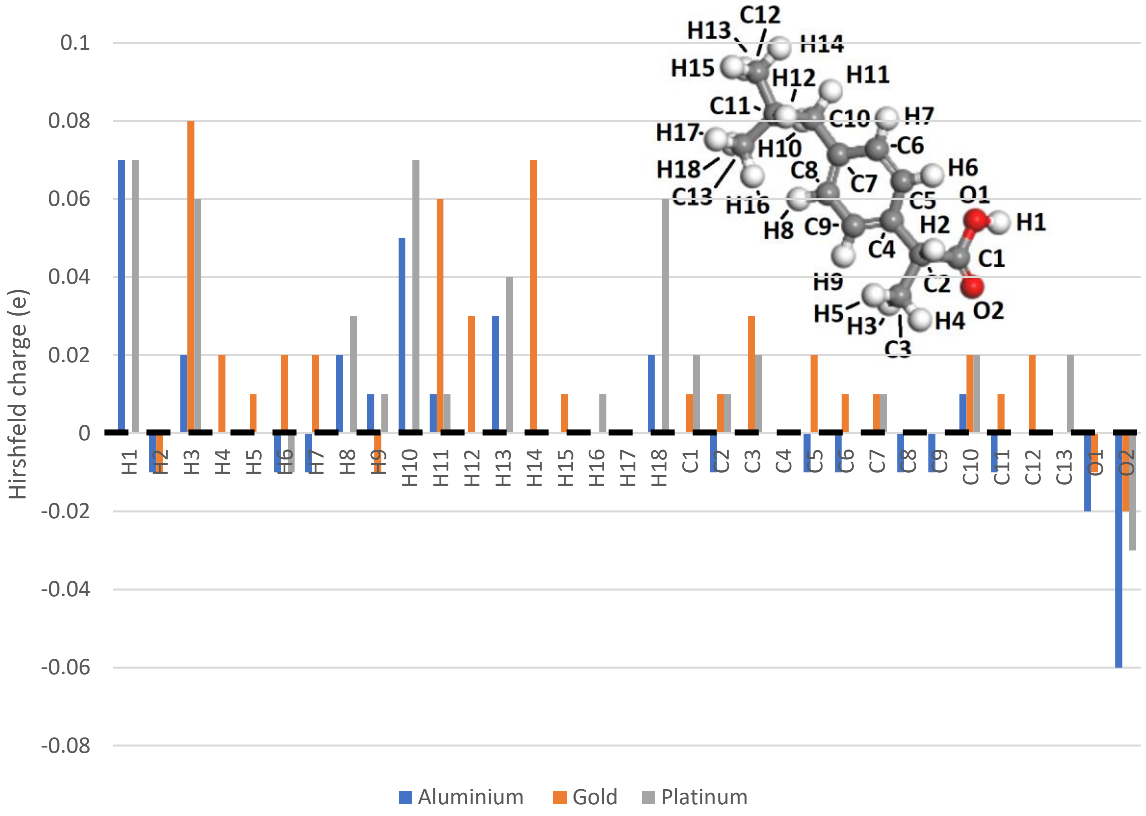

Figure 5.13 – *Hirshfeld charge difference of ibuprofen molecule on an Al, Au and Pt surface compared relative to the Hirshfeld charges on an isolated ibuprofen molecule.*

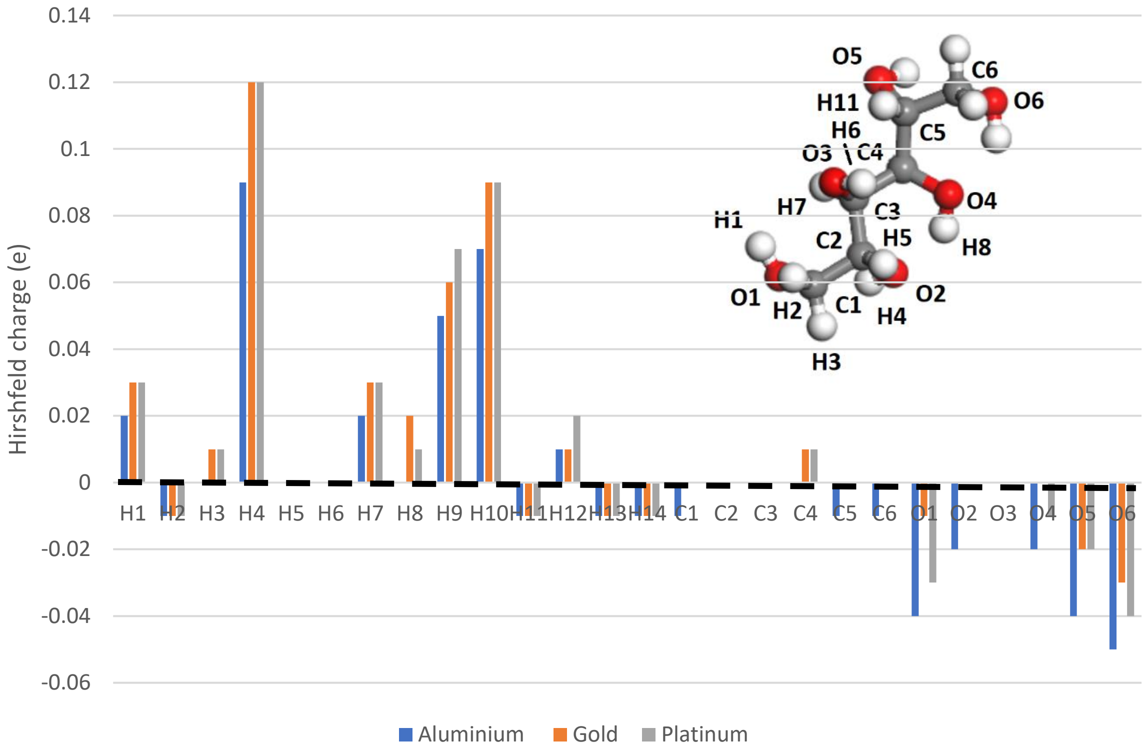

Figure 5.14 – *Hirshfeld charge difference of mannitol molecule on an Al, Au and Pt surface compared relative to the Hirshfeld charges on an isolated mannitol molecule.*

The redistribution of Hirshfeld charges resulting from API contact with the metal substrate is presented in Figures 5.11 to 5.14. It is consistently observed across all materials tested that oxygen atoms have a significantly reduced Hirshfeld charge after contact, which aligns well with the physical HOMO and LUMO locations reported in Figure 5.6. Carbon and hydrogen atoms exhibited a strong tendency to gain Hirshfeld charge. Analysing the total charge redistribution attributed to each atom type, it is evident that oxygen consistently loses Hirshfeld charge, meaning it becomes less negatively charged upon contact with the surfaces. Hydrogen, on the other hand, consistently gains Hirshfeld charge, becoming less positively charged when in contact with all surfaces tested. The behaviour of carbon was more variable. When molecules were on gold and platinum substrates, carbon consistently exhibited a net increase in Hirshfeld charge, indicating a negative charge. However, in the case of aluminium, there was a net decrease in Hirshfeld charge for carbon atoms, except in the case of aspirin on aluminium.

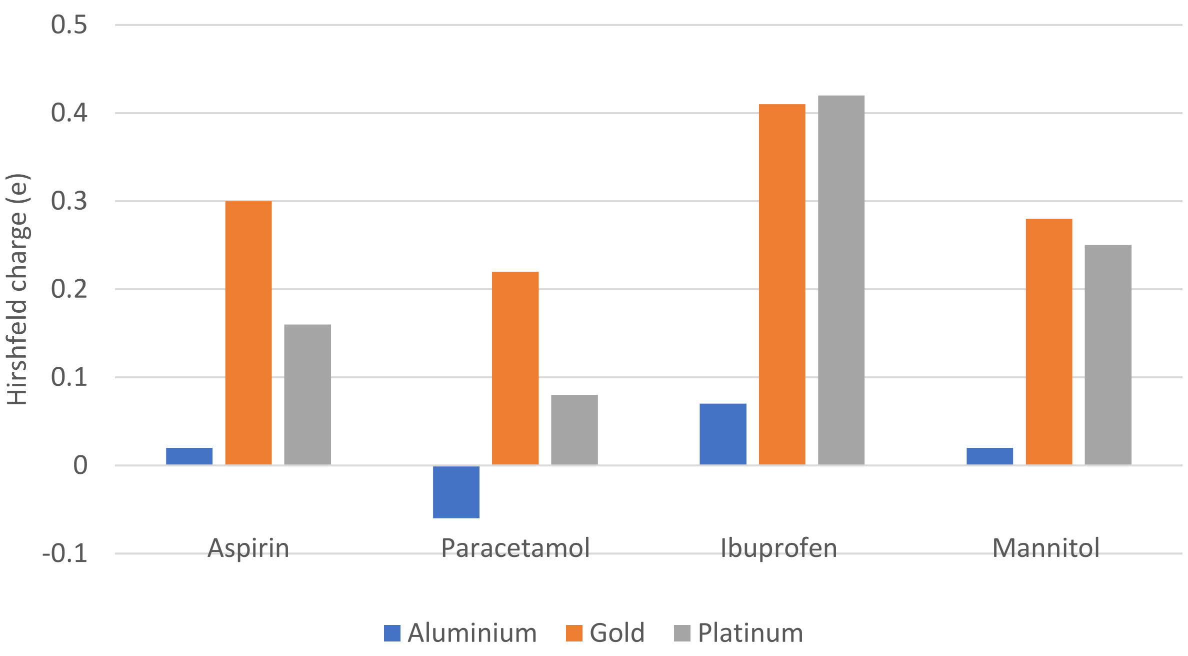

Figure 5.15 – *Total transferred Hirshfeld charge to each molecule by each test surface.*

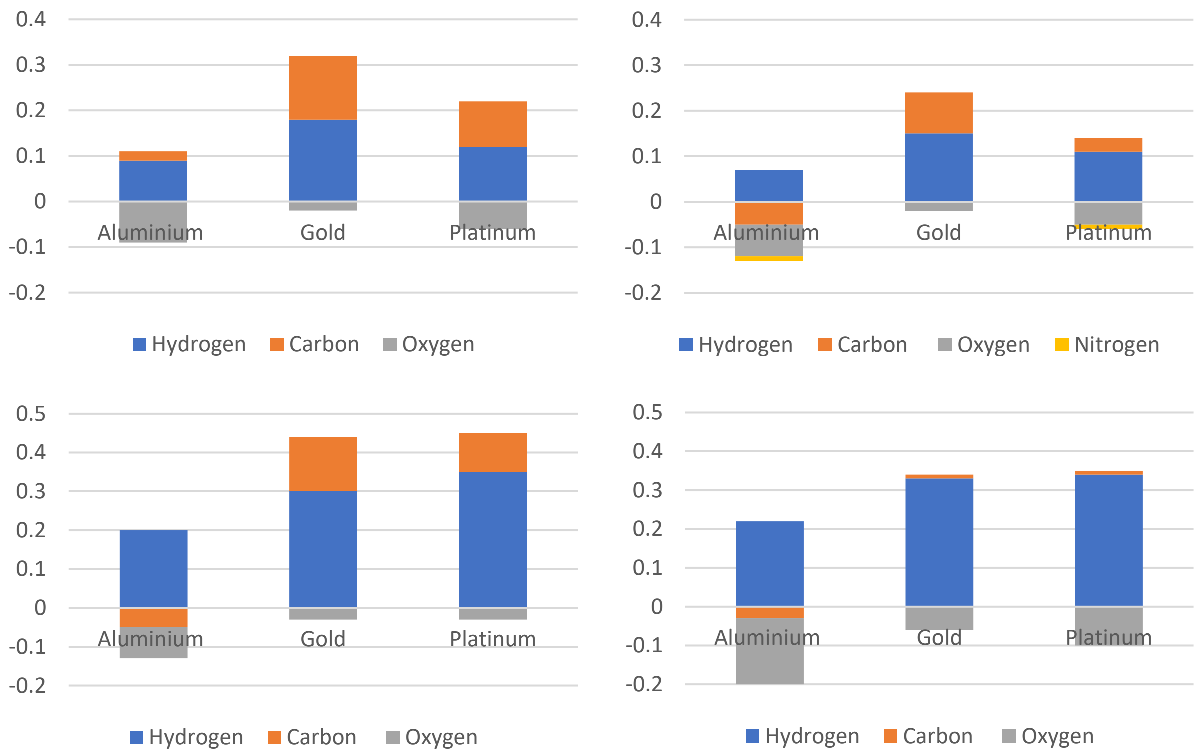

Figure 5.16 – *Contribution of each element to Hirshfeld charge transfer. Aspirin (top left). Paracetamol (top right). Ibuprofen (bottom left), Mannitol (bottom right).*

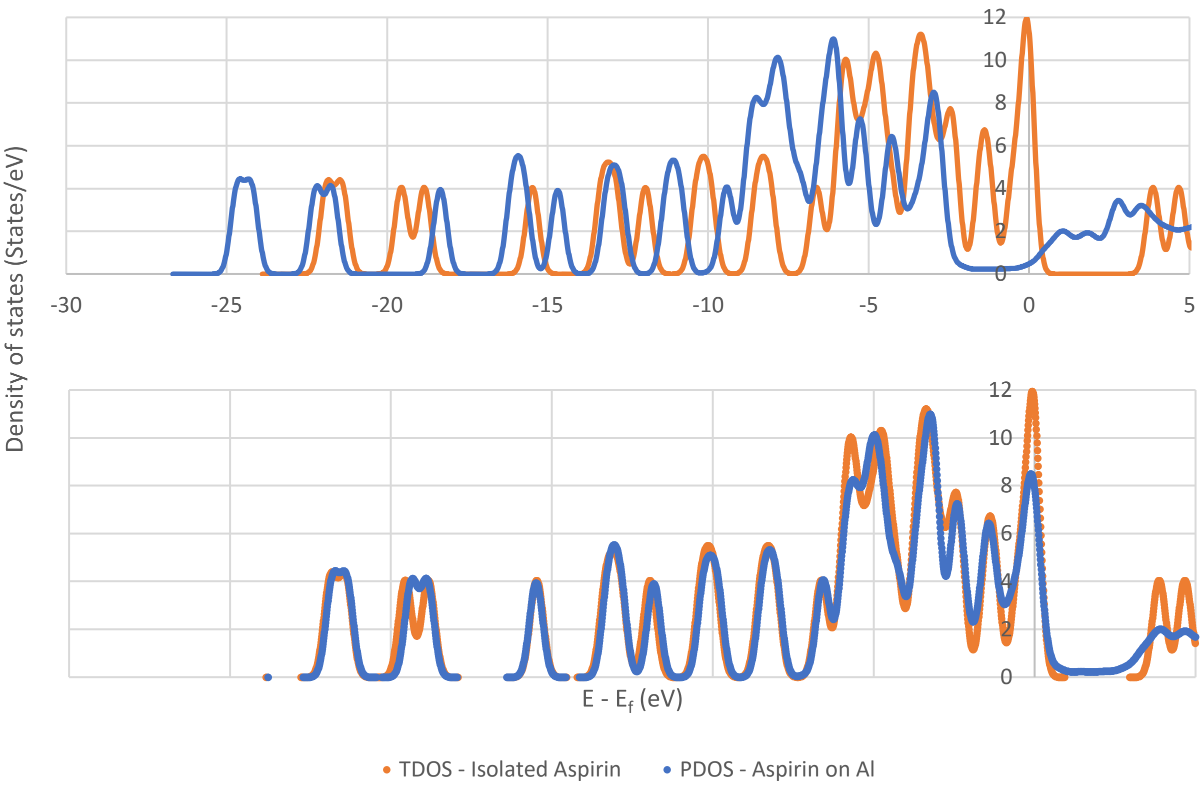

Figure 5.17 – *Projected density of states of aspirin relaxed on a aluminium (100) surface versus Total density of states for an isolated Aspirin. Uncorrected (top), Corrected (bottom).*

To further probe the underlying mechanism of charge transfer for pharmaceutical materials density of states (DOS) analysis was performed comparing the Total Density Of States (TDOS) of an isolated API molecule with the partial density of states (PDOS). A comparison of the DOS of an isolate molecule of aspirin and the PDOS of the aspirin contacting an aluminium surface is shown in Figure 5.17. In DOS calculations the states are usually calculated with respect to the Fermi level of a material (E_f) which is set at 0 in these plots. There is clearly a shift in the Fermi level occurring due to contact with the surface which is causing a synchronization between the DOS of an isolated molecule and the PDOS of the molecule placed on the surface. In order to perform better qualitative analysis of how the electron states of aspirin are impacted by contact with the aluminium surface the PDOS of the APIs tested are arbitrarily translated along the x-axis until the HOMO states are coincident, as shown in Figure 5.17. This methodology is similarly applied to the calculated DOS of aspirin, paracetamol, ibuprofen and mannitol as shown in Figures 5.18, 5.19, 5.20 and 5.21 respectively.

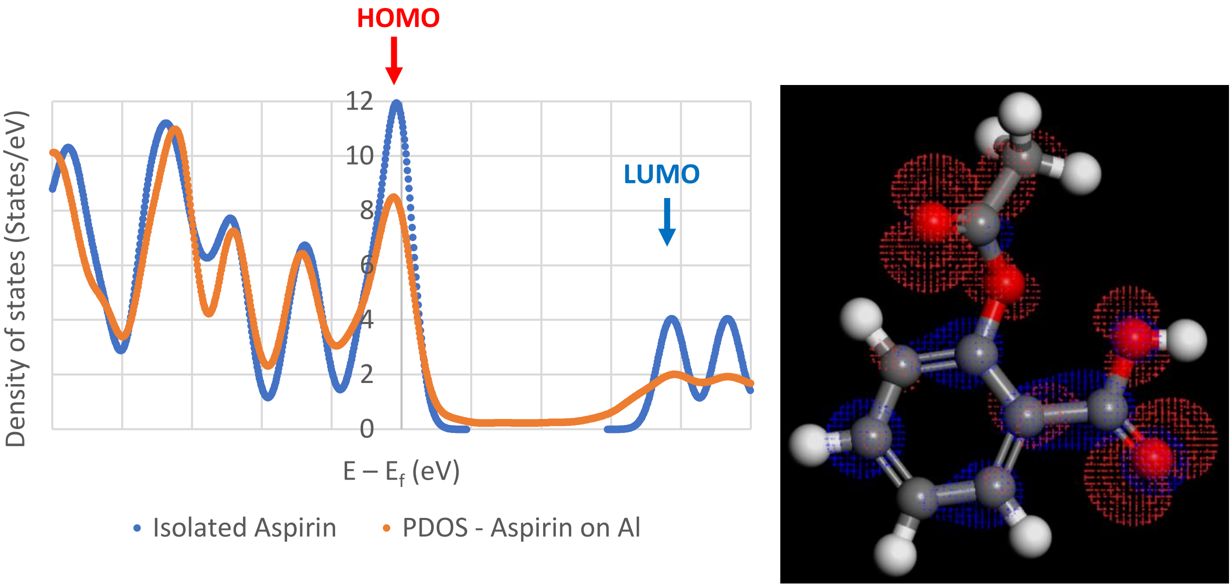

Figure 5.18 – *TDOS of isolated aspirin overlayed with the PDOS of aspirin relaxed onto an aluminium (100) surface (left). Image of corresponding location of HOMO and LUMO on molecule (right).*

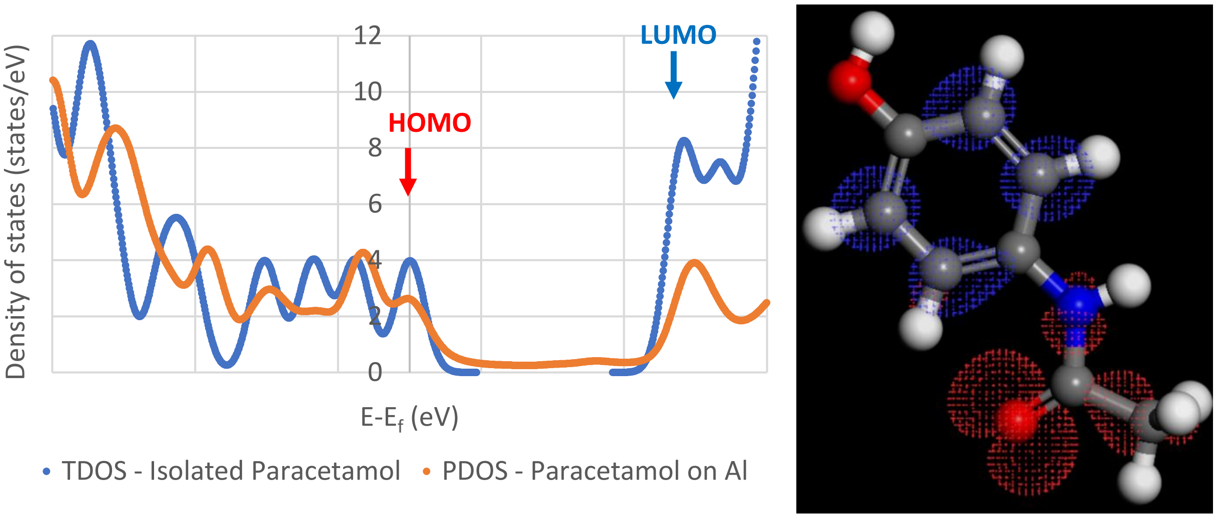

Figure 5.19 – *TDOS of isolated paracetamol overlayed with the PDOS of paracetamol relaxed onto an aluminium (100) surface (left). Image of corresponding location of HOMO and LUMO on molecule (right).*

The observation of the Projected Density of States (PDOS) of the API molecules on the aluminium surface suggests that the close contact of various molecules on the surface has a significant impact on the density of states for these materials. Aspirin, paracetamol, ibuprofen, and mannitol are all insulating materials, and as expected, they all exhibit a clear and distinct band gap between the HOMO and LUMO states, indicating insulating behaviour.

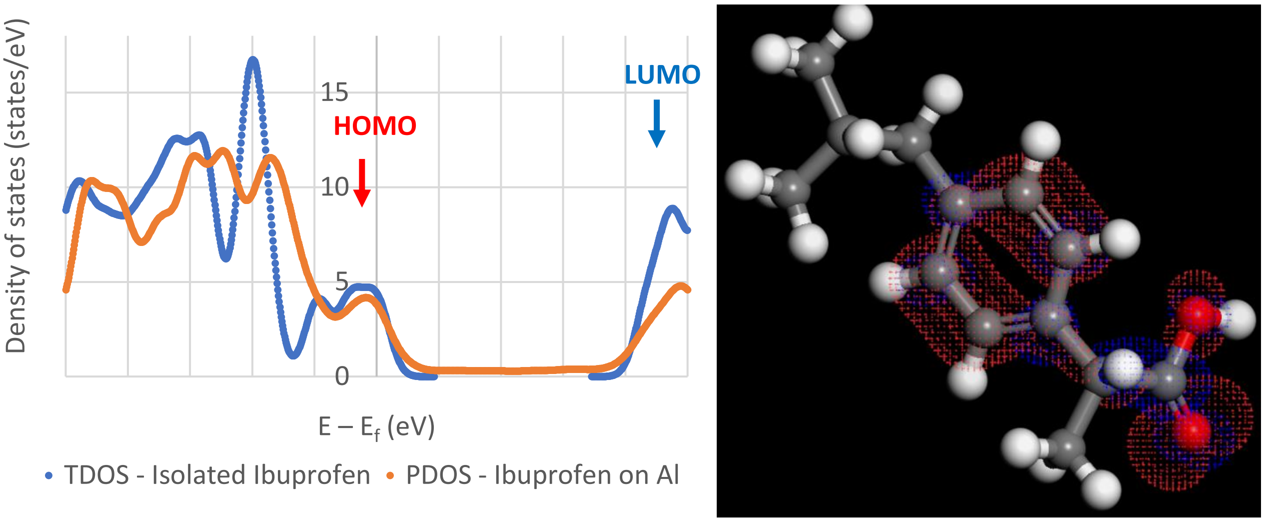

Figure 5.20 – *TDOS of isolated ibuprofen overlayed with the PDOS of ibuprofen relaxed onto an aluminium (100) surface (left). Image of corresponding location of HOMO and LUMO on molecule (right).*

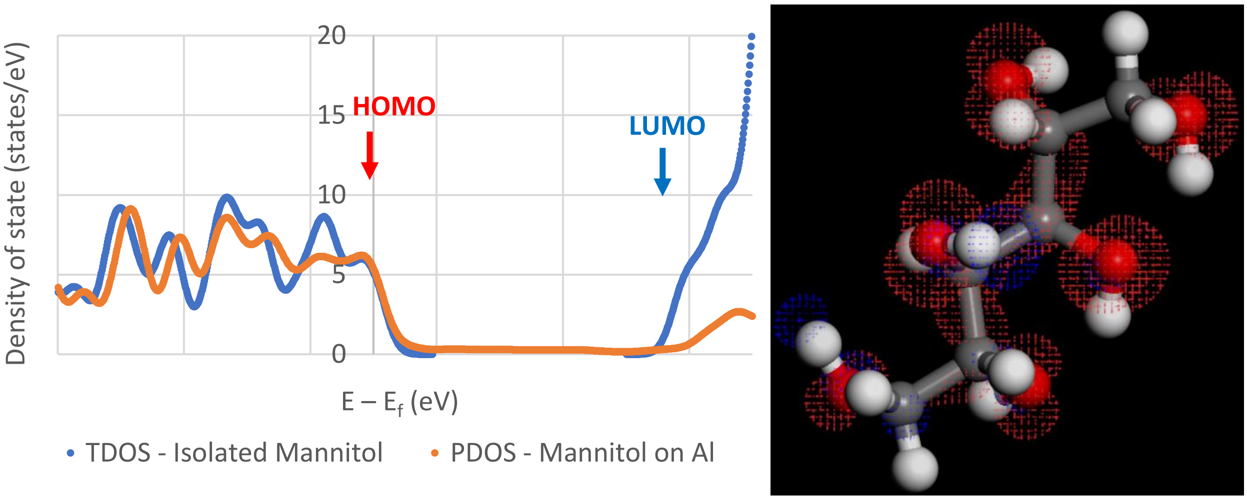

Figure 5.21 – *TDOS of isolated mannitol overlayed with the PDOS of mannitol relaxed onto an aluminium (100) surface (left). Image of corresponding location of HOMO and LUMO on molecule (right).*

Perhaps the most striking feature observed across all systems is the formation of mid-gap or surface states predicted by the calculations. From a mechanistic perspective, this is a crucial finding, as the disappearance of the band gap implies the presence of states that allow for the transfer of electrons in what is typically an insulating material. This phenomenon has also been documented in other publications where DFT has been used to model triboelectric charge transfer [210].

This research has been heavily influenced by the work of Wu et al. [54], who observed a similar disappearance of the band gap in their study; however, they did not provide an in-depth explanation in their paper. While investigating charge transfer mechanisms at solid-liquid interfaces, Nan et al. [244] reported the occurrence of surface states, leading to a broadening of the HOMO and LUMO peaks in DOS plots, thereby reducing the width of the band gap. Additionally, the formation of these so-called 'mid-gap' states has also been observed by Antony et al. [297] in their study of metal-silicon dioxide interfaces. It is hypothesized that this phenomenon may be due to the overlapping of orbitals, which generates the new states required for charge transfer.

Across all the systems studied, there is also a noticeable decrease in the number of LUMO electron states in the PDOS of the molecule. This indicates that contact between these materials can significantly impact the electronic states at the interface, further supporting the theoretical plausibility of electron transfer between materials that are typically insulating.

5.4 – Summary

This work employed DFT calculations to gain insights into the charging characteristics of common pharmaceutical materials. Initial calculations on isolated molecules aimed to identify the physical locations of the frontier orbitals on the molecules, with a focus on the HOMO orbitals that are crucial for triboelectric electron transfer. These results consistently showed that HOMO orbitals tend to concentrate around double-bonded oxygen atoms, suggesting their readiness to donate charge and indicating these regions as triboelectrically active. To further characterize different charging behaviours within the molecules, a slab-molecule approach was applied, inspired by the work of Wu et al. [54]. This approach revealed areas of significant charge density difference near the physical locations of the HOMOs, indicating potential charge transfer regions. Hirshfeld charge analysis demonstrated a substantial redistribution of charge upon contact with a surface, and the proximity to the surface played a significant role, with element-dependent behaviour observed. Additionally, DOS analysis of the contacting molecules revealed an intriguing smearing of electronic states at the surface, suggesting charge mobility between the surface and the molecule.

Chapter 6 – Conclusions and Future work

Triboelectric charging has a long history and has played a significant role in the discovery and development of electricity. However, the extensive literature on this topic reveals its inherent complexity, which has perplexed scientists and researchers since its discovery [1]. Even with advances in experimental and modeling techniques, the phenomenon continues to present difficulties in obtaining a definitive understanding of its underlying mechanism. The recent emergence of triboelectric nanogenerators has rekindled significant interest in triboelectrification and its fundamental mechanisms [62]. Researchers aim to enhance the design and performance of these devices. With the increasing availability of computational resources, first-principles calculations have become more accessible for studying triboelectric charging. Coupled with more sophisticated experimental techniques [216], these developments are helping to make progress in unravelling the underlying mechanisms of this phenomenon.

The advantage of computer simulations lies in their ability to precisely define the system under study. This precision is particularly crucial when investigating a phenomenon as sensitive as triboelectric charging, which is highly influenced by the environment and physical conditions of the system [1]. Furthermore, first-principles calculations offer the unique capability to study the atomic and electronic states, a key aspect for probing the fundamental mechanisms of triboelectric charging, such as electron [5] or ion transfer [46]. In this work, the first-principles modeling approach, specifically DFT, was employed to investigate the underlying mechanisms of triboelectric charging. DFT allows for the modeling of electrons, a level of detail often absent in macroscopic or mesoscopic modeling approaches. This technique was applied to study the electronic structure of various systems relevant to triboelectric charging.

Triboelectric charging exhibits a high degree of sensitivity to surface chemistry and environmental factors [15]. One of the earliest models devised for predicting triboelectric charging relied on the difference in material work functions [338]. While this model proved successful in many cases, it is notable that work function is frequently reported in triboelectric studies as a single, static value. In reality, work function is a dynamic property influenced by temperature, pressure, and surface chemistry [299]. This dynamic nature of work functions is well-recognized in fields such as semiconductors and photovoltaics but has often been overlooked in the context of modeling triboelectric charging. While early attempts in the 2000s used DFT to enhance our understanding of triboelectric charging [210], a significant surge in popularity has occurred more recently, driven by technological advancements and a focus on optimizing the design of Triboelectric Nanogenerator (TENG) devices [3]. However, a noticeable void exists in the literature when it comes to applying DFT calculations to comprehend the charge behaviour of particulate materials, especially in the realm of pharmaceuticals. This study aims to bridge this gap by applying established DFT approaches to novel systems, contributing to a more comprehensive understanding of triboelectric charging. By exploring the dynamic nature of work functions and extending DFT applications to particulate materials, particularly pharmaceuticals, this work seeks to advance the knowledge base and open avenues for improved design and performance of triboelectric systems.

In the initial results chapter of this thesis, the impact of various contaminant molecules on electronic structure properties relevant to triboelectric charging is investigated. The findings reveal a strong dependence of material work function on surface contamination, with certain contaminants consistently causing shifts in work function upward or downward respectively. The key conclusion from this study is that surface contamination can exert a significant influence on charge transfer, shedding light on experimentally observed phenomena, such as the formation of charge mosaics [36].

In the subsequent chapter, the investigation delves into the calculation of work functions for different facets of pharmaceutical materials, which is a rarely explored area. Unlike traditional approaches that consider work function as a static property, this study utilizes DFT calculations to predict effective work functions for various materials and facets. The results reveal significant variations not only among different materials but also among facets of the same material. Additionally, the study explores the influence of surface water, uncovering a complex relationship. These predictions offer valuable insights into the substantial charge build-up observed in the charging of identical materials and help elucidate the phenomenon of charge mosaics observed in other studies. This is in disagreement with other published works which report the work function of pharmaceutical materials to be a single value [310].

In the final and highly theoretical chapter of this thesis, first-principles calculations are employed to investigate the charging behaviour of individual functional groups within commonly encountered pharmaceutical materials. These materials are studied both in vacuum and while interacting with a metal surface. The analysis reveals clear trends in the location of frontier orbitals, which are crucial regions for charge transfer. Charge density difference plots highlight specific areas with significant changes in charge density distribution, and a correlation between charge density and distance from the surface is observed. Hirshfeld charge distribution analysis demonstrates that certain elements exhibit consistent charging trends in particular directions, and this behaviour depends on the type of metal surface. This underscores the significance of functional groups and elemental composition in charge distribution.

This work has illustrated the effectiveness of density functional theory in investigating properties relevant to triboelectric charging within precisely defined systems. The findings presented in this study offer valuable insights into various factors related to triboelectric charging, including the impact of surface contamination, the anisotropic work function, and the distinct interactions of individual functional groups with surfaces. Obtaining such comprehensive results through experimental means is inherently challenging due to limitations in precision, cleanliness, and the difficulty of measuring certain materials or molecular systems directly. The significance of these results lies in their theoretical underpinning of observed experimental phenomena related to triboelectric charging. Traditional experiments face constraints in achieving the necessary cleanliness and precision, and some materials pose challenges in obtaining reliable experimental work functions. Additionally, probing individual molecules directly remains a formidable task. The theoretical framework provided by our study addresses these limitations. These results lend theoretical support to the understanding of triboelectric charging behaviours, shedding light on the roles of humidity and surface contamination [25]. Moreover, the revealed variations in work function attributed to surface termination contribute to explaining the charging tendencies of identical materials [32]. Lastly, the observed influence of individual functional groups underscores the importance of strategic design decisions, offering a pathway to enhanced control over charging phenomena in pharmaceutical materials. In essence, this work contributes to bridging the gap between theory and experiment, providing a foundation for interpreting, and manipulating charging behaviours in practical applications.

As previously mentioned, the application of DFT to the investigation of triboelectric charging in powder systems, particularly beyond the development of TENG devices, is somewhat sparse in the literature. This presents a significant opportunity for the expansion and advancement of this field. For instance, there is little to no research applying Ab Initio Molecular Dynamics (AIMD) to model charge transfer at surfaces, which would offer a more continuous understanding of the processes. Furthermore, there is room for refining models to represent surface contamination more accurately in commonly used materials, and correlating these DFT results with experimental data can significantly enhance the overall understanding. Beyond the domain of TENG research, a substantial opportunity exists to improve the confidence in DFT modeling by establishing a strong correlation between experiments and electronic structure calculations, particularly in the triboelectric charging of particulate systems. Utilizing high-precision methods such as AFM [216] can serve as a practical approach to bridge the gap between theoretical predictions and experimental observations.

List of References

1. Lacks, D. J. & Shinbrot, T. Long-standing and unresolved issues in triboelectric charging. *Nat. Rev. Chem.* **3**, 465–476 (2019).

2. Matsusaka, S., Maruyama, H., Matsuyama, T. & Ghadiri, M. Triboelectric charging of powders: A review. *Chem. Eng. Sci.* **65**, 5781–5807 (2010).

3. Wang, Z. L. & Wang, A. C. On the origin of contact-electrification. *Mater. Today* **30**, 34–51 (2019).

4. Šutka, A. *et al.* Engineering Polymer Interfaces: A Review toward Controlling Triboelectric Surface Charge. *Adv. Mater. Interfaces* **n/a**, 2300323 (2023).

5. Ko, H., Lim, Y., Han, S., Jeong, C. K. & Cho, S. B. Triboelectrification: Backflow and Stuck Charges Are Key. *ACS Energy Lett.* **6**, 2792–2799 (2021).

6. Gibson, N. Static electricity — an industrial hazard under control? *J. Electrostat.* **40–41**, 21–30 (1997).

7. Pu, Y., Mazumder, M. & Cooney, C. Effects of Electrostatic Charging on Pharmaceutical Powder Blending Homogeneity. *J. Pharm. Sci.* **98**, 2412–2421 (2009).

8. Jantač, S., Konopka, L. & Kosek, J. Experimental study of triboelectric charging of polyethylene powders: Effect of humidity, impact velocity and temperature. *Adv. Powder Technol.* **30**, 148–155 (2019).

9. Taghavivand, M., Sowinski, A. & Mehrani, P. Triboelectric effects of continuity additives and a silica catalyst support on polyethylene fluidized bed wall fouling. *Chemical engineering science* vol. 245 116882 at https://doi.org/10.1016/j.ces.2021.116882 (2021).

10. Choi, K., Taghavivand, M. & Zhang, L. Experimental studies on the effect of moisture content and volume resistivity on electrostatic behaviour of pharmaceutical powders. *Int. J. Pharm.* **519**, 98–103 (2017).

11. Taghavivand, M., Mehrani, P., Sowinski, A. & Choi, K. Electrostatic charging behaviour of polypropylene particles during pulse pneumatic conveying with spiral gas flow pattern. *Chemical engineering science* vol. 229 116081 at https://doi.org/10.1016/j.ces.2020.116081 (2021).

12. Zhou, Q. *et al.* A study of charging characteristics of binary mixture of polyolefin particles by using horizontal airflow to separate large and small particles. *Powder Technol.*

13. Ohsawa, A. Brush and propagating brush discharges on insulating sheets in contact with a grounded conductor. *J. Electrostat.* **88**, 171–176 (2017).

14. Nifuku, M. & Katoh, H. A study on the static electrification of powders during pneumatic transportation and the ignition of dust cloud. *Powder Technol.* **135–136**, 234–242 (2003).

15. Harper, W. R. (Wallace R. *Contact and frictional electrification* . (Clarendon Press, 1967).

16. Yoshida, M. *et al.* Estimation of electrostatic charge distribution of flowing toner particles in contact with metals. *Powder Technol.* **135–136**, 23–34 (2003).

17. Gupta, R., Gidaspow, D. & Wasan, D. T. Electrostatic separation of powder mixtures based on the work functions of its constituents. *Powder Technol.* **75**, 79–87 (1993).

18. Kleber, W. & Makin, B. TRIBOELECTRIC POWDER COATING: A PRACTICAL APPROACH FOR INDUSTRIAL USE. *Part. Sci. Technol.* **16**, 43–53 (1998).

19. Jaworek, A., Krupa, A. & Czech, T. Modern electrostatic devices and methods for exhaust gas cleaning: A brief review. *J. Electrostat.* **65**, 133–155 (2007).

20. Tian, Z.-Q. & Wang, Z. L. Flexible triboelectric generator! *Nano energy*. vol. 1 328–334 at https://doi.org/10.1016/j.nanoen.2012.01.004 (2012).

21. Staniforth, J. N. & Rees, J. E. Powder mixing by triboelectrification. *Powder Technol.* **30**, 255–256 (1981).

22. Iversen, P. & Lacks, D. J. A life of its own: The tenuous connection between Thales of Miletus and the study of electrostatic charging. *J. Electrostat.* **70**, 309–311 (2012).

23. Ireland, P. M. Dynamic particle-surface tribocharging: The role of shape and contact mode. *J. Electrostat.* **70**, 524–531 (2012).

24. Greason, W. D. Investigation of a test methodology for triboelectrification. *J. Electrostat.* **49**, 245–256 (2000).

25. McCarty, L. S. & Whitesides, G. M. Electrostatic Charging Due to Separation of Ions at Interfaces: Contact Electrification of Ionic Electrets. *Angew. Chemie Int. Ed.* **47**, 2188–2207 (2008).

26. Lowell, J. The effect of an electric field on contact electrification. *J. Phys. D. Appl. Phys.* **14**, 1513 (1981).

27. Waitukaitis, S. R., Lee, V., Pierson, J. M., Forman, S. L. & Jaeger, H. M. Size-Dependent Same-Material Tribocharging in Insulating Grains. *Phys. Rev. Lett.* **112**, (2014).

28. Matsuyama, T. & Yamamoto, H. Maximum electrostatic charge of powder in pipe flow. *Advanced powder technology* vol. 21 350–355 at https://doi.org/10.1016/j.apt.2010.03.009 (2010).

29. Hu, J. *et al.* Triboelectric charging behavior of a rough surface sliding on a flat plane. *J. Electrostat.* **97**, 85–94 (2019).

30. Zou, H. *et al.* Quantifying the triboelectric series. *Nat. Commun.* **10**, (2019).

31. Šupuk, E. *et al.* Tribo-electrification of active pharmaceutical ingredients and excipients. *Powder Technol.* **217**, 427–434 (2012).

32. Forward, K. M., Lacks, D. J. & Sankaran, R. M. Charge Segregation Depends on Particle Size in Triboelectrically Charged Granular Materials. *Phys. Rev. Lett.* **102**, 28001 (2009).

33. Xu, C. *et al.* Contact-electrification between two identical materials: Curvature effect. *ACS Nano* **13**, (2019).

34. Mizzi, C. A., Lin, A. Y. W. & Marks, L. D. Does Flexoelectricity Drive Triboelectricity? *Phys. Rev. Lett.* **123**, 116103 (2019).

35. Landauer, J., Aigner, F., Kuhn, M. & Foerst, P. Effect of particle-wall interaction on triboelectric separation of fine particles in a turbulent flow. *Adv. Powder Technol.* **30**, 1099–1107 (2019).

36. Baytekin, H. T. *et al.* The Mosaic of Surface Charge in Contact Electrification. *Science (80-.).* **333**, 308 LP – 312 (2011).

37. Lee, V., James, N. M., Waitukaitis, S. R. & Jaeger, H. M. Collisional charging of individual submillimeter particles: Using ultrasonic levitation to initiate and track charge transfer. *Phys. Rev. Mater.* **2**, 35602 (2018).

38. Shah, U. V, Karde, V., Ghoroi, C. & Heng, J. Y. Y. Influence of particle properties on powder bulk behaviour and processability. *Int. J. Pharm.* **518**, 138–154 (2017).

39. Lacks, D. J. The Unpredictability of Electrostatic Charging. *Angewandte Chemie*. vol. 51 6822–6823 at https://doi.org/10.1002/anie.201202896 (2012).

40. Fotovat, F., Bi, X. T. & Grace, J. R. Electrostatics in gas-solid fluidized beds: A review. *Chem. Eng. Sci.* **173**, 303–334 (2017).

41. Chowdhury, F., Ray, M., Sowinski, A., Mehrani, P. & Passalacqua, A. A review on modeling approaches for the electrostatic charging of particles. *Powder Technol.* **389**, 104–118 (2021).

42. Wong, J., Kwok, P. C. L. & Chan, H.-K. Electrostatics in pharmaceutical solids. *Chem. Eng. Sci.* **125**, 225–237 (2015).

43. Maurer, R. J. *et al.* Advances in Density-Functional Calculations for Materials Modeling. *Annu. Rev. Mater. Res.* **49**, 1–30 (2019).

44. Latorre, C. A. *et al.* Simulating Surfactant–Iron Oxide Interfaces: From Density Functional Theory to Molecular Dynamics. *The journal of physical chemistry.* vol. 123 6870–6881 at https://doi.org/10.1021/acs.jpcb.9b02925 (2019).

45. Nikitina, E., Barthel, H. & Heinemann, M. Electron Transfer in Electrical Tribocharging Using a Quantum Chemical Approach. *The journal of imaging science and technology.* vol. 53 40503 at https://doi.org/10.2352/J.ImagingSci.Technol.2009.53.4.040503 (2009).

46. Gil, P. S. & Lacks, D. J. Humidity transforms immobile surface charges into mobile charges during triboelectric charging. *Phys. Chem. Chem. Phys.* **21**, 13821–13825 (2019).

47. Kang, D. *et al.* Deformation-contributed negative triboelectric property of polytetrafluoroethylene: A density functional theory calculation. *Nano Energy* **100**, 107531 (2022).

48. Sukhomlinov, S. V, Kickelbick, G., Mueser, M. H., Sukhomlinov, S. V & Müser, M. H. Mechanochemical Ionization: Differentiating Pressure-, Shear-, and Temperature-Induced Reactions in a Model Phosphate. *Tribology letters.* vol. 70 at https://doi.org/10.1007/s11249-022-01644-w (2022).

49. Lin, S. & Shao, T. Bipolar charge transfer induced by water: experimental and first-principles studies. *Phys. Chem. Chem. Phys.* **19**, 29418–29423 (2017).

50. Shen, X., Wang, A. E., Sankaran, R. M. & Lacks, D. J. First-principles calculation of contact electrification and validation by experiment. *J. Electrostat.* **82**, 11–16 (2016).

51. Fan, F.-R., Tian, Z.-Q. & Lin Wang, Z. Flexible triboelectric generator. *Nano Energy* **1**, 328–334 (2012).

52. Armitage, J. L., Ghanbarzadeh, A., Wang, C. & Neville, A. An investigation into the influence of tribological parameters on the operation of sliding triboelectric nanogenerators. *Tribol. Int.* **155**, 106778 (2021).

53. Wu, J. *et al.* Insights into the mechanism of metal-polymer contact electrification for triboelectric nanogenerator via first-principles investigations. *Nano Energy* **48**, 607–616 (2018).

54. Wu, J., Wang, X., Li, H., Wang, F. & Hu, Y. First-principles investigations on the contact electrification mechanism between metal and amorphous polymers for triboelectric nanogenerators. *Nano Energy* **63**, 103864 (2019).

55. Padhan, A. M. *et al.* NiO–Ti nanocomposites for contact electrification and energy harvesting: experimental and DFT+U studies. *Sustain. Energy Fuels* **6**, 2439–2448 (2022).

56. Wang, L., Dong, Y., Tao, J., Ma, T. & Dai, Z. Study of the mechanisms of contact electrification and charge transfer between polytetrafluoroethylene and metals. *J. Phys. D. Appl. Phys.* **53**, 285302 (2020).

57. Sun, M., Lu, Q., Wang, Z. L. & Huang, B. Understanding contact electrification at liquid–solid

interfaces from surface electronic structure. *Nat. Commun.* **12**, 1752 (2021).

58. Fatti, G., Righi, M. C., Dini, D. & Ciniero, A. Ab Initio Study of Polytetrafluoroethylene Defluorination for Tribocharging Applications. *ACS Appl. Polym. Mater.* **2**, 5129–5134 (2020).

59. Keithley, J. F. *The story of electrical and magnetic measurements : from 500 B.C. to the 1940s* . (IEEE Press, 1999). doi:10.1109/9780470546628.

60. Dibner, B. Ten founding fathers of the electrical science: II. Otto von Guericke: And the first electric machine. *Electr. Eng.* **73**, 396–397 (1954).

61. Gillispie, C. C. *Dictionary of Scientific Biography*. (Scribner, 1979).

62. Xu, C. *et al.* On the Electron-Transfer Mechanism in the Contact-Electrification Effect. *Adv. Mater.* **30**, 1706790 (2018).

63. Mirkowska, M., Kratzer, M., Teichert, C. & Flachberger, H. Atomic Force Microscopy as a Tool to Explore Triboelectrostatic Phenomena in Mineral Processing. *Chemie Ing. Tech.* **86**, 857–864 (2014).

64. Bailey, A. G. The charging of insulator surfaces. *J. Electrostat.* **51**–**52**, 82–90 (2001).

65. Galembeck, F. *et al.* Friction, tribochemistry and triboelectricity: recent progress and perspectives. *RSC Adv.* **4**, 64280–64298 (2014).

66. Horn, R. G., Smith, D. T. & Grabbe, A. Contact electrification induced by monolayer modification of a surface and relation to acid–base interactions. *Nature* **366**, 442–443 (1993).

67. Lowell, J. & Rose-Innes, A. C. Contact electrification. *Adv. Phys.* **29**, 947–1023 (1980).

68. Butt, H.-J. *Surface and interfacial forces* . (Wiley-VCH, 2018).

69. Raos, G., Zappone, B., Raos, G. & Zappone, B. Polymer Adhesion: Seeking New Solutions for an Old Problem. *Macromolecules.* vol. 54 10617–10644 at https://doi.org/10.1021/acs.macromol.1c01182 (2021).

70. Stoecker, H. *et al.* Generation of hard X-ray radiation using the triboelectric effect by peeling adhesive tape. *Journal of electrostatics* vol. 71 905–909 at https://doi.org/10.1016/j.elstat.2013.07.006 (2013).

71. Williams, M. W. Triboelectric charging in metal–polymer contacts – How to distinguish between electron and material transfer mechanisms. *Journal of electrostatics* vol. 71 53–54 at https://doi.org/10.1016/j.elstat.2012.11.006 (2013).

72. Baytekin, H. T. *et al.* Material Transfer and Polarity Reversal in Contact Charging. *Angewandte Chemie.* vol. 51 4843–4847 at https://doi.org/10.1002/anie.201200057 (2012).

73. Pandey, R. K. *et al.* Correlating Material Transfer and Charge Transfer in Contact Electrification. *Journal of physical chemistry.* vol. 122 16154–16160 at https://doi.org/10.1021/acs.jpcc.8b04357 (2018).

74. Li, G. B. *et al.* Experimental Investigation of Triboelectrification Behaviour in the Friction Process. *Lubricants.* vol. 10 180 at https://doi.org/10.3390/lubricants10080180 (2022).

75. Xie, Y., Li, Z., Xie, Y. & Li, Z. Triboluminescence: Recalling Interest and New Aspects. *Chem.* vol. 4 943–971 at https://doi.org/10.1016/j.chempr.2018.01.001 (2018).

76. Kitagawa, Y. *et al.* Tribo-Excited Chemical Reaction Using an Eu III Complex with a Stacked Anthracene Framework. *Chemistry : a European journal.* vol. 28 at https://doi.org/10.1002/chem.202104401 (2022).

77. Piperno, S. *et al.* Absorption vs. redox reduction of Pd2+ and Cu2+ on triboelectrically and naturally charged dielectric polymers. *PCCP : physical chemistry chemical physics.* vol. 14 5551–5557 at https://doi.org/10.1039/c2cp23000c (2012).

78. Sow, M. *et al.* Dependence of contact electrification on the magnitude of strain in polymeric materials. *Journal of Applied Physics* vol. 112 at https://doi.org/10.1063/1.4761967 (2012).

79. Sow, M. *et al.* Strain-Induced Reversal of Charge Transfer in Contact Electrification. *Angewandte Chemie.* vol. 51 2695–2697 at https://doi.org/10.1002/anie.201107256 (2012).

80. Sow, M. *et al.* Effects of material strain on triboelectric charging: Influence of material properties. *Journal of electrostatics* vol. 71 396–399 at https://doi.org/10.1016/j.elstat.2012.11.021 (2013).

81. Verners, O. *et al.* Smooth polymers charge negatively: Controlling contact electrification polarity in polymers. *Nano energy.* vol. 104 107914 at https://doi.org/10.1016/j.nanoen.2022.107914 (2022).

82. MEDLEY, J. A. Fractional Electrification of Polar Polymers. *Nature.* vol. 171 1077 at https://doi.org/10.1038/1711077a0 (1953).

83. MIZES, H. A. *et al.* Direct observation of ion transfer in contact charging between a metal and a polymer. *Applied physics letters* vol. 56 1597–1599 at https://doi.org/10.1063/1.103139 (1990).

84. LAW, K. Y. *et al.* Investigation of the Contact Charging Mechanism between an Organic Salt Doped Polymer Surface and Polymer-Coated Metal Beads. *Chemistry of materials.* vol. 7 2090–2095 at https://doi.org/10.1021/cm00059a016 (1995).

85. Diaz, A. F. Contact Electrification of Materials: The Chemistry of Ions on Polymer Surfaces. *The journal of adhesion.* vol. 67 111–122 at https://doi.org/10.1080/00218469808011102 (1998).

86. Pence, S., Novotny, V. J. & Diaz, A. F. Effect of Surface Moisture on Contact Charge of Polymers Containing Ions. *Langmuir* **10**, 592–596 (1994).

87. Wiles, J. A., Fialkowski, M., Radowski, M. R., Whitesides, G. M. & Grzybowski, B. A. Effects of Surface Modification and Moisture on the Rates of Charge Transfer between Metals and Organic Materials. *J. Phys. Chem. B* **108**, 20296–20302 (2004).

88. Burgo, T. A. L., Galembeck, F. & Pollack, G. H. Where is water in the triboelectric series? *J. Electrostat.* **80**, 30–33 (2016).

89. Moreira, K. S., Lermen, D., Campo, Y. A. S., Ferreira, L. O. & Burgo, T. A. L. Spontaneous Mosaics of Charge Formed by Liquid Evaporation. *Adv. Mater. Interfaces* **7**, 2000884 (2020).

90. Baytekin, H. T., Baytekin, B., Soh, S. & Grzybowski, B. A. Is Water Necessary for Contact Electrification? *Angew. Chemie Int. Ed.* **50**, 6766–6770 (2011).

91. Jonassen, N. *Electrostatics*. (Kluwer Academic Publishers, 2000). doi:10.1007/978-1-4757-1182-0.

92. Taylor, D. M. & Secker, P. E. *Industrial electrostatics : fundamentals and measurements*. (Research Studies Press ; J. Wiley, 1994).

93. Alcácer, L. Electronic Structure of Organic Semiconductors. *Polymers and small molecules* at https://doi.org/10.1088/2053-2571/aaddd8 (2018).

94. Benenson, W., Harris, J. ., Stocker, H. & Lutz, H. *Handbook of Physics*. (Springer-Verlag, 2002). doi:10.1007/0-387-21632-4.

95. Kwetkus, B. A. & Sattler, K. Contact charging of oxidized metal powders. *Zeitschrift f�r Phys. B Condens. Matter* **82**, 87–93 (1991).

96. GALLO, C. F., LAMA, W. L., Gallo, C. F. & Lama, W. L. Classical Electrostatic Description of the Work Function and Ionization Energy of Insulators. *IEEE Transactions on Industry Applications.* vol. 12 7–11 at https://doi.org/10.1109/TIA.1976.349379 (1976).

97. Gan, H. *et al.* Work function measurements of olivine: Implication to photoemission charging properties in planetary environments. *Advances in space research* vol. 56 2432–2438 at https://doi.org/10.1016/j.asr.2015.10.005 (2015).

98. Lin, L. *et al.* Work Function: Fundamentals, Measurement, Calculation, Engineering, and Applications. *Phys. Rev. Appl.* **19**, 37001 (2023).

99. Kim, J. W. & Kim, A. Absolute work function measurement by using photoelectron spectroscopy. *Current applied physics.* vol. 31 52–59 at https://doi.org/10.1016/j.cap.2021.07.018 (2021).

100. D K Davies. Charge generation on dielectric surfaces. *J. Phys. D. Appl. Phys.* **2**, 1533 (1969).

101. Chen, H. M. *et al.* Enhanced stretchable graphene-based triboelectric nanogenerator via control of surface nanostructure. *Nano energy.* vol. 58 304–311 at https://doi.org/10.1016/j.nanoen.2019.01.029 (2019).

102. Li, W. *et al.* Bidirectional electron transfer in Triboelectrification caused by friction-induced change in surface electronic structure. *Nano energy.* vol. 114 108667 at https://doi.org/10.1016/j.nanoen.2023.108667 (2023).

103. Lu, Y. *et al.* Constructing highly flexible dielectric sponge for enhancing triboelectric performance. *Chemical engineering journal* vol. 468 143802 at https://doi.org/10.1016/j.cej.2023.143802 (2023).

104. Hubner, M. *et al.* Influence of humidity on CO sensing with p-type CuO thick film gas sensors. *Sensors and actuators.* vol. 153 347–353 at https://doi.org/10.1016/j.snb.2010.10.046 (2011).

105. LEE, T. J. *et al.* Effect of Temperature on the Work-Function Minimum of Cesiated Tungsten Surfaces. *Journal of Applied Physics* vol. 40 3825–3827 at https://doi.org/10.1063/1.1658278 (1969).

106. Zuo, H. M. *et al.* Design of sensitive materials for nitrogen oxides detection. *Journal of Applied Physics* vol. 134 at https://doi.org/10.1063/5.0164049 (2023).

107. Li, W., Li, D. Y., Li, W. & Li, D. Y. On the correlation between surface roughness and work function in copper. *Journal of chemical physics.* vol. 122 at https://doi.org/10.1063/1.1849135 (2005).

108. Kaur, J., Kant, R., Kaur, J. & Kant, R. Curvature-Induced Anomalous Enhancement in the Work Function of Nanostructures. *The journal of physical chemistry letters.* vol. 6 2870–2874 at https://doi.org/10.1021/acs.jpclett.5b01197 (2015).

109. Liu, X. Y. *et al.* Effect of particle size on tribocharging. *Powder technology* vol. 375 199–209 at https://doi.org/10.1016/j.powtec.2020.07.078 (2020).

110. Clint, J. H., Dunstan, T. S., Clint, J. H. & Dunstan, T. S. Acid-base components of solid surfaces and the triboelectric series. *Europhysics letters.* vol. 54 320–322 at https://doi.org/10.1209/epl/i2001-00244-6 (2001).

111. Veregin, R. P. N. *et al.* A Bidirectional Acid-Base Charging Model for Triboelectrification: part 1. Theory. *The journal of imaging science and technology.* vol. 50 282–287 at

https://doi.org/10.2352/J.ImagingSci.Technol.(2006)50:3(282) (2006).

112. Knight, R. D. *Physics for Scientists and Engineers: A Strategic Approach with Modern Physics*. (Pearson, 2008).

113. Byun, K.-E. *et al.* Control of Triboelectrification by Engineering Surface Dipole and Surface Electronic State. *ACS Appl. Mater. Interfaces* **8**, 18519–18525 (2016).

114. Kim, J. *et al.* High Permittivity CaCu 3 Ti 4 O 12 Particle-Induced Internal Polarization Amplification for High Performance Triboelectric Nanogenerators. *Advanced energy materials.* vol. 10 at https://doi.org/10.1002/aenm.201903524 (2020).

115. Wang, J. *et al.* Achieving ultrahigh triboelectric charge density for efficient energy harvesting. *Nat. Commun.* **8**, (2017).

116. Xu, C. *et al.* Raising the Working Temperature of a Triboelectric Nanogenerator by Quenching Down Electron Thermionic Emission in Contact-Electrification. *Adv. Mater.* **30**, 1803968 (2018).

117. Xu, C. *et al.* Effects of Metal Work Function and Contact Potential Difference on Electron Thermionic Emission in Contact Electrification. *Adv. Funct. Mater.* **29**, 1903142 (2019).

118. Lin, S., Xu, L., Zhu, L., Chen, X. & Wang, Z. L. Electron Transfer in Nanoscale Contact Electrification: Photon Excitation Effect. *Adv. Mater.* **31**, 1901418 (2019).

119. Yanagida, K., Okada, O. & Oka, K. Low-Energy Electronic States Related to Contact Electrification of Pendant-Group Polymers: Photoemission and Contact Potential Difference Measurement. *Jpn. J. Appl. Phys.* **32**, 5603–5610 (1993).

120. Hashimoto, Y. Evaluation of Electronic States of Polymer Surface Using Photoelectron Spectroscopy in Air. *Electr. Eng. Japan* **188**, 9–17 (2014).

121. Lin, S., Xu, C., Xu, L. & Wang, Z. L. The Overlapped Electron-Cloud Model for Electron Transfer in Contact Electrification. *Adv. Funct. Mater.* **30**, 1909724 (2020).

122. Diaz, A. F. & Felix-Navarro, R. M. A semi-quantitative tribo-electric series for polymeric materials: the influence of chemical structure and properties. *J. Electrostat.* **62**, 277–290 (2004).

123. Kim, D. W., Kim, S. & Jeong, U. Lipids: Source of Static Electricity of Regenerative Natural Substances and Nondestructive Energy Harvesting. *Adv. Mater.* **30**, 1804949 (2018).

124. Özel, M. *et al.* Why Does Wood Not Get Contact Charged? Lignin as an Antistatic Additive for Common Polymers. *Chem. Mater.* **32**, 7438–7444 (2020).

125. Shaw, P. E., Jex, C. S. & Hardy, W. B. Tribo-electricity and friction. III.—Solid elements and textiles. *Proc. R. Soc. London. Ser. A, Contain. Pap. a Math. Phys. Character* **118**, 108–113 (1928).

126. Kaufman, G. K. Tribocharging and the triboelectric series. *Encyclopedia of Inorganic and Bioinorganic Chemistry* at (2011).

127. Pan, S. & Zhang, Z. Fundamental theories and basic principles of triboelectric effect: A review. *Friction* **7**, 2–17 (2019).

128. Liu, Z. Q. *et al.* Crystallization-Induced Shift in a Triboelectric Series and Even Polarity Reversal for Elastic Triboelectric Materials. *Nano letters.* vol. 22 4074–4082 at https://doi.org/10.1021/acs.nanolett.2c00767 (2022).

129. Seol, M. *et al.* Triboelectric Series of 2D Layered Materials. *Adv. Mater.* **30**, 1801210 (2018).

130. Yoo, D. *et al.* A Liquid Triboelectric Series. *Advanced materials.* at

https://doi.org/10.1002/adma.202300699 (2023).

131. Naik, S., Mukherjee, R. & Chaudhuri, B. Triboelectrification: A review of experimental and mechanistic modeling approaches with a special focus on pharmaceutical powders. *Int. J. Pharm.* **510**, 375–385 (2016).

132. Liu, J. *et al.* Separation and Quantum Tunneling of Photo-generated Carriers Using a Tribo-Induced Field. *Matter* **1**, 650–660 (2019).

133. Heinert, C., Sankaran, R. M. & Lacks, D. J. Electrostatic charge generation on material surfaces from the evaporation of liquids. *J. Electrostat.* **105**, 103450 (2020).

134. Biegaj, K. W., Rowland, M. G., Lukas, T. M. & Heng, J. Y. Y. Surface Chemistry and Humidity in Powder Electrostatics: A Comparative Study between Tribocharging and Corona Discharge. *ACS Omega* **2**, 1576–1582 (2017).

135. Biegaj, K., Kwek, J. W., Lukas, T., Rowland, M. & Heng, J. Y. Y. Novel Coupling of a Capacitive Probe with a Dynamic Vapor Sorption (DVS) Instrument for the Electrostatic Measurements of Powders. *Ind. Eng. Chem. Res.* **55**, 5585–5589 (2016).

136. Jallo, L. J. & Dave, R. N. Explaining Electrostatic Charging and Flow of Surface-Modified Acetaminophen Powders as a Function of Relative Humidity Through Surface Energetics. *J. Pharm. Sci.* **104**, 2225–2232 (2015).

137. Mohanta, S. K., Rath, S. S. & Dwari, R. K. Surface functionalization of coal and quartz with aniline: A study on work function and frictional charge. *Powder Technol.* **338**, 233–242 (2018).

138. Abdelaziz, K. M., Chen, J., Hieber, T. J. & Leseman, Z. C. Atomistic Field Theory for contact electrification of dielectrics. *J. Electrostat.* **96**, 10–15 (2018).

139. Wolloch, M., Levita, G., Restuccia, P. & Righi, M. C. Interfacial Charge Density and Its Connection to Adhesion and Frictional Forces. *Phys. Rev. Lett.* **121**, 26804 (2018).

140. Apodaca, M. M., Wesson, P. J., Bishop, K. J. M., Ratner, M. A. & Grzybowski, B. A. Contact Electrification between Identical Materials. *Angew. Chemie Int. Ed.* **49**, 946–949 (2010).

141. Kim, D. W., Lee, J. H., Kim, J. K. & Jeong, U. Material aspects of triboelectric energy generation and sensors. *NPG Asia Mater.* **12**, (2020).

142. Karner, S. *et al.* Surface roughness effects on the tribo-charging and mixing homogeneity of adhesive mixtures used in dry powder inhalers. *Powder technology* vol. 264 544–549 at https://doi.org/10.1016/j.powtec.2014.03.040 (2014).

143. Angus, J. C., Greber, I., Angus, J. C. & Greber, I. Tribo-electric charging of dielectric solids of identical composition. *Journal of Applied Physics* vol. 123 at https://doi.org/10.1063/1.5024742 (2018).

144. Helseth, L. E. The Influence of Microscale Surface Roughness on Water-Droplet Contact Electrification. *Langmuir* (2019) doi:10.1021/acs.langmuir.9b00988.

145. Wen, J. *et al.* An improved equivalent capacitance model of the triboelectric nanogenerator incorporating its surface roughness. *Nano energy.* vol. 96 107070 at https://doi.org/10.1016/j.nanoen.2022.107070 (2022).

146. Sutka, A. *et al.* Contact electrification between identical polymers as the basis for triboelectric/flexoelectric materials. *PCCP : physical chemistry chemical physics.* vol. 22 13299–13305 at https://doi.org/10.1039/d0cp01947j (2020).

147. Sutka, A. *et al.* Dramatic increase in polymer triboelectrification by transition from a glassy to rubbery state. *Materials horizons.* vol. 7 520–523 at https://doi.org/10.1039/c9mh01425j

(2020).

148. Bo, T. L. *et al.* The analysis of electrification in windblown sand. *Aeolian research.* vol. 11 15–21 at https://doi.org/10.1016/j.aeolia.2013.07.004 (2013).

149. Mukherjee, R. *et al.* Effects of particle size on the triboelectrification phenomenon in pharmaceutical excipients: Experiments and multi-scale modeling. *Asian journal of pharmaceutical sciences = 亚洲药物制剂科学(英文版).* vol. 11 603–617 at https://doi.org/10.1016/j.ajps.2016.04.006 (2016).

150. Sarkar, S., Chaudhuri, B., Sarkar, S. & Chaudhuri, B. Electrostatics effects in granular materials. *AIP Conference Proceedings* vol. 1542 117–120 at https://doi.org/10.1063/1.4811881 (2013).

151. Toth, J. R. *et al.* Particle-Size-Dependent Triboelectric Charging in Single-Component Granular Materials: Role of Humidity. *Industrial & engineering chemistry research.* vol. 56 9839–9845 at https://doi.org/10.1021/acs.iecr.7b02328 (2017).

152. Lacks, D. J., Sankaran, R. M., Lacks, D. J. & Mohan Sankaran, R. Contact electrification of insulating materials. *Journal of physics.* vol. 44 453001 at https://doi.org/10.1088/0022-3727/44/45/453001 (2011).

153. Chen, Z., Lu, Y., Manica, R. & Liu, Q. Curvature effects on liquid–solid contact electrification. *Nano energy.* vol. 89 106456 at https://doi.org/10.1016/j.nanoen.2021.106456 (2021).

154. Zielinski, M., Pope, M., Wang, N., Horvath, C. & Geacintov, N. E. Photoemission from adenine crystal: Solvation of a pre-ionizing state. **165**, 297–301 (1990).

155. Fu, R., Shen, X. & Lacks, D. J. First-Principles Study of the Charge Distributions in Water Confined between Dissimilar Surfaces and Implications in Regard to Contact Electrification. *J. Phys. Chem. C* **121**, 12345–12349 (2017).

156. Lu, C. X. *et al.* Temperature Effect on Performance of Triboelectric Nanogenerator. *Advanced engineering materials.* vol. 19 1700275 at https://doi.org/10.1002/adem.201700275 (2017).

157. Lin, S. *et al.* Electron Transfer in Nanoscale Contact Electrification: Effect of Temperature in the Metal–Dielectric Case. *Adv. Mater.* **31**, 1808197 (2019).

158. Duesenberg, B. *et al.* Temperature influence on the triboelectric powder charging during dry coating of polypropylene with nanosilica particles. *Powder technology* vol. 399 117224 at https://doi.org/10.1016/j.powtec.2022.117224 (2022).

159. Tan, C. *et al.* Revisiting Contact Electrification at Polymer–Liquid Interfaces. *Langmuir.* vol. 38 11882–11891 at https://doi.org/10.1021/acs.langmuir.2c01376 (2022).

160. Hao, Z. *et al.* Co-harvesting Light and Mechanical Energy Based on Dynamic Metal/Perovskite Schottky Junction. *Matter* **1**, 639–649 (2019).

161. Sun, L. L., Li, C., Chen, X. & Tang, W. Effect of ultraviolet light and ozone on electrification performance of polymers. *Nano Energy* **90**, 106587 (2021).

162. Tao, X. *et al.* Effect of Photo-Excitation on Contact Electrification at Liquid–Solid Interface. *ACS nano.* vol. 15 10609–10617 at https://doi.org/10.1021/acsnano.1c03358 (2021).

163. Melitz, W., Shen, J., Kummel, A. C. & Lee, S. Kelvin probe force microscopy and its application. *Surf. Sci. Rep.* **66**, 1–27 (2011).

164. Yin, J. & Nysten, B. Contact electrification and charge decay on polyester fibres: A KPFM study. *J. Electrostat.* **96**, 16–22 (2018).

165. Ahmed, A. *et al.* Toward High-Performance Triboelectric Nanogenerators by Engineering Interfaces at the Nanoscale: Looking into the Future Research Roadmap. *Adv. Mater. Technol.* 2000520 (2020) doi:10.1002/admt.202000520.

166. Jing, T., Xu, B. & Yang, Y. Liquid doping materials as micro-carrier of functional molecules for functionalization of triboelectric materials and flexible triboelectric nanogenerators for energy harvesting and gesture detection. *Nano Energy* **74**, 104856 (2020).

167. Murtomaa, M. *et al.* Effect of particle morphology on the triboelectrification in dry powder inhalers. *Int. J. Pharm.* **282**, 107–114 (2004).

168. Engers, D. A. *et al.* Triboelectric charging and dielectric properties of pharmaceutically relevant mixtures. *Journal of electrostatics* vol. 65 571–581 at https://doi.org/10.1016/j.elstat.2006.12.002 (2007).

169. Zhang, J. Y. *et al.* Electrochemistry on Tribocharged Polymers Is Governed by the Stability of Surface Charges Rather than Charging Magnitude. *Journal of the American Chemical Society*. vol. 141 5863–5870 at https://doi.org/10.1021/jacs.9b00297 (2019).

170. Sadewasser, S. & Glatzel, T. *Kelvin Probe Force Microscopy – Measuring and compensating Electrostatic forces*. (Springer, 2012).

171. Nonnenmacher, M., O'Boyle, M. P. & Wickramasinghe, H. K. Kelvin probe force microscopy. *Appl. Phys. Lett.* **58**, 2921–2923 (1991).

172. Cunningham, S. Dynamical studies of the single point contact electrification of inorganic and polymer substrates. *J. Electrostat.* **40–41**, 225–230 (1997).

173. Morita, S. & Sugawara, Y. Microscopic contact charging and dissipation. **393**, 310–318 (2001).

174. Knorr, N. & Vinzelberg, S. Charge Writing and Detection by EFM and KPFM Scanning Probe Techniques. *Microsc. Anal.* **26**, (2012).

175. Palleau, E., Ressier, L., Borowik, Ł. & Mélin, T. Numerical simulations for a quantitative analysis of AFM electrostatic nanopatterning on PMMA by Kelvin force microscopy. *Nanotechnology* **21**, 225706 (2010).

176. Yin, J., Vanderheyden, B. & Nysten, B. Dynamic charge transfer between polyester and conductive fibres by Kelvin probe force microscopy. *J. Electrostat.* **96**, 30–39 (2018).

177. Seidel, J. V *et al.* Relative permittivity estimation of wheat starch: A critical property for understanding electrostatic hazards. *J. Hazard. Mater.* **368**, 228–233 (2019).

178. Jin, Y. *et al.* Complete Prevention of Contact Electrification by Molecular Engineering. *Matter* **4**, 290–301 (2021).

179. DUKE, C. B. *et al.* Electronic structure of pendant-group polymers: Molecular-ion states and dielectric properties of poly(2-vinyl pyridine). *Physical review. B, Condensed matter.* vol. 18 5717–5739 at https://doi.org/10.1103/PhysRevB.18.5717 (1978).

180. Zeng, W. *et al.* Fiber-Based Wearable Electronics: A Review of Materials, Fabrication, Devices, and Applications. *Advanced materials.* vol. 26 5310–5336 at https://doi.org/10.1002/adma.201400633 (2014).

181. Chen, J., Wang, Z. L., Chen, J. & Wang, Z. L. Reviving Vibration Energy Harvesting and Self-Powered Sensing by a Triboelectric Nanogenerator. *Joule* vol. 1 480–521 at https://doi.org/10.1016/j.joule.2017.09.004 (2017).

182. Quan, T. *et al.* Hybridized Electromagnetic–Triboelectric Nanogenerator for a Self-Powered Electronic Watch. *ACS nano.* vol. 9 12301–12310 at https://doi.org/10.1021/acsnano.5b05598

(2015).

183. Lei, H. *et al.* Self-Assembled Porous-Reinforcement Microstructure-Based Flexible Triboelectric Patch for Remote Healthcare. *Nano-micro letters.* vol. 15 at https://doi.org/10.1007/s40820-023-01081-x (2023).

184. Fan, F. R. *et al.* Transparent Triboelectric Nanogenerators and Self-Powered Pressure Sensors Based on Micropatterned Plastic Films. *Nano letters.* vol. 12 3109–3114 at https://doi.org/10.1021/nl300988z (2012).

185. Yang, J. *et al.* Triboelectrification-Based Organic Film Nanogenerator for Acoustic Energy Harvesting and Self-Powered Active Acoustic Sensing. *ACS nano.* vol. 8 2649–2657 at https://doi.org/10.1021/nn4063616 (2014).

186. Yi, F. *et al.* Self-Powered Trajectory, Velocity, and Acceleration Tracking of a Moving Object/Body using a Triboelectric Sensor. *Advanced functional materials.* vol. 24 7488–7494 at https://doi.org/10.1002/adfm.201402703 (2014).

187. Wang, Z. L. Triboelectric Nanogenerators as New Energy Technology for Self-Powered Systems and as Active Mechanical and Chemical Sensors. *ACS nano.* vol. 7 9533–9557 at https://doi.org/10.1021/nn404614z (2013).

188. Chen, B. *et al.* Scavenging Wind Energy by Triboelectric Nanogenerators. *Advanced energy materials.* vol. 8 1702649 at https://doi.org/10.1002/aenm.201702649 (2018).

189. Wang, Z. L. *et al.* Toward the blue energy dream by triboelectric nanogenerator networks. *Nano energy.* vol. 39 9–23 at https://doi.org/10.1016/j.nanoen.2017.06.035 (2017).

190. Cui, X. J. *et al.* Triboelectric Nanogenerators for Harvesting Diverse Water Kinetic Energy. *Micromachines.* vol. 13 1219 at https://doi.org/10.3390/mi13081219 (2022).

191. Bai, Y. *et al.* Washable Multilayer Triboelectric Air Filter for Efficient Particulate Matter PM 2.5 Removal. *Advanced functional materials.* vol. 28 1706680 at https://doi.org/10.1002/adfm.201706680 (2018).

192. Cheng, J. *et al.* Triboelectric microplasma powered by mechanical stimuli. *Nature communications.* vol. 9 at https://doi.org/10.1038/s41467-018-06198-x (2018).

193. Matsumoto, M., Saito, S. & Ohmine, I. Molecular dynamics simulation of the ice nucleation and growth process leading to water freezing. *Nature.* vol. 416 409 at https://doi.org/10.1038/416409a (2002).

194. Gillan, M. J., Alfè, D., Brodholt, J., Vočadlo, L. & Price, G. D. First-principles modelling of Earth and planetary materials at high pressures and temperatures. *Reports Prog. Phys.* **69**, 2365–2441 (2006).

195. Becke, A. D. Perspective: Fifty years of density-functional theory in chemical physics. *J. Chem. Phys.* **140**, 18A301 (2014).

196. Jensen, J. H. *Molecular modeling basics* . (CRC, 2010).

197. Brazdova, V., Bowler, D. R. (David R. . & Dawsonera. *Atomistic computer simulations*. *Atomistic computer simulations : a practical guide* (Wiley-VCH, 2013).

198. van Eijck, B. P., Mooij, W. T. M. & Kroon, J. Ab initio crystal structure predictions for flexible hydrogen-bonded molecules. Part II. Accurate energy minimization. *J. Comput. Chem.* **22**, 805–815 (2001).

199. Zheng, Z., Tummala, N. R., Wang, T., Coropceanu, V. & Brédas, J.-L. Charge-Transfer States at Organic–Organic Interfaces: Impact of Static and Dynamic Disorders. *Adv. Energy Mater.* **9**, 1803926 (2019).

200. Fujita, T., Alam, M. K. & Hoshi, T. Thousand-atom ab initio calculations of excited states at organic/organic interfaces: toward first-principles investigations of charge photogeneration. *Phys. Chem. Chem. Phys.* **20**, 26443–26452 (2018).

201. Erker, S. & Hofmann, O. T. Fractional and Integer Charge Transfer at Semiconductor/Organic Interfaces: The Role of Hybridization and Metallicity. *J. Phys. Chem. Lett.* **10**, 848–854 (2019).

202. Le, J.-B. & Cheng, J. Modeling electrochemical interfaces from ab initio molecular dynamics: water adsorption on metal surfaces at potential of zero charge. *Curr. Opin. Electrochem.* **19**, 129–136 (2020).

203. Schöttner, L. *et al.* Doping-Induced Electron Transfer at Organic/Oxide Interfaces: Direct Evidence from Infrared Spectroscopy. *J. Phys. Chem. C* **124**, 4511–4516 (2020).

204. Gruenewald, M. *et al.* Integer Charge Transfer and Hybridization at an Organic Semiconductor/Conductive Oxide Interface. *J. Phys. Chem. C* **119**, 4865–4873 (2015).

205. Paulsson, M. & Datta, S. Thermoelectric effect in molecular electronics. *Phys. Rev. B* **67**, (2003).

206. Sanvito, S. Molecular spintronics. *Chem. Soc. Rev.* **40**, 3336–3355 (2011).

207. McMurry, J. *Organic Chemistry*. (Cengage Learning, 2011).

208. TANAKA, K. The Possibility of Developing Charge Control Agents using a Molecular Orbital Method. 電子写真学会誌 **31**, 392–399 (1992).

209. Laird, B. B., Ross, R. B. & Ziegler, T. Density-Functional Methods in Chemistry: An Overview. in *Chemical Applications of Density-Functional Theory* vol. 629 1 (American Chemical Society, 1996).

210. Yoshida, M., Ii, N., Shimosaka, A., Shirakawa, Y. & Hidaka, J. Experimental and theoretical approaches to charging behavior of polymer particles. **61**, 2239–2248 (2006).

211. Shirakawa, Y. *et al.* Quantum chemical calculation of electron transfer at metal/polymer interfaces. **21**, 500–505 (2010).

212. Gao, H. Q. *et al.* Investigation of Contact Electrification between 2D MXenes and MoS 2 through Density Functional Theory and Triboelectric Probes. *Advanced functional materials.* vol. 33 at https://doi.org/10.1002/adfm.202213410 (2023).

213. Willatzen, M., Lew Yan Voon, L. C. & Wang, Z. L. Quantum Theory of Contact Electrification for Fluids and Solids. *Adv. Funct. Mater.* **30**, 1910461 (2020).

214. Lacks, D. J., Duff, N. & Kumar, S. K. Nonequilibrium Accumulation of Surface Species and Triboelectric Charging in Single Component Particulate Systems. *Phys. Rev. Lett.* **100**, 188305 (2008).

215. Montgomery, D. J. Static Electrification of Solids. *Solid State Physics* 139 at https://doi.org/10.1016/S0081-1947(08)60565-2 (1959).

216. Wang, N., Zhao, X. B., Wang, N. & Zhao, X. Atomic Force Microscopy – A Powerful Tool for Studying Contact Electrification. *Advanced Materials Technologies* vol. 8 at https://doi.org/10.1002/admt.202201408 (2023).

217. Lehtola, S. A review on non-relativistic, fully numerical electronic structure calculations on atoms and diatomic molecules. *Int. J. Quantum Chem.* **119**, (2019).

218. Topham, B. J., Kumar, M. & Soos, Z. G. Profiles of Work Function Shifts and Collective Charge Transfer in Submonolayer Metal–Organic Films. *Adv. Funct. Mater.* **21**, 1931–1940

(2011).

219. Sholl, D. S. & Steckel, J. A. *DENSITY FUNCTIONAL THEORY - A Practical Introduction*. (John Wiley & Sons, Inc, 2009).

220. PAYNE, M. C. *et al.* Iterative minimization techniques for ab initio total-energy calculations: molecular dynamics and conjugate gradients. *Reviews of modern physics.* vol. 64 1045–1097 at https://doi.org/10.1103/RevModPhys.64.1045 (1992).

221. Lehtola, S. Assessment of Initial Guesses for Self-Consistent Field Calculations. Superposition of Atomic Potentials: Simple yet Efficient. *Journal of chemical theory and computation : JCTC.* vol. 15 1593–1604 at https://doi.org/10.1021/acs.jctc.8b01089 (2019).

222. Martin, R. M. *Electronic Structure: Basic Theory and Practical Methods*. (Cambridge University Press, 2004). doi:DOI: 10.1017/CBO9780511805769.

223. Broyden, C. G. A CLASS OF METHODS FOR SOLVING NONLINEAR SIMULTANEOUS EQUATIONS. *Mathematics of computation.* vol. 19 557 at (1965).

224. Pulay, P. Convergence acceleration of iterative sequences. the case of scf iteration. *Chem. Phys. Lett.* **73**, 393–398 (1980).

225. Arrigoni, M. & Madsen, G. K. H. Comparing the performance of LDA and GGA functionals in predicting the lattice thermal conductivity of III-V semiconductor materials in the zincblende structure: The cases of AlAs and BAs. *Comput. Mater. Sci.* **156**, 354–360 (2019).

226. Perdew, J. P., Burke, K. & Ernzerhof, M. Generalized Gradient Approximation Made Simple. *Phys. Rev. Lett.* **77**, 3865–3868 (1996).

227. Alfe, D., Gillan, M. J., Alfè, D. & Gillan, M. J. The energetics of oxide surfaces by quantum Monte Carlo. *Journal of physics : Condensed matter.* vol. 18 L435–L440 at https://doi.org/10.1088/0953-8984/18/35/L01 (2006).

228. Sun, J. W. *et al.* Accurate first-principles structures and energies of diversely bonded systems from an efficient density functional. *Nature chemistry.* vol. 8 831–836 at https://doi.org/10.1038/NCHEM.2535 (2016).

229. STEPHENS, P. J. *et al.* Ab Initio Calculation of Vibrational Absorption and Circular Dichroism Spectra Using Density Functional Force Fields. *Journal of physical chemistry.* vol. 98 11623–11627 at https://doi.org/10.1021/j100096a001 (1994).

230. Vanderbilt, D. Soft self-consistent pseudopotentials in a generalized eigenvalue formalism. *Phys. Rev. B* **41**, 7892–7895 (1990).

231. Klimeš, J. & Michaelides, A. Perspective: Advances and challenges in treating van der Waals dispersion forces in density functional theory. *J. Chem. Phys.* **137**, 120901 (2012).

232. Grimme, S. Accurate description of van der Waals complexes by density functional theory including empirical corrections. *Journal of computational chemistry* vol. 25 1463–1473 at https://doi.org/10.1002/jcc.20078 (2004).

233. Grimme, S. Semiempirical GGA-type density functional constructed with a long-range dispersion correction. *J. Comput. Chem.* **27**, 1787–1799 (2006).

234. Tao, J. M. *et al.* Accurate van der Waals coefficients from density functional theory. *Proceedings of the National Academy of Sciences of the United States of America.* vol. 109 18–21 at https://doi.org/10.1073/pnas.1118245108 (2012).

235. Tkatchenko, A. & Scheffler, M. Accurate Molecular Van Der Waals Interactions from Ground-State Electron Density and Free-Atom Reference Data. *Phys. Rev. Lett.* **102**, 73005 (2009).

236. Renne, M. J. & Nijboer, B. R. A. Microscopic derivation of macroscopic Van der Waals forces. *Chem. Phys. Lett.* **1**, 317–320 (1967).

237. Bereau, T. & von Lilienfeld, O. A. Toward transferable interatomic van der Waals interactions without electrons: The role of multipole electrostatics and many-body dispersion. *J. Chem. Phys.* **141**, 34101 (2014).

238. Tkatchenko, A., Distasio, R. A., Car, R. & Scheffler, M. Accurate and Efficient Method for Many-Body van der Waals Interactions. *Phys. Rev. Lett.* **108**, (2012).

239. Wang, Z., Jin, J. & Liu, M. Atomic Charge Schemes Comparison for Fe Single Atom in Graphitic Carbon: Insights from Quantum Simulations and Machine Learning. *J. Phys. Chem. C* **127**, 17345–17354 (2023).

240. Wang, B., Rong, C., Chattaraj, P. K. & Liu, S. A comparative study to predict regioselectivity, electrophilicity and nucleophilicity with Fukui function and Hirshfeld charge. *Theor. Chem. Acc.* **138**, 124 (2019).

241. Wang, L., Tao, J., Ma, T. & Dai, Z. The electronic behaviors and charge transfer mechanism at the interface of metals: A first-principles perspective. *J. Appl. Phys.* **126**, 205301 (2019).

242. Obot, I. B. *et al.* Density functional theory (DFT) as a powerful tool for designing new organic corrosion inhibitors. Part 1: An overview. *Corrosion science* vol. 99 1–30 at https://doi.org/10.1016/j.corsci.2015.01.037 (2015).

243. Nan, Y. *et al.* Physical mechanisms of contact-electrification induced photon emission spectroscopy from interfaces. *Nano research.* at https://doi.org/10.1007/s12274-023-5674-2 (2023).

244. Nan, Y., Shao, J., Willatzen, M. & Wang, Z. L. Understanding Contact Electrification at Water/Polymer Interface. *Research : a science partner journal.* vol. 2022 1–10 at https://doi.org/10.34133/2022/9861463 (2022).

245. Mulliken, R. S. Electronic Population Analysis on LCAO–MO Molecular Wave Functions. I. *J. Chem. Phys.* **23**, 1833–1840 (1955).

246. Du, X., Gao, X., Qiu, K., Luo, Z. & Cen, K. The Reaction of Poisonous Alkali Oxides with Vanadia SCR Catalyst and the Afterward Influence: A DFT and Experimental Study. *J. Phys. Chem. C* **119**, 1905–1912 (2015).

247. Hirshfeld, F. L. Bonded-atom fragments for describing molecular charge densities. *Theoretica chimica acta.* vol. 44 129–138 at https://doi.org/10.1007/BF00549096 (1977).

248. Bader, R. F. W. Atoms in molecules. *Accounts of Chemical Research.* vol. 18 9–15 at https://doi.org/10.1021/ar00109a003 (1985).

249. Yun, H. & He, R. A Theoretical Model to Predict Contact Electrification. *J. Energy Resour. Technol.* **144**, (2022).

250. Ciniero, A. *et al.* Defects drive the tribocharging strength of PTFE: An ab-initio study. *Nano energy.* vol. 112 108502 at https://doi.org/10.1016/j.nanoen.2023.108502 (2023).

251. Marenich, A. V, Jerome, S. V, Cramer, C. J. & Truhlar, D. G. Charge Model 5: An Extension of Hirshfeld Population Analysis for the Accurate Description of Molecular Interactions in Gaseous and Condensed Phases. *J. Chem. Theory Comput.* **8**, 527–541 (2012).

252. Manz, T. A. & Limas, N. G. Introducing DDEC6 atomic population analysis: part 1. Charge partitioning theory and methodology. *RSC Adv.* **6**, 47771–47801 (2016).

253. Gross, K. C., Seybold, P. G. & Hadad, C. M. Comparison of different atomic charge schemes for predicting p$K_a$variations in substituted anilines and phenols*. *Int. J. Quantum Chem.* **90**,

445–458 (2002).

254. Rigby, J., Izgorodina, E. I., Rigby, J. & Izgorodina, E. I. Assessment of atomic partial charge schemes for polarisation and charge transfer effects in ionic liquids. *PCCP : physical chemistry chemical physics.* vol. 15 1632–1646 at https://doi.org/10.1039/c2cp42934a (2013).

255. Liu, S. Z., Luan, B. Q., Liu, S. & Luan, B. Benchmarking various types of partial atomic charges for classical all-atom simulations of metal–organic frameworks. *Nanoscale.* vol. 14 9466–9473 at https://doi.org/10.1039/d2nr00354f (2022).

256. Hinchliffe, A. *Molecular Modelling for Beginners*. (John Wiley & Sons Ltd., 2008).

257. Andrews, D. H. The Relation Between the Raman Spectra and the Structure of Organic Molecules. *Phys. Rev.* **36**, 544–554 (1930).

258. Cramer, C. J. *Essentials of Computational Chemistry: Theories and Models*. (Wiley, 2004).

259. MAYO, S. L. *et al.* DREIDING: a generic force field for molecular simulations. *Journal of physical chemistry.* vol. 94 8897–8909 at https://doi.org/10.1021/j100389a010 (1990).

260. Rappe, A. K., Casewit, C. J., Colwell, K. S., Goddard, W. A. I. I. I. & Skiff, W. M. UFF, a full periodic table force field for molecular mechanics and molecular dynamics simulations. *J. Am. Chem. Soc.* **114**, 10024–10035 (1992).

261. DAUBEROSGUTHORPE, P. *et al.* Structure and energetics of ligand binding to proteins: Escherichia coli dihydrofolate reductase-trimethoprim, a drug-receptor system. *Proteins : structure, function and genetics.* vol. 4 31–47 at https://doi.org/10.1002/prot.340040106 (1988).

262. Sun, H. Force field for computation of conformational energies, structures, and vibrational frequencies of aromatic polyesters. *Journal of computational chemistry* vol. 15 752–768 at https://doi.org/10.1002/jcc.540150708 (1994).

263. Sun, H. COMPASS: An ab Initio Force-Field Optimized for Condensed-Phase ApplicationsOverview with Details on Alkane and Benzene Compounds. *The journal of physical chemistry.* vol. 102 7338–7364 at https://doi.org/10.1021/jp980939v (1998).

264. Sun, H. *et al.* COMPASS II: extended coverage for polymer and drug-like molecule databases. *J. Mol. Model.* **22**, 47 (2016).

265. Akkermans, R. L. C., Spenley, N. A. & Robertson, S. H. COMPASS III: automated fitting workflows and extension to ionic liquids. *Mol. Simul.* **47**, 540–551 (2021).

266. Robinson, R. L. M. *et al.* Evaluation of Force-Field Calculations of Lattice Energies on a Large Public Dataset, Assessment of Pharmaceutical Relevance, and Comparison to Density Functional Theory. *Journal of chemical information and modeling.* vol. 59 4778–4792 at https://doi.org/10.1021/acs.jcim.9b00601 (2019).

267. Case, D. A. *et al.* The Amber biomolecular simulation programs. *Journal of computational chemistry* vol. 26 1668–1688 at https://doi.org/10.1002/jcc.20290 (2005).

268. BROOKS, B. R. *et al.* CHARMM : A program for macromolecular energy, minimization, and dynamics calculations. *Journal of computational chemistry* vol. 4 187–217 at https://doi.org/10.1002/jcc.540040211 (1983).

269. Van der Spoel, D. *et al.* GROMACS: Fast, flexible, and free. *Journal of computational chemistry* vol. 26 1701–1718 at https://doi.org/10.1002/jcc.20291 (2005).

270. Thompson, A. P. *et al.* LAMMPS - a flexible simulation tool for particle-based materials modeling at the atomic, meso, and continuum scales. *Computer physics communications* vol. 271 108171 at https://doi.org/10.1016/j.cpc.2021.108171 (2022).

271. Phillips, J. C. *et al.* Scalable molecular dynamics with NAMD. *Journal of computational chemistry* vol. 26 1781–1802 at https://doi.org/10.1002/jcc.20289 (2005).

272. Eastman, P. *et al.* OpenMM 7: Rapid development of high performance algorithms for molecular dynamics. *PLoS computational biology.* vol. 13 e1005659 at https://doi.org/10.1371/journal.pcbi.1005659 (2017).

273. Dassault Systemes. BIOVIA MATERIALS STUDIO FORCITE - DATASHEET. https://www.3ds.com/assets/invest/2023-10/biovia-material-studio-forcite.pdf (2024).

274. Hafner, J. Ab-initio simulations of materials using VASP: Density-functional theory and beyond. *Journal of computational chemistry* vol. 29 2044–2078 at https://doi.org/10.1002/jcc.21057 (2008).

275. Giannozzi, P. *et al.* QUANTUM ESPRESSO: a modular and open-source software project for quantum simulations of materials. *Journal of physics : Condensed matter.* vol. 21 395502 at https://doi.org/10.1088/0953-8984/21/39/395502 (2009).

276. Blaha, P. *et al.* WIEN2k: An APW+lo program for calculating the properties of solids. *Journal of chemical physics.* vol. 152 at https://doi.org/10.1063/1.5143061 (2020).

277. Clark, S. J. *et al.* First principles methods using CASTEP. **220**, 567–570 (2005).

278. Lejaeghere, K. *et al.* Reproducibility in density functional theory calculations of solids. *Science.* vol. 351 at https://doi.org/10.1126/science.aad3000 (2016).

279. Wu, C. *et al.* Triboelectric Nanogenerator: A Foundation of the Energy for the New Era. *Advanced energy materials.* vol. 9 1802906 at https://doi.org/10.1002/aenm.201802906 (2019).

280. Tan, D., Willatzen, M. & Wang, Z. L. Electron transfer in the contact-electrification between corrugated 2D materials: A first-principles study. *Nano Energy* **79**, 105386 (2021).

281. Escobar, J. V., Hernandez-Hernandez, M. C., Escobar, J. V. & Hernández-Hernández, M. C. Discharge dynamics from an x-ray generating tribosource. *Applied physics letters* vol. 122 61602 at https://doi.org/10.1063/5.0127155 (2023).

282. Kolehmainen, J. *et al.* Triboelectric charging of monodisperse particles in fluidized beds. *AIChE journal* vol. 63 1872–1891 at https://doi.org/10.1002/aic.15541 (2017).

283. Wang, L., Tao, J., Ma, T. & Dai, Z. The electronic behaviors and charge transfer mechanism at the interface of metals: A first-principles perspective. *J. Appl. Phys.* **126**, 205301 (2019).

284. Segall, M. D. *et al.* First-principles simulation: ideas, illustrations and the CASTEP code. *J. Phys. Condens. Matter* **14**, 2717–2744 (2002).

285. Al-Mahayni, H., Wang, X., Harvey, J.-P., Patience, G. S. & Seifitokaldani, A. Experimental methods in chemical engineering: Density functional theory. *Can. J. Chem. Eng.* **99**, 1885–1911 (2021).

286. Probert, M. Atomistic Computer Simulations: A Practical Guide, by V. Brázdová and D.R. Bowler. *Contemp. Phys.* **54**, 270–271 (2013).

287. Laasonen, K., Car, R., Lee, C. & Vanderbilt, D. Implementation of ultrasoft pseudopotentials in ab initio molecular dynamics. *Phys. Rev. B* **43**, 6796–6799 (1991).

288. Yates, J. R., Pickard, C. J. & Mauri, F. Calculation of NMR chemical shifts for extended systems using ultrasoft pseudopotentials. *Phys. Rev. B* **76**, 24401 (2007).

289. Kahn, A. Fermi level, work function and vacuum level. *Materials horizons.* vol. 3 7–10 at https://doi.org/10.1039/c5mh00160a (2016).

290. Cahen, D., Kahn, A., Cahen, D. & Kahn, A. Electron Energetics at Surfaces and Interfaces: Concepts and Experiments. *Advanced materials.* vol. 15 271–277 at https://doi.org/10.1002/adma.200390065 (2003).

291. Kittel, C. & McEuen, P. *Introduction to Solid State Physics*. (Wiley, 2018).

292. RAMSTAD, A. *et al.* Theoretical study of the Si(100) surface reconstruction. *Physical review. B, Condensed matter.* vol. 51 14504–14523 at https://doi.org/10.1103/PhysRevB.51.14504 (1995).

293. Gross, A., Sakong, S., Groß, A. & Sakong, S. Ab Initio Simulations of Water/Metal Interfaces. *Chemical reviews.* vol. 122 10746–10776 at https://doi.org/10.1021/acs.chemrev.1c00679 (2022).

294. Turetta, N. *et al.* Au(111) Surface Contamination in Ambient Conditions: Unravelling the Dynamics of the Work Function in Air. *Advanced materials interfaces.* vol. 8 at https://doi.org/10.1002/admi.202100068 (2021).

295. Zhang, Y.-Y. First-principles study of electronic properties of interfacial atoms in metal-metal contact electrification. *Chinese Phys. B* **22**, 53403 (2013).

296. Zhang, Y. & Shao, T. Effect of contact deformation on contact electrification: a first-principles calculation. *J. Phys. D. Appl. Phys.* **46**, 235304 (2013).

297. Antony, A. C., Thelen, D., Zhelev, N., Adib, K. & Manley, R. G. Electronic charge transfer during metal/SiO2 contact: Insight from density functional theory. *J. Appl. Phys.* **129**, 65304 (2021).

298. Tao, J., Wang, L., Kong, K., Hu, M. & Dai, Z. Contact Electrification of Biological and Bio-Inspired Adhesive Materials on SiO2 Surfaces: Perspectives from DFT Calculations. *Biomimetics* vol. 7 at https://doi.org/10.3390/biomimetics7040216 (2022).

299. Kawano, H. Effective Work Functions of the Elements: Database, Most probable value, Previously recommended value, Polycrystalline thermionic contrast, Change at critical temperature, Anisotropic dependence sequence, Particle size dependence. *Prog. Surf. Sci.* **97**, 100583 (2022).

300. Patra, A. *et al.* Properties of real metallic surfaces: Effects of density functional semilocality and van der Waals nonlocality. *Proceedings of the National Academy of Sciences of the United States of America.* vol. 114 E9188–E9196 at https://doi.org/10.1073/pnas.1713320114 (2017).

301. BANGE, K. *et al.* The surface chemistry of H2O on clean and oxygen-covered Cu(110). *Surface science* vol. 137 38–64 at https://doi.org/10.1016/0039-6028(84)90675-7 (1984).

302. Musumeci, F., Pollack, G. H., Musumeci, F. & Pollack, G. H. Influence of water on the work function of certain metals. *Chemical physics letters* vol. 536 65–67 at https://doi.org/10.1016/j.cplett.2012.03.094 (2012).

303. Jia, B. *et al.* The electron transfer mechanism between metal and silicon oxide composites for triboelectric nanogenerators. *Adv. Compos. Hybrid Mater.* **5**, 3223–3231 (2022).

304. Li, L. *et al.* Understanding the Ferroelectric Polymer–Metal Contact Electrification for Triboelectric Nanogenerator from Molecular and Electronic Structure. *Adv. Funct. Mater.* **32**, 2109949 (2022).

305. Nakayama, Y. *et al.* Photoemission measurement of extremely insulating materials: Capacitive photocurrent detection in photoelectron yield spectroscopy. *Appl. Phys. Lett.* **92**, 153306 (2008).

306. Neff, J. L. & Rahe, P. Insights into Kelvin probe force microscopy data of insulator-supported molecules. *Phys. Rev. B* **91**, 85424 (2015).

307. Singh-Miller, N. E. & Marzari, N. Surface energies, work functions, and surface relaxations of low-index metallic surfaces from first principles. *Phys. Rev. B* **80**, 235407 (2009).

308. Anagaw, A. Y., Wolkow, R. A. & DiLabio, G. A. Theoretical Study of Work Function Modification by Organic Molecule-Derived Linear Nanostructure on H−Silicon(100)-2 × 1. *J. Phys. Chem. C* **112**, 3780–3784 (2008).

309. Tran, R. *et al.* Anisotropic work function of elemental crystals. *Surf. Sci.* **687**, 48–55 (2019).

310. Brunsteiner, M., Zellnitz, S., Pinto, J. T., Karrer, J. & Paudel, A. Can we predict trends in tribo-charging of pharmaceutical materials from first principles? *Powder Technol.* **356**, 892–898 (2019).

311. Groom, C. R., Bruno, I. J., Lightfoot, M. P. & Ward, S. C. The Cambridge structural database. *Acta Crystallogr. Sect. B Struct. Sci. Cryst. Eng. Mater.* **72**, 171–179 (2016).

312. Liu, D. C. & Nocedal, J. On the limited memory BFGS method for large scale optimization. *Math. Program.* **45**, 503–528 (1989).

313. Docherty, R., Clydesdale, G., Roberts, K. J. & Bennema, P. Application of Bravais-Friedel-Donnay-Harker, attachment energy and Ising models to predicting and understanding the morphology of molecular crystals. *Journal of physics.* vol. 24 89–99 at https://doi.org/10.1088/0022-3727/24/2/001 (1991).

314. Kumar, S., Sinha, N., Goel, S. & Kumar, B. Trypan blue stained KAP crystal: A comparative study on morphological, structural, optical, di-/piezo-electric and mechanical properties. *Chinese J. Phys.* **72**, 655–669 (2021).

315. Goel, S. *et al.* Optical, piezoelectric and mechanical properties of xylenol orange doped ADP single crystals for NLO applications. *Arab. J. Chem.* **13**, 146–159 (2020).

316. Goel, S., Sinha, N., Yadav, H. & Kumar, B. On the prediction of external shape of ZnO nanocrystals. *Physica.* vol. 106 291–297 at https://doi.org/10.1016/j.physe.2018.08.014 (2019).

317. Khan, B. A. *et al.* Design, synthesis, crystal structures, computational studies, in vitro and in silico monoamine oxidase-A&B inhibitory activity of two novel S-benzyl dithiocarbamates. *J. Mol. Struct.* **1265**, 133317 (2022).

318. West, D. *et al.* Importance of the correct Fermi energy on the calculation of defect formation energies in semiconductors. *Applied physics letters* vol. 101 82105 at https://doi.org/10.1063/1.4745779 (2012).

319. Li, Q., Gusarov, S., Kovalenko, A., Veregin, R. P. N. & Veregin, R. P. N. Interfacial Water and Triboelectric Charging: A Theoretical Study of the Role of Water on the PMMA/Silica Tribopair. *The journal of imaging science and technology.* vol. 59 40502–40515 at https://doi.org/10.2352/J.ImagingSci.Technol.2015.59.4.040502 (2015).

320. Golchoobi, A. & Pahlavanzadeh, H. Extra-framework charge and impurities effect, Grand Canonical Monte Carlo and volumetric measurements of CO 2 /CH 4 /N 2 uptake on NaX molecular sieve. *Separation science and technology.* vol. 52 2499–2512 at https://doi.org/10.1080/01496395.2017.1345942 (2017).

321. Arefi, H. H., Fagas, G., Arefi, H. H. & Fagas, G. Chemical Trends in the Work Function of Modified Si(111) Surfaces: A DFT Study. *Journal of physical chemistry.* vol. 118 14346–14354 at https://doi.org/10.1021/jp502464r (2014).

322. Fall, C. J., Binggeli, N. & Baldereschi, A. Anomaly in the anisotropy of the aluminum work function. *Phys. Rev. B* **58**, R7544–R7547 (1998).

323. Heng, J. Y. Y., Bismarck, A. & Williams, D. R. Anisotropic surface chemistry of crystalline

pharmaceutical solids. *AAPS PharmSciTech* **7**, E12–E20 (2006).

324. Wilson, R. G. Vacuum Thermionic Work Functions of Polycrystalline Be, Ti, Cr, Fe, Ni, Cu, Pt, and Type 304 Stainless Steel. *Journal of Applied Physics* vol. 37 2261–2267 at https://doi.org/10.1063/1.1708797 (1966).

325. Mukherjee, R. *et al.* Effects of particle size on the triboelectrification phenomenon in pharmaceutical excipients: Experiments and multi-scale modeling. *Asian J. Pharm. Sci.* **11**, 603–617 (2016).

326. Naik, S. *et al.* Quantification of Tribocharging of Pharmaceutical Powders in V-Blenders: Experiments, Multiscale Modeling, and Simulations. *Journal of pharmaceutical sciences.* vol. 105 1467–1477 at https://doi.org/10.1016/j.xphs.2015.12.024 (2016).

327. Marri, I. *et al.* Surface chemistry effects on work function, ionization potential and electronic affinity of Si(100), Ge(100) surfaces and SiGe heterostructures. *Phys. Chem. Chem. Phys.* **22**, 25593–25605 (2020).

328. Jooya, H. Z. *et al.* Mechanisms for carbon adsorption on Au(110)-(2 × 1): A work function analysis. *Surf. Sci.* **677**, 232–238 (2018).

329. Panda, P. K. *et al.* Contact electrification through interfacial charge transfer: a mechanistic viewpoint on solid–liquid interfaces. *Nanoscale Advances* vol. 4 884–893 at https://doi.org/10.1039/d1na00467k (2022).

330. D'Arrigo, J. S. Screening of membrane surface charges by divalent cations: an atomic representation. *Am. J. Physiol. Physiol.* **235**, C109–C117 (1978).

331. Shah, U. V *et al.* Effect of crystal habits on the surface energy and cohesion of crystalline powders. *Int. J. Pharm.* **472**, 140–147 (2014).

332. Heng, J. Y. Y., Bismarck, A., Lee, A. F., Wilson, K. & Williams, D. R. Anisotropic Surface Energetics and Wettability of Macroscopic Form I Paracetamol Crystals. *Langmuir* **22**, 2760–2769 (2006).

333. Sotthewes, K., Gardeniers, H. J. G. E., Desmet, G. & Jimidar, I. S. M. Triboelectric Charging of Particles, an Ongoing Matter: From the Early Onset of Planet Formation to Assembling Crystals. *ACS Omega* **7**, 41828–41839 (2022).

334. Li, L.-H., Kontsevoi, O. Y. & Freeman, A. J. Atomic-Scale Understanding of the Interaction of Poly(3-hexylthiophene) with the NiO (100) Surface: A First-Principles Study. *J. Phys. Chem. C* **118**, 20298–20305 (2014).

335. Saha, S. K. *et al.* Density functional theory and molecular dynamics simulation study on corrosion inhibition performance of mild steel by mercapto-quinoline Schiff base corrosion inhibitor. *Physica.* vol. 66 332–341 at https://doi.org/10.1016/j.physe.2014.10.035 (2015).

336. Veregin, R. P. N. *et al.* Linking the Chemistry and Physics of Electronic Charge Transfer in Insulators: Theory and Experiment. *The journal of imaging science and technology.* vol. 57 30401–30412 at https://doi.org/10.2352/J.ImagingSci.Technol.2013.57.3.030401 (2013).

337. Tao, J., Wang, L., Li, J. & Dai, Z. Contact Electrification and Adhesion Between Carbon Nanotube and Graphene on Metal Surfaces: Insights from First-principles Study. *J. Bionic Eng.* **19**, 103–112 (2022).

338. Lowell, J. & Brown, A. Contact electrification of chemically modified surfaces. *J. Electrostat.* **21**, 69–79 (1988).

Appendix

Table A.1 – *Table Showing raw data from the bulk optimisation study showing Optimisation approach, Calculated lattice parameters and calculation time.*

Material	Optimisation Approach	Lattice Parameter (Å)	Calculation time (s)
Al	Experimental (Imported)	4.0495	N/A
	FF- COMPASSIII	4.035935	0.47
	DFT - PBE GGA	4.039541	163.88
	DFT - LDA	3.983271	189.17
Pt	Experimental (Imported)	3.9239	N/A
	FF- COMPASSIII	3.910307	0.53
	DFT - PBE GGA	3.970155	2873.53
	DFT - LDA	3.895176	2013.2
Cu	Experimental (Imported)	3.6147	N/A
	FF- COMPASSIII	3.606366	0.45
	DFT - PBE GGA	3.629682	698.91
	DFT - LDA	3.516091	939.33
Au	Experimental (Imported)	4.0783	N/A
	FF- COMPASSIII	4.064632	0.48
	DFT - PBE GGA	4.159351	2394.77
	DFT - LDA	4.049646	2457.62
Ag	Experimental (Imported)	4.0857	N/A
	FF- COMPASSIII	4.070678	0.42
	DFT - PBE GGA	4.155573	2517.75
	DFT - LDA	4.009241	2232.23
Pd	Experimental (Imported)	3.8907	N/A
	FF- COMPASSIII	3.880025	0.91
	DFT - PBE GGA	3.840959	2265.27
	DFT - LDA	3.942671	1407.78